Bolt Beranek and Newman Inc.

NASA Contractor Report 172546

Methods for Designing Treatments to Reduce Interior Noise of Predominant Sources and Paths in a Single Engine Light Aircraft

R.E. Hayden, P.J. Remington, M.A. Theobald, J.F. Wilby

Bolt Beranek and Newman Inc.
Cambridge, MA 02238

Contract NAS1-16138
March 1985

National Aeronautics and Space Administration

Langley Research Center
Hampton, Virginia 23665

METHODS FOR DESIGNING TREATMENTS TO REDUCE INTERIOR NOISE OF PREDOMINANT SOURCES AND PATHS IN A SINGLE ENGINE LIGHT AIRCRAFT

by

R.E. Hayden
P.J. Remington
M.A. Theobald
J.F. Wilby

Prepared Under Contract No. NAS1-16138

by

Bolt Beranek and Newman Inc.
Cambridge, MA 02238

for

National Aeronautics and Space Administration
Langley Research Center
Hampton, VA 23665

LIST OF FIGURES

LIST OF TABLES

characteristics sufficient to identify treatment concepts for each.

The study concentrated on laboratory tests of a specially fabricated fuselage section of a single-engine aircraft, shown in Fig. 1 (and described in detail in App. A). The lab tests consisted of path diagnoses and a brief wind tunnel test to investigate airflow-induced noise, as well as evaluation of several generic treatment concepts.

Flight test data from Phase 1 was used in conjunction with additional data taken on a brief flight test to provide source levels; these source levels were then combined with the path data obtained in the laboratory tests to allow rank-ordering of the dominant source/path combinations over the entire frequency range of interest.

The following source/path combinations were found to contribute measurably to the cabin noise (A-weighted level, and/or speech interference level):

Source	Path(s)
Propeller airborne noise	(a) Through firewall via engine compartment (b) Through roof and skin panels
Exhaust noise	Through shin panels (and possibly through engine compartment)
Structureborne noise from engine/propeller combination	Through mounts, support frame (spider), and firewall
Airflow over landing gear cutouts	Not explicitly determined, but assumed to be through wheel well structure

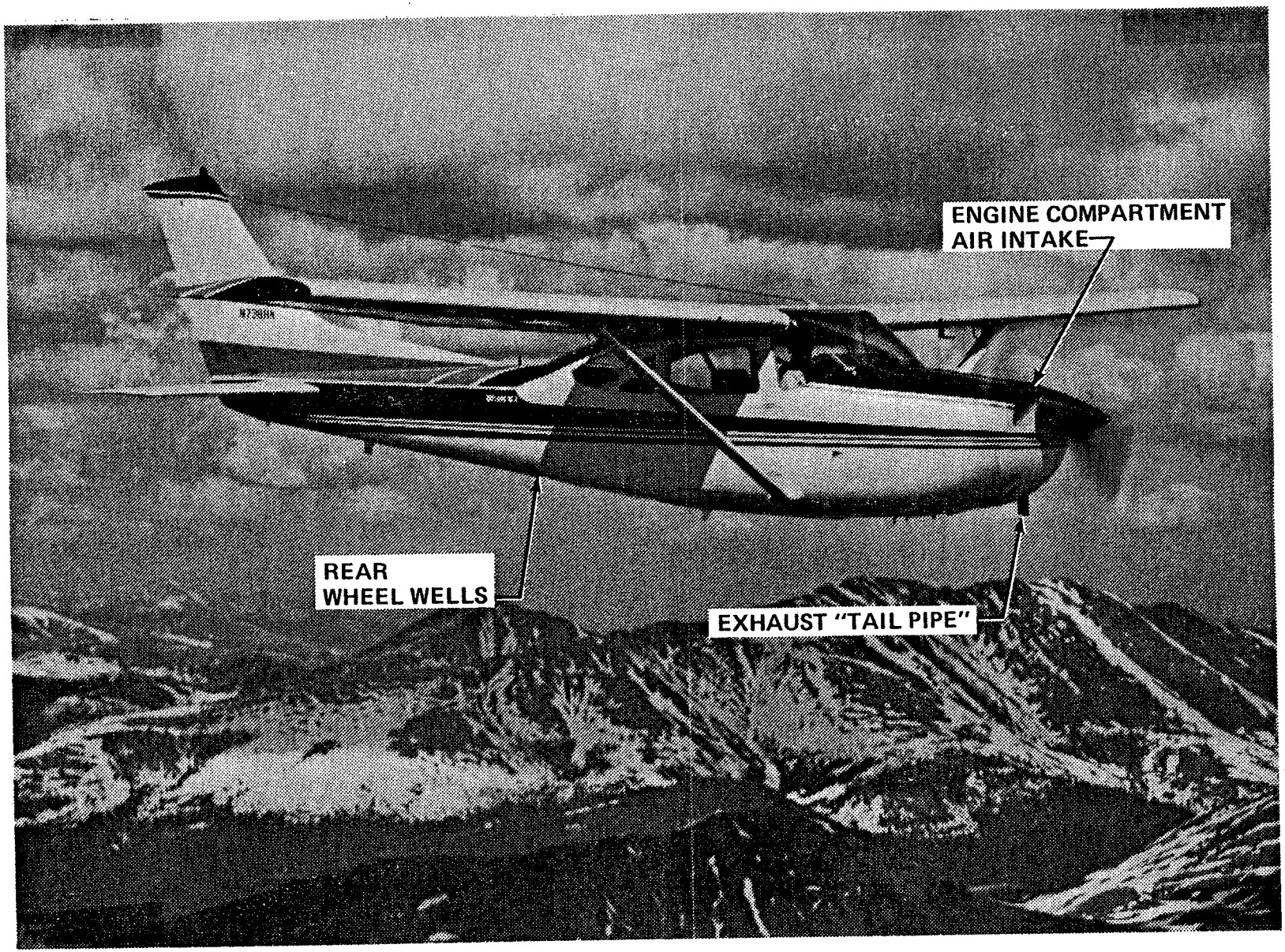

FIGURE 1. AIRCRAFT USED FOR THIS STUDY.

Noise reduction concepts explicitly studied in the laboratory included:

- Two types of firewall stiffening which reduced the prop blade rate tone transmission at 80 Hz by up to 8 dB;
- Two-stage vibration isolators for reducing structure-borne noise; these isolators were not as effective as expected due to the rapidly-changing admittance characteristics of the attachment points and due to resonances in the support structure itself;
- Stiffening the engine support structure to change admittance characteristics in particular frequency bands;
- Use of wheel well covers to reduce airflow source noise.

Other standard techniques, such as panel stiffening, special mufflers, use of damping and absorption, were evaluated for their applicability, but not actually tested, because of resource limitations in the project. As a result, this report serves as a status report which should prove to be a helpful guide to engineers attempting to design noise control solutions for light aircraft, but does not in itself provide a handbook of validated noise control measures.

This report is organized as to provide a succinct summary of the diagnosis of this particular aircraft (Sec. 2), and a summary of noise control concepts (Sec. 3), followed by extensive details of every aspect of the study which are described in nine appendices. The appendices include theoretical considerations regarding sources, paths, and measurement methods; data from laboratory and flight tests on each source/path combination of interest; predicted contributions of each source/path combination to the cabin noise levels; and discussion of noise control methods applicable to each source/path combination. The appendices are organized as follows:

Appendix A: Description of the Test Aircraft (physical characteristics, performance, construction and photographs)

Appendix B: Flight Tests to Obtain Diagnostic Data (excerpts from flight test conducted in this phase)

Appendix C: Noise Reduction Measurement and Improvement for Various Exterior Panels, Windows, and Firewalls (methods for and results of transmission loss estimates of individual sections of the aircraft as well as a discussion of the firewall stiffening study)

Appendix D: Contribution and Treatment of Cabin Noise Resulting From Exhaust Noise (source and path data from flight and lab tests)

Appendix E: Contribution and Treatment of Cabin Noise Resulting from Propeller Airborne Noise (source level estimates at different locations on the aircraft, estimates of several path contributions, and discussion of treatment options)

Appendix F: Contribution and Treatment of Cabin Noise Resulting from Airborne Noise in the Engine Compartment (flight and lab data, estimates of contribution to cabin noise and application of stiffened firewall)

Appendix G: Noise Due to Airflow (review of flight observations, discussion of analytical considerations, and a description of the unique wind tunnel experiment)

Appendix H: Contribution and Treatment of Cabin Noise Resulting from Engine and Propeller-Induced Structureborne Noise (theoretical aspects, diagnostic methods, flight and ground test observations, two-stage isolator design and testing and stiffened support results)

Appendix I: Considerations Relating to Sensor Performance in the Measurement of Sound in Moving Airstreams and on Aircraft Surfaces (data and techniques for measuring sound in the presence of moving airstreams, including a newly-developed surface-mounted microphone for flight surveys).

2. SUMMARY OF SOURCE/PATH DIAGNOSIS

2.1 Setting Engineering Goals

It is generally accepted that two common measures of human response to sound provide a good measure of the acceptability of aircraft interior spaces: the A-weighted sound pressure level (dBA) and the speech interference level (SIL [0.5,1,2,4]).

Reference 1 reviewed a study which correlated the percentage of test subjects highly annoyed by recorded aircraft interior sound as a function of the two measures mentioned. These results are plotted in Fig. 2, along with two bars at the left of the plot which give the range of data measured on the test aircraft with a standard production interior. The intercepts of the flight data with the dBA-vs-annoyance and SIL-vs-annoyance curves show that between 78% and 90% of the test subjects would be highly annoyed when exposed to the cabin environment in the aircraft selected for our study (which was typical of the larger fleet).

An optimistic but meaningful goal for a noise control program might be to improve the environment such that only half as many passengers would find it objectionable; thus, for illustrative purposes, one can define a "goal" as shown by the shaded area on the ordinate between the 40% and 50% marks. Translating the goal for "% annoyed" back to the trend curves allows the direct determination of the required reduction in noise levels, i.e., 9-13 dBA and 9-12 dB SIL. Using 12 dBA and 12 dB SIL as a goal for reduction, we can now examine means for arriving at an engineering criterion for implementing the goal.

Figure 3 shows a band of one-third octave spectra (shaded) which represents the range of A-weighted levels measured during several flights (at 2400 rpm). Below the data band, two curves have been shown - one a constant dBA curve (flat) and the other

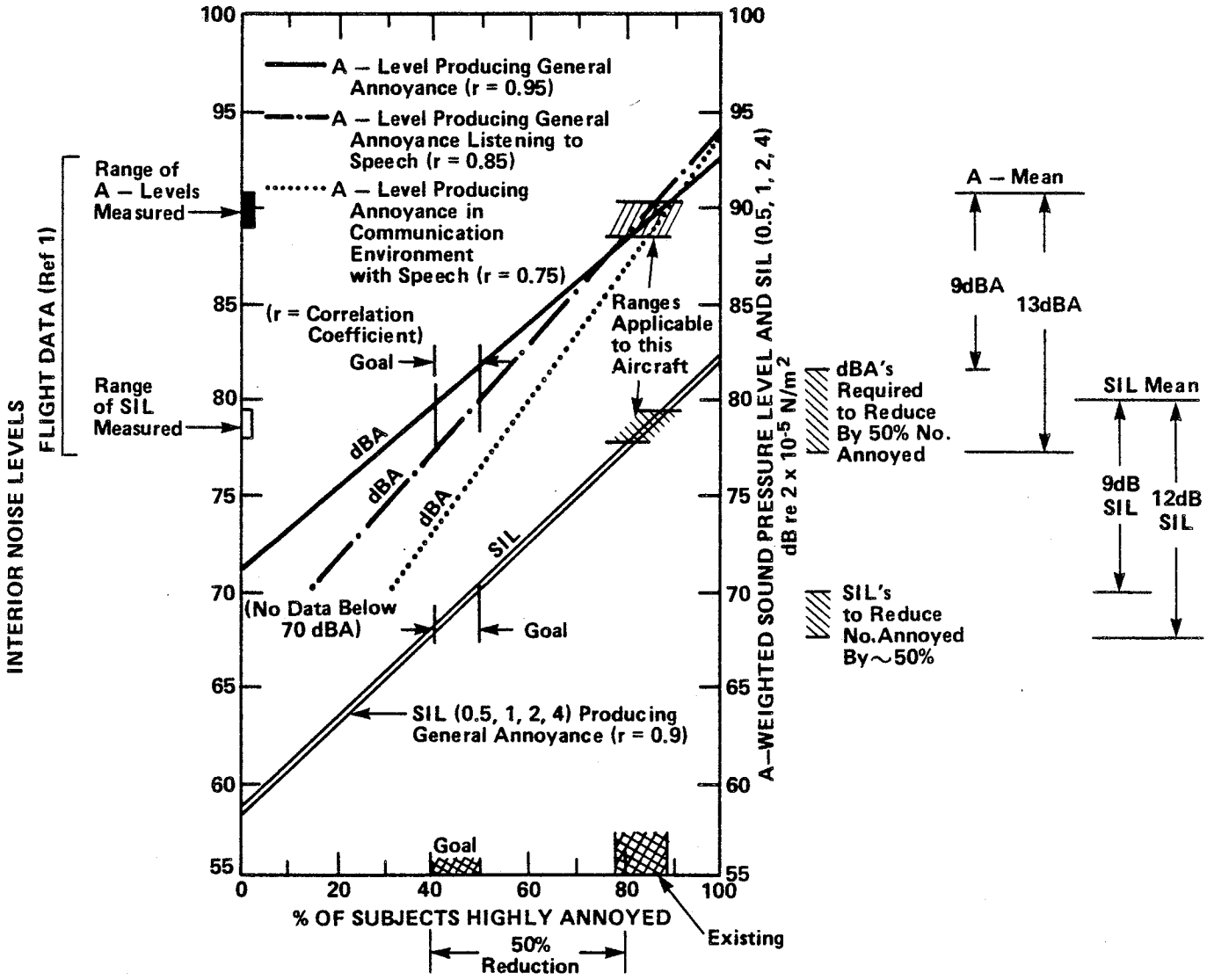

SUBJECTIVE RESPONSES TO G/A INTERIOR NOISE
(Ref 21 of Ref 1)

FIGURE 2. USE OF FLIGHT AND PSYCHOACOUSTIC DATA TO DERIVE ENGINEERING REQUIREMENTS.

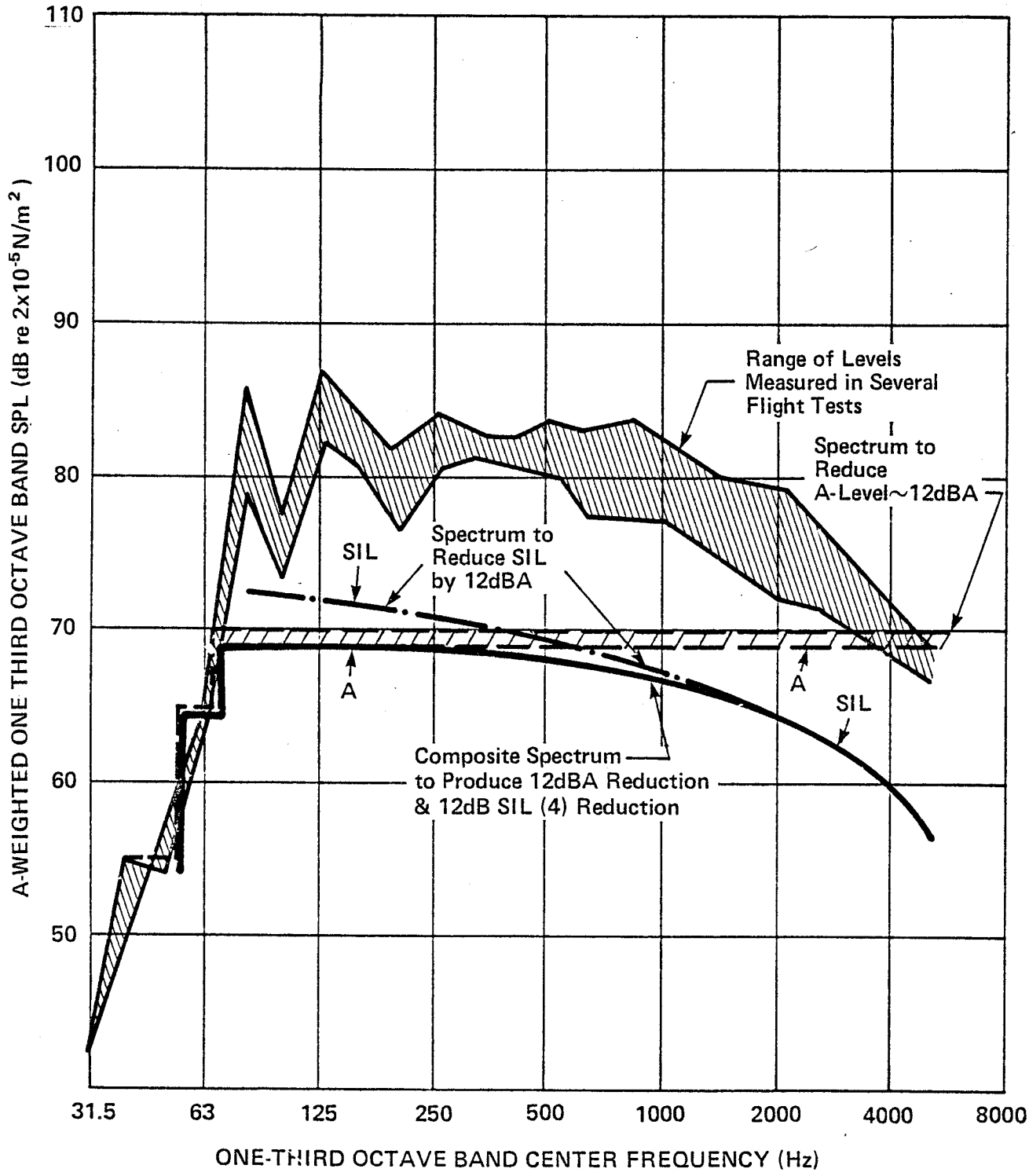

FIGURE 3. DERIVATION OF SPECTRUM REQUIRED TO REDUCE A-LEVELS AND SIL BY 12 DB WHICH WOULD EFFECT A 50% REDUCTION IN NUMBER OF PASSENGERS ANNOYED.

a constant SIL curve. Since we are trying to reduce both the A-level and the SIL by the same amount, a composite "goal spectrum" can be formed simply by taking the lower of the two curves in each one-third octave band. Obviously, other shapes of curves which would lead to the same result are possible, but this approach will define the noise reduction needed to arrive at a balanced cabin noise spectrum.

2.2 Identification of Source/Path Combinations

The diagnosis of a complex aircraft requires a systematic plan such that all appropriate parameters are measured or estimated. The most convenient model for such a diagnosis is one which identifies each source of acoustic energy (radiated sound, structural vibration, or unsteady airflow) and then identifies all the paths by which the energy reaches the cabin.

Figures 4 through 7 provide such diagrams for the airborne radiation from the propeller; airborne radiation from the engine exhaust, engine casing and intakes, and engine/propeller structureborne vibration; unsteady aerodynamic excitation and a composite diagram showing all source/paths combined. Appendices D through H discuss the diagnosis of these source/path combinations in detail. Appendix C provides a separate section dealing with the performance of various parts of the aircraft structure from the point of view of reducing airborne sound transmission. In situ, element-by-element noise reduction mesurements are provided, as well as an analysis and test of means for changing the acoustic characteristics of selected panels.

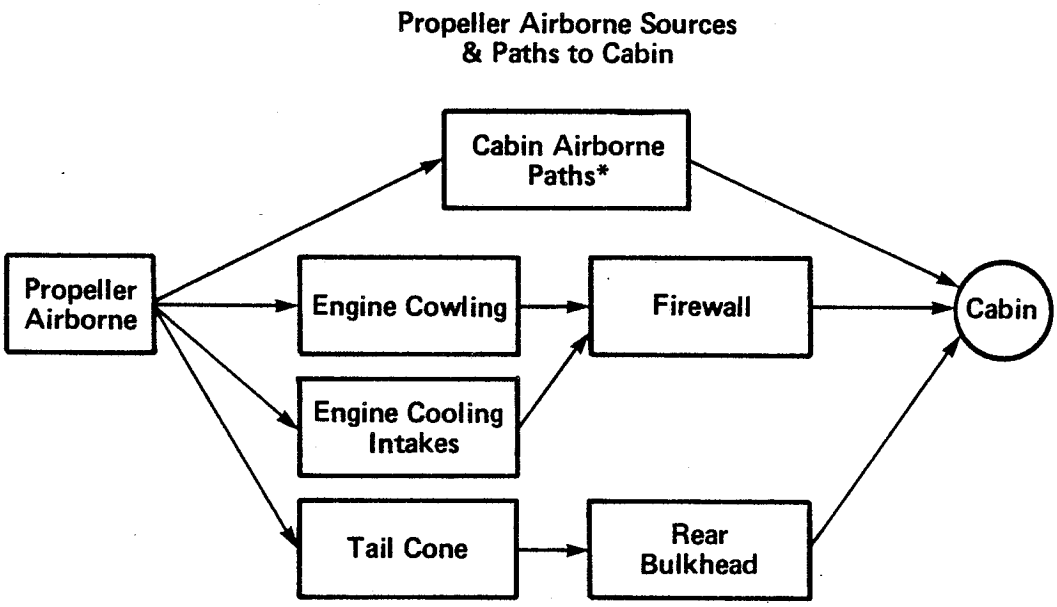

*Cabin Airborne Paths Include:

- Windshield
- Doors
- Door Leaks
- Windows
- Window Leaks
- Walls
- Floor
- Overhead
- Ventilation Ducts

FIGURE 4. PROPELLER SOURCE/PATH DIAGRAM

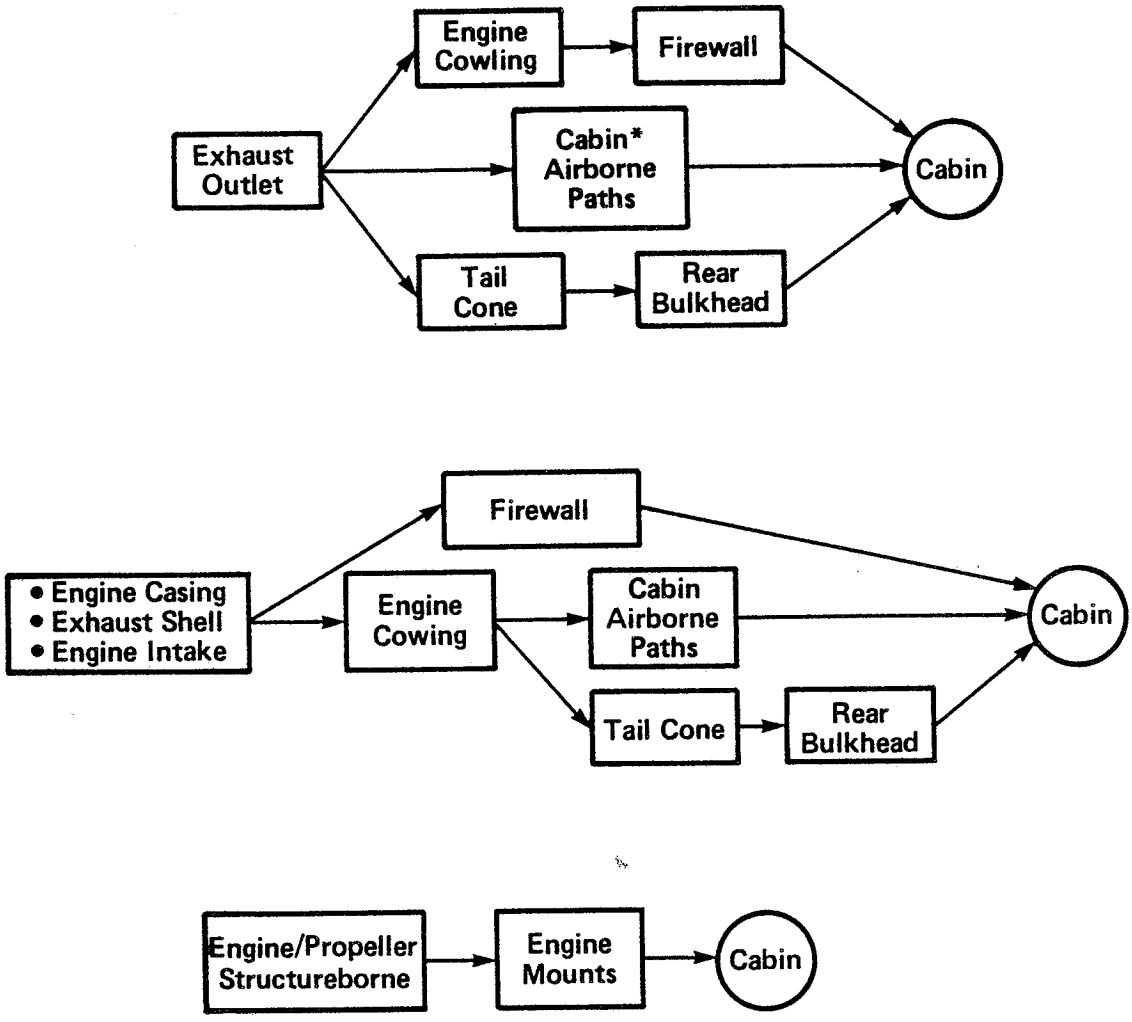

FIGURE 5. ENGINE SOURCES AND PATHS.

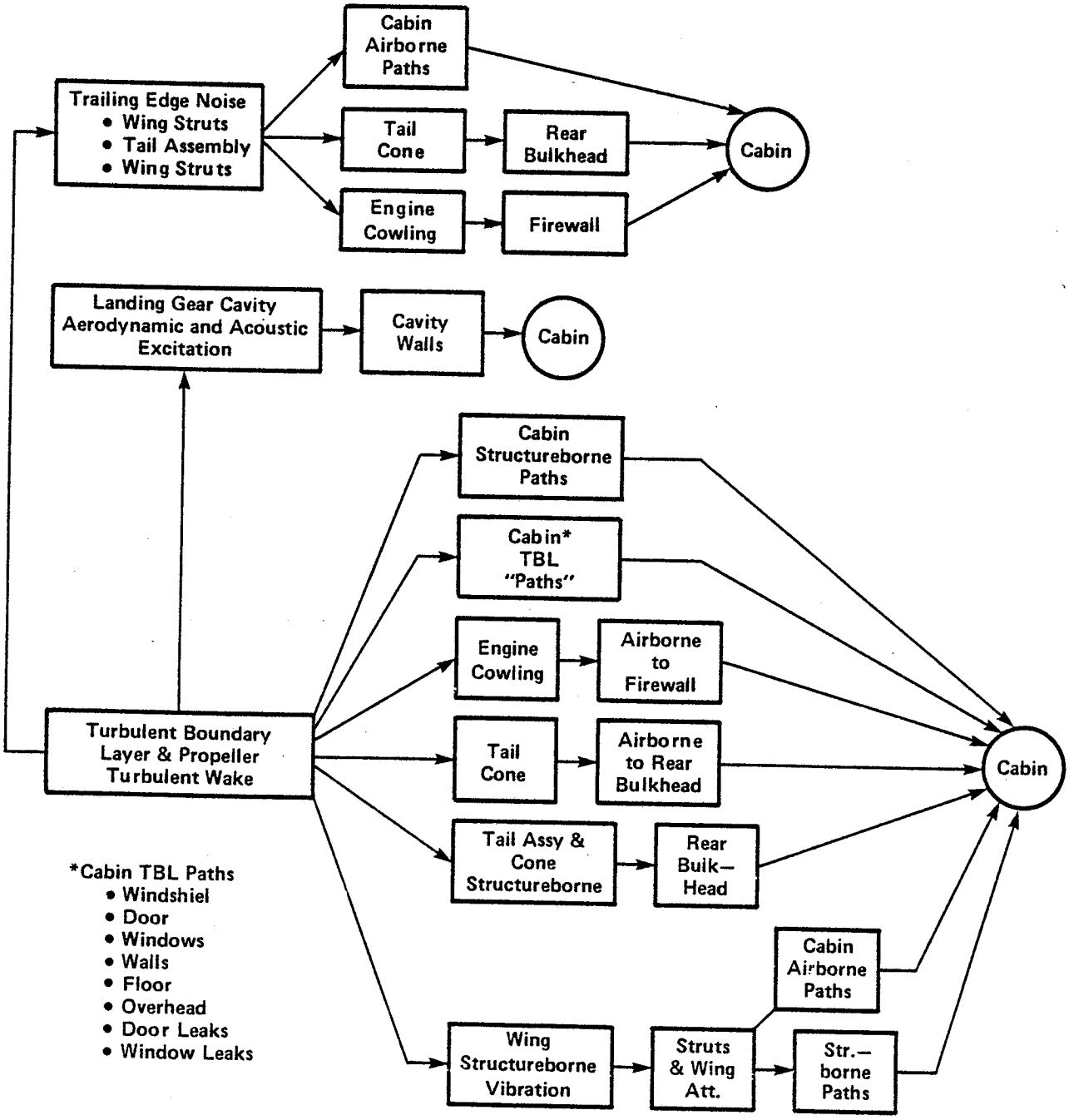

FIGURE 6. AERODYNAMIC SOURCES AND PATHS.

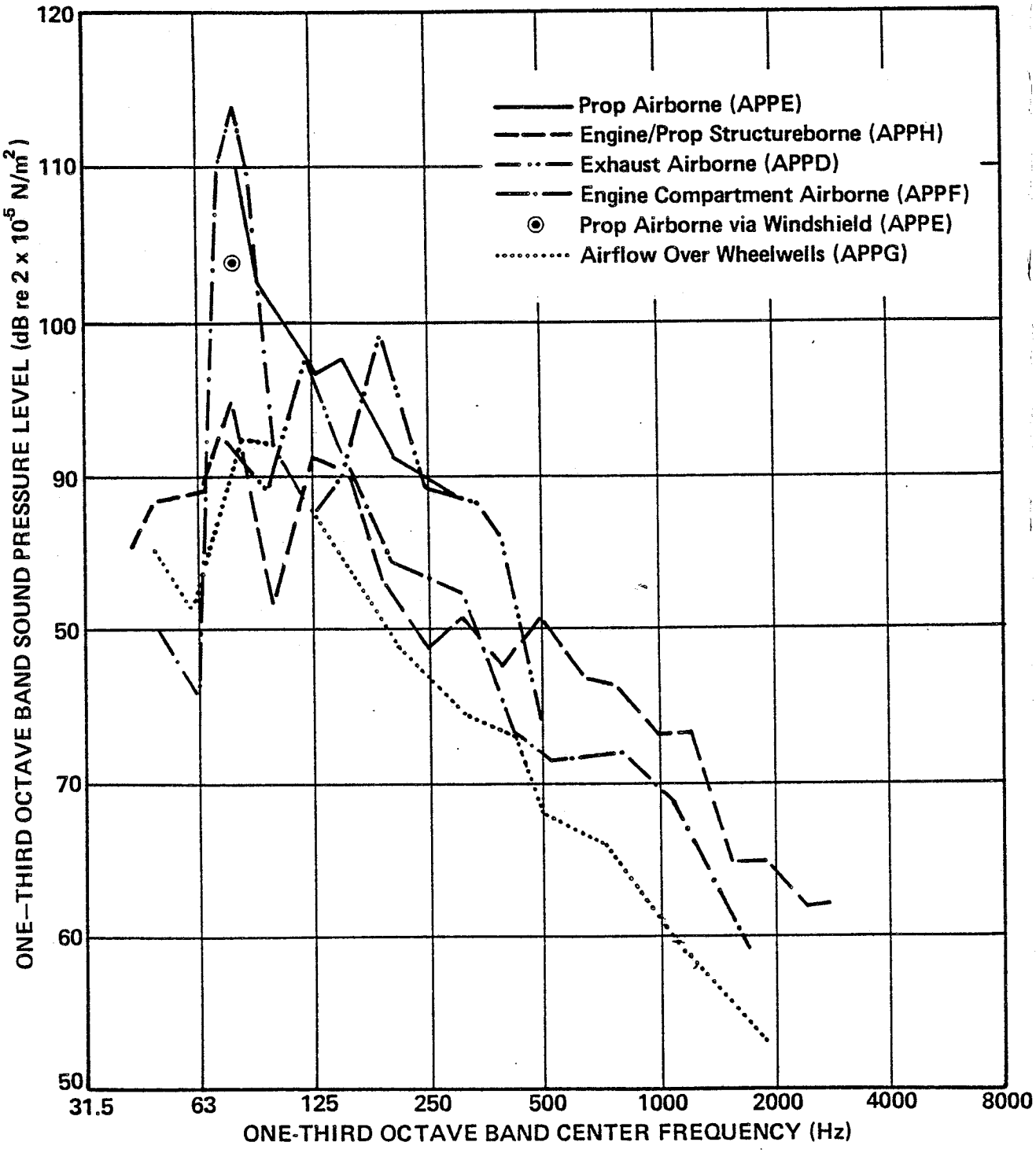

FIGURE 8. PREDICTED SOURCE/PATH COMBINATIONS FOR 2400 RPM LEVEL FLIGHT

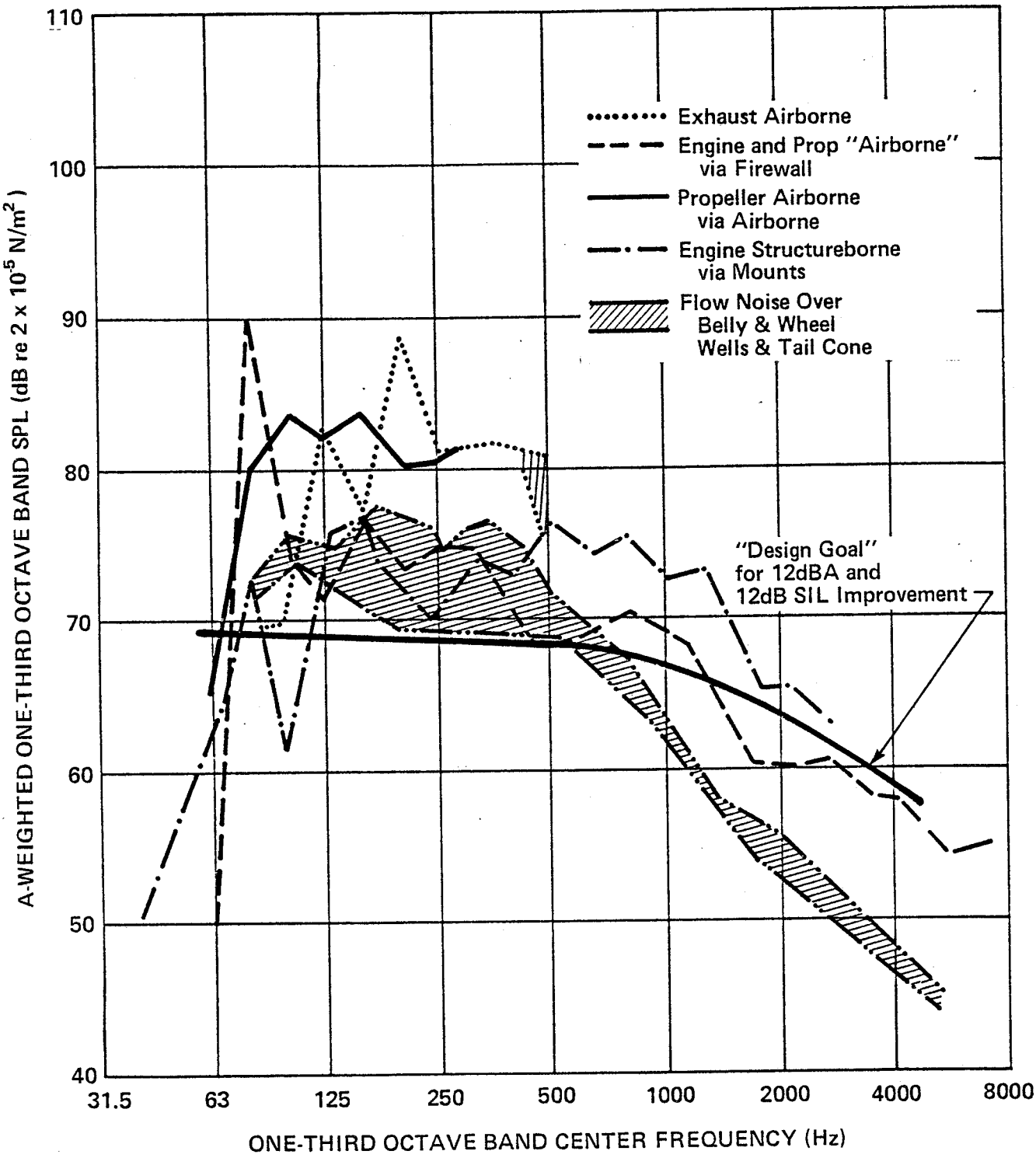

FIGURE 9. A-WEIGHTED COMPONENT SPECTRA COMPARED WITH "GOAL."

transmission characteristics and in defining the relative roles of skin and structural members in the sound transmission process. Intensity methods could be useful in this context, although use of such methods does not inherently solve the fundamental problem of identifying how the energy reached a particular panel. In the area of engine/propeller structureborne noise transmission, the principal effects to be explored further are the mount-to-mount variations in admittance and in-flight vibration levels; the techniques we have described will serve as a basis for undertaking such a study. The role of airflow still remains a key problem in the diagnosis. Improved estimates could be made using computational fluid dynamics programs to calculate the local flow field properties around the aircraft (recognizing that the programs do not account well for flow separation and that such separated flow regions do exist and are important in relation to cabin noise) and through the use of tests in low noise wind tunnels or engine-off dive tests. The role of the tail and wings in creating structureborne vibration resulting from aerodynamic excitation should be clarified through the use of a combination of flight tests (to gather excitation data and to measure typical vibration levels) and laboratory tests to develop appropriate transfer functions.

Because of the overall complexity of the problem of predicting source and path characteristics on a small aircraft, one can count on a lengthy, time-consuming process, requiring a full complement of analytical and experimental tools, as well as both ground and flight tests, if a diagnosis is to be developed which will allow optimum selection and application of treatment concepts.

3. TREATMENT REQUIREMENTS AND CONCEPTS

3.1 Requirements

Using the illustrative criterion curve developed in Sec. 2.1 and the predicted source-path contributions developed in Apps. D through H and summarized in Sec. 2.3, a goal for noise reduction for each source/path combination can be quantified. Figure 10(a) summarizes the overall "requirement" as determined by the range of levels measured in the Phase 1 and Phase 2 flight tests. Most bands require 10 dB of reduction with several requiring 15-18 dB reduction. Figure 10(b) breaks down the noise reduction required by source/path combination. At 80 Hz, the propeller airborne noise, which reaches the cabin via the engine compartment through the firewall and via the roof, is clearly the dominant source, followed by airborne propagation through the windshield. Exhaust noise and propeller airborne noise dominate the rest of the spectra out to around 500 Hz. Important, although weaker, contributions from engine/propeller structureborne and airflow-induced noise can also be seen. Above 500 Hz, all the source/path combinations shown do not add up to the required reduction. This is due primarily to limitations in the diagnosis imposed by sensor response or "contamination" of acoustic pressures by hydrodynamic pressures. Note that because of the residual ambiguities in the diagnosis and variations in flight measurements, the required reductions shown may vary somewhat from aircraft to aircraft.

prop wake is the convected spiraling wake pattern which creates periodic deflections of the aircraft structure as it passes. These deflections include the creation of unsteady forces and moments on the tail section, which in turn creates structureborne vibration propagating toward the cabin. The relative role of these non-acoustic disturbances created by the propeller is largely unknown. However, in the first instance, it is easy to visualize a re-arrangement of the air intake system which would reduce the periodic modulation of the air entering the engine compartment. Thus, pending verification of the mechanism on specific aircraft (which could be done, for example, by temporarily blocking or changing the shape of the intake), one could, in principle, reduce the blade passage rate disturbances which excite the firewall. The modification of the general wake structure which may be exciting the fuselage and empennage is less straightforward. However, propellers which are designed with an aerodynamically optimized distribution of wake along the prop radius may have weaker root and tip vortices and thus create a less intense excitation. The latter point is highly speculative but could be kept in mind in development of a new aircraft or selection of advanced propellers as retrofits to existing models.

The engine, as a source, is difficult to modify, since the engine is usually offered to the airframe manufacturers as a unit. If one could view exhaust muffling as "source reduction," the present study would indicate that use of an improved muffler would produce a substantial benefit in the cabin noise level. We did not do a detailed survey of the sources of casing-radiated noise in the engine compartment, but in doing such a survey, one might expect to find "acoustic hot spots" which could be modified to reduce the overall level of noise in that area (vibrating valve covers, oil lines, etc). However, such an effort should only be undertaken if it has been clearly established that the engine casing noise is contributing to noise in the cabin

environment in a given frequency range. Finally, it is not clear how one could easily reduce the vibrational energy of the engine, except perhaps at the rotational rate and first few harmonics. However, as is discussed in detail in Appendix H, there is a great deal that can and should be done to improve the dynamic characteristics of the system comprised of the engine, its mounts, its suspension, and the airframe to which it is attached.

Airflow-generated noise can, in principle, be reduced at the source when the true source is separated flow (such as around a wheel cavity, external mirror or other protuberance, and at the aft end of the cabin). Localized aerodynamic "cleanup" may be fruitful in terms of reducing interior noise levels (depending on the aircraft and the location and details of the local flow separation) and can always be tolerated (and welcomed) from a performance standpoint.

3.2.2 Path treatment

General Approaches

Path treatments can be classified either as major structural changes or as "add-on" devices. A major structural change could take the form of a very stiff or very flexible tail cone, a re-supporting of the engine/propeller combination, or replacing a section of the aircraft with an alternate material (composite). Such major structural changes can be most effective in certain instances, but are usually ruled out as retrofit possibilities due to the cost of re-tooling and re-certification. The second category of path treatments, the use of "add-ons," is most often turned to in both light and large transport aircraft - use of "add-ons." Such treatments may involve local stiffening or thickening of structural elements, use of double wall structures, application of damping, increasing absorption, and use of vibration isolators (passive or active).

Application to Test Aircraft

Fuselage Treatments for Reducing Transmission of Airborne Sound - "Sidewall Treatments": In the identification, analysis, and optimization of potential concepts for high acoustic performance "sidewalls" (on other parts of the aircraft), it is vital at the outset to classify the mechanism(s) which causes the high transmission loss. If one wishes to obtain high sound transmission loss, one must select panel configurations where the sound wave incident on the source side of the panel produces the lowest possible compression of fluid at the cabin side. Low compression of the cabin-side fluid is obtained by:

(1) low vibration response of the inside face of the panel;

(2) low radiation efficiency of the inside face of the panel achieved through novel design;

(3) a combination of measures 1 and 2.

Low vibration response of the inside face of the "panel" can be obtained by:

- designing the "panel" so that it has poor coupling to the outside sound field;
- avoiding resonant buildup of the structural response by making the panel response stiffness-controlled or, if this is not possible, by providing sufficient damping to minimize resonant response of the structure;
- decoupling the motion of the inside surface from the outside surface (double-wall concept).

Low radiation efficiency of the inside face of the panel may be achievable through novel design measures which are highly effective in selected narrow frequency regions and work for both the forced and resonant motion of the panel, or by conventional measures (such as providing for low bending stiffness) which are

effective only for the resonant motion of the panel and do not affect the manner in which sound is radiated by the forced motion. In all cases, the end result must be the smallest possible motion of interior panels and frame covers, and/or the lowest radiation efficiency possible. In principle, reduction of sound transmission through a sidewall structure may be achieved by:

- mass effects
- stiffness effects
- damping of resonant structural modes or dissipation of acoustic waves
- impedance mismatching
- mode conversion.

The first three concepts are well understood, taken by themselves, or in straightforward combinations. Recent studies of sidewall sound transmission [3,4] into high speed propeller-driven aircraft have explored the reduction of sound transmission in traditional skin-stringer constructions using a variety of single- and double-wall constructions. Conceptual approaches to achieving impedance mismatching or mode conversion include:

(1) "Tuning" of the skin-stringer structure to couple (or decouple), optimally, the modes of the exterior skin panels and the supporting stringers, while damping the modes into which the energy has been "redistributed" [5];

(2) Use of tuned acoustic elements in the airspace between the skin and trim panel, which drastically change the impedance in the "transmission line";

(3) Use of alternate gasses in the space between skin and trim panels, again to change the impedance drastically;

(4) Use of special constructions in the airspace, such as very stiff and damped or very limp elements, which may be viewed as a "triple wall" construction;

(5) Use of dynamic absorbers on either the skin, stringers, frames or trim panels. These absorbers could include traditional spring-mass concepts, or novel concepts such as those described below;

(6) Use of a trim panel system with dynamic properties which result in poor coupling to the air gap and to the structureborne vibration at its supports.

Some of these concepts cannot be realistically considered for general use on single engine light aircraft - i.e., conceptual approach 3 above, but could be employed on modular elements (such as windows), or on larger twin-engine aircraft. Specific lightweight schemes embodying these basic concepts need to be identified and analyzed for their applicability to realistic general aviation aircraft. Ultimately, some combination of traditional and novel approaches may be necessary to achieve the high transmission loss (and thermal insulation) required to achieve comfortable cabin environments in advanced propeller-driven aircraft of all types.

For propeller-driven light aircraft, those concepts which are applicable in realistic acoustic/structural environments will need to provide substantial noise reduction at low frequencies (60-200 Hz), where excitation wavelengths are much larger than typical stringer and frame spacing, where the structure is sufficiently compliant to complicate the use of tuned structure or tuned panel concepts, and where the frame can be a significant radiator on the interior, thus requiring good isolation of the interior trim panels. Concepts that provide the necessary transmission loss at low frequencies may be ineffective at higher

frequencies, and therefore may need to be augmented with concepts which perform best in the higher end of the frequency range of interest.

Implementation of any concept on pressurized aircraft must be compatible with the requirement for pressurization, which produces significant stiffening of the skin and frame structure, and which could be deleterious to the performance of alternate gasses that might be placed in flexible containers in the space between the skin and interior trim panels.

The theory and experience base for use of simple applications of mass stiffness and damping is well documented, e.g., Ref. 6, and will not be discussed here in general terms. However, some of the more promising new concepts applicable to light aircraft are not as well documented and warrant further discussion. Most of the relevant effort is summarized in ongoing work related to the advanced high speed propeller-driven transport aircraft ("Propfan") which will require substantial noise reduction of discrete frequency propeller noise at low frequencies.

Double-Wall Structures

Analytical noise control studies [2,3,4,7] for propfan aircraft have relied mainly on fairly conventional approaches in terms of add-on materials. These materials involve the design of the sidewall treatment which is located between the fuselage skin and the cabin interior. Essentially, these treatments consist of a double-wall system in which the outer wall is formed by the fuselage skin and the inner wall by the cabin trim panel. In between, the space is filled by porous acoustic insulation material, with or without an airgap. Two sidewall treatments proposed for propfan aircraft [2,3,4] are shown schematically in Fig. 11. The improvement relative to a single wall structure is illustrated generically in Fig. 12.

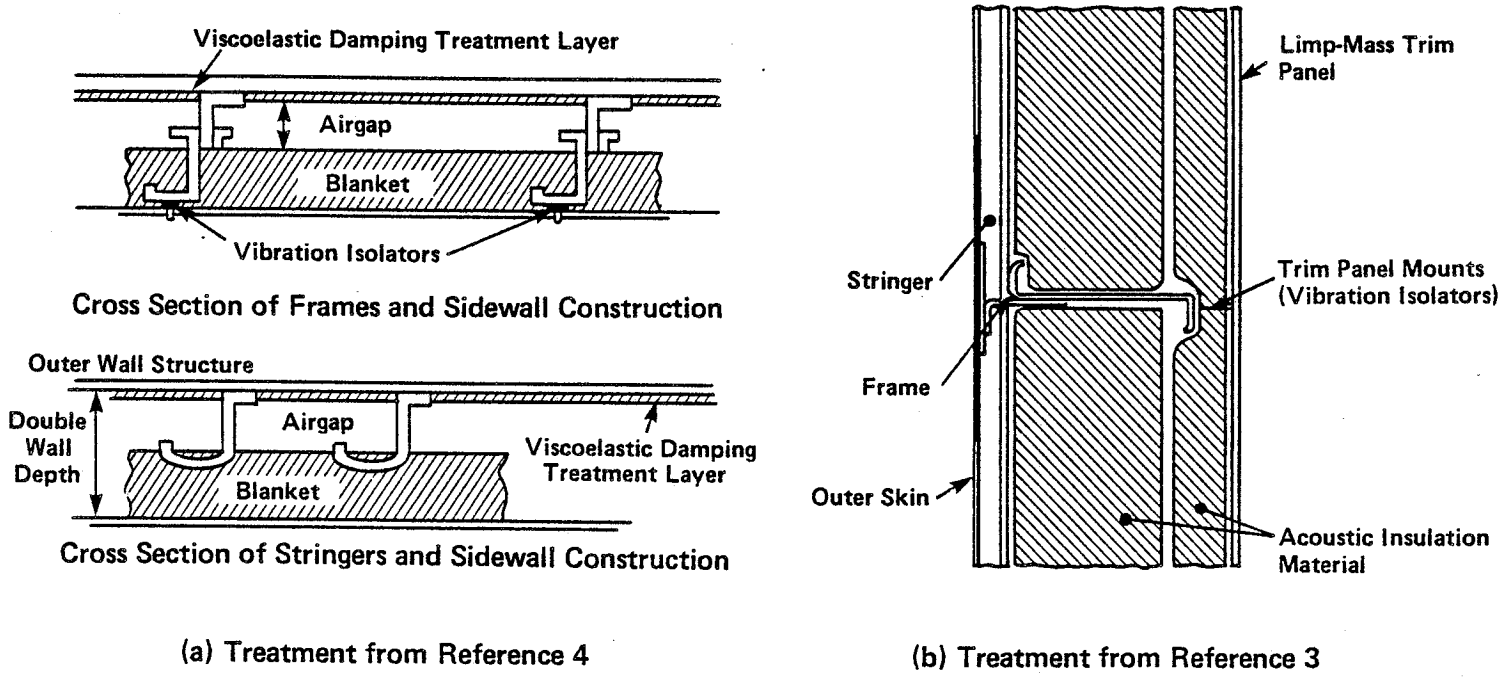

(a) Treatment from Reference 4

(b) Treatment from Reference 3

FIGURE 11. SIDEWALL TREATMENTS PROPOSED FOR PROPFAN AIRPLANES

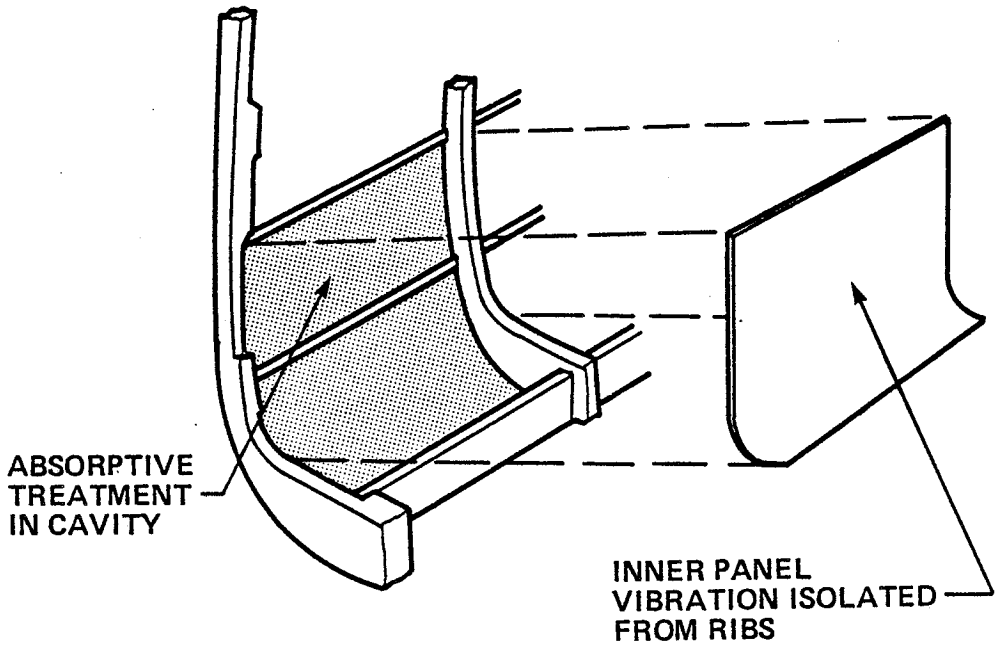

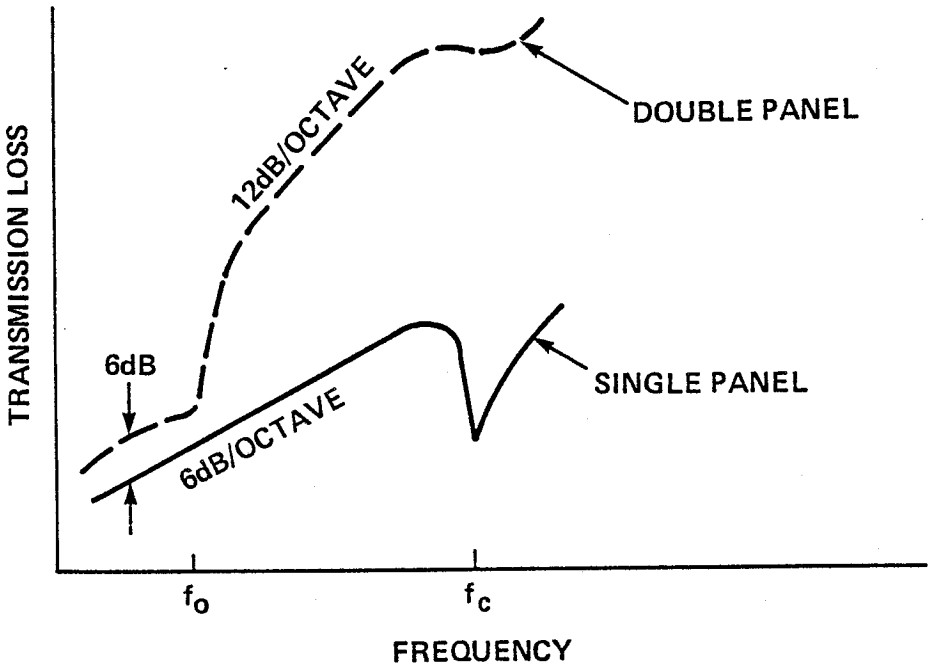

FIGURE 12. SCHEMATIC ILLUSTRATION OF DOUBLE WALL STRUCTURE AND IDEALIZED PERFORMANCE RELATIVE TO SINGLE WALL STRUCTURE.

Two characteristics of the treatments should be noted. First, the cabin trim is assumed to be limp rather than stiff, as is the case in current designs. The requirement that the trim be "limp" is made in order to satisfy assumptions that the trim be locally reacting, and that it responds according to the mass-law dependency. Secondly, the trim is mechanically isolated from the fuselage structure. This is particularly important because, at frequencies associated with the first and second harmonics of the blade passage frequency, vibration levels of the frame and stringers are similar in magnitude to those of the skin panels [1].

It can be observed in Fig. 11(a) that a viscoelastic damping treatment layer is added to the fuselage skin panel. This treatment provides mass and damping to the skin panels, although tests on turbofan aircraft [8] indicate that the damping effect is negligible below the fundamental frequency of the panel - typically about 500 Hz. Damping augmentation is possible at low frequencies only if the vibrational energy in the stringers and frames can be dissipated - this is a much more difficult task than simply applying damping material to skin panels.

The sidewall treatment proposed in [7] is somewhat different from those of [2,3,4] in that the trim panel is constructed from stiff honeycomb material. Such materials are usually found to have poor transmission loss characteristics. However, the acoustic performance in the sidewall proposed in [1] is improved by adding mass to the trim panel. A second difference between the sidewall proposed in [7] and in [3,4] lies in the choice of primary structure. Rather than using skin panels of constant thickness, the structure [7] utilized "isogrid" panels which consist of integrally stiffened plates having a triangular grid of rib stiffeners. These panels are based on applications to advanced spacecraft designs. The advantage claimed for the isogrid structures is that of increased noise transmission loss

at low and mid frequencies. The claim is based, in part, on transmission loss measurements on sample flat panels exposed to broadband reverberant excitation. The actual response of curved structures exposed to discrete frequency acoustic excitation incident within a narrow range of angles may be somewhat different.

The noise reduction potential of the basic skin-stringer fuselage structure is still open to discussion, but exploratory analyses [3,4] have so far failed to identify any large benefits. However, the analyses have been rather limited and have not sought structures with frequency characteristics that can be tuned to specific excitation frequencies. The analyses do suggest that the structural modal densities are quite high, even at the blade passage frequency, so that it will be difficult to design skin-stringer structures that have no resonance in certain specified frequency bands associated with harmonics of the blade passage frequency.

The ongoing Propfan studies have shown that structural design changes, when applied in conjunction with conventional add-on acoustic materials, may result in sidewall treatments that are optimized for minimum weight penalty.

Tuned Structures

The notion of tuning a structure so that its response will be optimally mismatched to the excitation is not new. However, the intrinsic problem with tuned structures of this type is their poor performance at frequencies other than one or two tuning frequencies. Such systems are difficult to apply to systems with high modal densities, such as may exist in the sidewall of a typical general aviation aircraft.

A different type of tuned structure has been proposed by Sen Gupta [5]. The "intrinsically tuned structure" attempts to match the resonant frequency of a skin panel with the corresponding

resonance of its stringer supports; damping is applied to the stringer flange. Calculations show that the response of the panel at its fundamental resonance disappears and is replaced by modes above and below the resonance, which can be damped at the stringer flanges. This concept is only applicable in the frequency range above that where frame motion is important and below the point where the modal density of the panel becomes high. Therefore, it is probably not applicable to reducing the first and second harmonics of typical propeller blade passing frequencies, unless it can be applied to the more difficult problem of modifying frame response. This concept may also be incompatible with variations in pressurization which affect the panel frequencies differently than those of the stringer.

Use of Composite and Honeycomb Elements for Skin or Trim Panels: Lightweight, stiff, honeycomb-backed composite panels seem appealing as structures for reducing low frequency sound transmission because of the high stiffness-to-weight ratios which can be achieved using them. However, experience to date has revealed that stiff lightweight structures are good sound transmitters at low frequency as a result of this low critical frequency. Honeycomb simply bonded to an isotropic panel does not effectively stiffen the panel at low frequencies, but instead acts only like additional mass. Some studies have been done to quantify the possible effects of conventional honeycomb on typical transport structures [9] and have shown unimpressive results.

Dym [11] and Herron [10] have shown that one has to select honeycomb cores which are either very stiff, or very soft, to develop extraordinary transmission loss.

Therefore, investigation of the use of composite panels with or without honeycomb should focus on unique possibilities associated with the inherent anisotropy which can be developed, or

should focus on airframe integration schemes which take advantage of the high stiffnesses possible when the composite panel is applied over a span equivalent to many stringer or frame spacings, either by replacing some of the airframe structure with equivalently stiff integrated structure, or by somehow carrying the stiff skin across several frames.

Dynamic Absorbers

Broadband "waveguide" dynamic absorbers: Classical dynamic absorbers or "tuned dampers" have been studied and applied extensively [12,13]. Aircraft such as the DC-9 and Gulfstream Aerospace Commander use dynamic absorbers to reduce structure-borne and airborne sound transmission. It is well-known that the addition of such absorbers to a structural system can alter its dynamic and sound-transmission characteristics significantly, particularly at frequencies in the vicinity of the absorber's resonance. For other frequencies, however, the use of classical absorbers may be detrimental because they may produce a resonant response of a higher mode.

Thus, a classical absorber intended for noise reduction in propeller aircraft would need to be tuned to the fundamental blade passage frequency or a harmonic of it and would need to be relatively highly damped to accomodate changes in this frequency within its bandwidth, and would also need to be reasonably unaffected by changes in temperature, pressure, aircraft altitude, and other environmental factors. As was previously indicated, a typical light aircraft's sidewall response (and attendant sound radiation) shows that in the frequency range where the prop frequencies would exist, frames and panels respond more-or-less equally, while at higher frequencies the panel motion is dominant. Therefore, different absorbers or groups of absorbers would need to be used for each significant harmonic of the blade passage frequency, resulting in considerable complexity and increase in weight.

Absorbers with distributed masses and stiffnesses e.g., absorbers consisting of elastic beams, plates or rings, have also been investigated to some extent [15, 16]. They suffer much the same limitations as classical absorbers, although distributed absorbers can, at least in theory, suppress vibrations in several frequency bands. (See App. H for a discussion of application of these to this test aircraft.)

In contrast to the aforementioned absorbers, which depend on resonant response of a dynamic system, so-called "waveguide absorbers" depend on non-resonant wave propagation for the extraction of vibratory energy from the structure to which they are attached [17].

The principle of this novel waveguide absorber concept can be illustrated (and also realized practically) in terms of a tapered bar (Fig. 13). The wider, larger end of the bar (shown cross-sectionally) is attached to the structure whose vibrations are to be reduced, and the bar's narrower end is provided with a damping arrangement, such as a viscoelastic coating. This bar acts somewhat like a reversed acoustic horn: as the structure vibrates, it causes compressional waves to propagate along the rod; the amplitude of the waves increases as the rod narrows, and the greater motions in the narrow region facilitate the absorption of energy by the damping arrangement. The waveguide absorber thus removes energy from the vibrating structure at all frequencies at which it can support waves; below a certain cutoff frequency it cannot do this and acts essentially like a lumped mass [17].

The previous discussion described the waveguide absorber principle of action in terms of compressional waves. However, the same idea applies also to torsional, flexural, and combined wave systems. In fact, an absorber consisting of a tapered rod that has been twisted about its axis coiled into a tapered helix and potted in high-damping plastic, has been found to provide

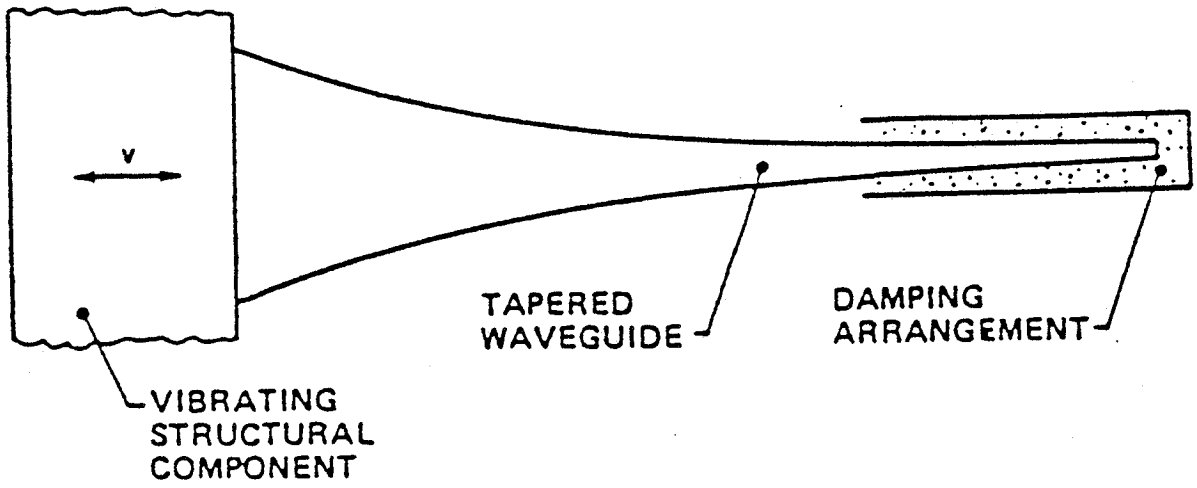

FIGURE 13. WAVEGUIDE ABSORBER.

effective broadband damping by virtue of the many different wave types it can propagate. Some other realizations of such absorbers are described in [14], along with experimental results obtained on several such absorbers.

Application to Test Aircraft

The theory for dynamic absorbers is well-developed for use on relatively simple or clearcut applications, but may be difficult to apply in a complex, interconnected structure such as the test aircraft used in this study. The key to selecting treatments for a complex noise generating and transmitting structure such as a single- engine light aircraft is to ensure that the diagnosis is so complete and thorough that the selection and application of treatments will become clearcut.

3.2.3 Candidate treatments for test aircraft

In Table 1, we list some candidate treatments for each of the major source/path combinations identified in this study.

The parametric relationships for each class of these treatments are developed in Apps. C through H. Some pertinent variables are summarized in Table 2 for each category.

TABLE 1

CANDIDATE TREATMENT CONCEPTS

Source/Path Combination	Generic Treatment Concept
Propeller Airborne	• thicker windows • double windows • stiffer firewall to move resonance frequency away from propeller blade passing frequency • heavier firewall or double firewall • heavier inner trim panel in cabin roof • double wall structure on roof • heavier rear bulkhead • absorption in vent ducts • increase in cabin absorption • better door & window seals
Engine Casing, Intake, Exhaust Shell Radiation	• same as Propeller Airborne (above) • absorption in engine compartment
Exhaust Outlet Airborne	• same as Propeller Airborne (above) • improved muffler

TABLE 1 (cont'd)

Source/Path Combination	Generic Treatment Concept
Engine/Propeller Structureborne	• improved engine mounts • 2-stage engine mounts • stiffen engine support structure • cabin panel damping • cabin absorption
Landing Gear Cavity Aerodynamic Excitation	• increased TL of cavity walls by increased thickness or double-wall structure • absorption in floor cavity • double barrier
Turbulent Boundary Layer Propeller Wake	• damping of cabin walls, engine cowling, tail cone, wing panels, wing strut • panel stiffening to reduce modal density, e.g., honeycomb panels • absorption in tail cone • improve TL of rear bulkhead • reinforce cabin and wing where struts attach

TABLE 2. TYPICAL PERFORMANCE OF GENERIC TREATMENT CONCEPTS APPLIED TO TEST AIRCRAFT

1) Increased Skin or Window Thickness

A) Reduction of noise caused by hydrodynamically-generated skin vibration: $NR_H = 30 \log (t_{after}/t_{before})$

B) Reduction of noise caused by acoustically-generated skin vibration: $NR_H = 20 \log (t_{after}/t_{before})$

C) For each doubling of thickness:
"Hydrodynamic" Noise Reduction = 9 dB
"Acoustic" Noise Reduction = 6 dB

D) Approximate weight penalty for doubling thickness of skin and windows: { 11 kg (windows)
28 kg (cabin)

2) Damping (Aluminum tape, aluminum tape foam backed or viscoelastic layer)

A) Reduction of noise caused by hydrodynamic and/or structureborne excited vibration:
$NR = 10 \log (\eta_{after}/\eta_{before})$, where
[η = loss factor]

B) Reduction of Noise Caused by Acoustic Excitation:
NR = negligible

C) Typical Weight Penalty for general application of 8 mm thick viscoelastic layer: ~ 13.6 kg (tail cone), ~ 13.6 kg (cabin)

TABLE 2 (cont'd)

3) Two-Stage Isolators (working into high impedance foundation)

A) Noise reduction (above resonant frequency) = 40 log f (note, degradation occurs in some frequencies below $\sqrt{\frac{2k}{m}}$)

B) Weight penalty = 2 kg/mount

4) Double-Wall Structures (properly isolated from stringers and frames)

A) Noise reduction

1) at double wall resonant frequency f_{dw} (assuming wall filled with appropriate absorption): up to 11 dB

2) above f_{dw}: NR $\approx$ (40-60) log f/f_{dw}

3) below f_{dw}: NR $\propto$ (20-30) log f_{dw}/f

B) Weight Penalty (relative to NO treatment)

Approx: 3-8 kg/m^2

(typical area: roof - 1.5m^2
sidewalls - 3m^2 each
firewall - 1m^2
cabin total $\approx$ 8.5m^2 $\rightarrow$ 30-70 kg)

Note: Deduct normal trim weight to get net weight penalty.

3.3 Summary of Specific Concepts Evaluated on this Aircraft

As previously mentioned, all candidate path treatments could not be evaluated through use of prototype hardware, due to the limitations on program resources and the extensive effort required to complete the diagnosis and investigation of treatments for the structureborne noise. The priority for treatment testing was given to those areas which had been subjected, in the course of this study, to unusually complicated analysis or testing and/or which represented a previously-unexplored source/path combination. It was felt that, in particular, certain sidewall treatment concepts are documented sufficiently to allow their correct application, once a proper diagnosis has provided unambiguous definition of the noise reduction required through a particular path [2,6].

The treatments actually tested were designed to be placed as close to the source as possible, thus "breaking" the transmission path before the energy associated with a particular source/path combination became distributed throughout the aircraft structure. The treatments included those shown in Table 3. The treatments described in Table 3 are discussed in detail in Apps. C through H, along with analyses of the predicted effectiveness of other, more standard, types of path treatments. Of the additional concepts studied analytically, the most promising is the use of double-wall structures. A properly-designed double-wall can provide reductions of airborne sound in excess of 10 dB at all frequencies, thus in and of itself nearly meeting the illustrative noise reduction goal set forth in Sec. 2.1 and 3.1 for those source/path combinations which involve acoustic transmission through the fuselage structure.

TABLE 3: TREATMENT SUMMARY

	Treatment Evaluated	Source/Path Treated	Results and Comments
1)	Firewall stiffening through use of discrete stiffeners	Engine/propeller airborne through engine compartment and firewall	8 dB improvement in critical 80 Hz band; degradation in 63 Hz band not critical unless degradation extends too far toward 80 Hz.
2)	Two-stage isolators	Engine/propeller structureborne	Actual test results on prototype were erratic and not encouraging due to erroneous design information; diagnosis revealed strong variations in mechanical admittance of support structure and elastomer properties different than quoted by manufacturer. Revised design not tested, but good high frequency performance should be possible
3)	Stiffened engine support structure	Engine/propeller structureborne	"Quick look" test of generic approach showed dB improvements; general trend warrants detailed study by manufacturers
4)	Wheel well covers	Airflow/wheel well	10 dBA reduction; evaluation was done to take advantage of unusual setup; full airflow simulation including propwash may change results

4. SUMMARY AND CONCLUSIONS

This report describes a laboratory study of a single-engine aircraft in which a detailed diagnosis of interior noise sources and paths was carried out. Preliminary designs for several treatment concepts were undertaken and several prototype treatments were evaluated on a partial fuselage being used as a test bed. Further flight testing and treatment evaluations are recommended.

The primary diagnostic approach taken was the use of the transfer function technique in which the path between a given source and the cabin is characterized in terms of its conversion (transfer) of the excitation energy into interior acoustic pressures. Once each path is characterized, source characteristics associated with the flight condition of interest are calculated or measured, from which the contribution of each source/path combination to the total cabin acoustic environment can then be calculated. This technique further allows for explicit specification of the frequency spectrum of the reduction in transmitted energy required for each path. Such a specification serves as a guide to the selection of concepts for noise reduction and for evaluating performance of particular designs. As a practical matter, the diagnosis of a particular aircraft usually requires several iterations, with primary source/path combinations being treated first to allow secondary paths or secondary source/path combinations to be quantified.

In the tests and analyses performed on the particular single engine aircraft, a large number of source/path combinations were contributing more or less equally to the cabin A-weighted level. Through the use of the transfer function technique, several instances were found where the excitation frequency corresponded with a path resonance or minimum in the path loss spectrum; such findings provide opportunities to gain significant noise reduc-

tion at a particular frequency by relatively minor adjustments in the path characteristics. The primary source/path combinations which were discovered on the particular aircraft tested were:

- propeller airborne sound transmitted via the roof, firewall, and windshield;
- propeller/engine structureborne vibration transmitted via the engine mount structure and firewall attachment points;
- exhaust noise transmitted through the skin near the exhaust opening (and also through the engine compartment/firewall path);
- airflow-induced noise transmitted via wheel wells, and through other parts of the fuselage (not localized in the study).

These results are probably typical of other aircraft with similar characteristics.

Treatments for these key source/path combinations were investigated in general terms and also in specific conceptual design studies. Propeller airborne sound can be reduced to the (sample) cabin noise goal through use of roof, firewall, and windshield stiffening and through use of double-wall constructions near the roof and on the firewall. Other treatments are possible but do not provide an efficient use of weight.

Structureborne sound arising from the engine propeller combination proved to be the most difficult to control due to the complex dynamic characteristics of the entire mounting system, the nonuniform distribution of mean and dynamic forces in the system, the apparent nonlinear behavior of standard engine isolation mounts, and the variability of loading (vibration) with flight conditions. We believe that a substantial redesign of the

engine mounting system (including firewall attachment details) would be required to achieve a weight-efficient means of controlling this source. Airflow contributions to the cabin environment appear to be surprisingly high.

A novel experiment revealed that separated flow over the wheel wells may be responsible for some of the broadband levels; in such a case, an aerodynamic cleanup would solve the problem, as would a more robust structure between the cavities and the cabin. Other sources of airflow-induced noise were not isolated in sufficient detail to enable treatment design. However, it is noted that double-wall structures designed to reduce transmission of airborne sound would also provide control of airflow-generated sound radiating from the aircraft skin, provided that essential precautions in the design of the interior panel were taken.

The work we have described does not take one all the way from the point of an undiagnosed aircraft to the point of proven and optimized noise control designs. However, the extent to which flight and ground tests may (and must) be used in concert to arrive at a meaningful diagnosis has been demonstrated. We believe that the noise control measures identified, if carried forward by a usual design evolution process, would provide 10-12 dBA and 10-12 dB SIL reductions of noise in the cabin of the test aircraft. Thus, this report may serve its readers as a guide, but not as a catalog of proven guaranteed solutions. Indeed, if this program, in both its phases, has demonstrated anything as a certainty, it is that <u>each aircraft has unique characteristics which must be fully understood before efficient noise control measures can be applied</u>.

References

1. Hayden, R.E., B.S. Murray and M.A. Theobald, "A Study of Interior Noise Levels, Noise Sources and Transmission Paths in Light Aircraft," NASA CR-172152, July 1983.

2. Wilby, J.F., "The Prediction of Interior Noise of Propeller-Driven Aircraft: A Review," SAE Technical Paper 830737, 1983.

3. Rennison, D.C., et al, "Interior Noise Control Prediction Study for High-Speed, Propeller-Driven Aircraft," NASA CR-159200, 1979.

4. Revell, J.D., et al, "Analytical Study of Interior Noise Control by Fuselage Design Techniques on High-Speed, Propeller-Driven Aircraft," NASA CR-159222, 1980.

5. Sen Gupta, G., "Low Frequency Cabin Noise Reduction Based on the Intrinsic Structural Tuning Concept," NASA CR-145262, 1978.

6. Beranek, L.L., Noise Reduction, McGraw-Hill, 1971.

7. Goldsmith, I.M., "A Study to Define the Research and Technology Requirements for Advanced Turbo/Propfan Transport Aircraft," NASA CR-166138, 1981.

8. Bhat, W.V. and J.F. Wilby, "Interior Noise Radiated by an Airplane Fuselage Subjected to Turbulent Boundary Layer Excitation and Evaluation of Noise Reduction Treatments," J. Sound and Vibration, 18, 4, 449-464, 1971.

9. Wilby, J.F., and J.I. Smullen, "Interior Noise of STOL Aircraft and Helicopters," J. Noise Control Engineering, Vol 12, No. 3, 1978.

10. Dym, C.L., "Optimal Acoustic Design of Sandwich Panels," JASA, 1978.

11. Heron, K.H., "Acoustic Radiation from Honeycomb Sandwich Plates," Symposium on Interior Noise in Helicopters, University of Southampton, England, 1979.

12. Reed, F.E., "Dynamic Vibration Absorbers and Auxiliary Mass Dampers," Chapter 6 of Shock and Vibration Handbook, 2nd Edition, Ed. by C.M. Harris and C.E. Crede, McGraw-Hill Book Co., Inc., New York, 1976.

13. Den Hartog, J.P. Mechanical Vibration, McGraw-Hill Book Co., Inc., New York, 4th Edition, 1956.

14. Snowdon, J.C., Vibration and Shock in Damped Mechanical Systems, John Wiley & Sons, Inc., New York, 1968.

15. Snowdon, J.C., "Platelike Dynamic Vibration Absorbers," J. Engineering for Industry (Trans. ASME) pp. 88-93, 1975.

16. Nobile, M.A., and J.C. Snowdon, "Viscously Damped Absorbers of Novel Design," J. Acoust. Soc. Am., 61, 5 pp. 1198-1208, 1977.

17. Ungar, E.E., and L.G. Kurzweil, "Preliminary Evaluation of Waveguide Absorbers," AFWAL-TR-83-3125, 1984.

APPENDIX A

DESCRIPTION OF THE TEST AIRCRAFT

A. DESCRIPTION OF THE TEST AIRCRAFT

A.1 Overview

The aircraft used for this study was a Cessna R182 single engine utility aircraft (Skylane), which had been selected from those tested in Ref. 1 based upon review of the fleet survey data and discussions with manufacturers, of the following factors:

- Contemporary design (of airframe, propeller, and engine);
- Popularity of type (past sales, and sales trends, as a percent of the total fleet);
- Typicality of noise levels, as deduced from flight test program in Ref. 1;
- Availability of test aircraft for substantial ground and flight testing, and availability of new fuselage for lab tests;
- Possibility of configuration changes on test aircraft or lab test article.

The aircraft, shown in Fig. A.1, is a high-wing, single-engine design with a retractable undercarriage. It is powered by a six-cylinder horizontally-opposed engine and had been tested [1] with both two- and three-blade propellers, and with and without a turbocharger. The maximum takeoff weight was 1400 kg (3100 lb) for both versions. The aircraft had also been tested [1] with three different levels of interior treatment, ranging from none to a standard production interior. For the diagnostic and prototype work, the two-bladed, normally-aspirated, standard production interior configuration was used.

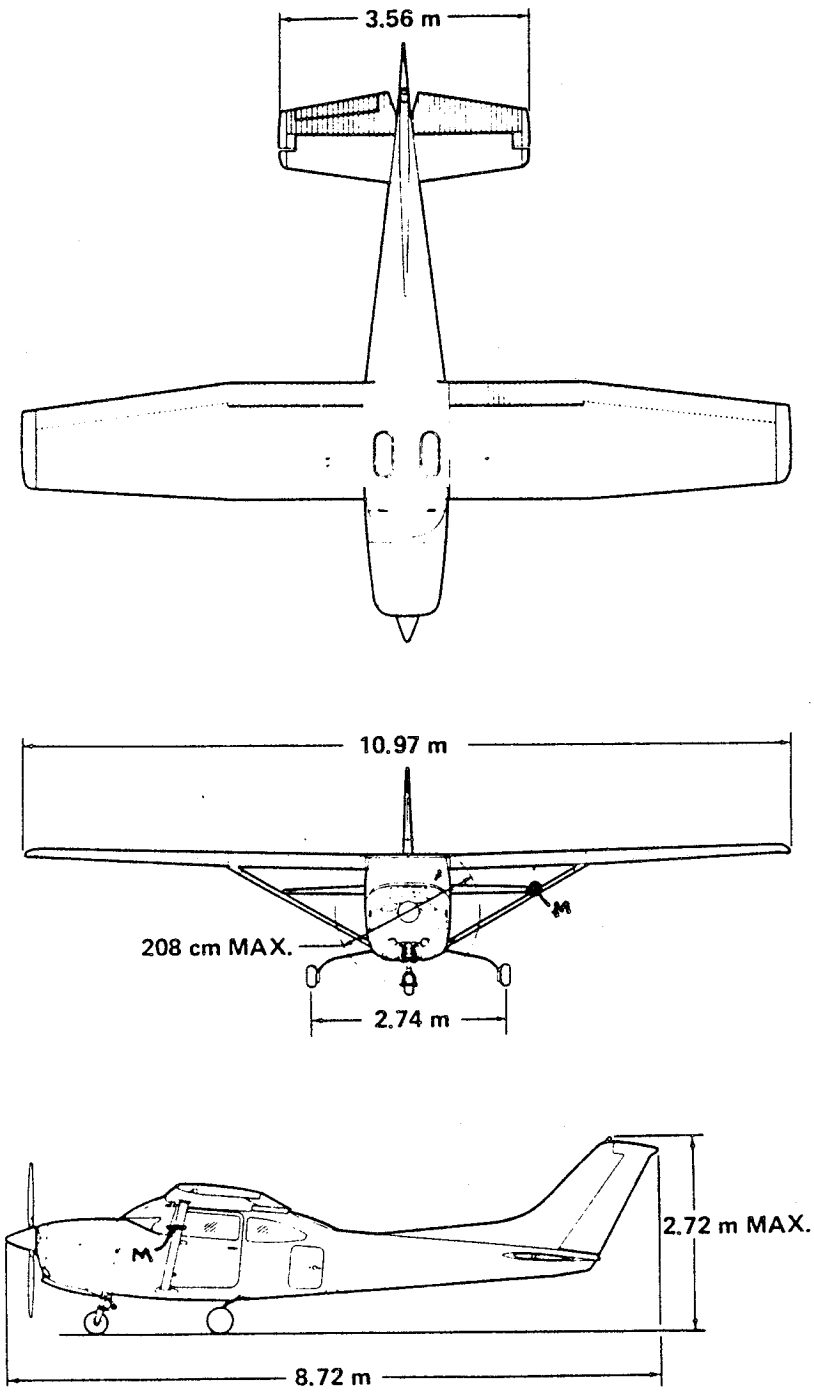

FIGURE A.2 GENERAL ARRANGEMENT OF TEST AIRCRAFT.

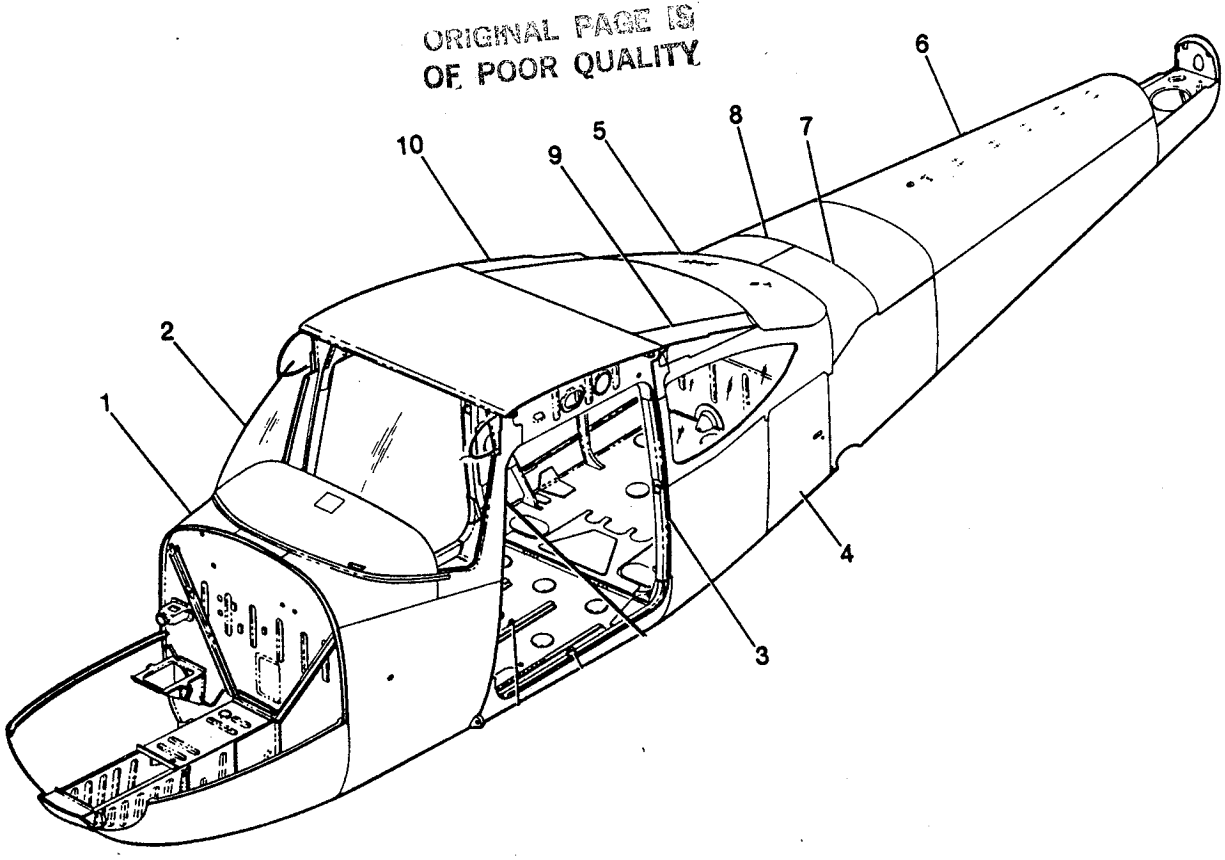

Key	Description
1	Fuselage structure assy - forward
2	Windshield installation
3	Center cabin section assy
4	Baggage door installation
5	Aft cabin windows installation
6	Tailcone assy - fuselage
7	Skin-upper aft LH
	Skin-upper aft LH
8	Skin-upper aft RH
	Skin-upper aft RH
9	Fillet assy - wing to fuselage LH
10	Fillet assy - wing to fuselage RH

FIGURE A.3 FUSELAGE DETAILS.

TABLE FOR FIGURE A.4

Figure and Index No.	Description	Units Per Assy	Usable On Code
4A-	Structure Assy-LH Wing Integral Fuel Cell	1	B
	Structure Assy-LH Wing Integral Fuel Cell	1	C
	Structure Assy-RH Wing Integral Fuel Cell	1	A
- 1	Leading Edge Assy	1	
- 2	Skins & Stringers Installation	1	
- 3	Spar assy	1	
- 4	Fuel Cell Assy-Integral	1	
- 5	Stiffener-LH Wing	1	
- 6	Bracket assy	1	
- 8	Rib-Leading Edge-LH Sta. 100.00	1	
-10	Rib Assy-LH and Doubler Sta. 100.00	1	
-14	Rib Assy-Trailing Edge LH Sta. 100.50	1	
	Rib Assy-Trailing Edge RH Sta. 100.50	1	
	Angle-LH	1	
	Angle-RH	1	
-15, 17,10 20,21	Ribs - Sta. 118.00	1	
-17	Rib - Sta. 136.00	1	
-18	Rib-Trailing Edge Sta. 136.00	1	
-19	Rib Assy-LH - Sta. 154.00	1	
	Rib Assy-RH - Sta. 154.00	1	
-20	Rib - Sta. 172.00	1	
-21	Rib - Sta. 190.00	1	
-22	Rib Assy-LH - Sta. 208.00	1	

A -- R182 & TR182 Serial R18200584 & On
FR182 Serial FR18200020 & On
B -- R182 & TR182 Serial R18200584 Thru R18201628
FR182 Serial FR18200021 Thru FR18200070
C -- R182 & TR182 Serial R18201629 & On

the normal operation is at a constant speed of 2400 rpm on 2100 rpm (economy mode). Typical power requirements and airspeed for this aircraft are plotted as a function of altitude in Fig. A.5. Variations from these typical curves on non-standard days or for other loadings will be expected and are discussed in Ref. A.1.

The nominal wing specific loading of the aircraft is 851 N/m^2 (17.8 psf) and the specific power loading is 6.0 kg/hp (13.2 lb/hp).

Some of the details of the aircraft which directly or indirectly affect the cabin noise are described below. Other details are provided in subsequent appendices in conjunction with discussion of a particular source and path combination.

A.4 Air Induction and Exhaust Systems

The engines air induction system receives ram air through an intake scoop in the upper left hand engine cowling (Fig. A.1). The intake scoop is covered by an air filter which removes dust and other foreign matter from the induction air. Airflow passing through the filter enters an airbox. After passing through the airbox, induction air enters the inlet in the carburetor which is below the engine, and is then ducted to the engine cylinders through intake manifold tubes.

Exhaust gas from each cylinder passes through riser assemblies to a muffler and short tailpipe on each side of the engine (turbocharged versions have only a single tailpipe on the left side of the aircraft). Shrouds are constructed around the outside of the mufflers to form heating chambers. The left muffler supplies heat to the carburetor, and the right muffler supplies heat to the cabin.

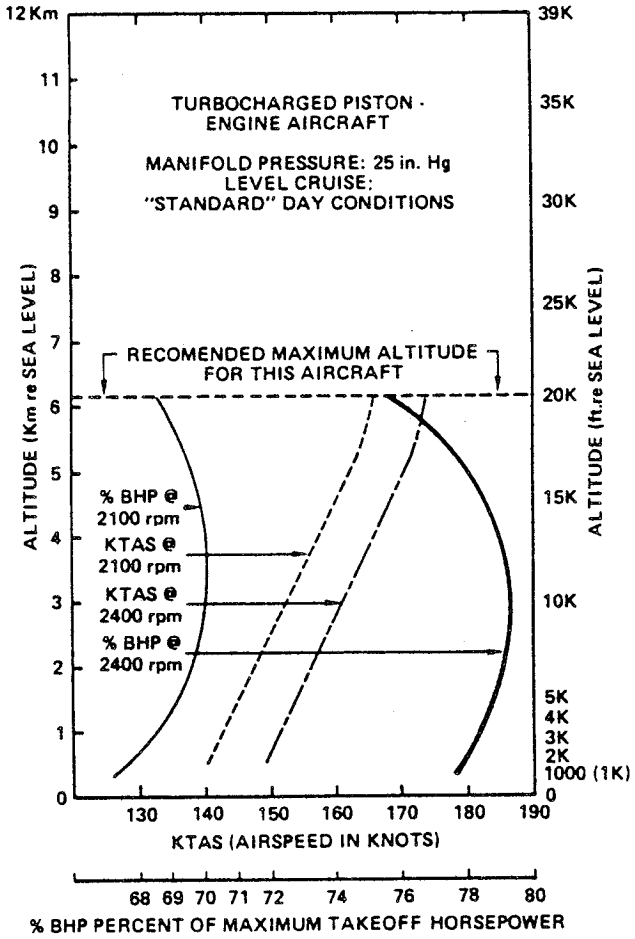

FIGURE A.5 TYPICAL AIRCRAFT PERFORMANCE AT TWO ENGINE SPEEDS AND VARIOUS ALTITUDES.

A.5 Cabin Ventilation Systems

A primary path for engine, propeller, or airflow noise in light aircraft is through ventilation, heating, or air conditioning ducts. Also, elements of these systems often become significant noise sources themselves. Although the systems on the test aircraft were not explicitly studied (vents were blocked and sealed), a description of such systems is provided below for completeness of the aircraft configuration summary.

Figure A.6 shows a schematic layout of the cabin heating and ventilation system (Ref. A.1). Front cabin heat and ventilating air is supplied by outlet holes spaced across a cabin manifold just forward of the pilot's and copilot's feet. Rear cabin heat and air is supplied by two ducts from the manifold, one extending down each side of the cabin to an outlet at the front door post at floor level. Windshield defrost air is also supplied by a duct leading from the cabin manifold to an outlet on top of the antiglare shield. Separate adjustable ventilators supply additional ventilation air to the cabin. One ventilator near each upper corner of the windshield supplies air for the pilot and copilot, and two ventilators are available for the rear cabin area to supply air to the rear seat passengers.

Air conditioning is an option on this aircraft, and, as such, becomes an additional potential noise source and/or path for sound generated by other sources. The air conditioning system provides cooled air to the cabin during hot weather operations, both on the ground and in flight. Cool air is directed through ducts above the headliners to four individually adjustable outlets, one above each seat.

In this system (see Fig. A.7), a belt-driven compressor and a high pressure switch are located on the left front side of the engine, while the evaporator, condensor, blowers and other

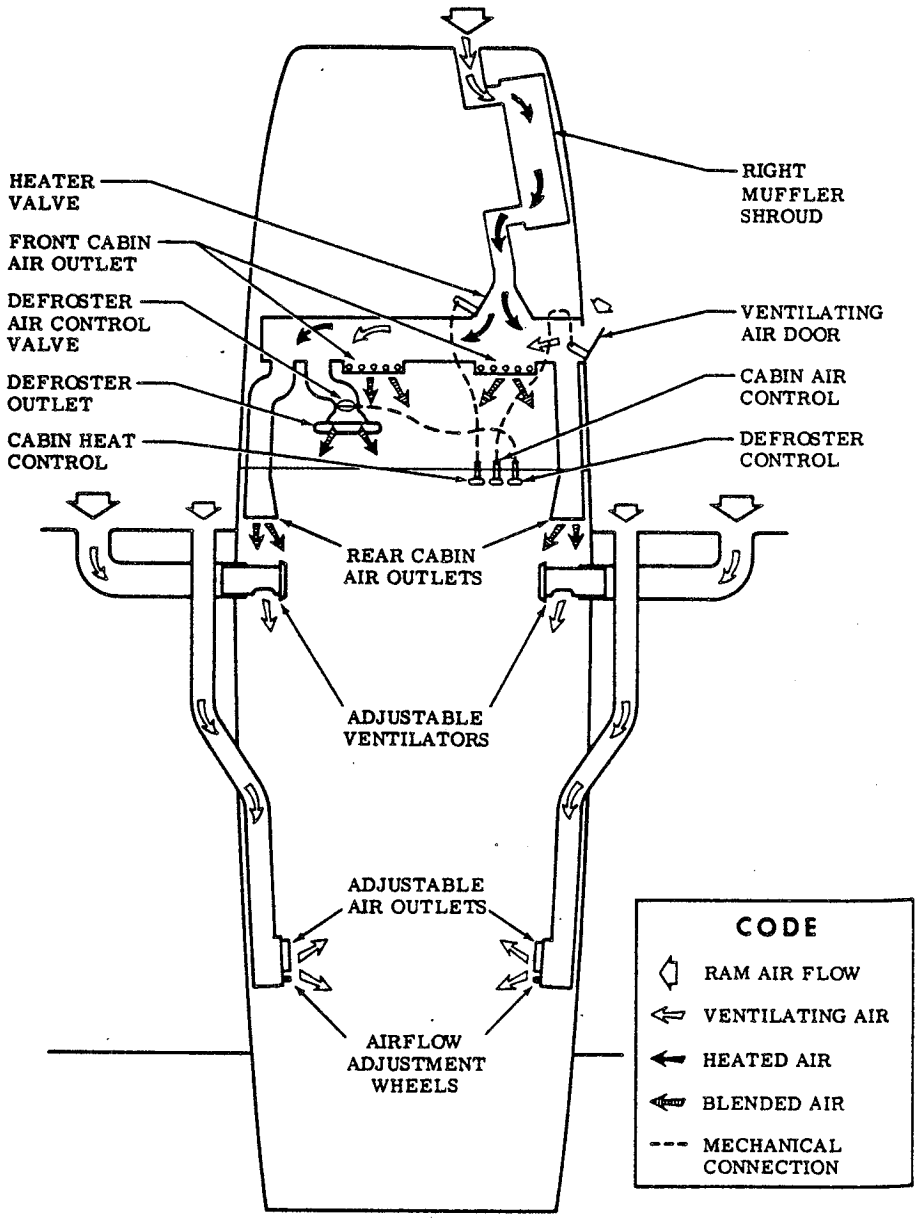

FIGURE A.6 CABIN HEATING, VENTILATING, AND DEFROSTING SYSTEM.

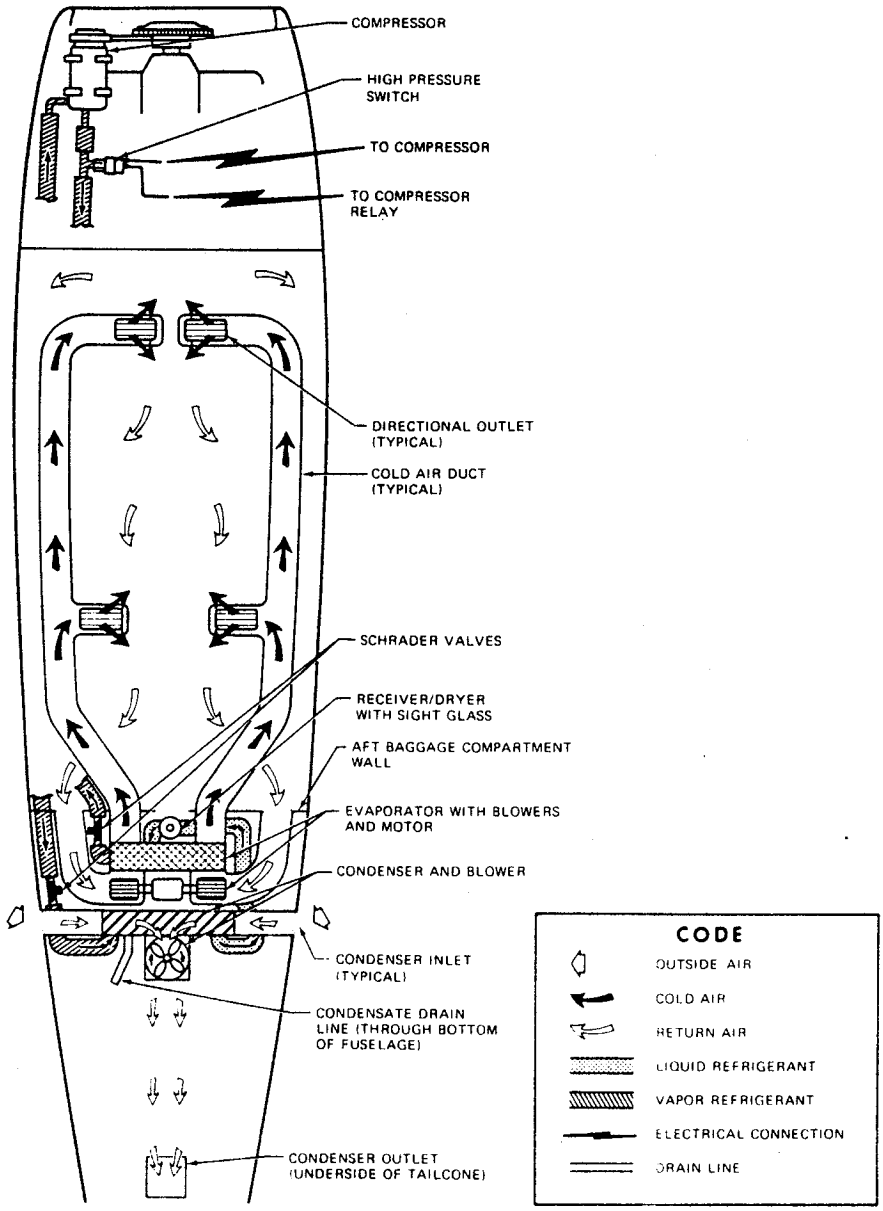

FIGURE A.7 AIR CONDITIONING SYSTEM.

components are combined into an integral unit located above the main landing gear wheel well, aft of the baggage compartment wall.

A.6 Fuselage for Lab Testing

A fuselage section was fabricated by Cessna Aircraft Company for use in laboratory testing of source/path combinations, transmission loss characteristics of different parts of the aircraft, structureborne transmission, airflow-induced pressures and cabin noise, panel damping, and preliminary evaluations of selected candidate treatment concepts. The fuselage section was outfitted with a production interior and included a standard "soundproofing package." No engine, landing gear, wing or wing struts, or empennage were included.

Figures A.8 through A.10 show several views of the fuselage in the test facility, prior to suspension of the fuselage from its wing root attachment points, and prior to complete installation of floor treatment in the semi-anechoic facility.

Figure A.11 and the associated table provide a schematic of the standard soundproofing package. Other more detailed views of the fuselage are contained in the sections which follow.

FIGURE A.8 OVERVIEW OF FUSELAGE IN TEST FACILITY.

FIGURE A.9 VIEWS OF ENGINE COWLING AND MOUNTING SPIDER.

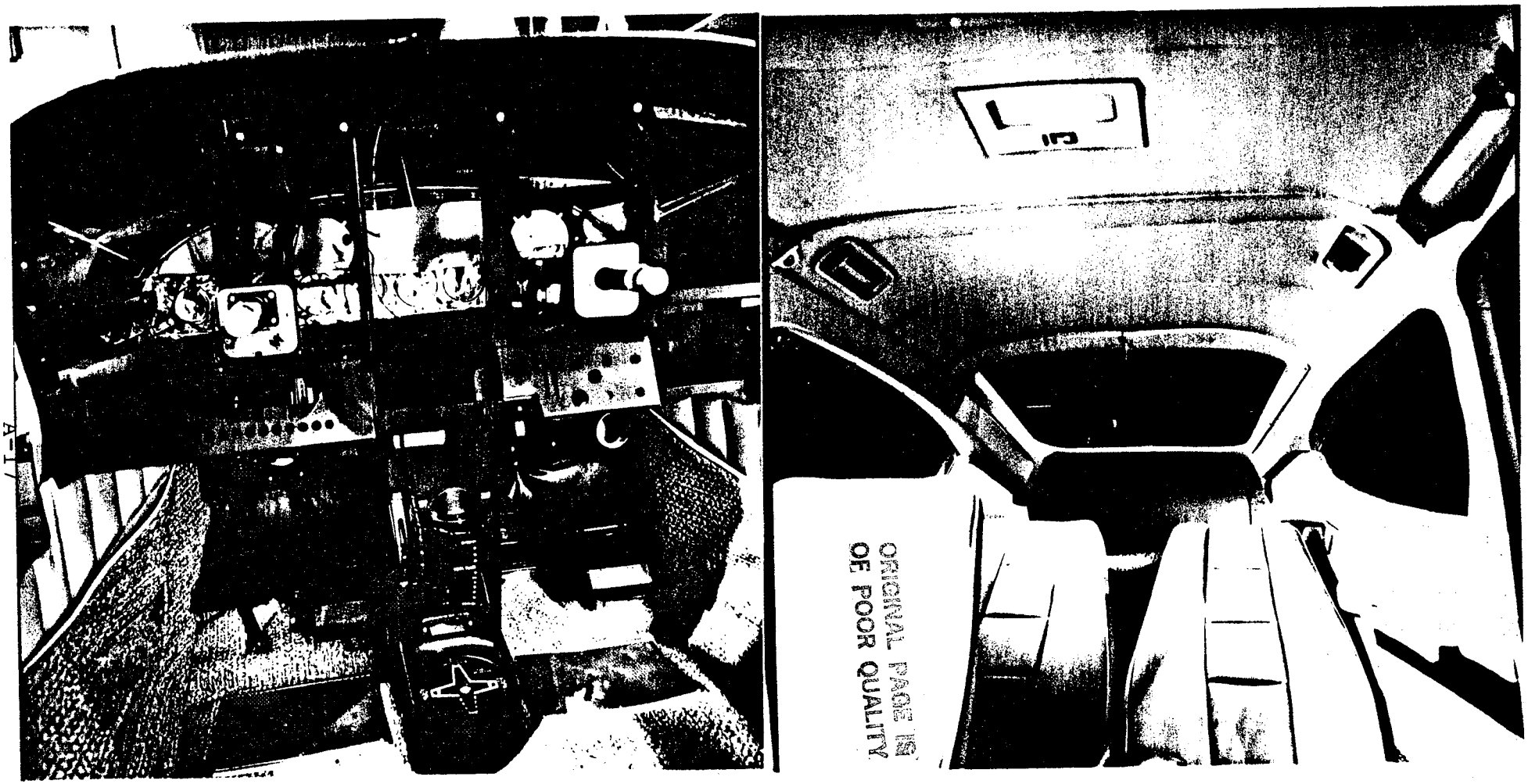

FIGURE A.10 TWO VIEWS OF CABIN INTERIOR.

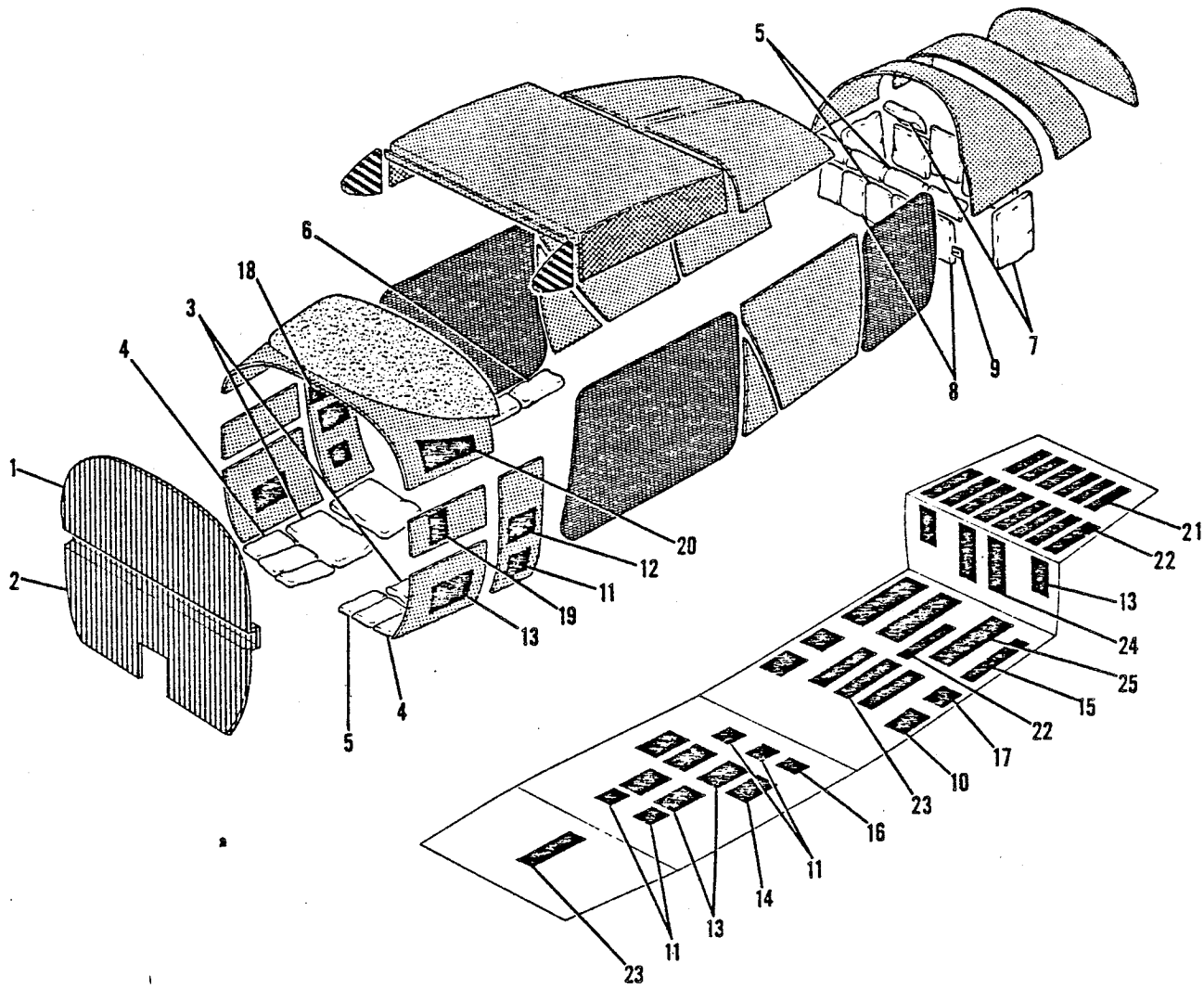

	Typical Thickness
CES 1109 CLASS 1A Soundproofing - Fiberglass (See Parts Listings)	1"
CES 1109 CLASS 1B Soundproofing - Fiberglass (See Parts Listings)	2"
CES 1109 CLASS 1C Soundproofing - Fiberglass (See Parts Listings)	½"
CES 1109 CLASS 1G Soundproofing - Fiberglass (See Parts Listings)	1"
CES 1109 CLASS 1H Soundproofing - Fiberglass (See Parts Listings)	1"
CES 1109 CLASS IV Polymeric Sheet (See Parts Listings)	.035 Damping Material
Embossed Soundfoam (See Parts Listings)	3/4" Sound Foam

FIGURE A.11 STANDARD SOUNDPROOFING PACKAGE.

FIGURE AND INDEX NO.	PART NUMBER	DESCRIPTION 1 2 3 4 5 6 7	UNITS PER ASSY
55 -		SOUNDPROOFING INSTALLATION	NP
- 1	SEE FIG 53	SOUNDPROOFING ASSY-UPPER FIREWALL	1
- 2	SEE FIG 53	SOUNDPROOFING ASSY-LWR FIREWALL	1
- 3	07C0762-4	BAG-SOUNDPROOFING	4
- 4	C7CC762-5	BAG-SOUNDPROOFING	4
- 5	C7C0762-6	BAG-SOUNDPROOFING	7
- 6	0700762-21	BAG-SOUNDPROOFING	4
- 7	2215001-16	BAG-SOUNDPROOFING	7
- 8	2215001-17	BAG-SOUNDPROOFING	4
- 9	0700762-9	SEAL-BAGGAGE DOOR	1
-10	1200217-26	PANEL-SOUNDPROOFING	2
-11	1700127-7	PANEL-SOUNDPROOFING	6
-12	1700127-8	PANEL-SOUNDPROOFING	2
-13	1700127-9	PANEL-SOUNDPROOFING	8
-14	1700127-10	PANEL-SOUNDPROOFING	2
-15	1700127-13	PANEL-SOUNDPROOFING	1
-16	1700127-14	PANEL-SOUNDPROOFING	1
-17	1700127-19	PANEL-SOUNDPROOFING	2
-18	1700127-22	PANEL-SOUNDPROOFING RH ONLY	1
-19	1700127-23	PANEL-SOUNDPROOFING LH ONLY	1
-20	1700127-24	PANEL-SOUNDPROOFING LH ONLY	1
-21	1700127-26	PANEL-SOUNDPROOFING	6
-22	1700127-27	PANEL-SOUNDPROOFING	9
-23	1700127-28	PANEL-SOUNDPROOFING	4
-24	1700127-29	PANEL-SOUNDPROOFING	2
-25	1700127-23	PANEL-SOUNDPROOFING	3
	CES1109CLASS1A *	SOUNDPROOFING-FIBERGLASS MAT 1 IN. THICK BKI	AR
	CES1109CLASS1B *	SOUNDPROOFING-FIBERGLASS MAT 2 IN. THICK	AR
	CES1109CLASS1C *	SOUNDPROOFING-FIBERGLASS MAT 1/2 IN. THICK BKI	AR
	CES1109CLASS1G *	SOUNDPROOFING-FIBERGLASS MAT 1 IN. THICK BKI	AR
	CES1109CLASS1H *	SOUNDPROOFING-FIBERGLASS MAT 1 IN. THICK BKI	AR
	C7C0762-32 *	SOUNDPROOFING-EMBOSSED SOUNDFOAM 3/4 IN. THICK	AR
	CES1109CLASS4 *	SOUNDPROOFING-POLYMERIC SHEET .C35 IN. THICK BKI	AR

FIGURE A.11 (cont'd)

REFERENCES FOR APPENDIX A

A.1 Cessna Aircraft Company, "Information Manual: Model R182," published annually by Cessna Aircraft Company, Wichita, KS.

A.2 Cessna Aircraft Company, "Illustrated Parts Catalog, Models R182 and TR182," published annually or updated as required by Cessna Aircraft Company, Wichita, KS.

APPENDIX B

FLIGHT TESTS TO OBTAIN DIAGNOSTIC DATA

B. FLIGHT TESTS TO OBTAIN DIAGNOSTIC DATA

B.1 Introduction

Flight tests conducted during the survey phase of this study [1] provided a substantial quantity of diagnostic data which has been used for determining source levels and propagation paths. One finding from the preliminary source/path study carried out in Ref. 1 was that the multiplicity of apparently nearly equal source/path combinations created a requirement for more detailed data. Two sets of flight tests were planned - one to fill in a few key gaps on exterior source levels, and a second to provide detailed data on key issues and to check out generic treatments. Unfortunately, due to project schedules and resources which were needed for laboratory tests, the second series of flight tests never took place. However, the brief test series provided some additional useful data which, when combined with the Phase 1 survey results and the laboratory tests that are described in the following appendices, improved the definition of the relative importance of various source/path combinations. Certain Phase 1 data are summarized below, along with the data from the flight test conducted in this phase. Additional data are included in each of the appendices which follow in support of the diagnosis of a particular source/path combination being discussed.

B.2 Flight Test of Cessna R182

B.2.1 Summary

This flight test had a number of purposes:

- To obtain exterior noise data on the fuselage near the exhaust outlet and on the windshield using a new "stick-on" microphone design, to record vibration data at the microphone locations, and to record cabin interior noise data;

- To use this data to assess vibration sensitivity problems with the stick-on microphone which was included in plans for subsequent detailed tests;
- To compare noise and vibration levels during a dive with the engine off with those noise and vibration levels during cruise, to validate observations from Ref. 1;
- To carefully examine and photograph the aircraft so that we could properly configure the special test fuselage in our laboratory.

Data was obtained for three flight conditions, normal cruise, economy cruise, and dive, at all locations except the accelerometer at the exhaust microphone. That transducer showed anomolously low vibration levels leading us to believe that it fell off early in the flight. Laboratory data on the vibration sensitivity of the "tape-on" microphone indicate that, in some low frequency bands, vibration sensitivity may be a problem.

Dive noise and vibration levels proved to be only slightly below steady cruise levels. This appeared to be a consequence of the engine windmilling at an rpm nearly equivalent to that associated with steady cruise.

B.2.2 Noise and Vibration Measurement System

The aircraft tested was a 1979 Cessna R182 with a naturally-aspirated engine and two-bladed propeller. The engine had been run for 828 hours. There was a finished interior in the aircraft but the interior trim was slightly different from the interior in our laboratory fuselage, probably reflecting the difference in model years. The instrumentation chain used is sketched in Fig. B.1. The location of the various instruments was as follows:

- Windshield microphone - center of windshield above compass mount;

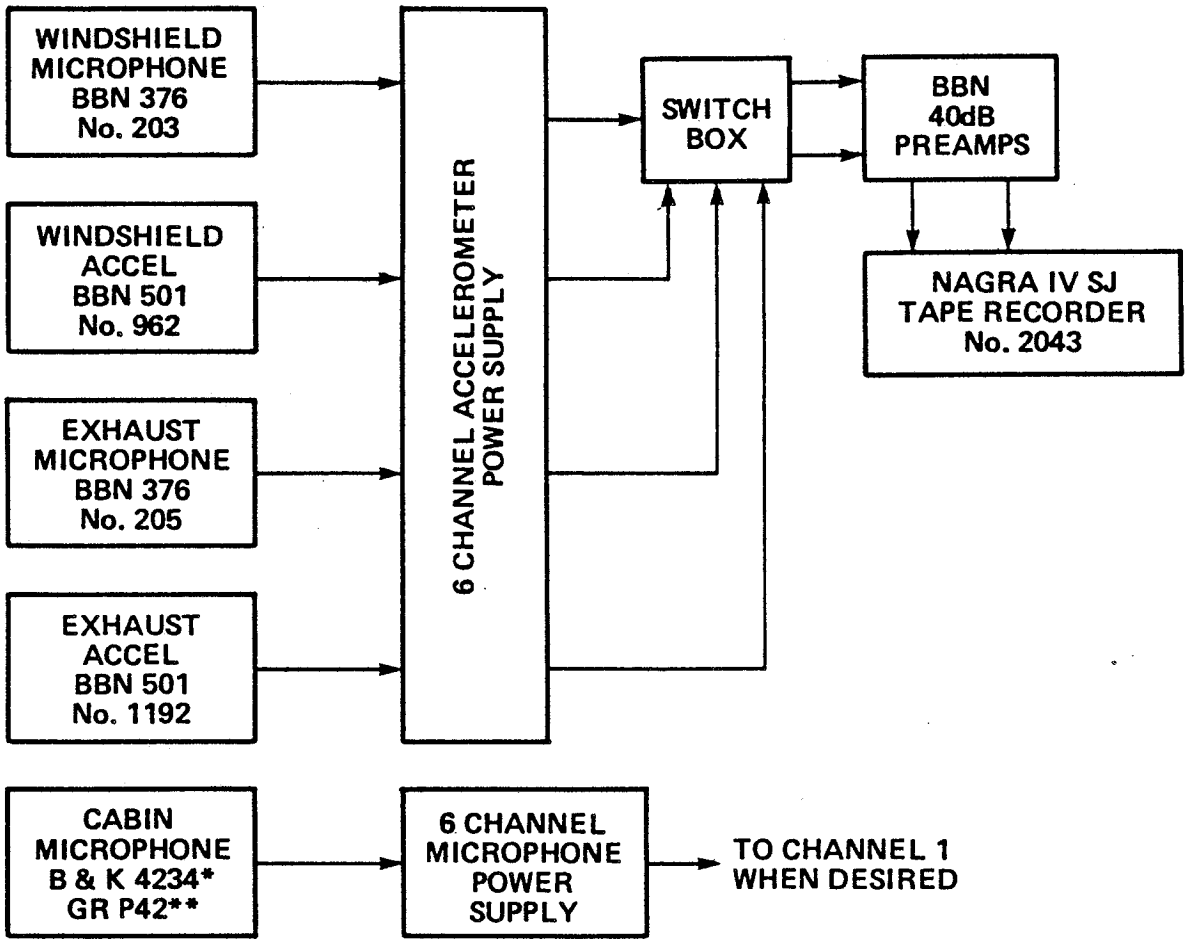

FIGURE B.1 INSTRUMENTATION CHAIN FOR FLIGHT TEST.

- Windshield accelerometer - inside surface of windshield next to compass mount;
- "Exhaust" microphone - on starboard side of the body of the fuselage, between the double line of rivets connecting the cabin floor to the wall of fuselage oppposite the exhaust outlet;
- "Exhaust" accelerometer - on the skin of the starboard side of the fuselage inside the cabin approximately 5 cm above floor and 5 cm aft of the firewall;
- Cabin microphone - at ear level halfway between pilot and copilot positions.

The flight conditions at which data were taken was as follows:

- Standard cruise - 75% of full power at 2400 rpm

  Altitude: 2270 m
  Temperature: -21°C
  Speed: 145 kts (indicated air speed)
  Manifold Pressure: 559 mm Hg (22 in. Hg)

- Economy Mode - 65% of full power at 2100 rpm

  Altitude: 2270 m
  Temperature: -21°C
  Speed: 140 kts (indicated air speed)
  Manifold Pressure: 553 mm Hg (22 in. Hg)

- Dive - engine throttled back, 2200 rpm

  Altitude: 2270 m
  Temperature: -21°C
  Speed: 140-150 kts (indicated air speed)
  Heading: down
  Manifold Pressure: 0

Data from all transducers were analyzed for each test mode and one-third octave band and narrowband (2.5 Hz bandwidth, 0-1000 Hz) spectra are included in this report. The levels from the exhaust accelerometer, however, appeared to be anomalously low and is not reported further in this study.

To execute the dive tests without contamination from engine and propeller sources, it would be desirable (and is apparently possible) to install a feathering propeller so that one can stop the engine completely (such as was done with certain twin-engine aircraft tested in Ref. 1.)

B.2.3 Vibration Sensitivity of "Stick-On" Microphone

Laboratory testing of the BBN 376 microphone indicated that, when used in the configuration shown in Figure B.2, the microphone provides a simple, accurate and reliable means for measuring noise exterior to the aircraft. Its major drawback is the vibration sensitivity of the microphone. Preliminary measurements indicate that 1 g lateral vibration at 100 Hz is sensed as 103 dB sound pressure level. Laboratory measurements to obtain vibration sensitivity data at other frequencies are described in App. I. It is useful to examine the implications of the

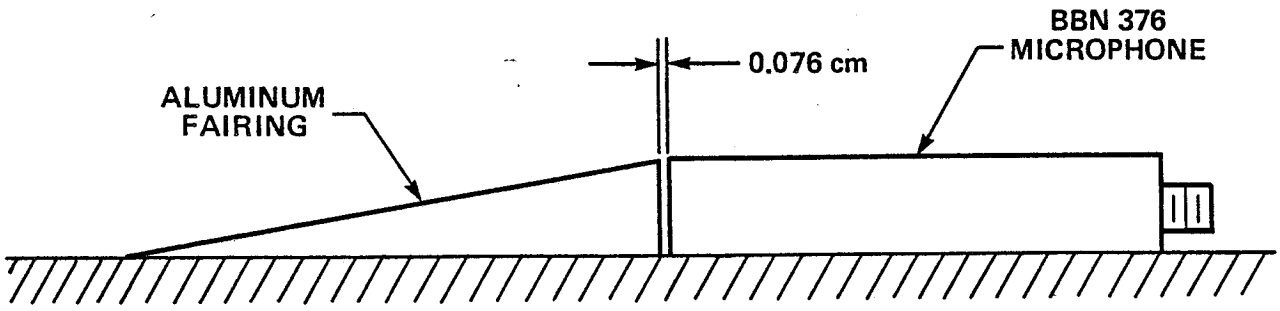

FIGURE B.2. "STICK-ON" EXTERIOR MICROPHONE.

transducer having the same vibration sensitivity at other frequencies as it has at 100 Hz. Figure B.3 shows the estimated microphone signal due to the measured vibration at the windshield and compares it to the signal measured in flight in the economy mode. Above 100 Hz there does not seem to be a vibration sensitivity problem. However, at 63 and 80 Hz the vibration sensitivity of the microphone might present a problem. Further discussion of calibrations on this microphone is presented in App. I.

B.2.4 Dive Noise and Vibration Levels

During the dive tests described herein it was found that the engine windmills at approximately 2200 rpm. Noise and vibration levels in dive, straight and level cruise, and in economy mode were observed to be quite similar (see Figs. B.4 and B.5). This result may indicate that some of the cabin noise attributed to "airflow" is actually structureborne vibration and perhaps "backfire" airborne noise from the engine.

B.2.5 Selected cabin acoustic data from flight test

Figure B.6 shows representative cabin acoustic data taken in an R182 aircraft during Phase 1 of this program (see App. A of Ref. 1) for the reference cruise condition (75% power, 2400 rpm, altitude approximately 5000 ft). Figure B.7 compares the Phase 1 data with data taken from the aircraft which was available for this test, at comparable operating settings (note that both curves are A-weighted in Figure B.7. The comparison shows that this aircraft is somewhat noisier than the one tested in Ref. 1; this may be due to differences in source strengths caused by substantial differences in density (temperature), or to the fact that more time was available in the tests in Ref. 1 to block air conditioning vents, seal leaks, etc., than in this test (which was aimed primarily at obtaining external levels). The

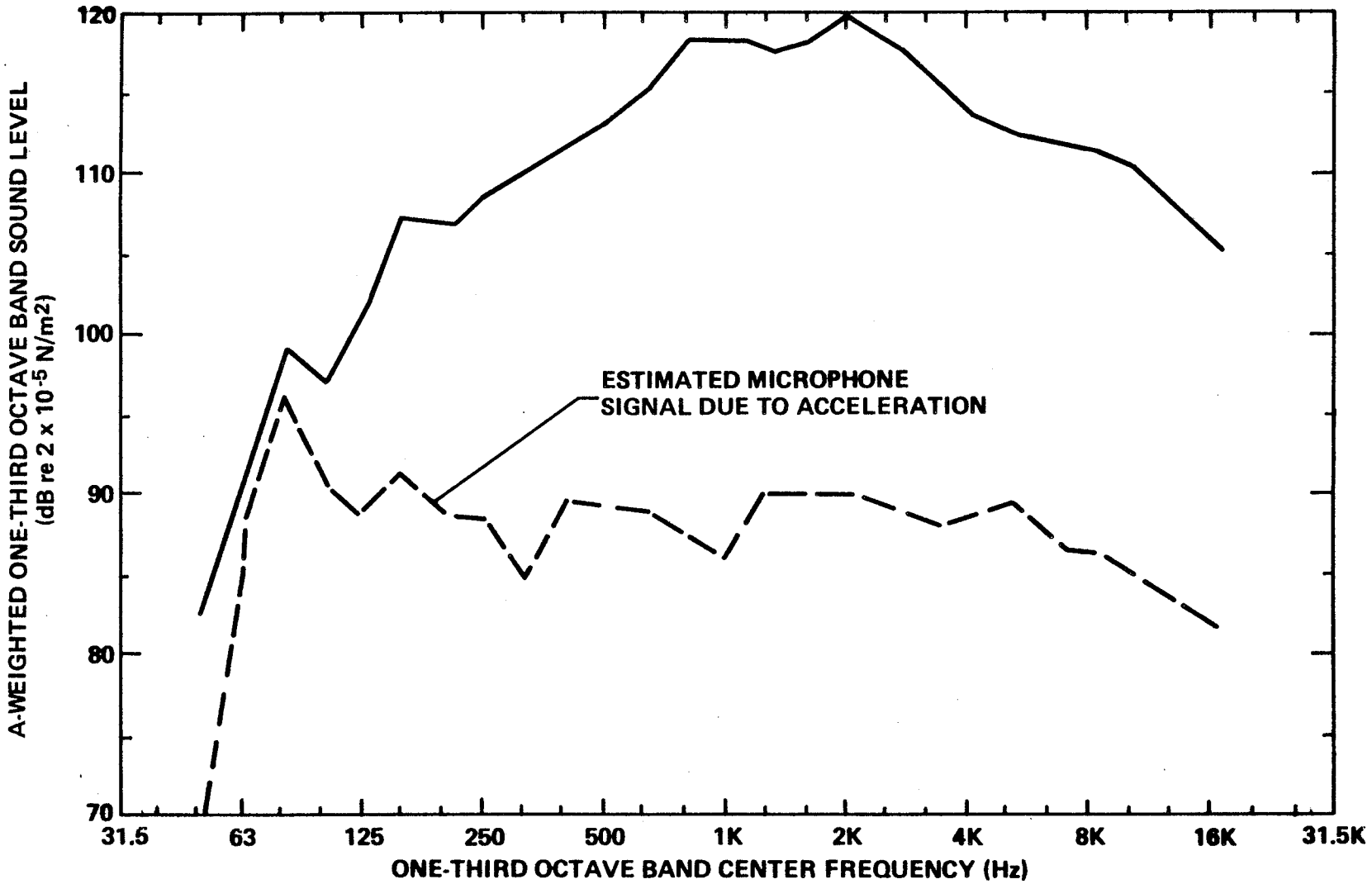

FIGURE B.3. INDICATED SOUND LEVEL AND VIBRATION-INDUCED OUTPUT OF SURFACE-MOUNTED MICROPHONE AT THE WINDSHIELD DURING LEVEL FLIGHT, 2100 RPM, 65% POWER, 2270m (7500 FT).

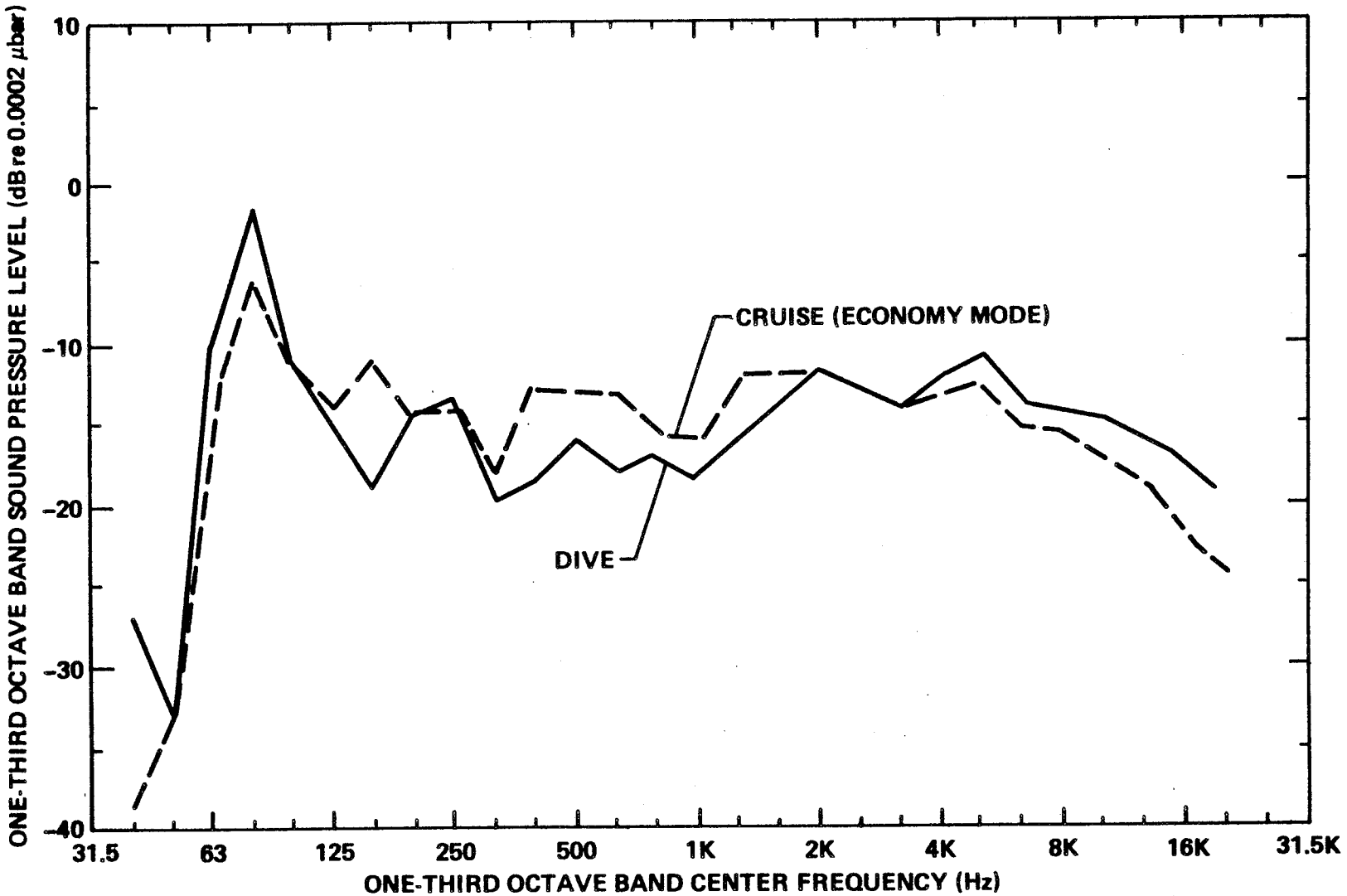

FIGURE B.4. TYPICAL WINDSHIELD ACCELERATION LEVELS DURING CRUISE AND DIVE.

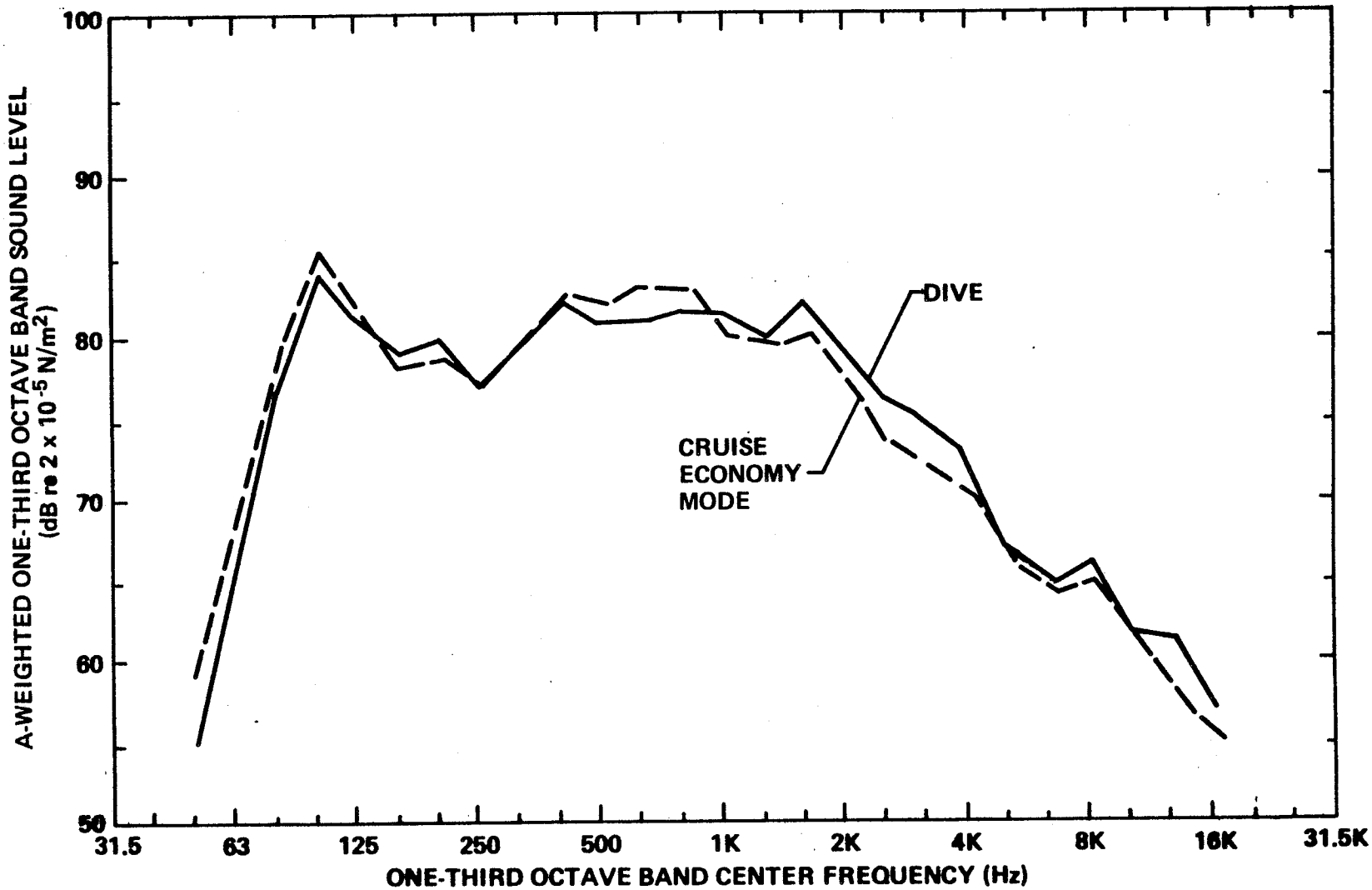

FIGURE B.5. TYPICAL LEVELS AT CABIN MICROPHONE DURING CRUISE AND DIVE.

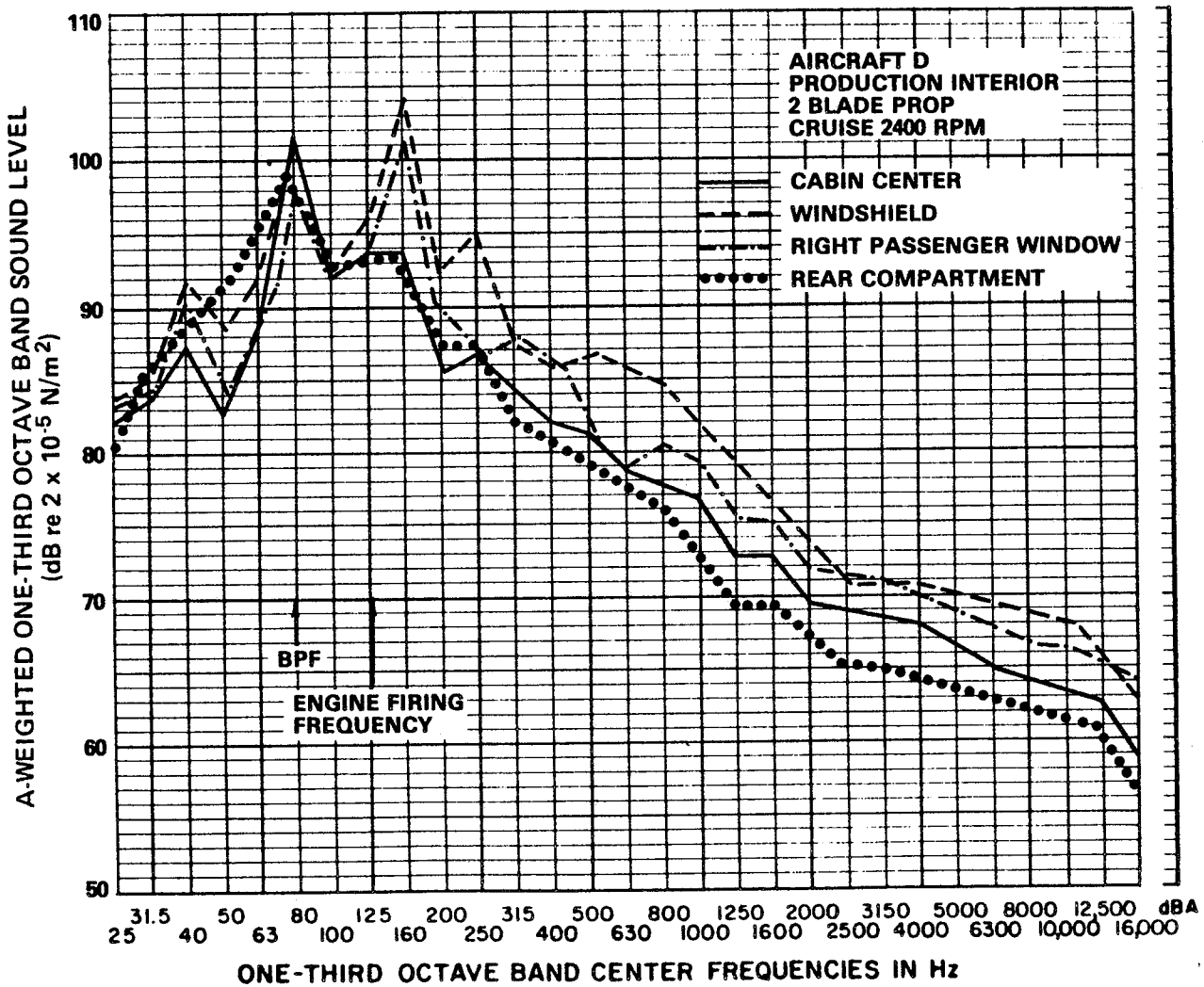

FIGURE B.6 CABIN NOISE SURVEY IN AIRCRAFT D IN CRUISE CONDITION.

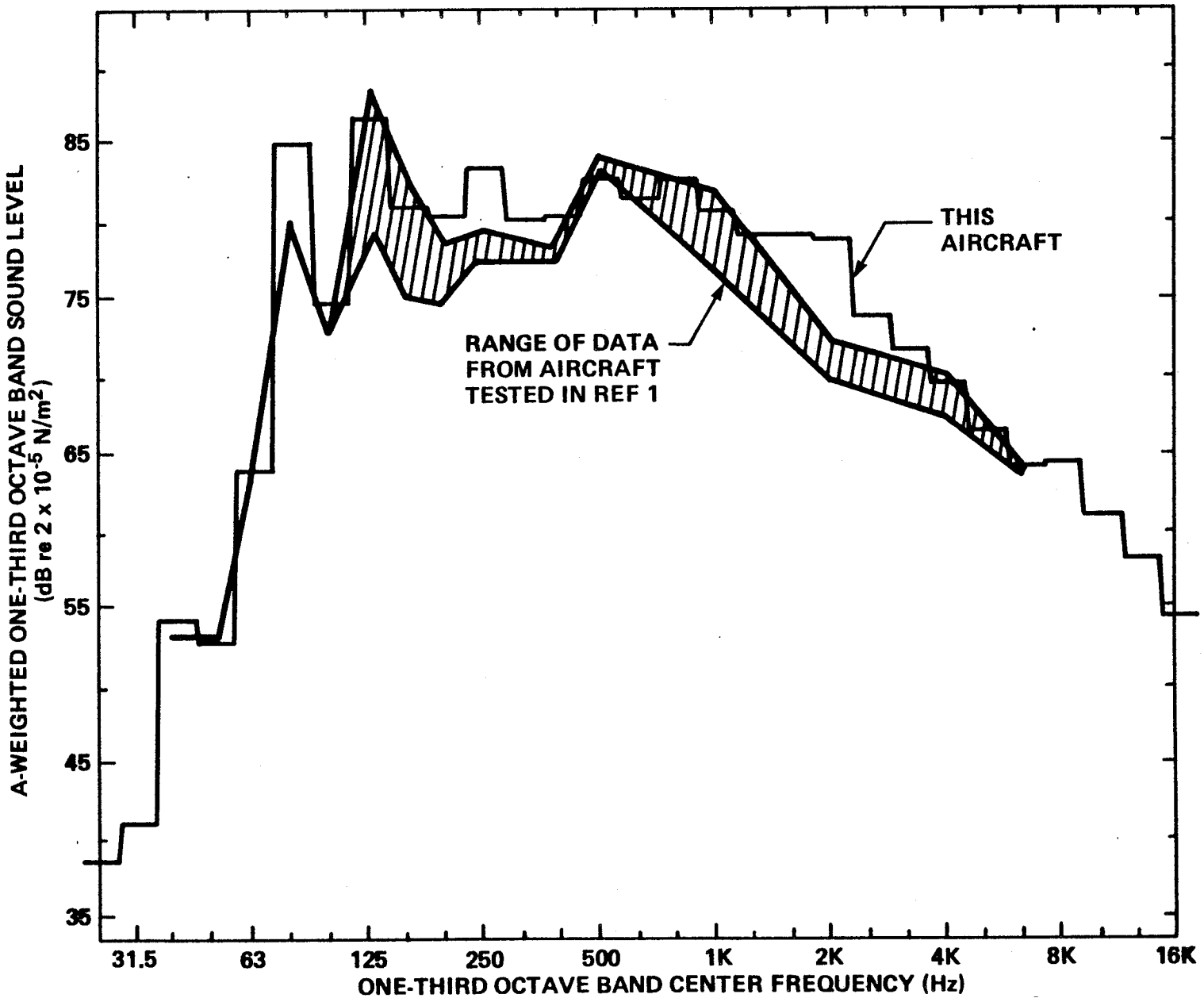

FIGURE B.7. MID-CABIN 1/3-OCTAVE ACOUSTIC LEVELS IN TEST AIRCRAFT COMPARED TO REF. 1.

differences are not great considering the general variability in levels documented in Ref. 1.

Figure B.8 provides the one-third octave spectrum at mid-cabin for the 2100 rpm level cruise, and Fig. B.9 illustrates the spectrum for the dive conditions.

Figures B.10 through B.12 provide narrowband spectra for the three cases illustrated in Figs. B.7 through B.9.

B.2.6 Selected vibration data from flight test

Vibration measurements were performed during the flight test primarily to assist in interpreting external acoustic data from the "stick-on" acoustic sensor which was being evaluated during the flight. Phase 1 testing (Ref. 1) included limited vibration surveys around the inside of the cabin, which are illustrated in Fig. B.13 for reference purposes. Figure B.14 provides one-third octave vibration data on the windshield for the Phase 2 test flight; this data shows levels considerably higher than those observed in the Phase 1 test, probably due to differences in accelerometer location, and possibly due to differences in structureborne vibration through the engine mounts which, as reported in Ref. 1 and App. H, may be substantial from mount to mount. Figures B.15 through B.19 provide additional windshield vibration, for reference purposes.

Other vibration data acquired during this test appears elsewhere in the report in conjunction with discussion of a particular source/path diagnosis and treatment.

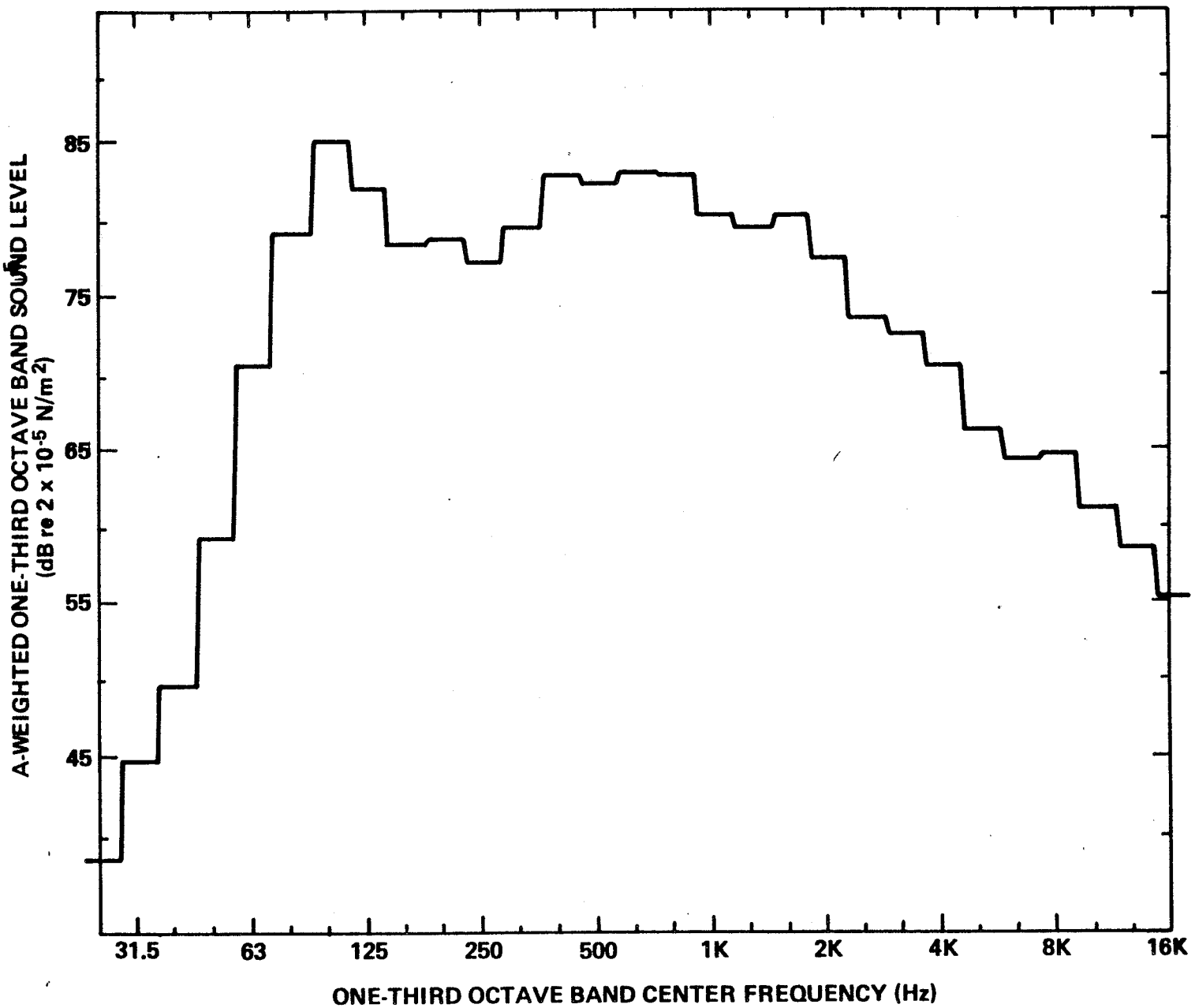

FIGURE B.8. MID-CABIN 1/3 OCTAVE ACOUSTIC SPECTRUM FOR 2100 RPM CRUISE.

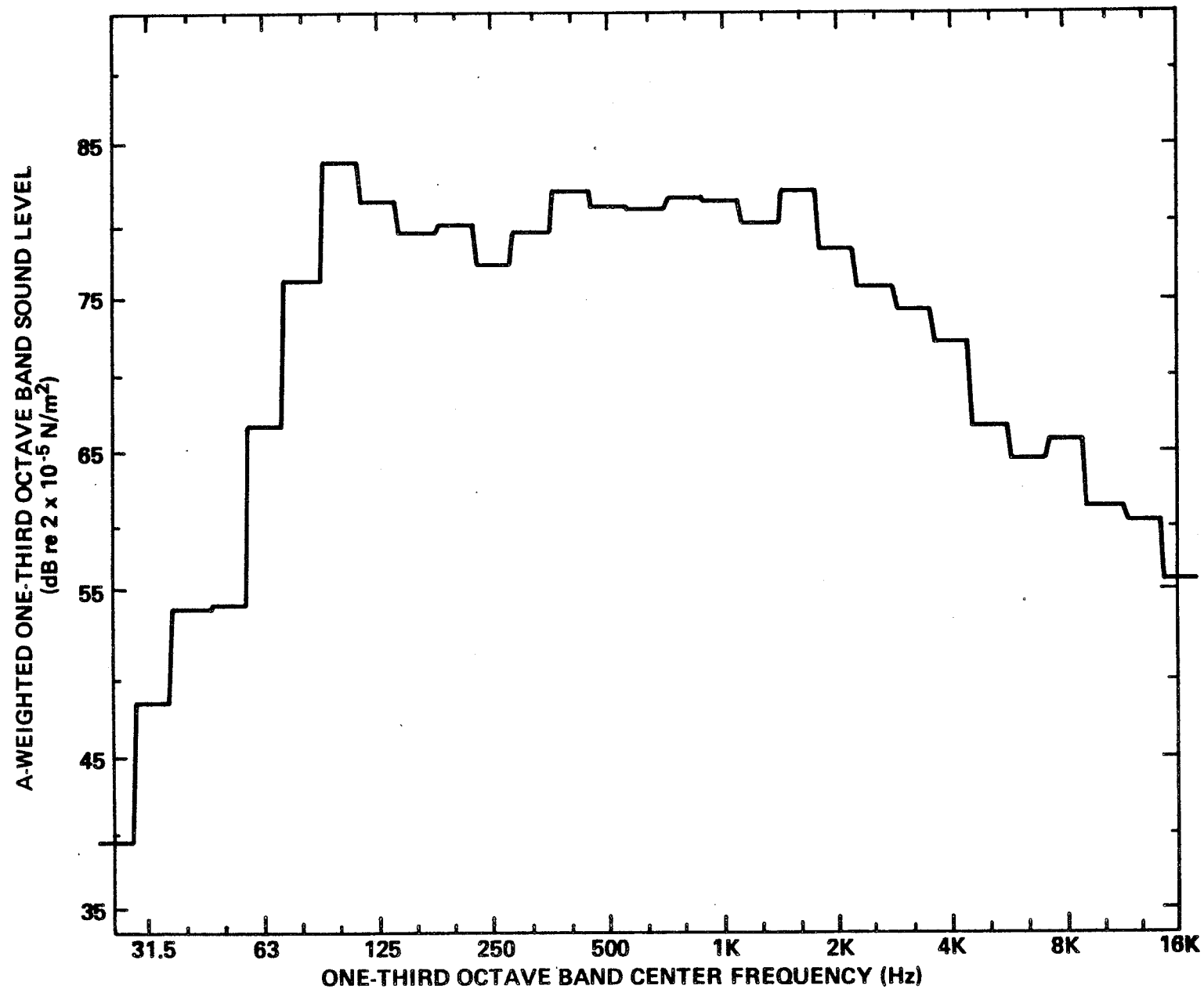

FIGURE B.9. MID-CABIN 1/3 OCTAVE SPECTRUM DURING DIVE (ENGINE AT IDLE WINDMILLING AT AROUND 2200 RPM)

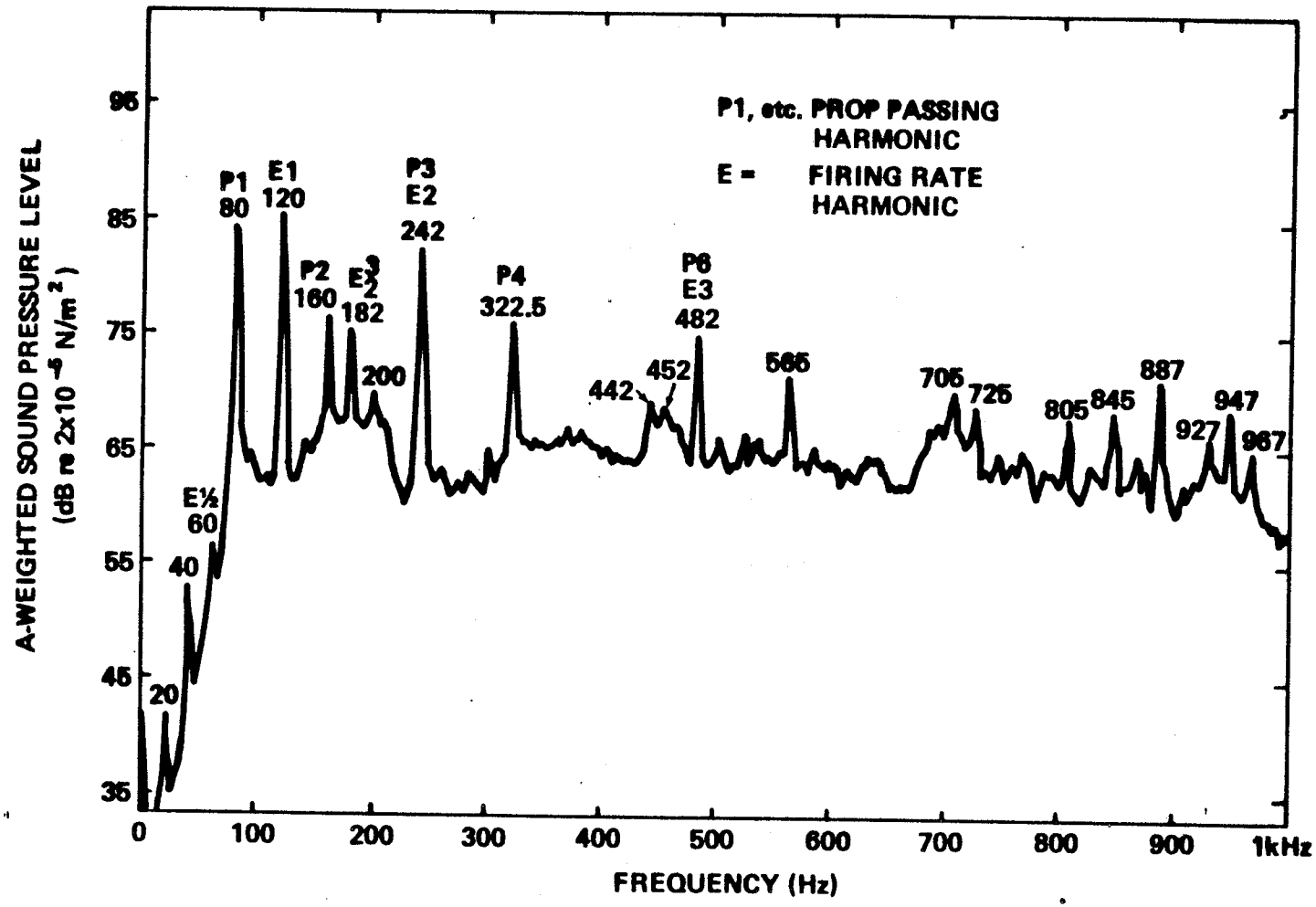

FIGURE B.10. NARROWBAND SPECTRUM (2.5 HZ BANDWIDTH) OF MID-CABIN LEVELS FOR 75% POWER/2400 RPM LEVEL FLIGHT CONDITION.

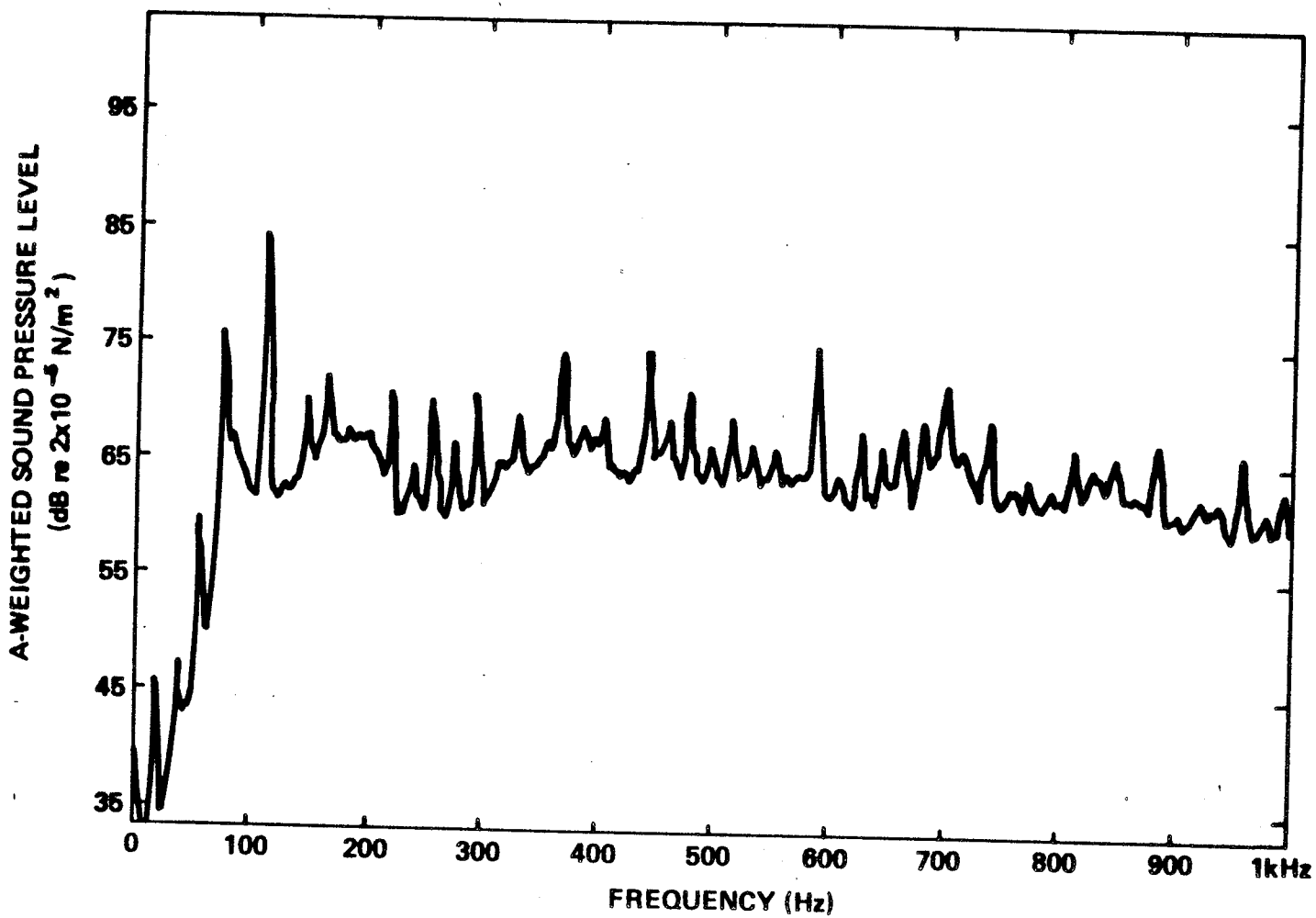

FIGURE B.11. A-WEIGHTED NARROWBAND SPECTRUM OF MID-CABIN LEVELS FOR 60% POWER 2100 RPM, LEVEL FLIGHT CONDITION.

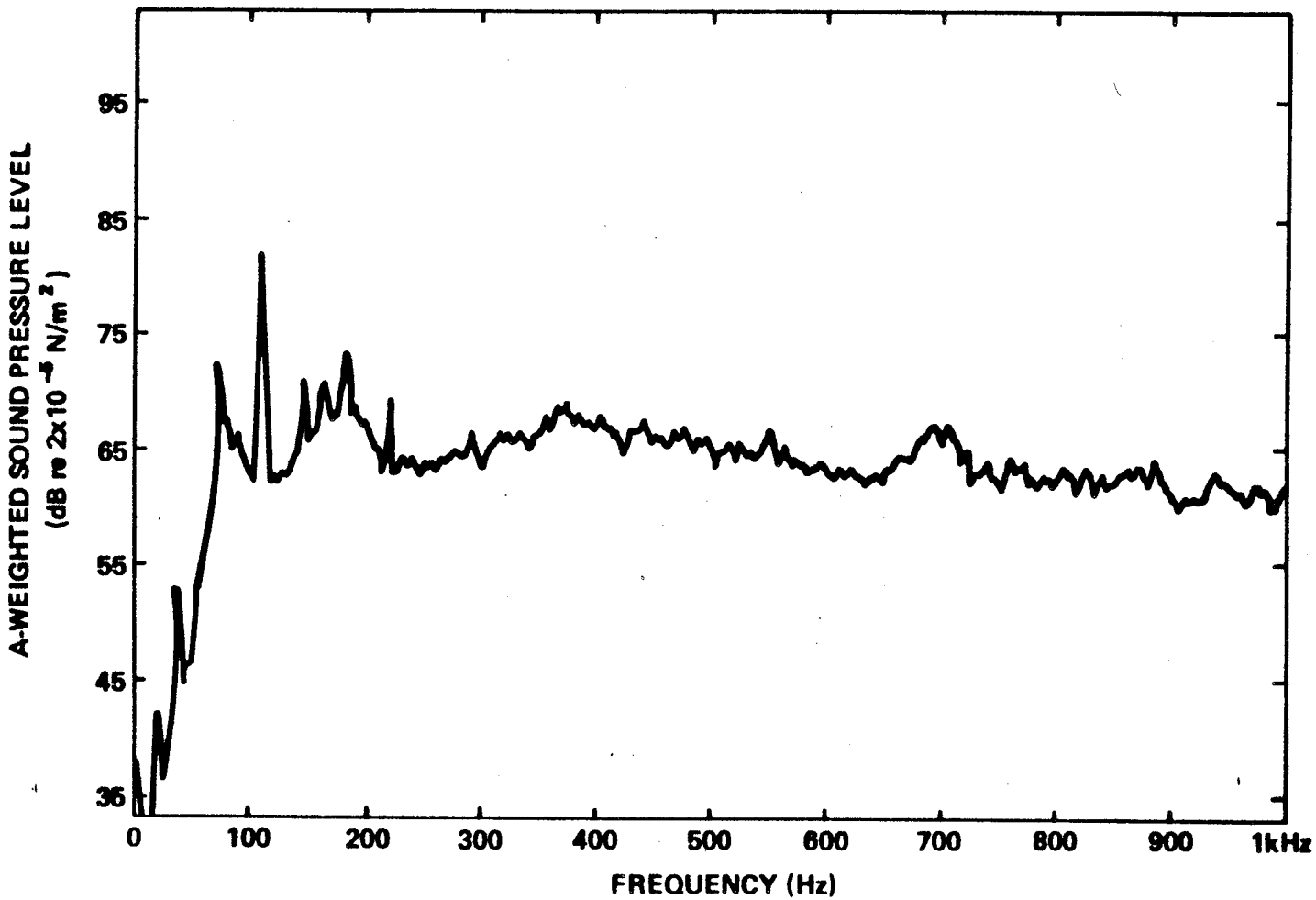

FIGURE B.12. A-WEIGHTED NARROWBAND SPECTRUM OF MID-CABIN LEVELS DURING DIVE.

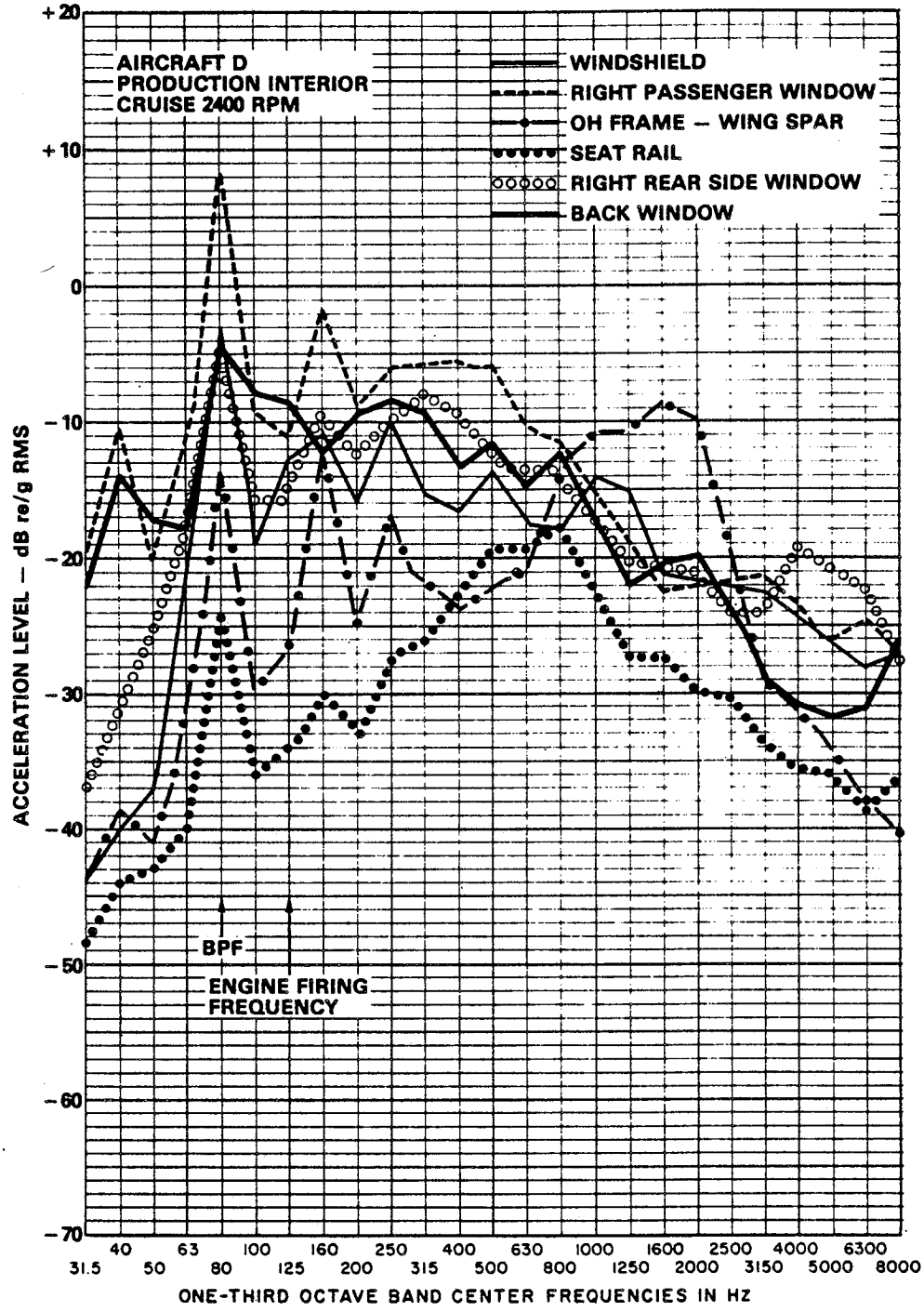

FIGURE B.13. VIBRATION SURVEY ON INTERIOR SURFACES ON AIRCRAFT D IN CRUISE CONDITION (REF 1, APPENDIX A)

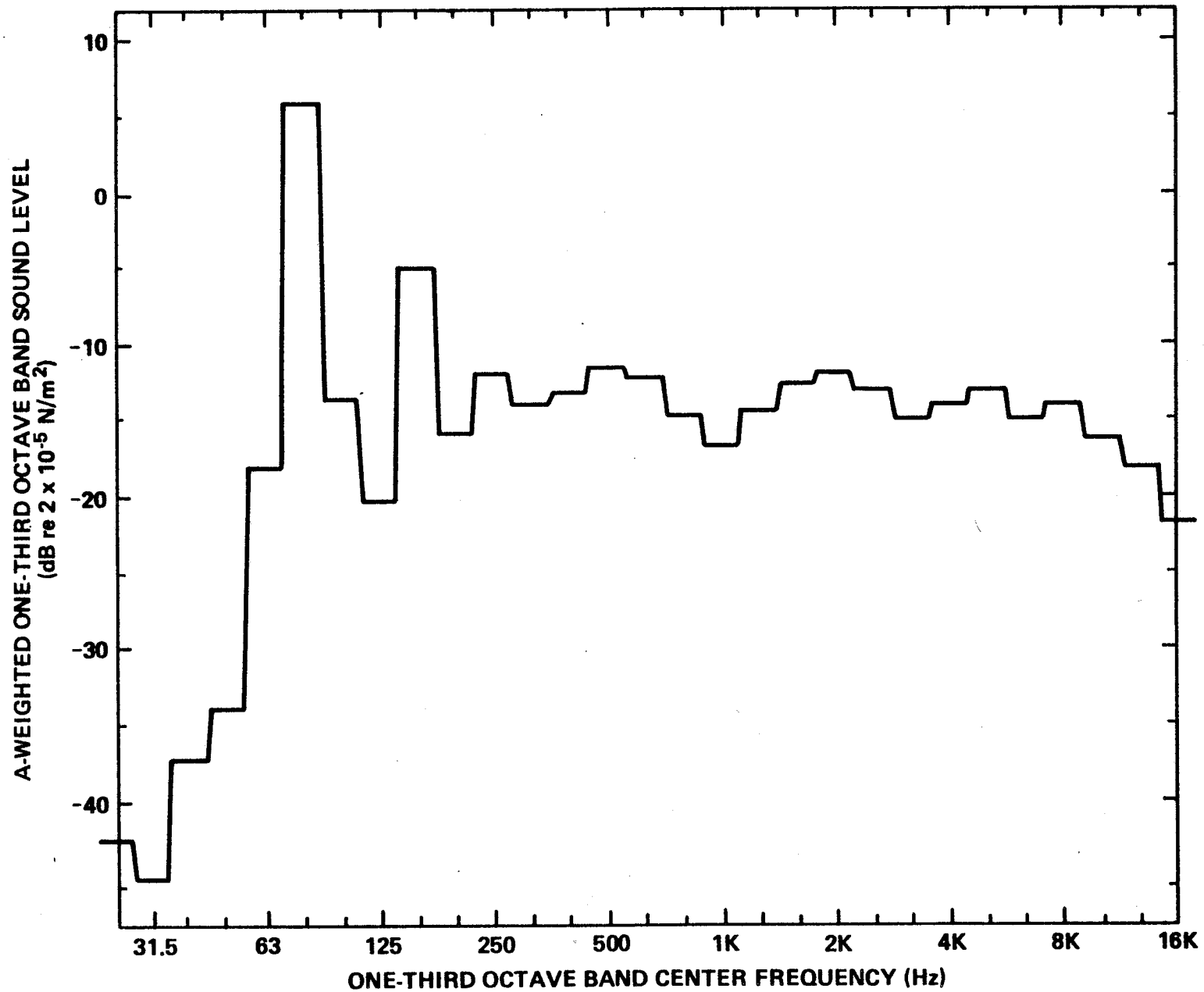

FIGURE B.14. 1/3 OCTAVE SPECTRUM WINDSHIELD VIBRATION FOR 2400 RPM CRUISE CONDITION (FLAT WEIGHTING).

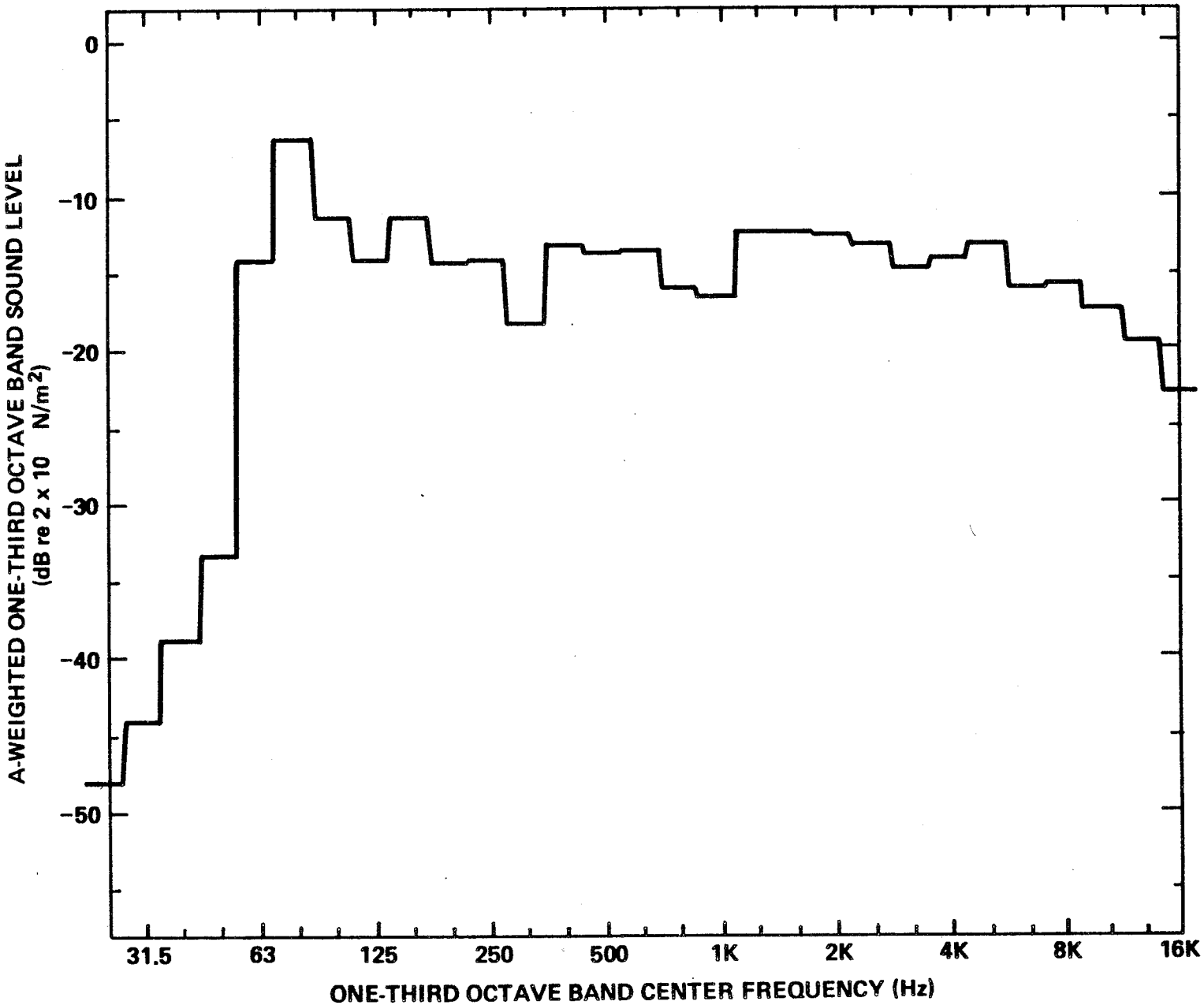

FIGURE B.15. 1/3 OCTAVE SPECTRUM WINDSHIELD VIBRATION FOR 2100 RPM CRUISE CONDITION.

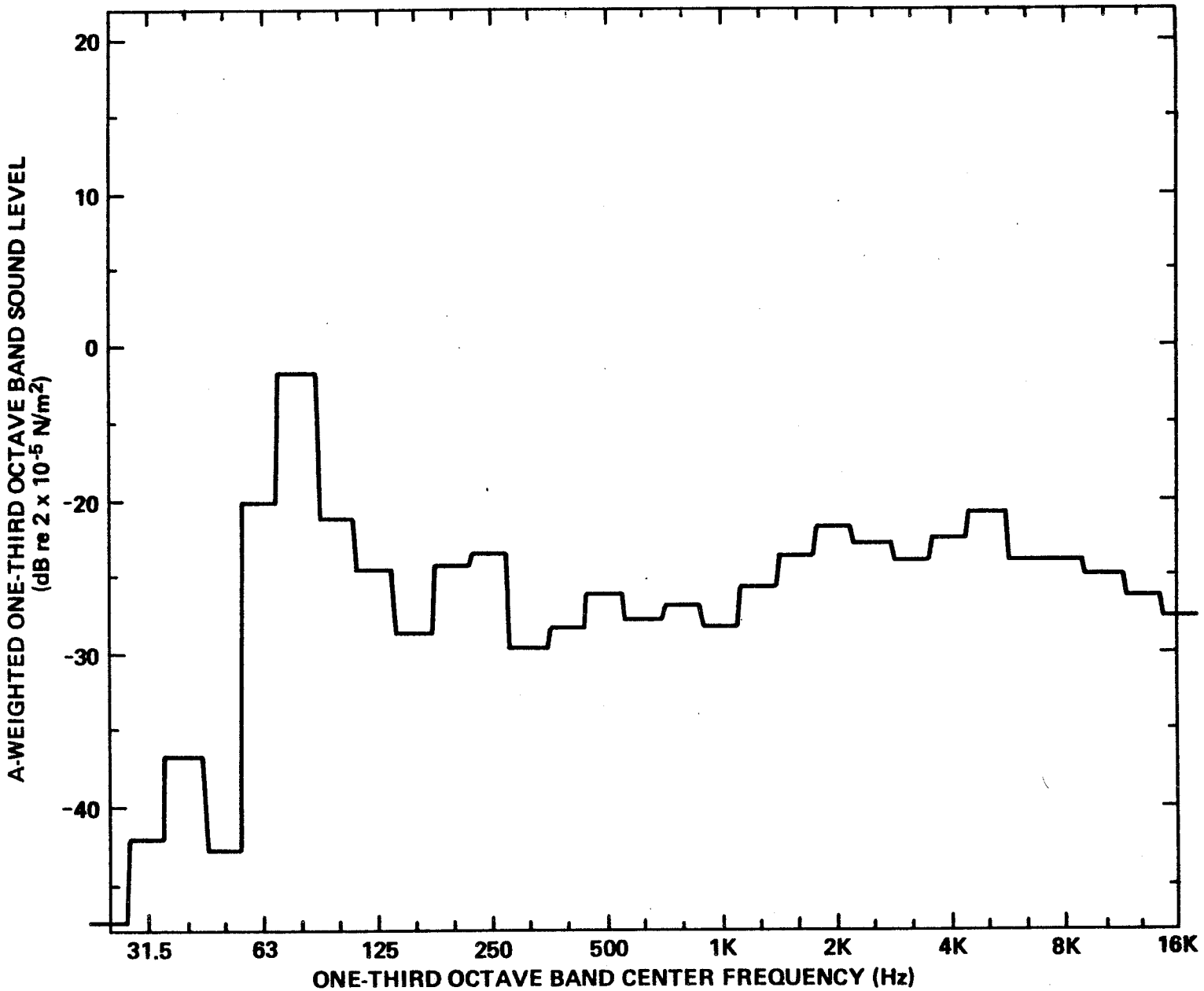

FIGURE B.16. 1/3 OCTAVE SPECTRUM OF WINDSHIELD VIBRATION DURING DIVE TEST.

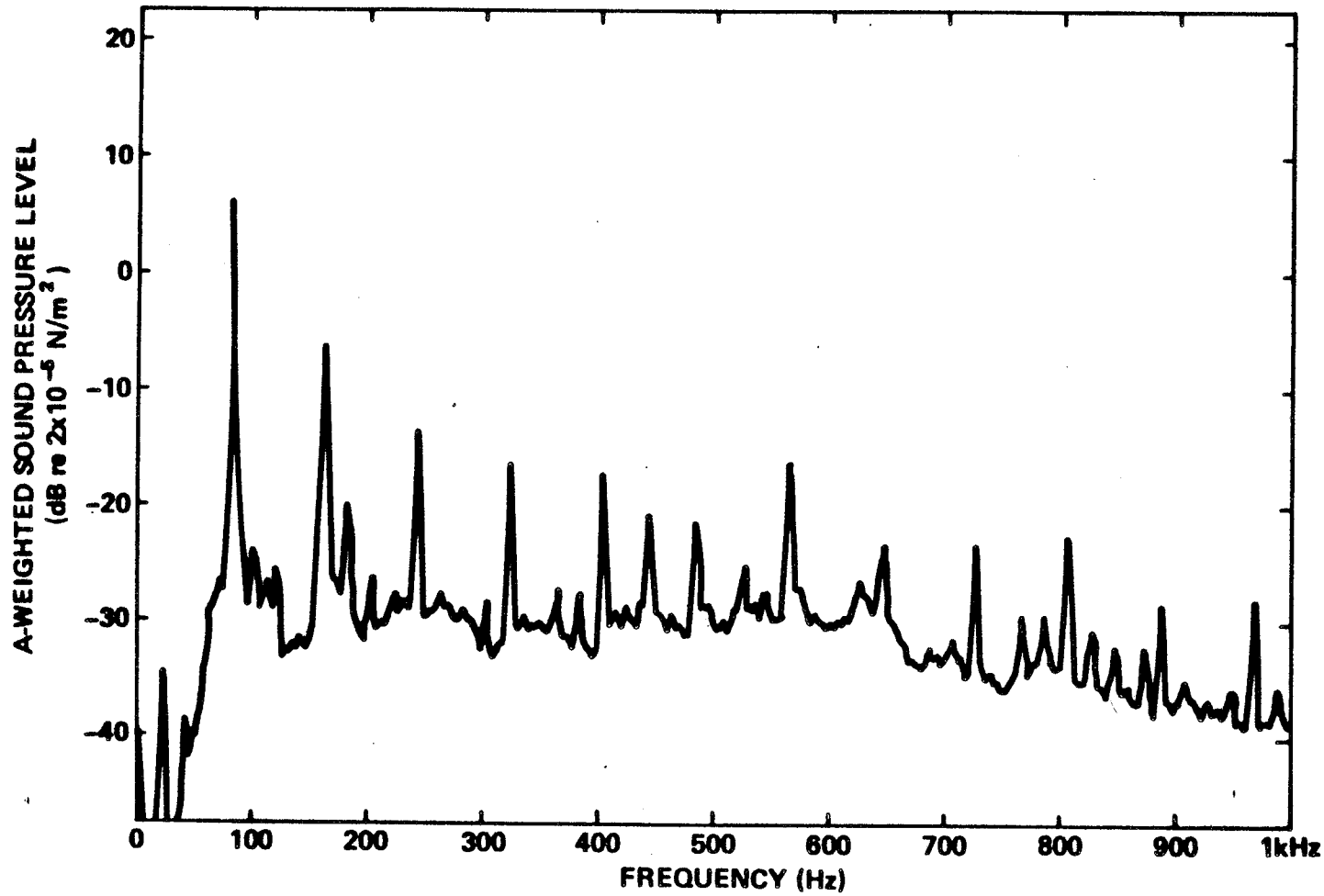

FIGURE B.17. NARROWBAND SPECTRUM OF WINDSHIELD VIBRATION DURING 2400 RPM CRUISE.

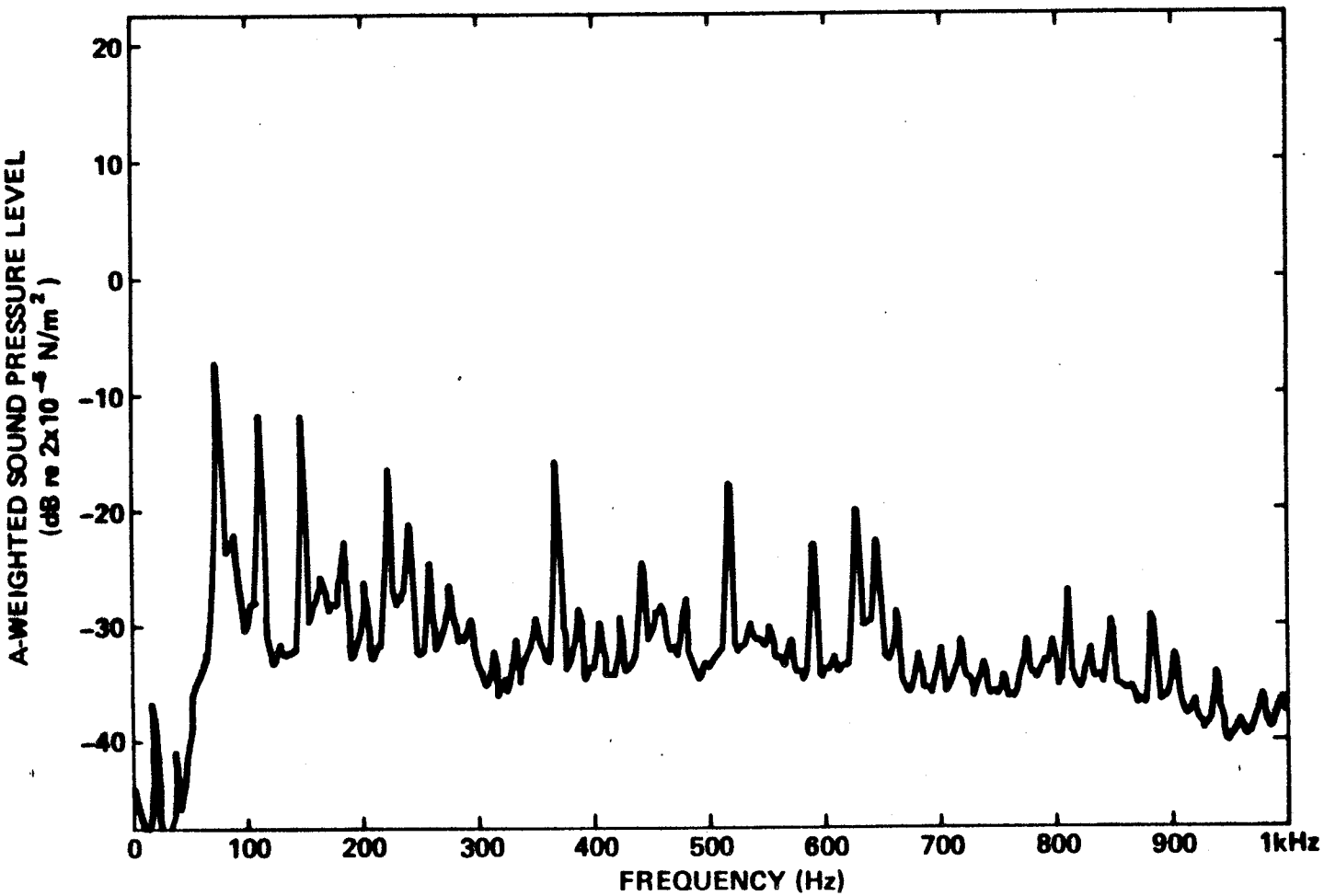

FIGURE B.18. NARROWBAND SPECTRUM OF WINDSHIELD VIBRATION DURING 2100 RPM CRUISE.

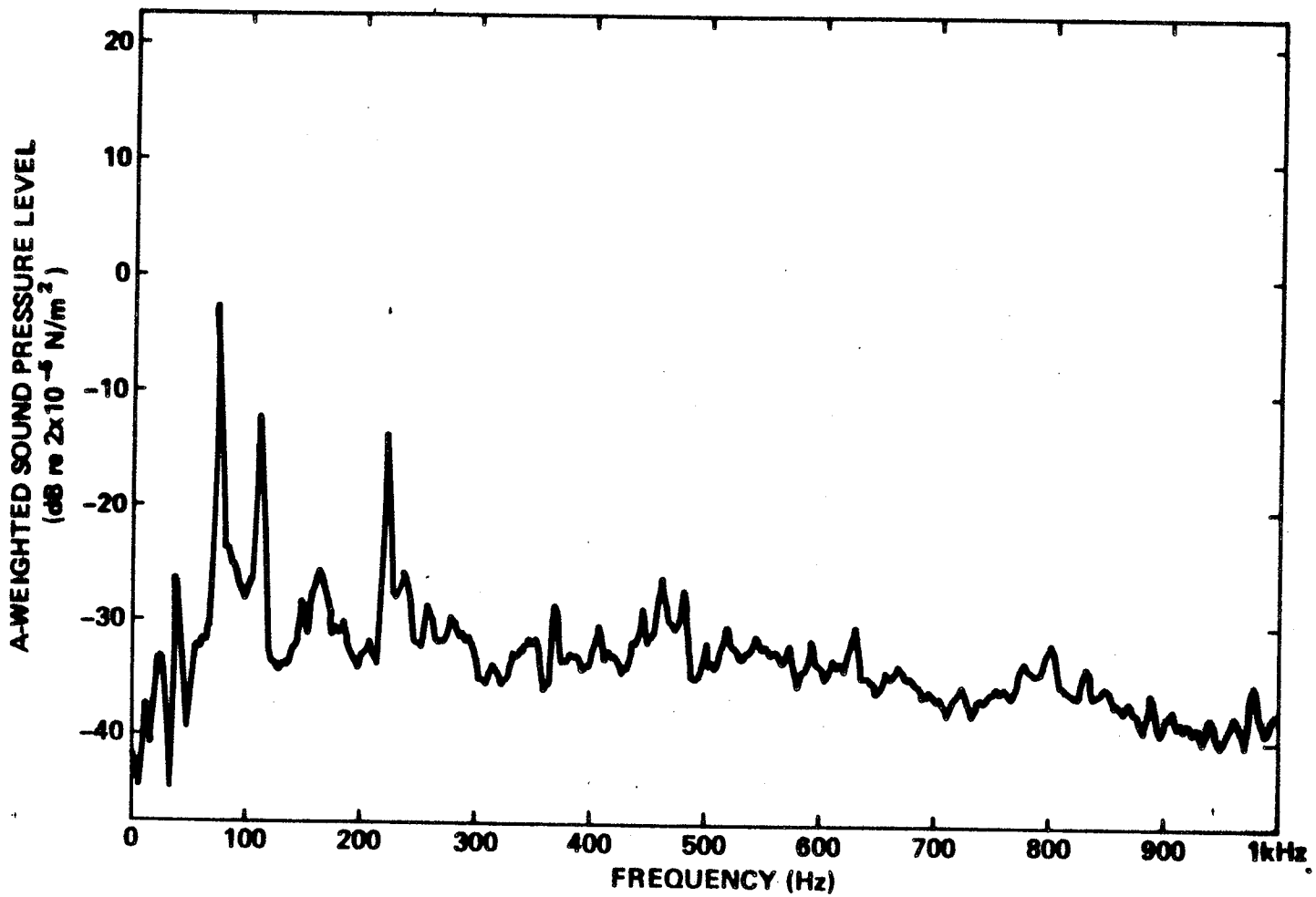

FIGURE B.19. NARROWBAND SPECTRUM OF WINDSHIELD VIBRATION DURING DIVE.

APPENDIX C

NOISE REDUCTION MEASUREMENT AND IMPROVEMENT FOR VARIOUS EXTERIOR PANELS, WINDOWS, AND FIREWALL

C. NOISE REDUCTION MEASUREMENT AND IMPROVEMENT FOR VARIOUS EXTERIOR PANELS, WINDOWS, AND FIREWALL

C.1 Introduction

This section summarizes the measurements carried out to quantify the paths for airborne noise into the Cessna R182 cabin. Three sources of airborne noise were considered:

- propeller airborne noise
- engine airborne noise
- exhaust noise

and the following paths from each source were examined:

- windshield
- firewall
- roof
- rear window
- side windows
- shin panel
- rear side panel
- floor
- rear bulkhead
- doors.

In general, transmission through the roof, windshield, and firewall dominated the sound level inside the cabin to such an extent that quantifying the strength of the other paths was difficult. Consequently, the results presented here focus primarily on those paths.

We also examined, experimentally, the possibility of stiffening the firewall to reduce the sound transmission through that path. The primary contribution to cabin interior noise from that path was in the 80 Hz one-third octave band. At so low a frequency, stiffening appeared to be the technique most likely to be successful in increasing the transmission loss of the firewall.

C.2 Test Configuration

The fuselage of a Cessna R182 with a finished interior was suspended as shown in Fig. C.1, and all cabin panels, windows, etc. were covered with 5 cm (2 in.) of glass fiber and 0.5 lb/ft^2 leaded vinyl. Before beginning testing, we found that we had to cover the windshield and firewall (see Figs. C.2 and C.3) with a second layer of glass fiber and leaded vinyl, because the sound transmitted through these paths was so dominant, especially for the simulated propeller noise source. A loudspeaker was mounted forward of the aircraft, as shown in Fig. C.4., to simulate airborne noise from the propeller. The exhaust and engine airborne noise were simulated, as described in App. D and App. F, respectively. Finally a loudspeaker was placed in the tail cone to examine sound transmission through the rear bulkhead. Noise measurements were made outside the aircraft cabin very close to the panel of interest* (2.5 to 5 cm away) and at four locations inside the cabin:

- the cabin center
- above the dashboard behind the windshield
- the co-pilot's right ear
- the back seat.

---

*For the rear bulkhead, the noise was measured at a convenient position inside the tail cone, and the difference between that microphone and the cabin microphone was used to characterize the sound transmission through that panel. With this transfer function we can use these measurements in conjunction with flight measurements of the noise in the tail cone to characterize the sound transmission through the rear bulkhead.

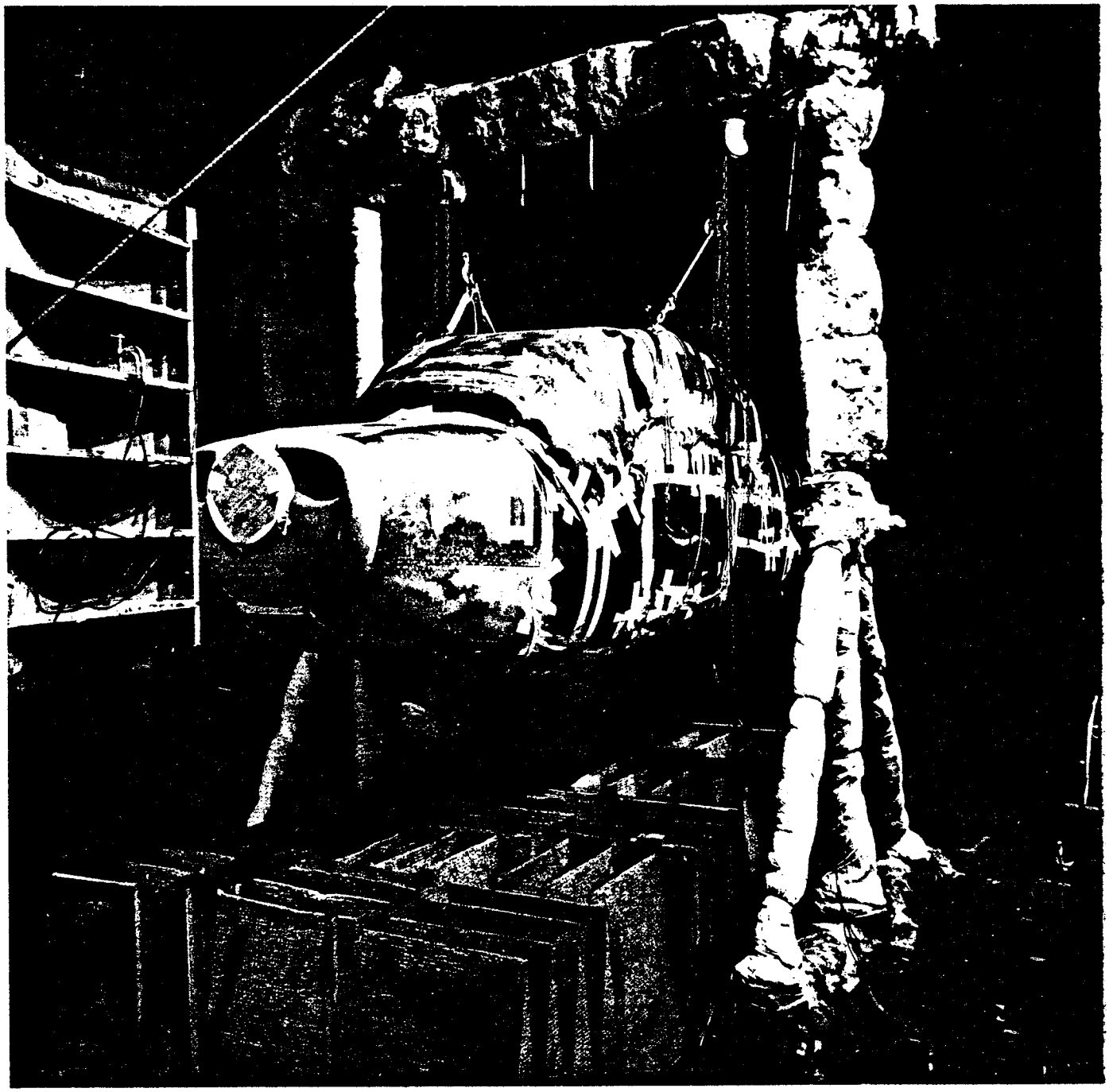

FIGURE C.1. THE CESSNA R182 FUSELAGE SET-UP FOR TESTING.

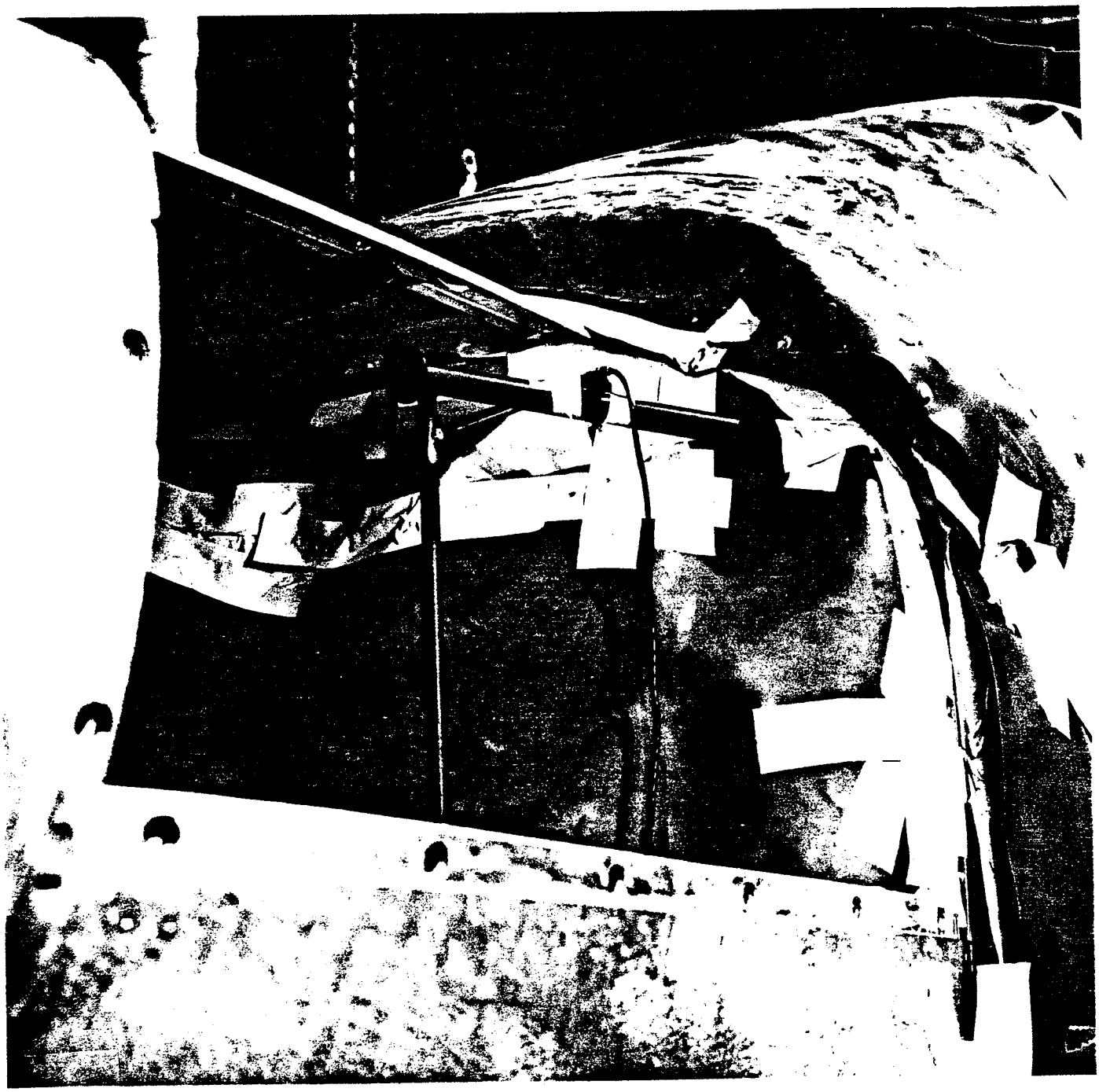

FIGURE C.2. THE FIREWALL OF THE FUSELAGE PREPARED FOR TESTING SHOWING THE MICROPHONE PLACED TO MONITOR ENGINE COMPARTMENT NOISE.

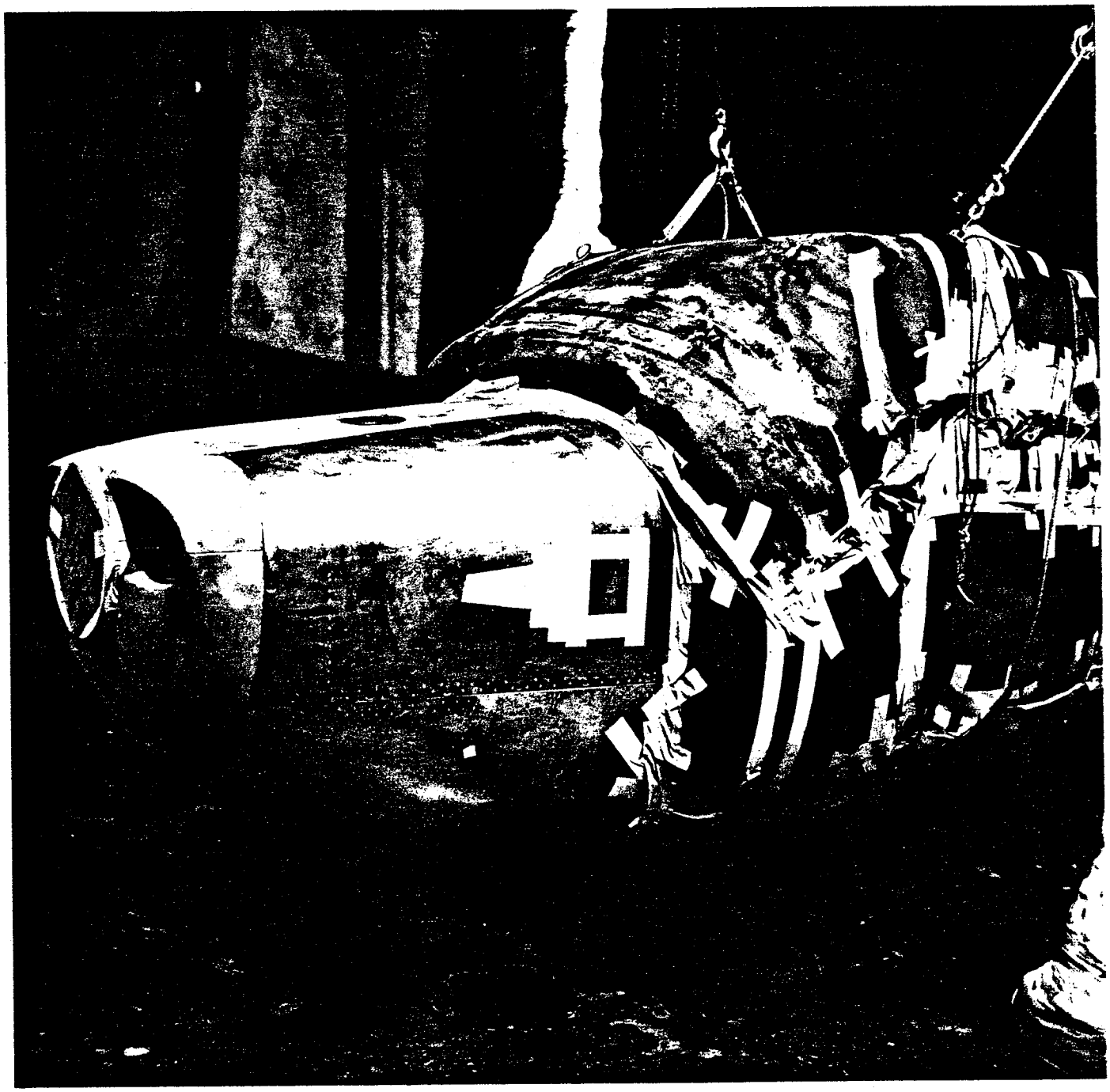

FIGURE C.3. THE SECOND LAYER OF LEADED VINYL AND FIBERGLASS ON THE WINDSHIELD.

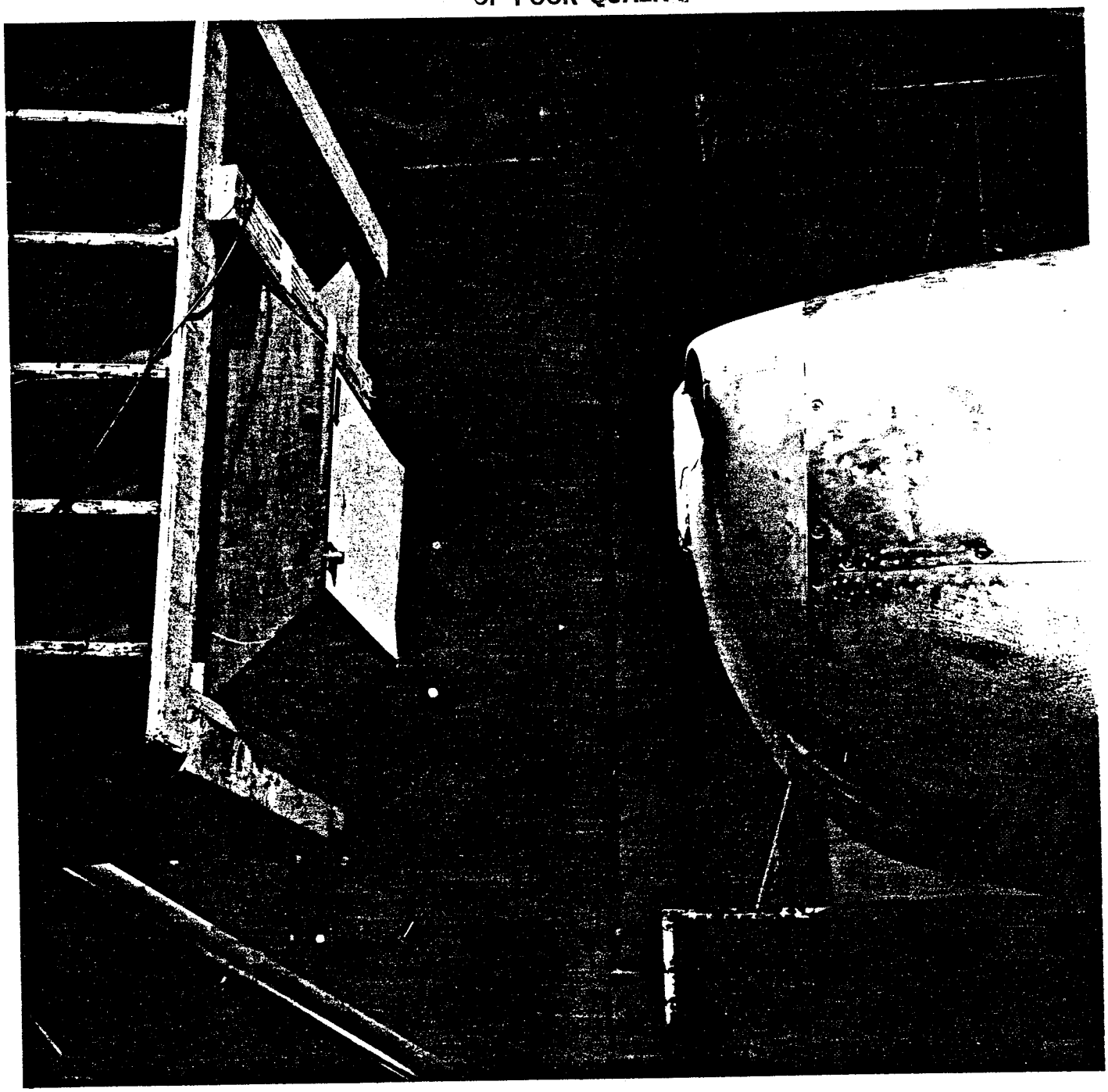

FIGURE C.4. THE LOUDSPEAKER USED TO SIMULATE PROPELLER AIRBORNE SOUND.

The noise reduction is characterized by the difference in noise levels between the outside microphone and an interior microphone or the average of the interior microphones. Measurements of airborne sound outside the aircraft using a flush-mounted microphone (see App. B) can then be used in conjunction with these cabin noise reduction measurements to predict the sound levels entering the cabin via the various paths.

C.3 Test Results

C.3.1 Cabin Noise Reduction

To obtain estimates of the noise reduction associated with each panel of the cabin, we began by making measurements of interior noise due to each source with the cabin fully "wrapped." Figure C.5 shows the change in cabin interior noise as a consequence of wrapping the cabin in glass fiber and leaded vinyl as described above. The wrapping reduced the noise in the cabin by 5 to 25 dB in every one-third octave band except 160 Hz, 200 Hz, and 315 Hz. We then exposed the panel of interest and measured the change in cabin interior noise. Figure C.6 shows the fuselage configuration for windshield and side window measurements. As mentioned earlier, in many cases exposing a panel resulted in a negligible increase in cabin interior noise. In fact, for the propeller source, the noise in the cabin changed significantly only when the roof, windshield, or firewall was exposed to the sound field. For the engine noise source, only uncovering the firewall increased the cabin noise, and for the exhaust noise source, only uncovering the underbelly of the aircraft or one skin panel had any effect on cabin noise.

The noise reduction for the firewall, roof, and windshield with the propeller source operating is shown in Figs. C.7, C.8, and C.9, respectively. At the bottom of the figures is the increase in noise in each one-third octave band from the fully

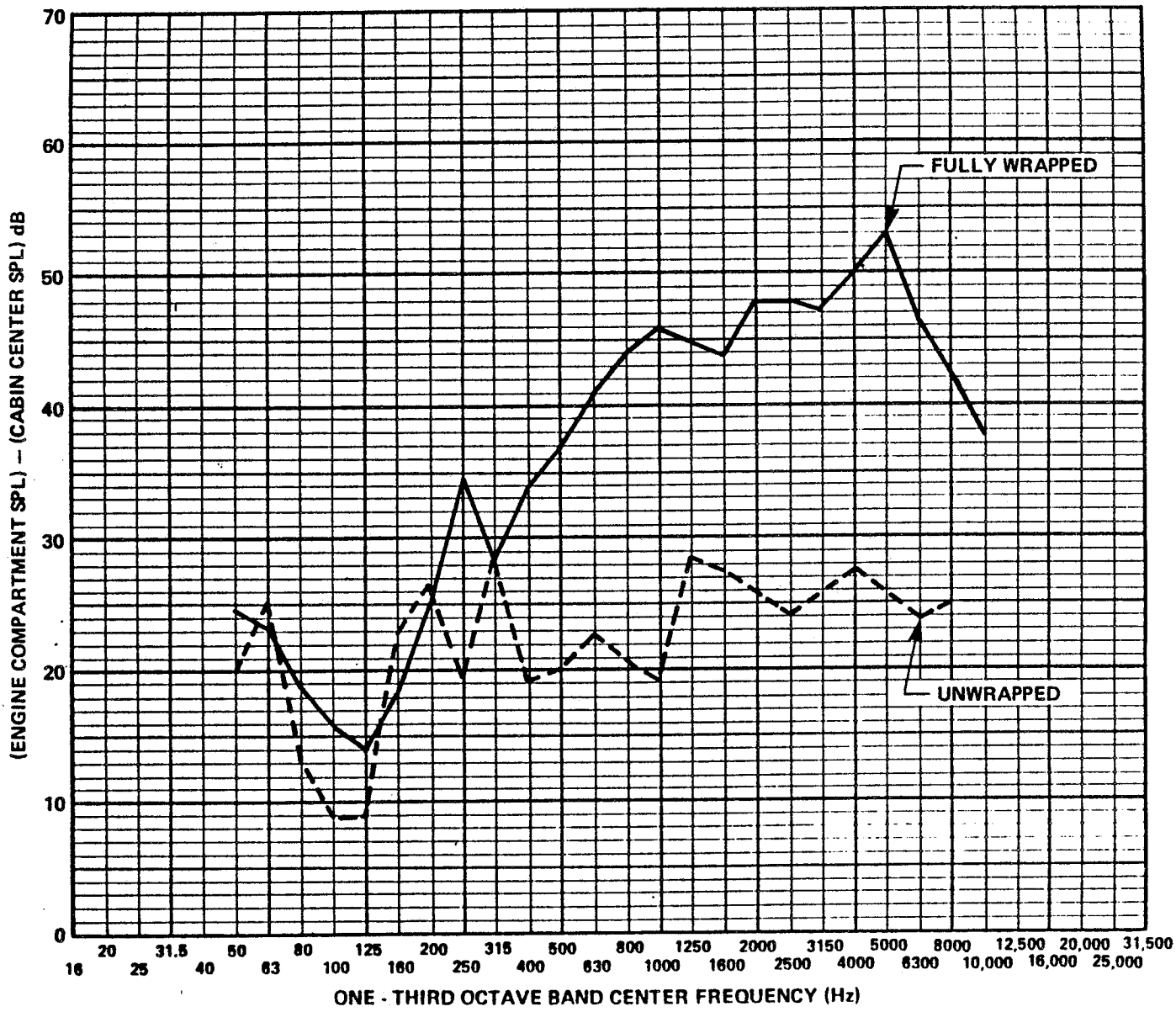

FIGURE C.5. COMPARISON OF CABIN INTERIOR NOISE WRAPPED AND UNWRAPPED (PROPELLER SOURCE).

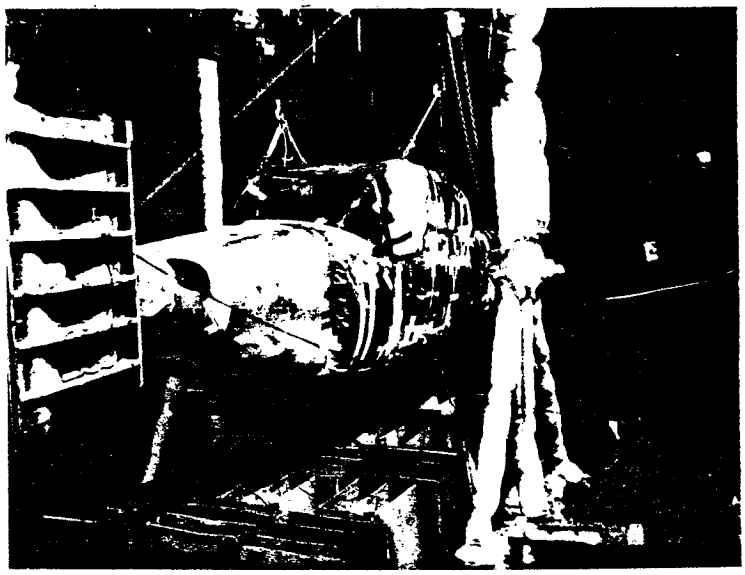

WINDSHIELD

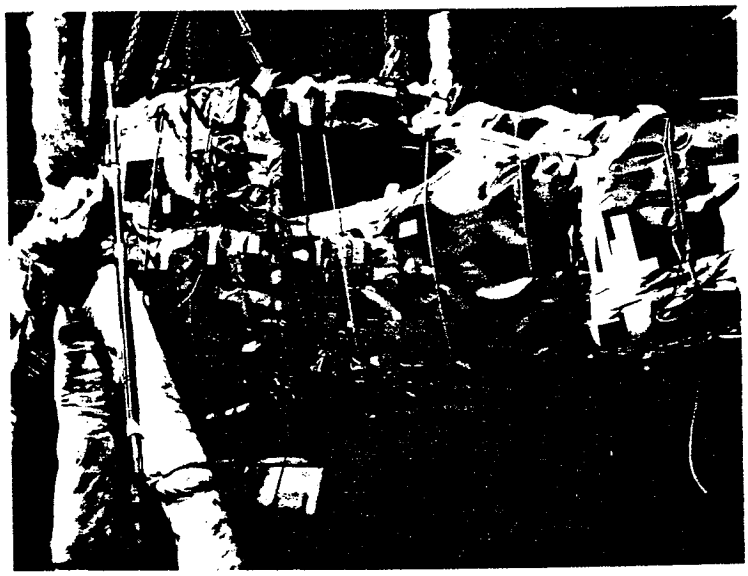

SIDE WINDOW

FIGURE C.6. FUSELAGE CONFIGURATION FOR THE NOISE REDUCTION MEASUREMENTS OF WINDSHIELD AND SIDE WINDOW.

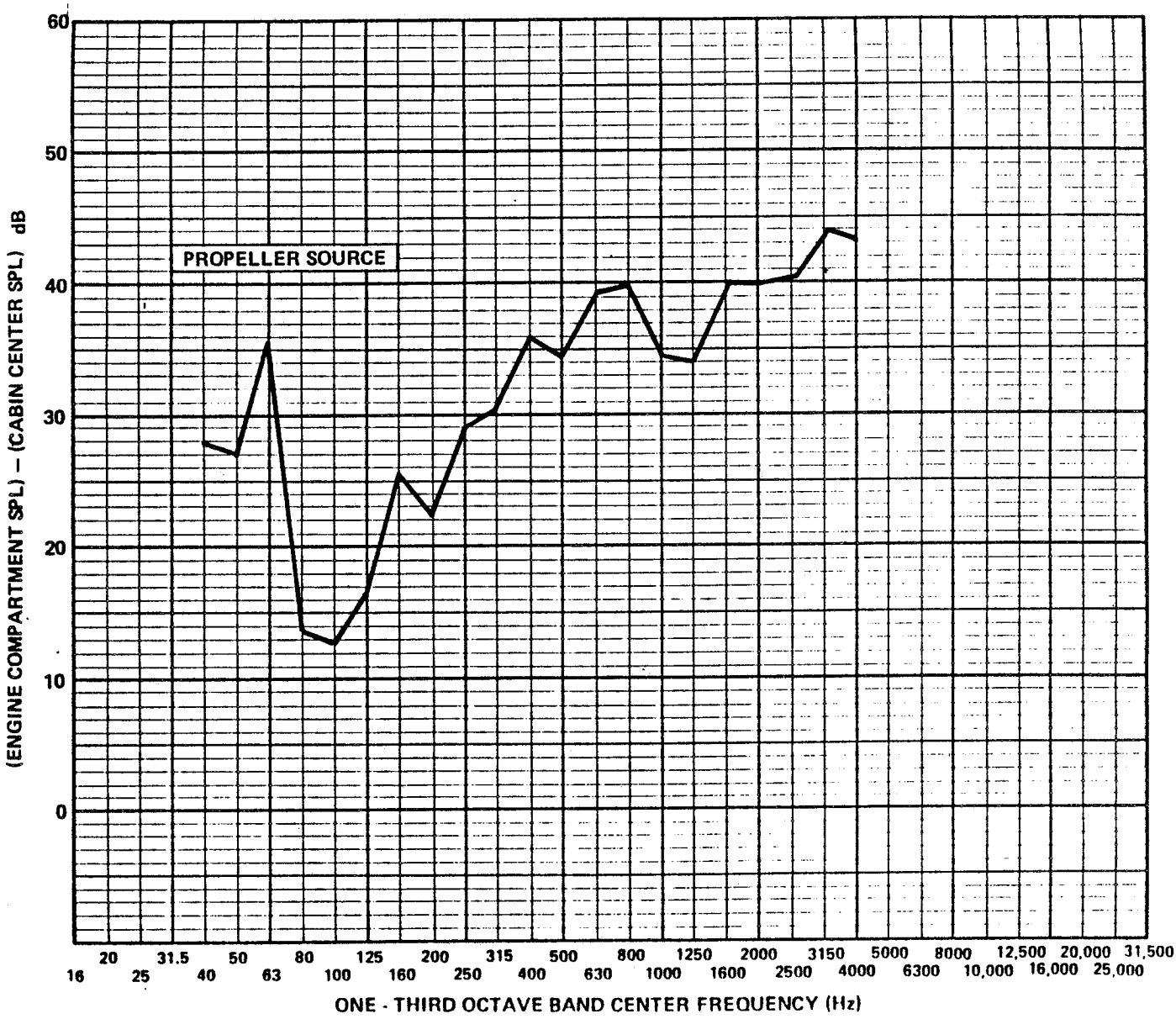

FIGURE C.7. NOISE REDUCTION THROUGH THE UNSTIFFENED FIREWALL.

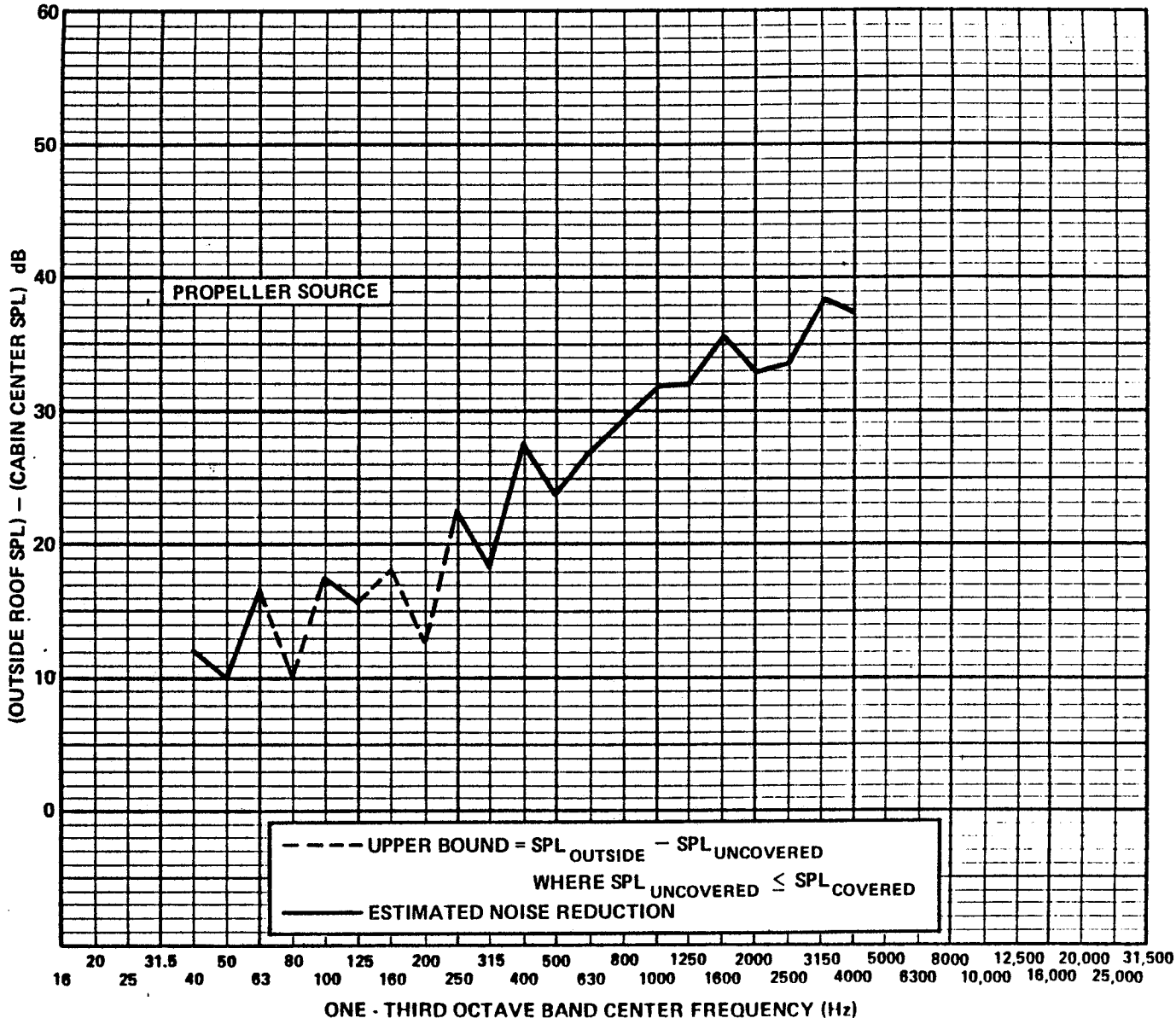

FIGURE C.8 NOISE REDUCTION THROUGH THE ROOF.

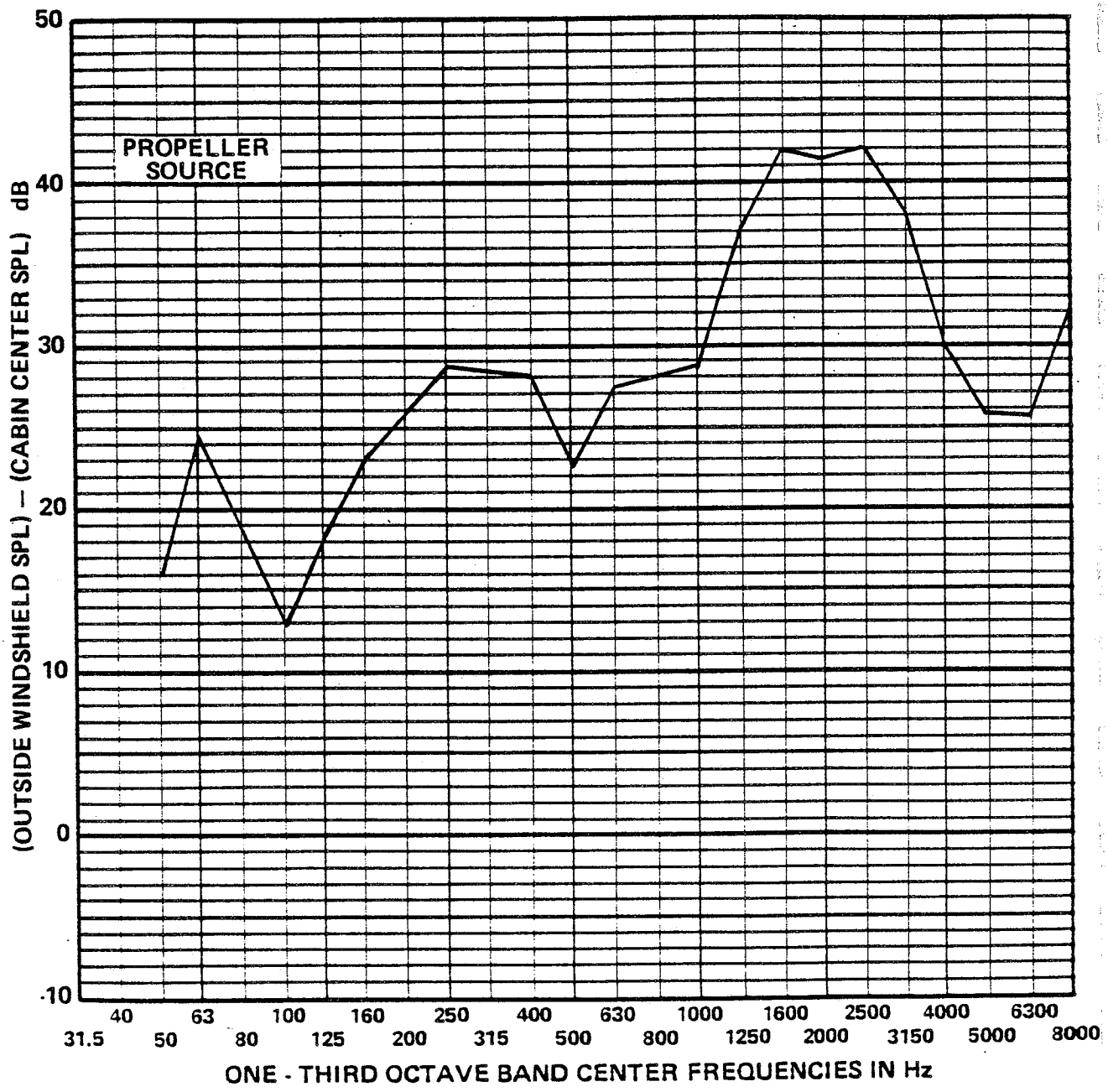

FIGURE C.9 NOISE REDUCTION THROUGH THE WINDSHIELD.

covered condition, caused by uncovering the panel of interest. In some bands, the noise did not increase or decreased slightly, making it impossible to estimate the noise reduction at those frequencies. Where an increase did occur, we corrected the cabin sound level by

$$SPL_{corrected} = SPL_{uncovered} - SPL_{fully\ covered},$$

where (1) $SPL_{uncovered}$ is the sound pressure level in the cabin after remvoving the covering on the panel of interest and $SPL_{covered}$ is the cabin sound pressure level with all panels covered; and (2) $A - B = 10 \log (10^{A/10} - 10^{B/10})$ for the engine source, the firewall noise reduction is shown in Fig. C.10 and agrees reasonably well with Fig. C.7. For the exhaust source, the noise reduction for the right shin panel and the cabin floor is shown in Figs. C.11 and C.12, respectively. The noise reduction of the rear bulkhead (for airborne sound in the tail cone) is shown in Fig. C.13.

The data in Figs. C.7 through C.13 show numerous "peaks and valleys" which are thought to be associated with radiation from frame elements (which have much lower coincidence frequencies than the skin), curvature effects, resonances of the built-up structure (including "multi-wall" effects of existing trim panels), and at low frequencies, coupling with acoustic modes of the cabin. These peaks and valleys can be troublesome in achieving the broadband reductions required for this aircraft. However, at low frequencies the valleys (frequencies at which abnormally low noise reduction occurs) can be shifted in frequency by structural stiffening, mass additions, or double wall structures, so that these low noise reductions do not occur at those frequencies associated with propeller or engine firing fundamental frequencies and their harmonics; such shifting can produce large incremental reductions of propeller and engine noise transmission through a particular path.

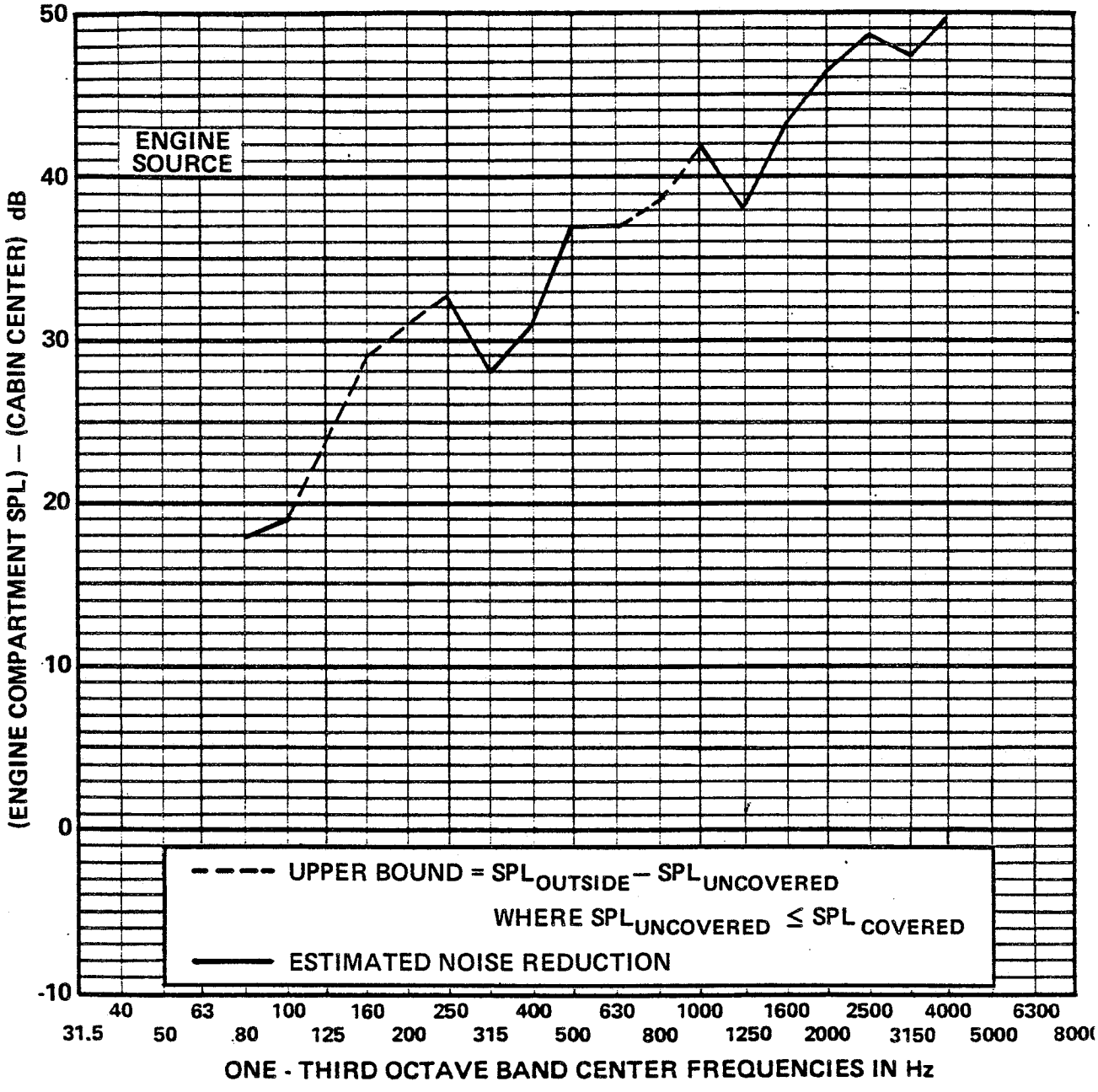

FIGURE C.10 FIREWALL NOISE REDUCTION FOR THE ENGINE SOURCE.

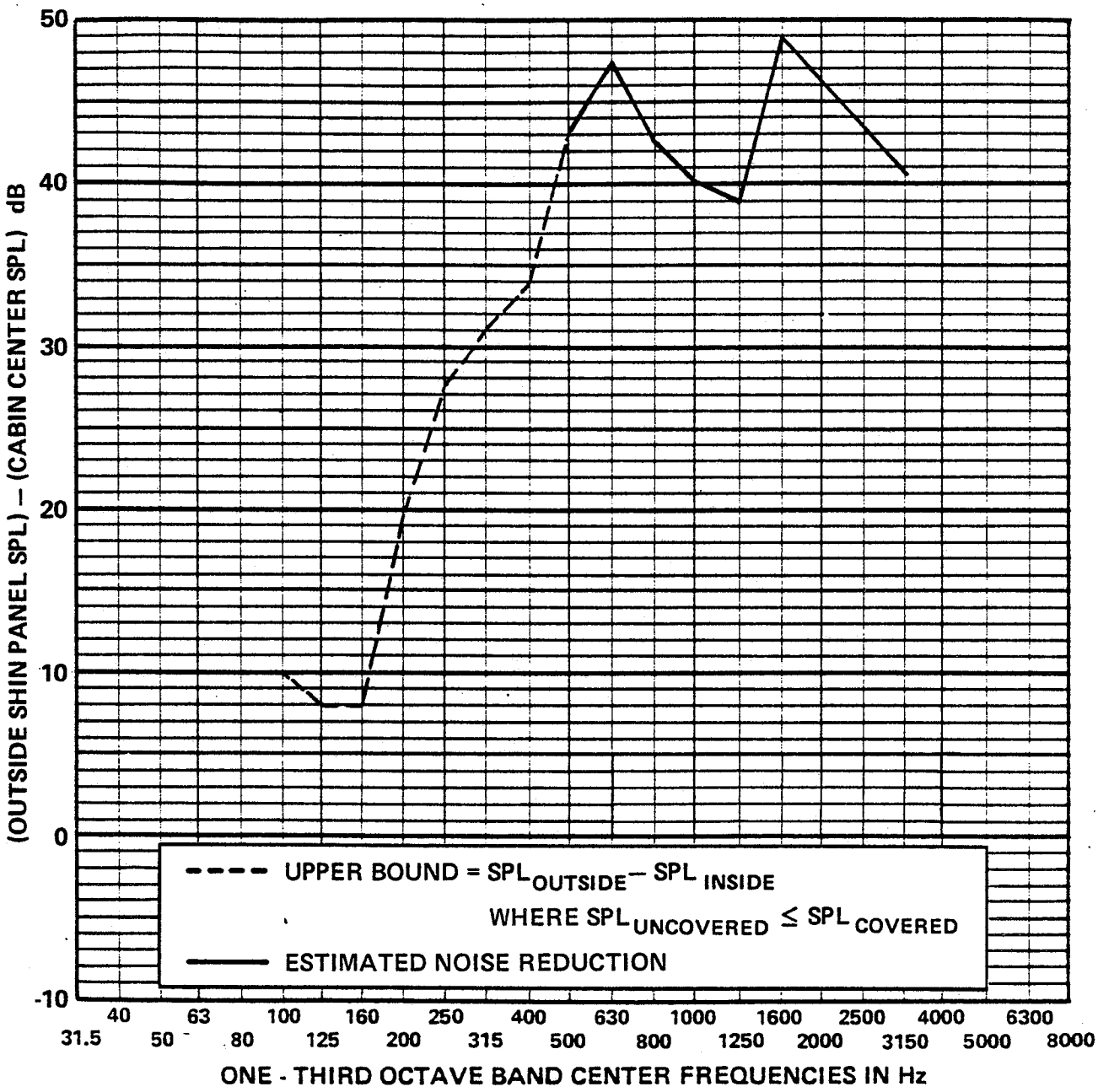

FIGURE C.11. NOISE REDUCTION OF THE RIGHT SHIN PANEL (EXHAUST SOURCE).

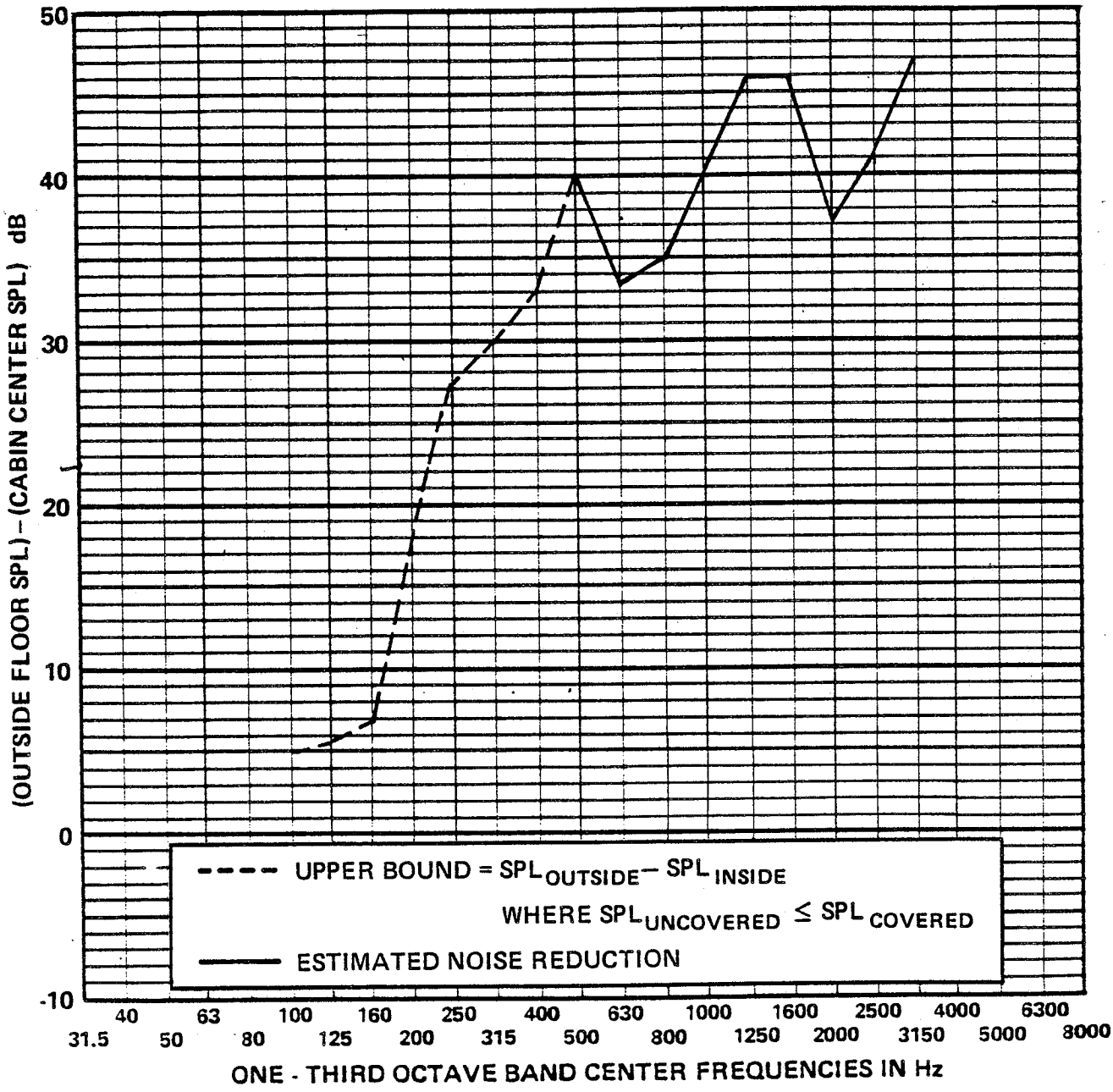

FIGURE C.12 NOISE REDUCTION OF CABIN FLOOR (EXHAUST SOURCE).

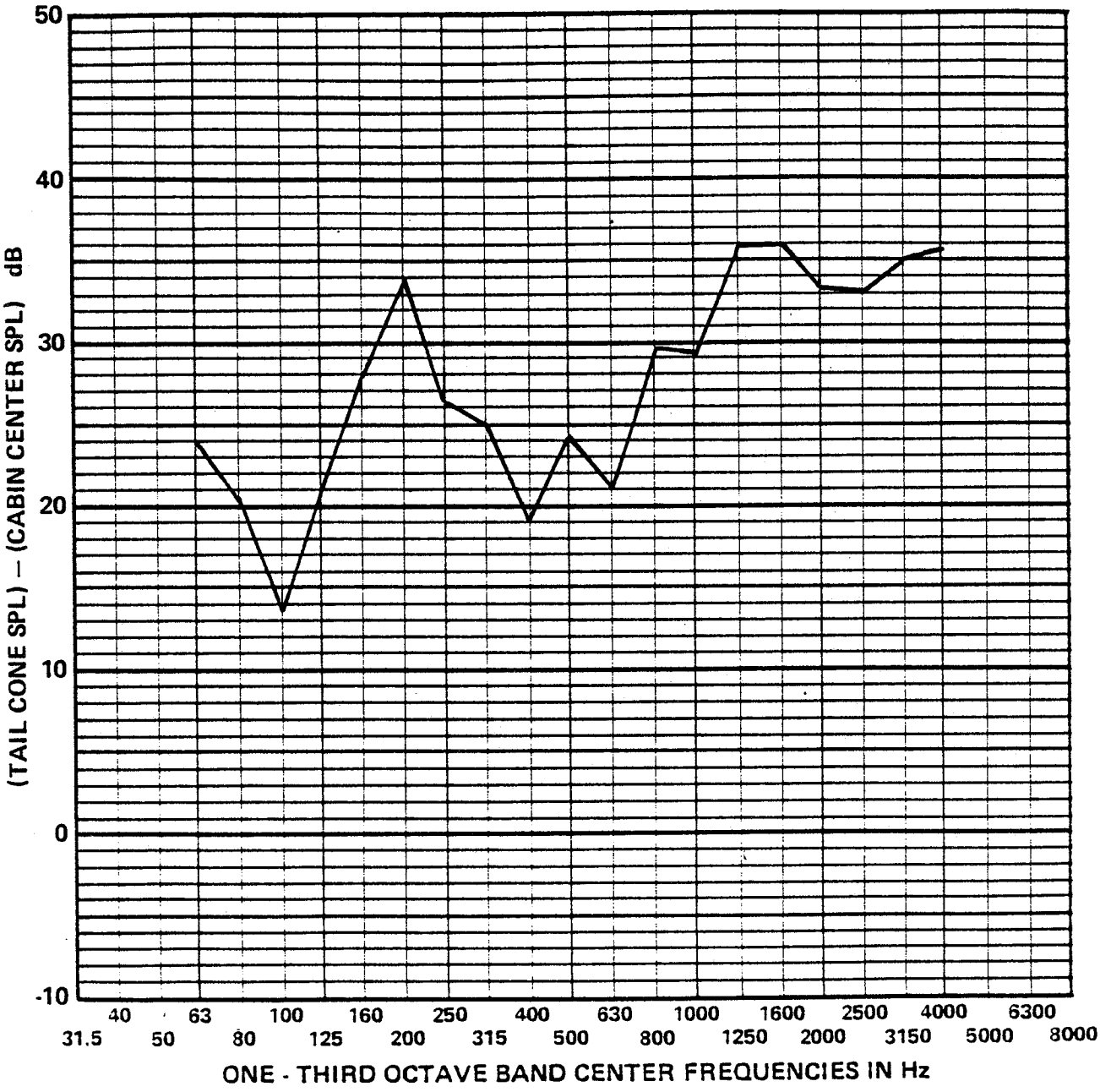

FIGURE C.13 NOISE REDUCTION OF THE REAR BULKHEAD (TAIL CONE SOURCE).

C.4 Comparison with Theoretical Transmission Loss

The above test results can be transformed from noise reduction to transmission loss (TL) through the following equation:

$$TL = 10 \log \frac{\overline{p^2}_{cabin}}{p^2_{outside}} + 10 \log(\alpha S_{cabin}) - 10 \log(S_{panel}), \quad (C.1)$$

where αS_{cabin} is the room constant for the cabin and S_{panel} is the projected area of the panel of interest normal to the direction of sound propagation. For the windshield, 6 dB must be added to the right side of the equation because the outside microphone is very close to the surface, and one would expect the sound pressure at the microphone to be twice the incident sound pressure. The area of the firewall and the projected area of the windshield are each about 1 m^2,and the area of the roof is about 1.5 m^2. The room constant for the cabin was measured using a calibrated sound source (ILG Blower); the values of room constant shown in Table C.1 are based on the average noise level at 4 locations in the cabin for three source positions. Figure C.14 compares the predicted transmission loss of the firewall with the transmission loss estimated from the noise reduction measurements. The firewall is a fairly complicated structure made up of a number of stiffeners and double thicknesses of aluminum sheet. Using an assumed thickness of 0.063 in. and using mass law with coincidence effects, we have generated a predicted transmission loss that agrees well with measurements.

For the windshield and roof, similar comparisons are shown in Figs. C.15 and C.16, respectively. For the predictions at these locations, we have used the random incidence mass law since it appears most appropriate when the sound is nearly at grazing incidence. The predictions agree well with measurements for the windshield, they are but underestimated when compared with the measurements for the roof. The roof has a great deal of fiberglass and vinyl trim that is not accounted for in our simple model; these materials may account for the increased TL.

Table C.1

ROOM CONSTANT FOR THE CESSNA R182 CABIN

1/3 Octave Center Frequency (Hz)	Sabine Absorption Coefficient (dB re $1m^2$)
100	2.0
125	5.6
160	5.1
200	5.9
250	3.2
315	9.3
400	10.0
500	11.1
630	8.7
800	8.6
1000	9.3
1250	8.5
1600	8.0
2000	9.0
2500	8.3
3150	8.7
4000	8.5
5000	8.4
6300	8.2
8000	8.9
10,000	7.7

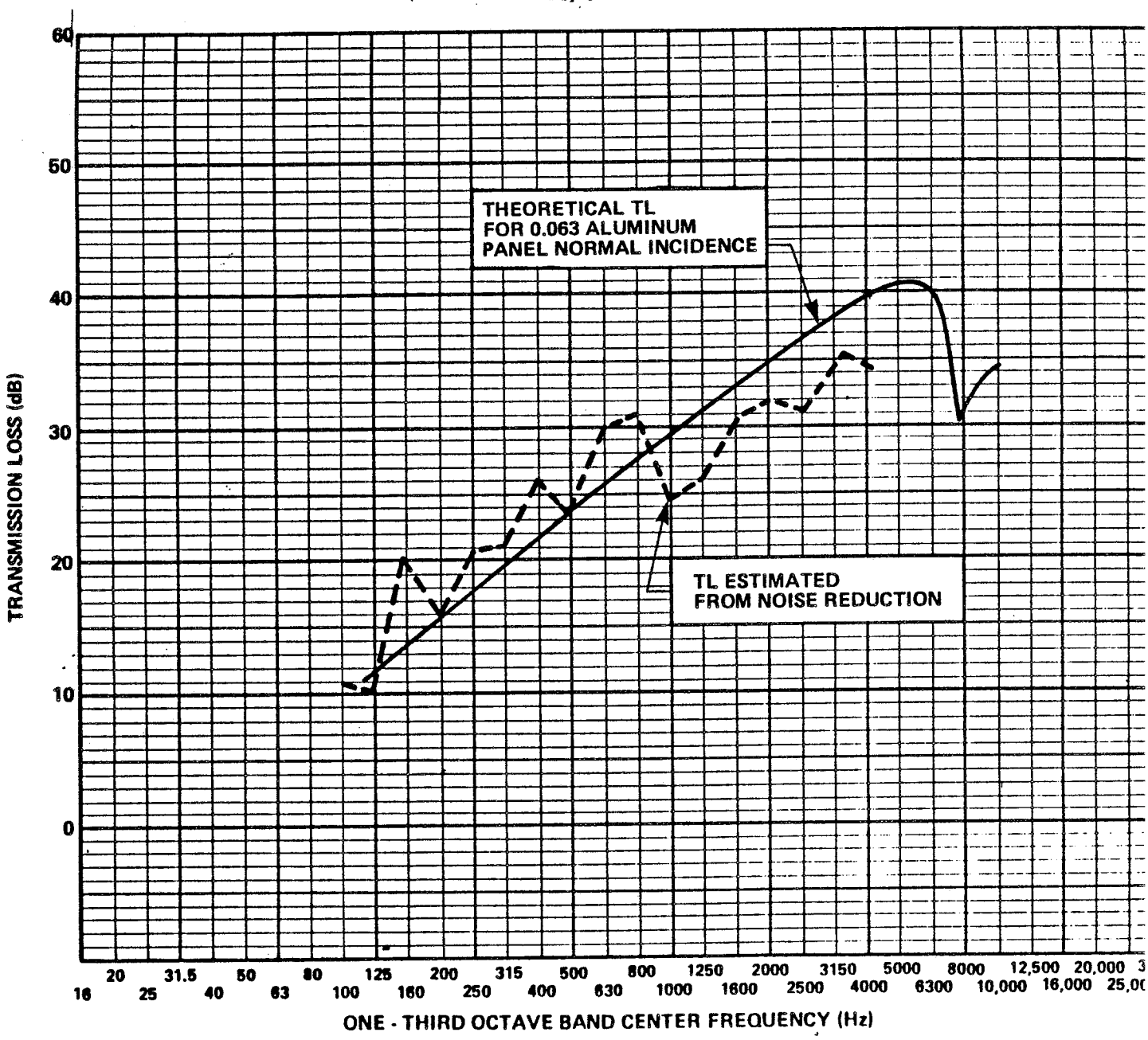

FIGURE C.14. FIREWALL TRANSMISSION LOSS: COMPARISON OF THEORY AND MEASUREMENT.

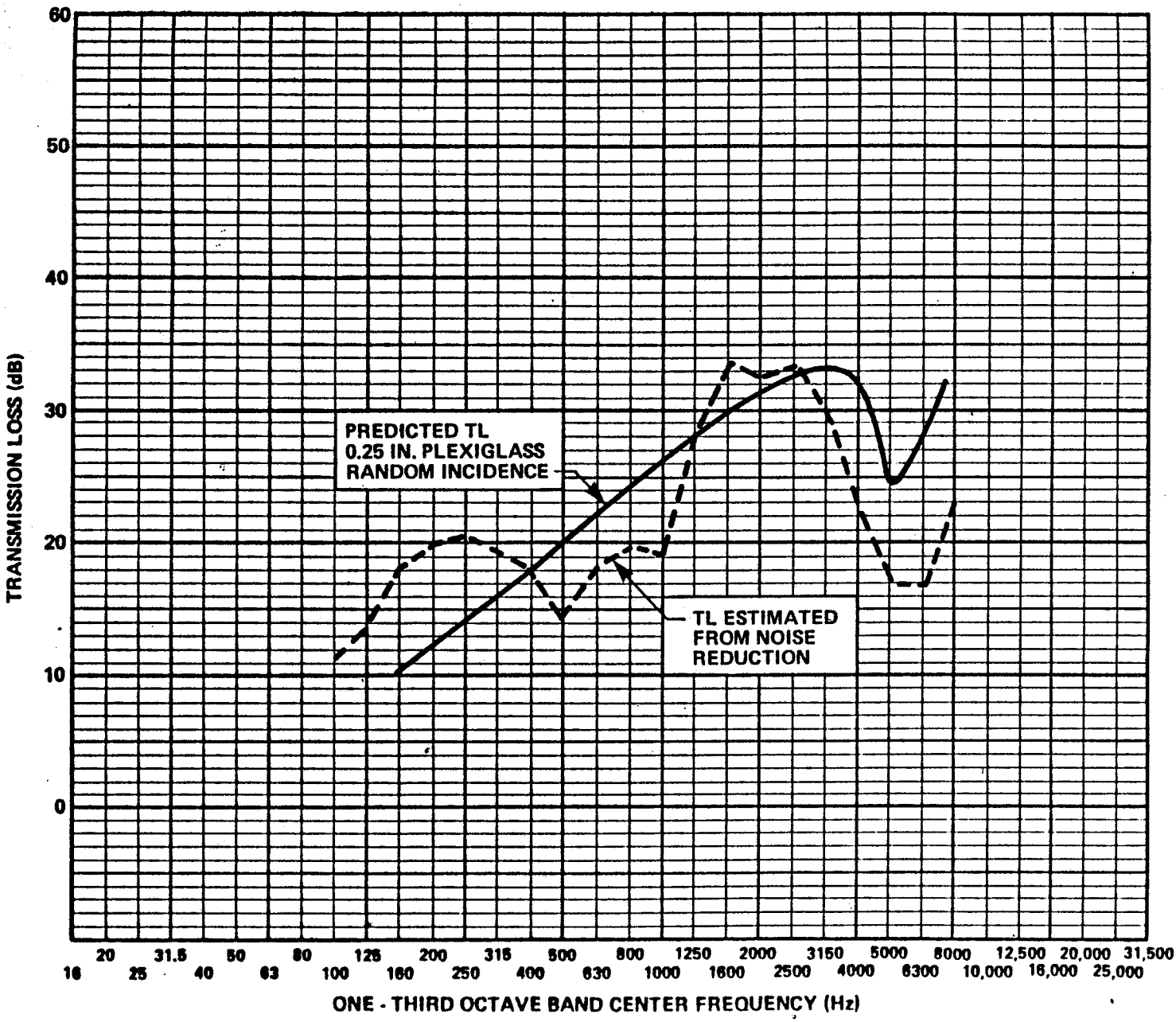

FIGURE C.15. WINDSHIELD TRANSMISSION LOSS: COMPARISON OF PREDICTIONS AND MEASUREMENTS.

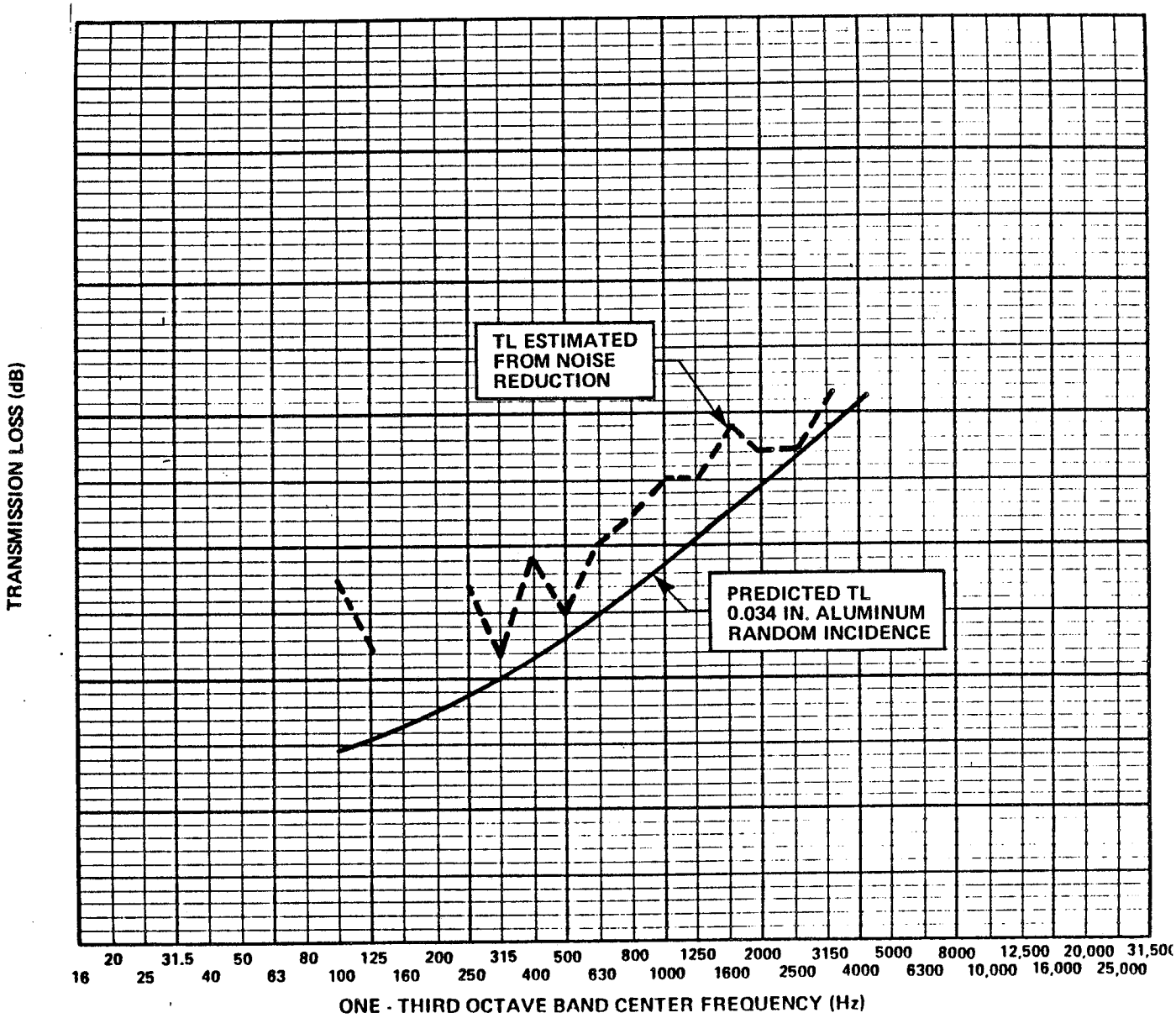

FIGURE C.16. ROOF TRANSMISSION LOSS: COMPARISON OF PREDICTIONS AND MEASUREMENTS.

C.5 Improved Noise Reduction Due to Firewall Stiffening

An earlier set of measurements that included both laboratory and flight tests (App. F) showed that airborne noise transmission through the firewall occurred primarily in the 80 Hz one-third octave band. To increase the transmission loss of the firewall at so low a frequency generally requires stiffening rather than increased mass. In addition, the shape of the noise reduction versus frequency curve in Fig. C.7 below 125 Hz is characteristic of a panel that is stiffness-controlled. Consequently, we added stiffening beams to the firewall in two stages, as indicated in Fig. C.17. The first stage, which we have called level 1, consisted of just the 1-1/2 x 1-1/2 x 3/16 aluminum angle glued to the center of the firewall, as shown in the figure. Level 2 of stiffening was this angle, plus the 1 x 1 x 3/16 channel attached to the firewall with epoxy in the pattern shown in Fig. C.17. The stiffeners were fastened to the firewall with epoxy because it was convenient to do so. In a production aircraft, the stiffeners would be welded or riveted. The placement of the stiffeners was determined by a vibration survey of the firewall. Two surveys were carried out with the excitation provided by the speaker simulating the propeller. The first survey identified the center of the firewall, an area of high vibration, as suitable for a stiffener. The 1-1/2 x 1-1/2 x 3/16 angle was glued on and the survey repeated. Again areas of high vibration were selected as likely sites for the addition of stiffeners and the 1 x 1 x 3/16 channels were glued to those locations.

Figure C.18 shows the change in noise reduction due to the addition of the stiffeners. Level 1 of stiffening gave a 4 dB increase in noise reduction at 80 Hz, and level 2 gave an additional 4 dB. This implies an 8 dB reduction in airborne sound transmission through the firewall at 80 Hz. At higher frequency, there is no consistent change in the noise reduction as one would expect. To improve the noise reduction at higher frequency, a double walled construction or simply a thicker firewall would be required.

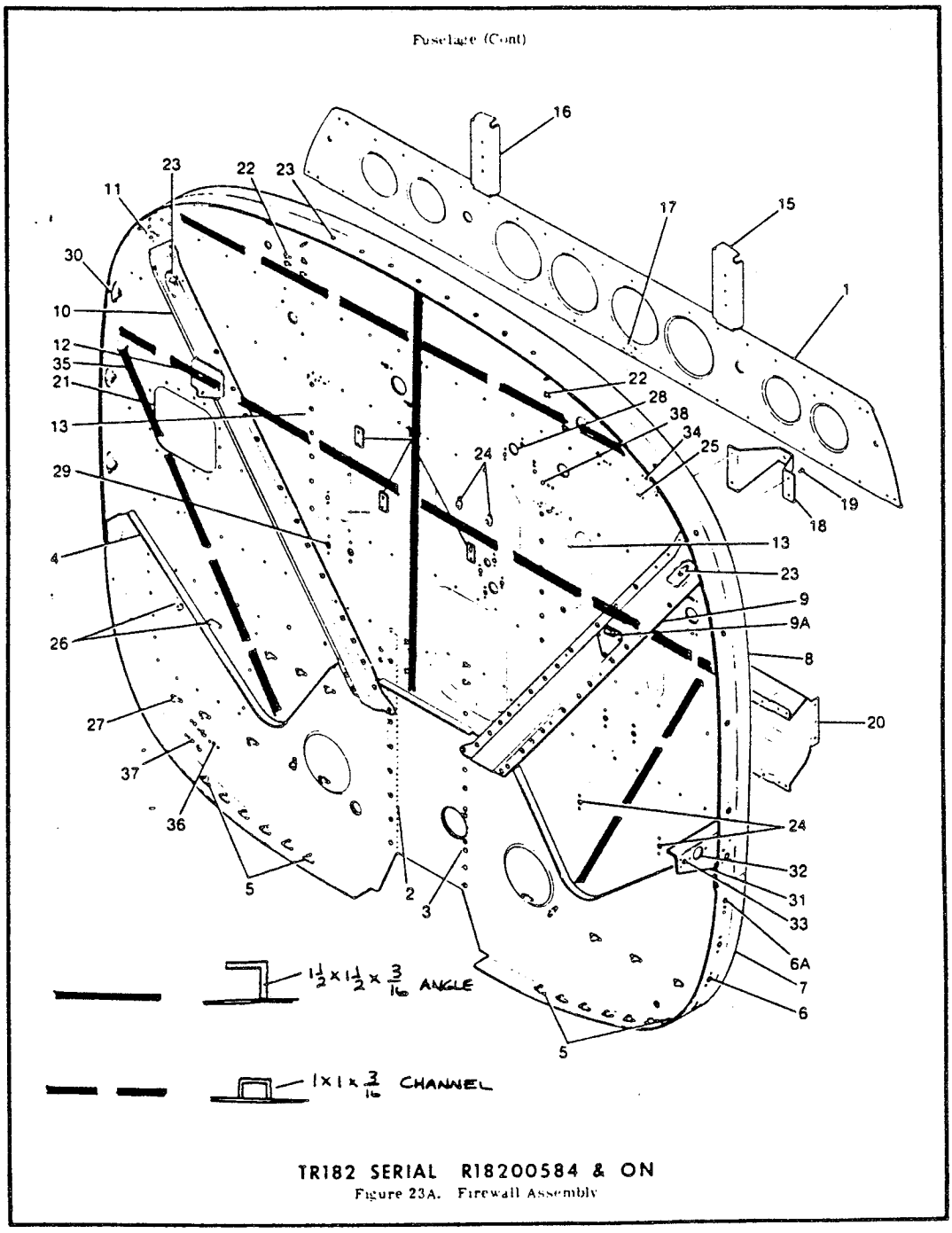

FIGURE C.17. PLACEMENT OF FIREWALL STIFFENERS.

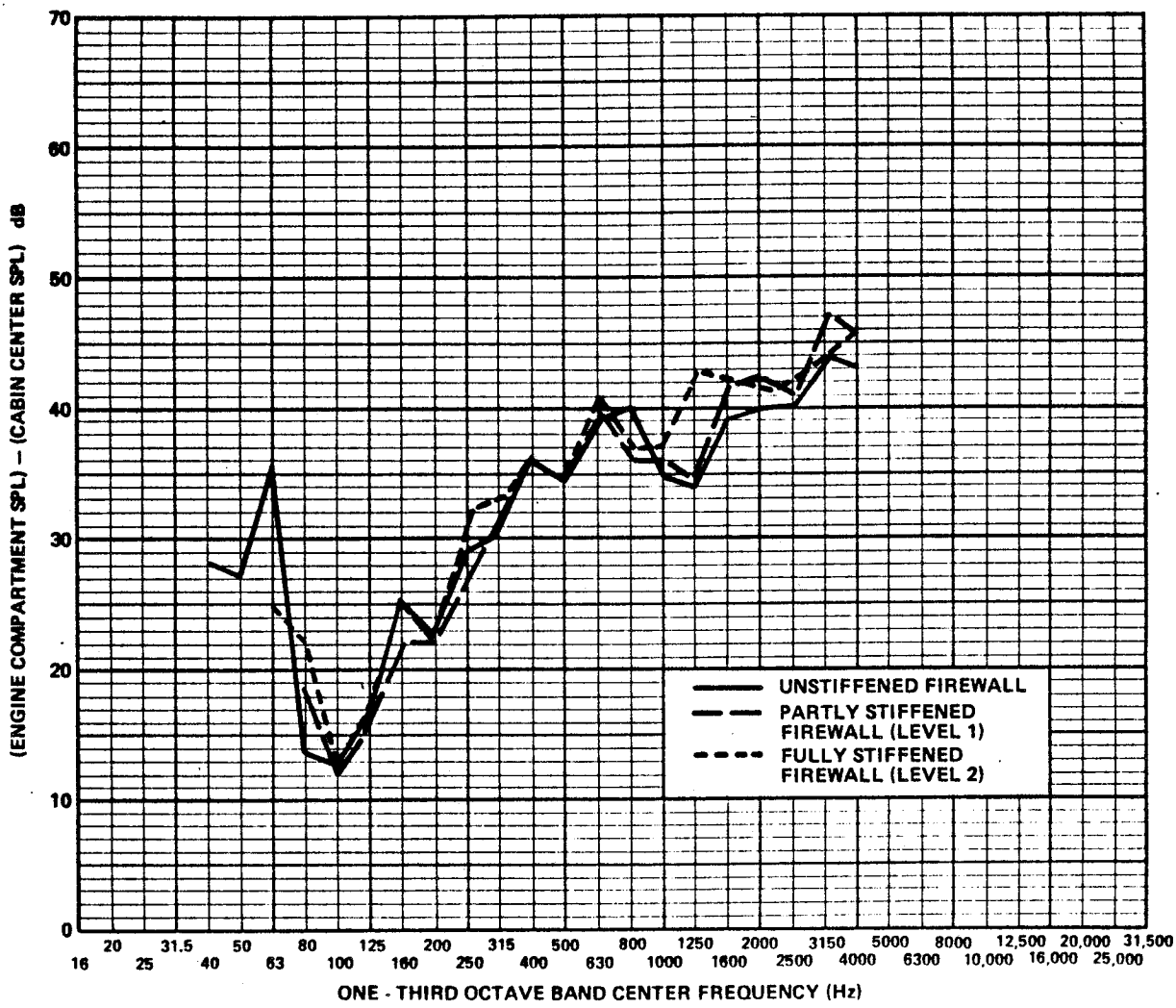

FIGURE C.18. CHANGE IN FIREWALL NOISE REDUCTION DUE TO TWO LEVELS OF STIFFENING.

APPENDIX D

CONTRIBUTION AND TREATMENT OF CABIN NOISE RESULTING FROM EXHAUST NOISE

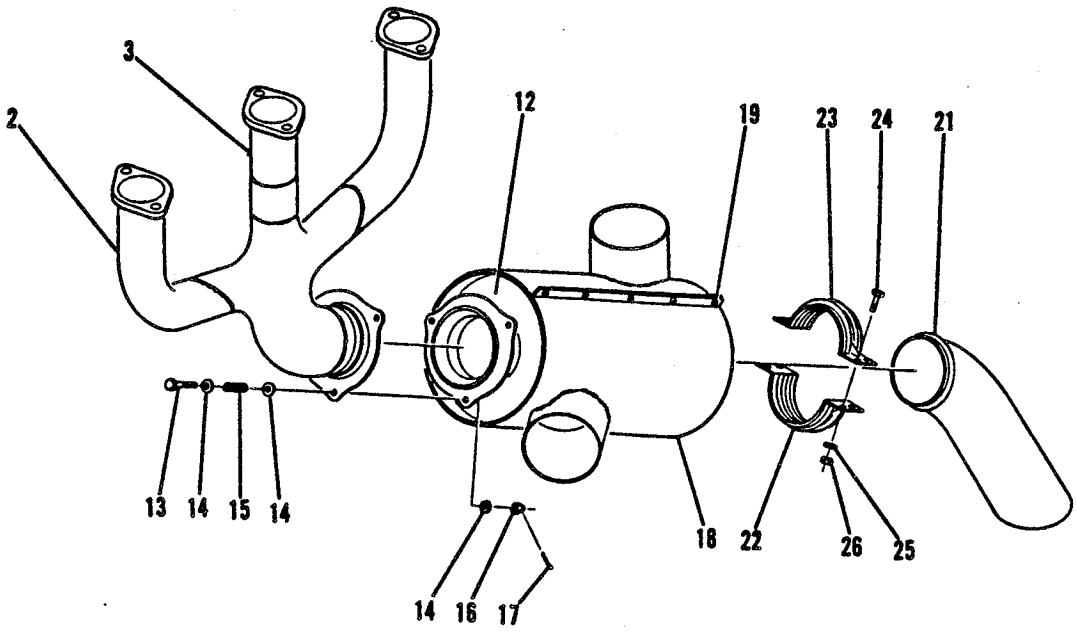

RH SIDE

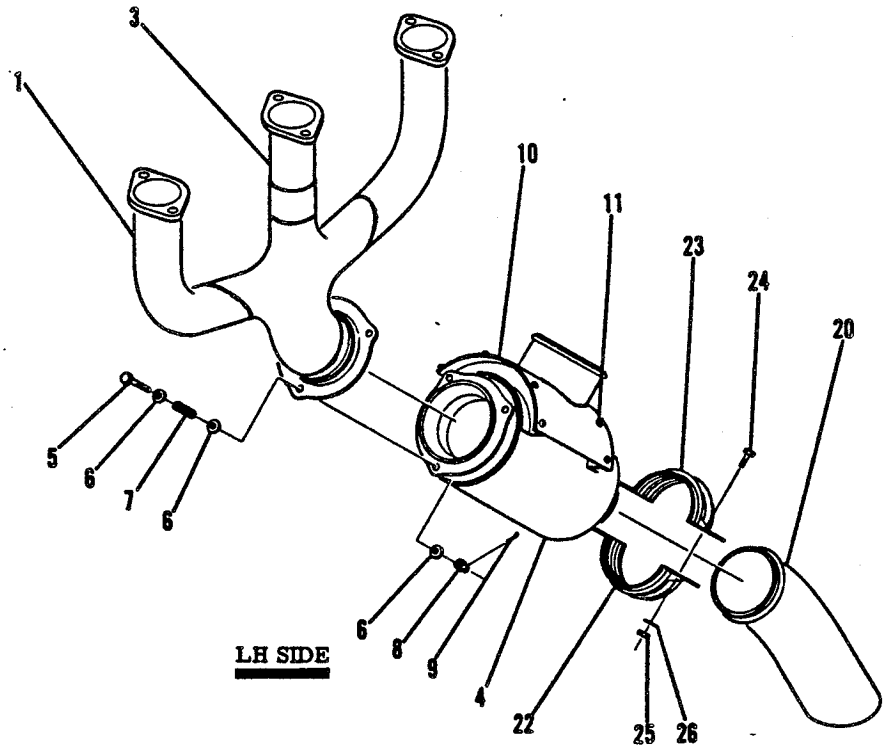

LH SIDE

FIGURE D.1 EXHAUST SYTEM OF R182 (TWO EXHAUST STACKS).

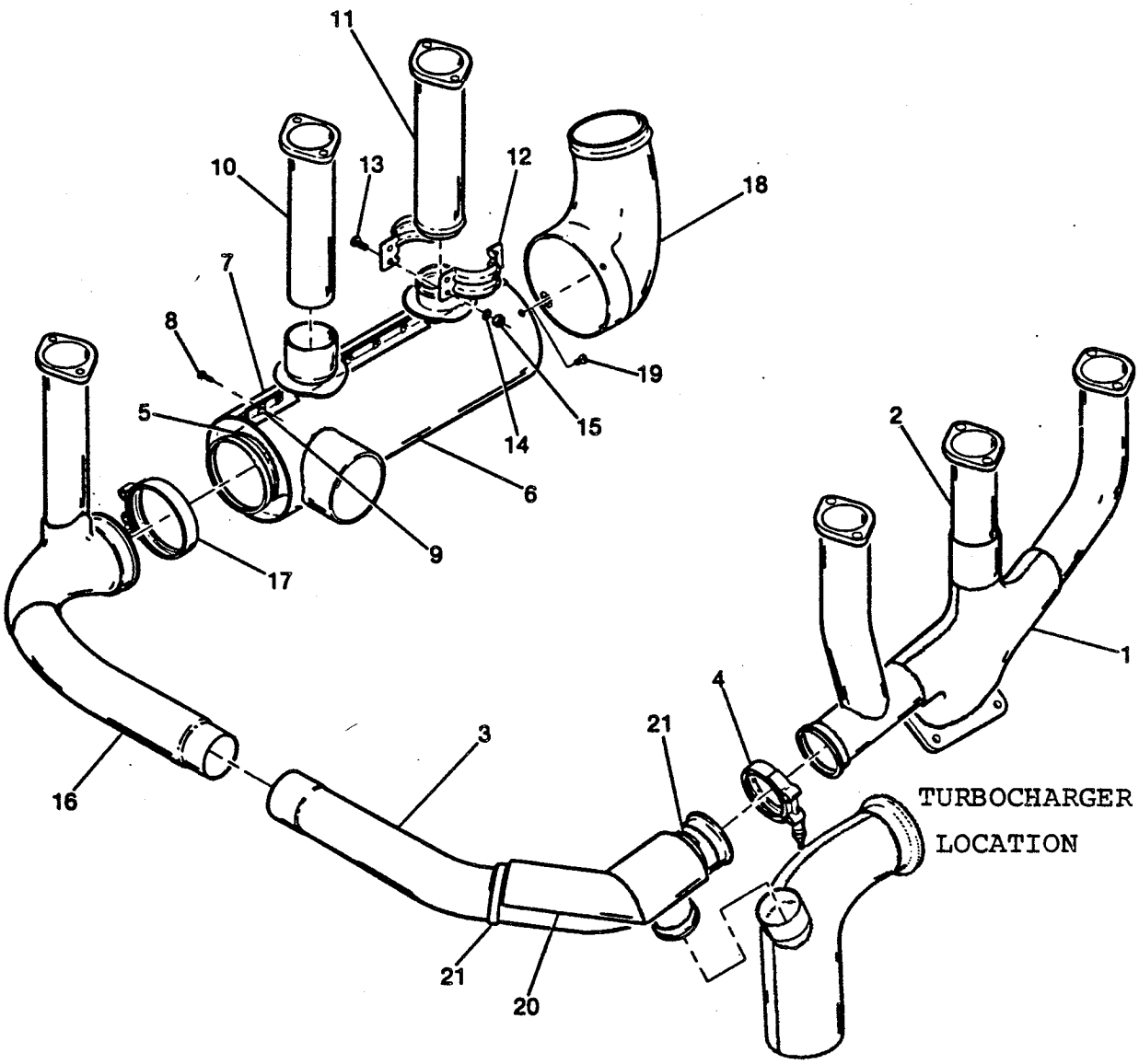

FIGURE D.2 EXHAUST SYSTEM OF TR182 (ONE EXHAUST STACK, TURBO-CHARGED).

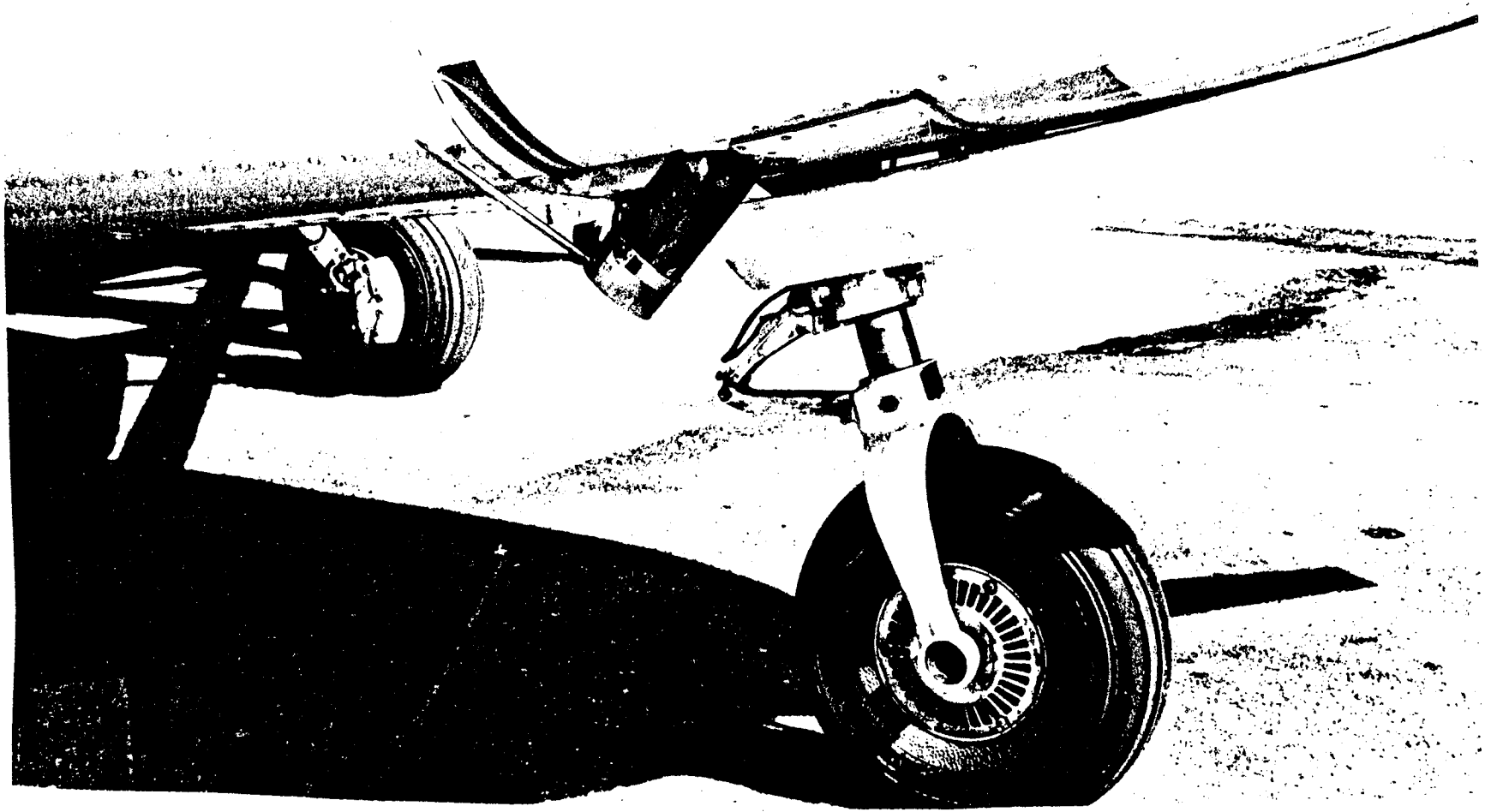

FIGURE D.3 PROBE MICROPHONE MOUNTED ON STARBOARD EXHAUST STACK OF R182.

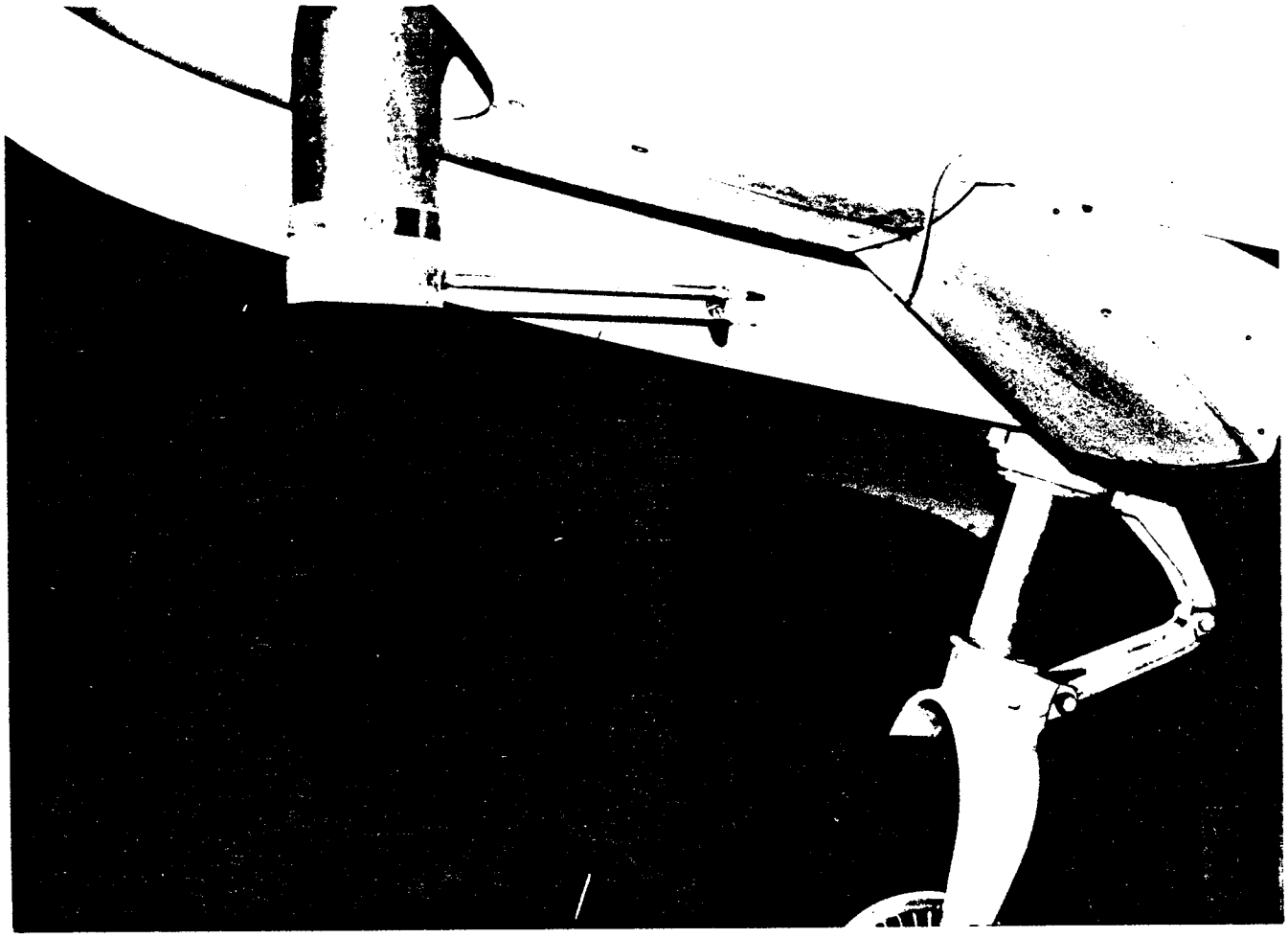

FIGURE D.4 PROBE MICROPHONE MOUNTED ON EXHAUST STACK OF TR182.

In-Pipe Measurements

For the first method, a high-temperature microphone was arranged in a probe tube at the outlet plane of the exhaust stack (see Figs. D.3 and D.4). The gas flow past the probe is hot (≈1120°K) and has a velocity of about M = 0.2 (relative to the atmosphere). The relationship between the acoustic pressure measured at the exit plane of the stack and the farfield acoustic pressure can be estimated as follows.

Consider the geometry shown in Fig. D.5.

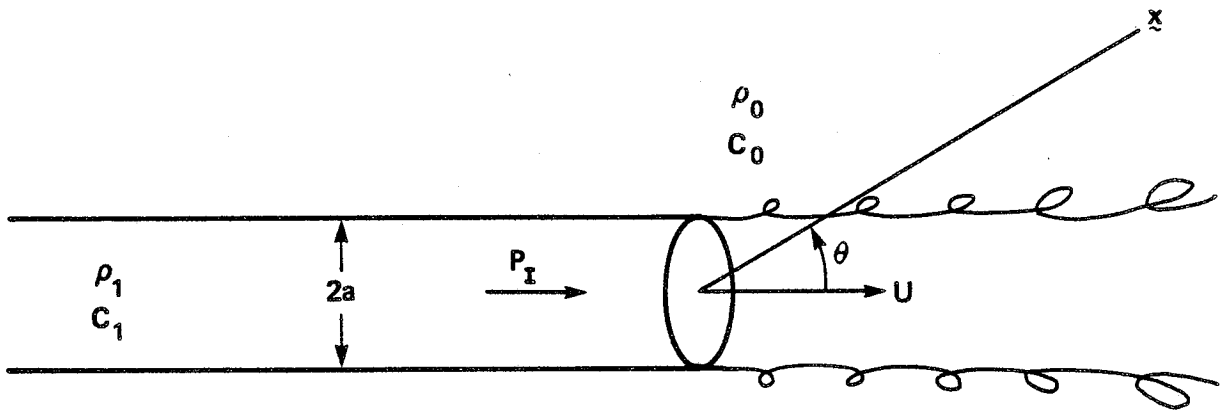

FIGURE D.5 SCHEMATIC OF EXHAUST PIPE.

Assume that: $a << \lambda$ (acoustic wavelength)

$\frac{\omega a}{U}$ is small (ω = radian frequency);

M_j ($= U/c_1$) is small (up to 0.3).

Let $p_I e^{ik_1 x_1/(1+M_j)}$ denote the presssure perturbation incident on the pipe exit from upstream. The corresponding incident power flux W_o is

$$W_o = \frac{\pi a^2 (1+M_j)^2}{\rho_1 c_1} p_I^2. \qquad (D.1)$$

From Eq. (4.2) of [Ref. D.2], the acoustic pressure p_a satisfies

$$\frac{p_a^2}{\rho_0 c_0} = \frac{W_0 \frac{\rho_0 c_0}{\rho_1 c_1} (k_0 a)^2}{4\pi |\underset{\sim}{x}|^2 (1-M_0 \cos\theta)^4 (1+M_j)^2} \qquad (D.2)$$

when $\upsilon \simeq 1$, $\zeta = \mu << 1$, $M_j^2 << 1$.

Hence, using Eqs. (D.1) and (D.2).

$$p_a^2 = 1/4\, p_I^2 \left(\frac{\rho_0 c_0}{\rho_1 c_1}\right)^2 (k_0 a)^2 \left(\frac{a}{|\underset{\sim}{x}|}\right)^2 \frac{1}{(1-M_0 \cos\theta)^4}. \qquad (D.3)$$

In the pipe, the net pressure perturbation is given by

$$p_D = p_I \left[e^{ik_1 x_1/(1+M_j)} + R\left(\frac{1+M_j}{1-M_j}\right) e^{-ik_1 x_1/(1-M_j)} \right], \qquad (D.4)$$

where for low values of Mach number, Strouhal number and for a pipe opening:

$$R \simeq -\ 1-2M_j - \tfrac{1}{2}(k_0 a)^2\ (\frac{\rho_0 c_0}{\rho_1 c_1}) + 2ik_1\lambda. \qquad (D.5)$$

(See Eq. (3.29) of Ref. D.2.)

Using (D.5) in Eq. (D.4), expanding for small M_j and $k_1 x_1$ so that x_1 is well within an acoustic wavelength of the pipe exit plane, where $x_1=0$:

$$p_D = p_I \cdot\ 2ik_1(x_1-\lambda). \qquad (D.6)$$

(Note: $x_1<0$ in the pipe)

Let L = distance upstream of nozzle exit at which p_D is measured,

$$\text{then } p_D = -\frac{2i\omega}{c_1}\ (L+\lambda)p_I\ . \qquad (D.7)$$

Using this in (3):

$$\overline{p_A^2} = \frac{1}{16}\ \overline{p_D^2}\ (\frac{a}{|\underset{\sim}{x}|})^2\ (\frac{a}{L+\lambda})^2 \frac{(\rho_0/\rho_1)^2}{(1-M_0\cos\theta)^4}\ . \qquad (D.8)$$

This relationship holds if standing wave effects in the exhaust system are negligible. The main effect on our measured data at the exhaust stack is to increase the effective radiated acoustic power because of the difference in densities between the heated exhaust and the cool surroundings. The estimated increase in radiated power in the test aircraft is large, being about 12 dB using exhaust gas parameters provided by Avco Lycoming.

Sidewall Measurements

The second method for obtaining exhaust pressures incident upon the sidewall was to attach a small pressure sensor with a

nose cone fairing to the surface of the fuselage near the exhaust stack. This sensor was calibrated in a low-noise wind tunnel where it was shown to sense the acoustic pressure correctly at grazing incidence in the presence of flow at flight speeds (see App. I).

D.3. Review of Available Data on Source Levels and Spectra

Various measured flight data are summarized below. Measurements using the probe microphone have been performed on the normally aspirated R182 and the turbocharged TR182, each fitted with both two- and three-blade propellers (see Fig. D.6). The acoustic pressures at the exhaust stack are 2 to 3 dB lower for the turbocharged version at firing frequency (120 Hz to 2400 rpm cruise). No variation is introduced by changing the number of propeller blades, indicating that this measurement is not contaminated by propeller noise. A narrowband analysis of the noise spectrum measured by the probe microphone is shown in Fig. D.7(a). The resonance of the probe tube is plainly visible and indicates that tone data above about 400 Hz are not reliable. Also shown, in Fig. D.7(b), is a spectrum measured on the wing microphone (described in Ref. 1). The simple assumption of spherical spreading from a small source (the exhaust stack) over a distance of about 1 m to the wing microphone is the basis for the calculated exhaust levels shown. No allowance for temperature differences was made, yet the agreement appears to be reasonable, particularly at the 120 Hz firing frequency.

Flight measurements performed using the surface microphone mounted near the exhaust stack are shown in Figs. D.8 through D.11 for two cruise conditions in both narrow (2.5 Hz) and one-third octave bands. These data were A-weighted at the time of recording because of dynamic range limitations of the recorder. Note that this measurement is contaminated by propeller noise (tones are visible in narrowband plots) and that broadband noise

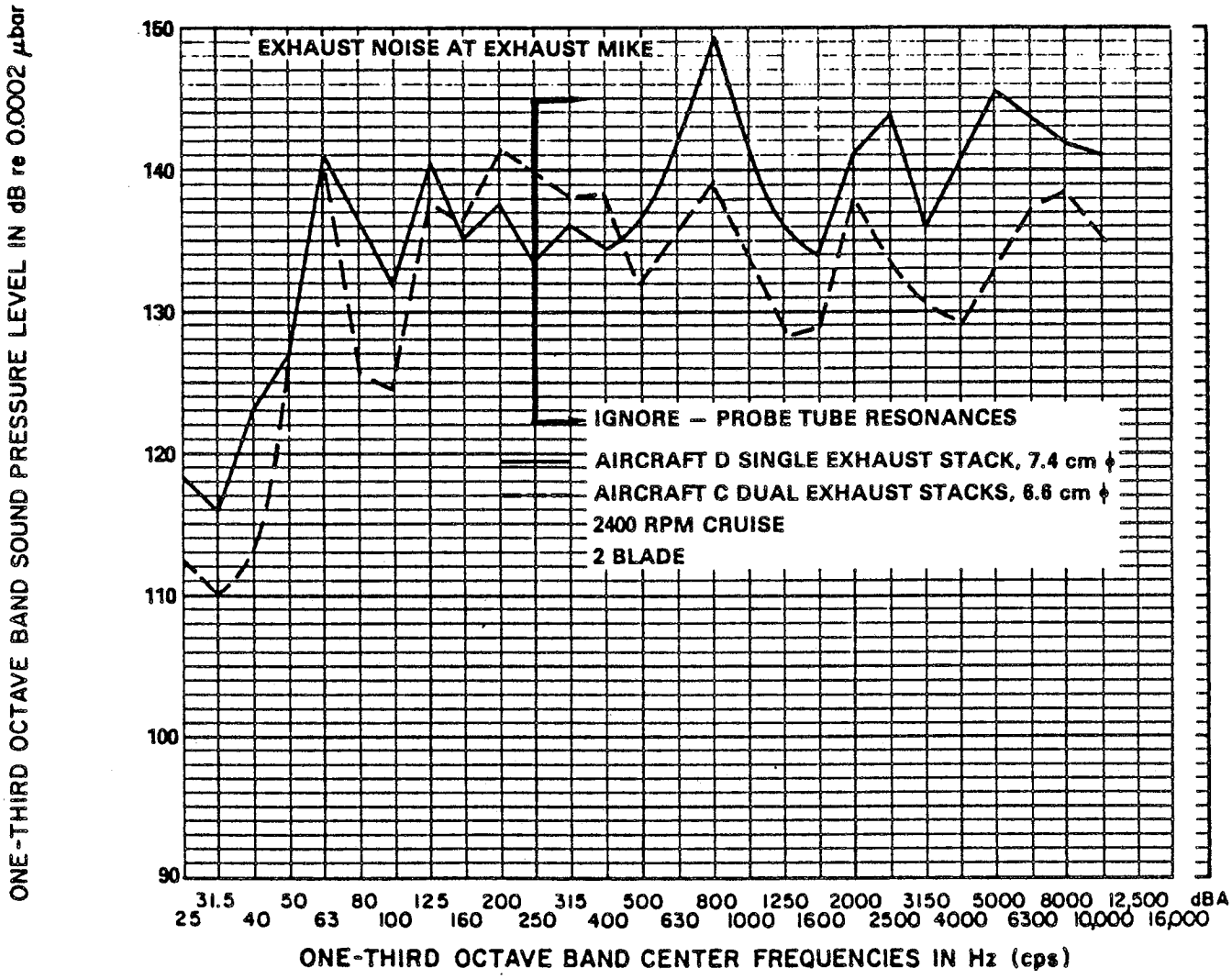

FIGURE D.6 EXHAUST PRESSURES MEASURED NEAR TAILPIPE EXIT IN-FLIGHT (SEE REF. 1).

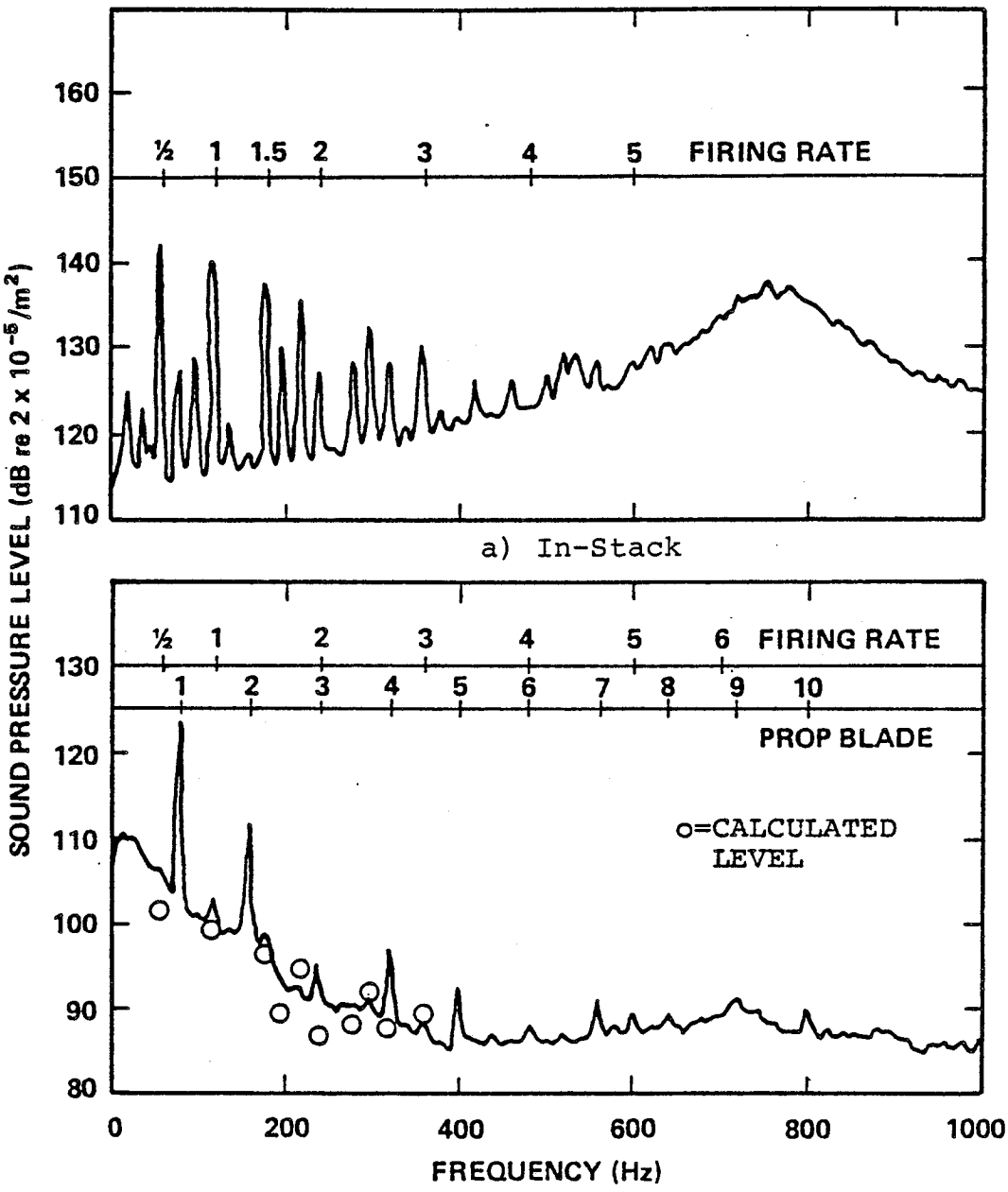

FIGURE D.7 NARROWBAND ANALYSIS OF EXHAUST NOISE AT STACK AND AT WING STRUT MICROPHONE.

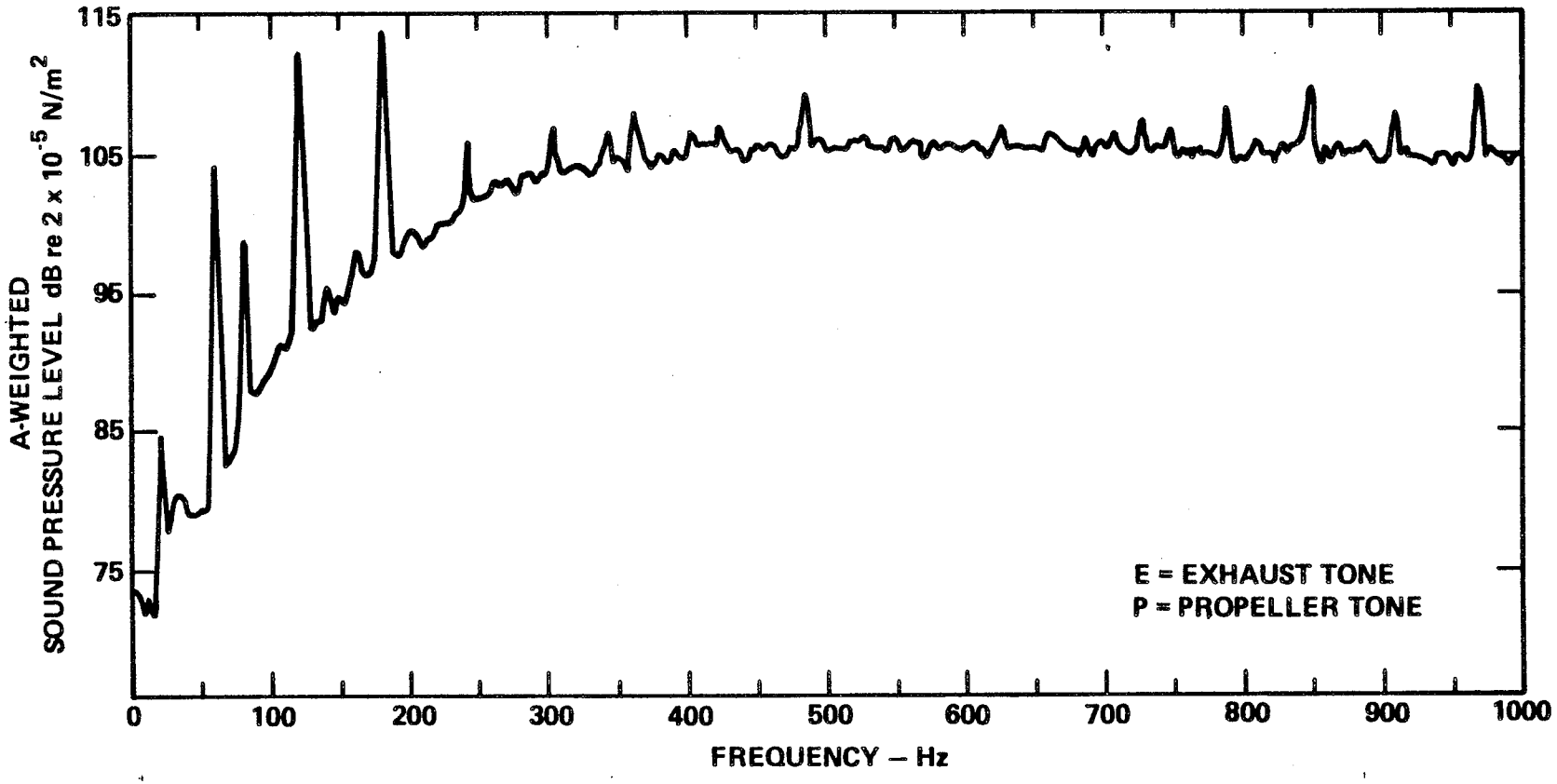

FIGURE D.8 NARROWBARD ANALYSIS OF NOISE AT SURFACE MICROPHONE NEAR STARBOARD EXHASUT STACK. R182 WITH TWO BLADE PROPELLER, CRUISE AT 2400 RPM (2½ Hz BANDWIDTH).

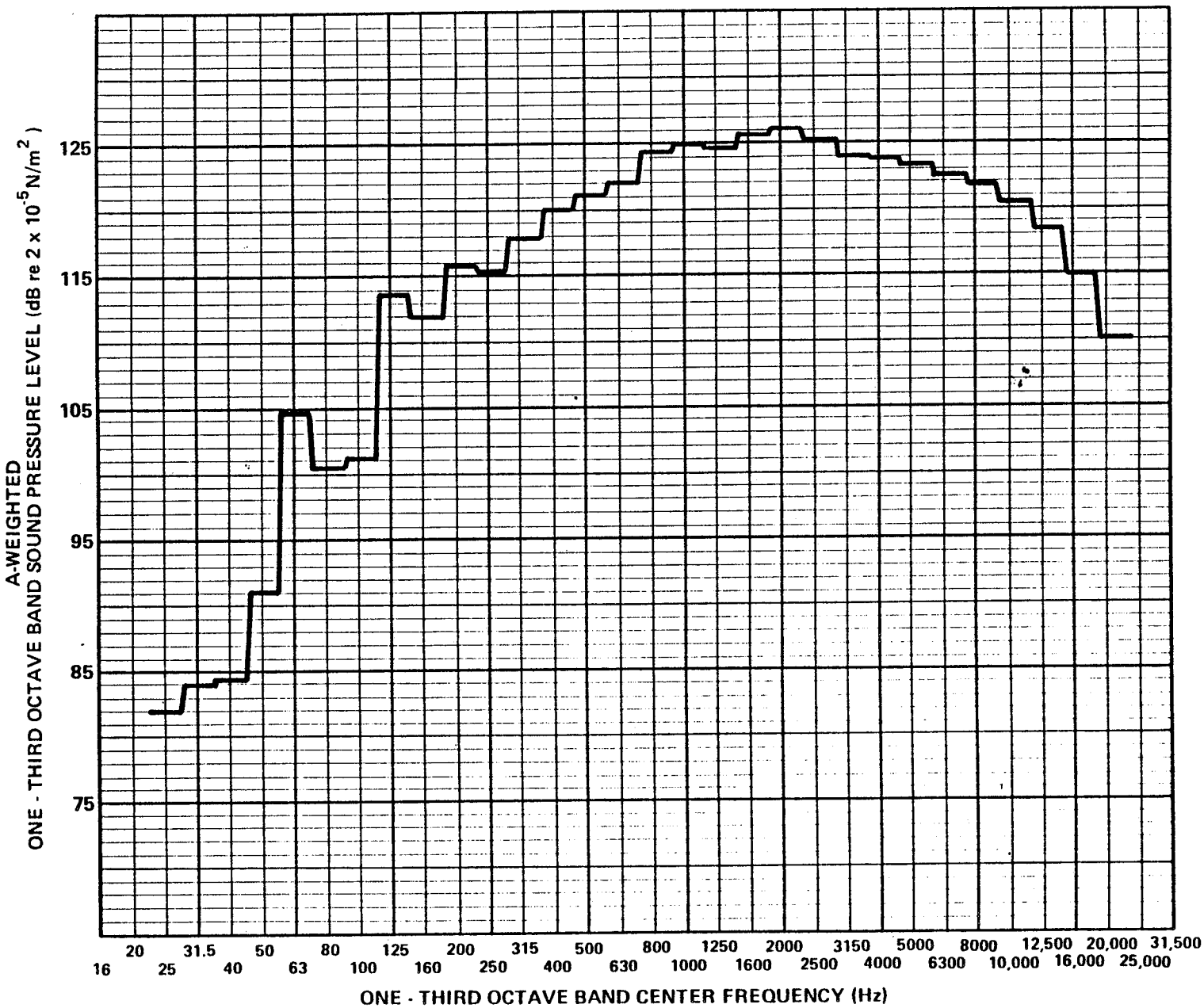

FIGURE D.9 NOISE SPECTRUM AT SURFACE MIRCOPHONE NEAR STARBOARD EXHAUST STACK (R182 WITH TWO BLADE PROPELLER, CRUISE AT 2400 RPM).

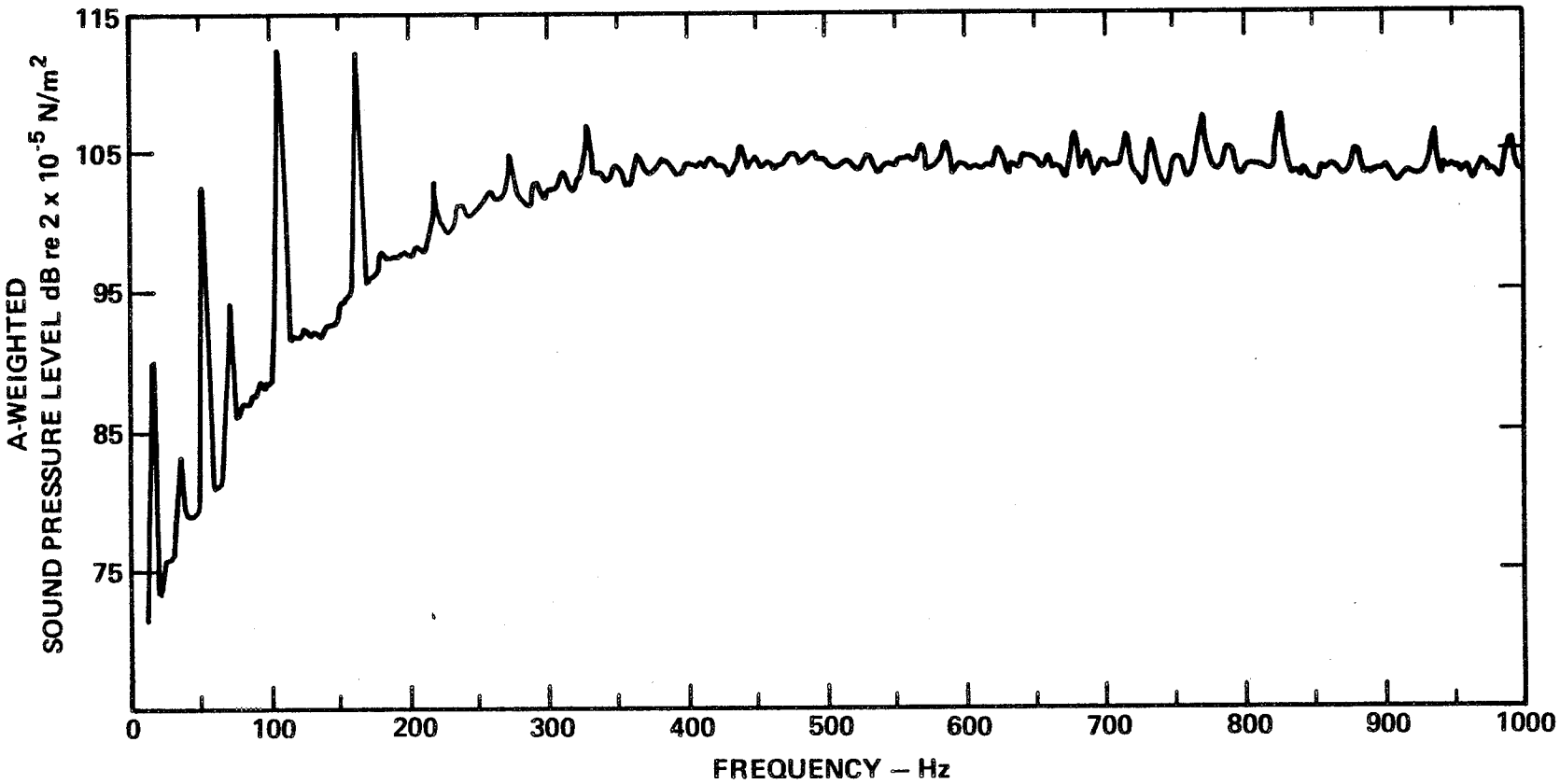

FIGURE D.10 NARROWBAND ANALYSIS OF NOISE AT SURFACE MICROPHONE NEAR STARBOARD EXHAUST STACK. R182 WITH TWO BLADE PROPELLER, CRUISE AT 2100 RPM (2½ HZ BANDWIDTH).

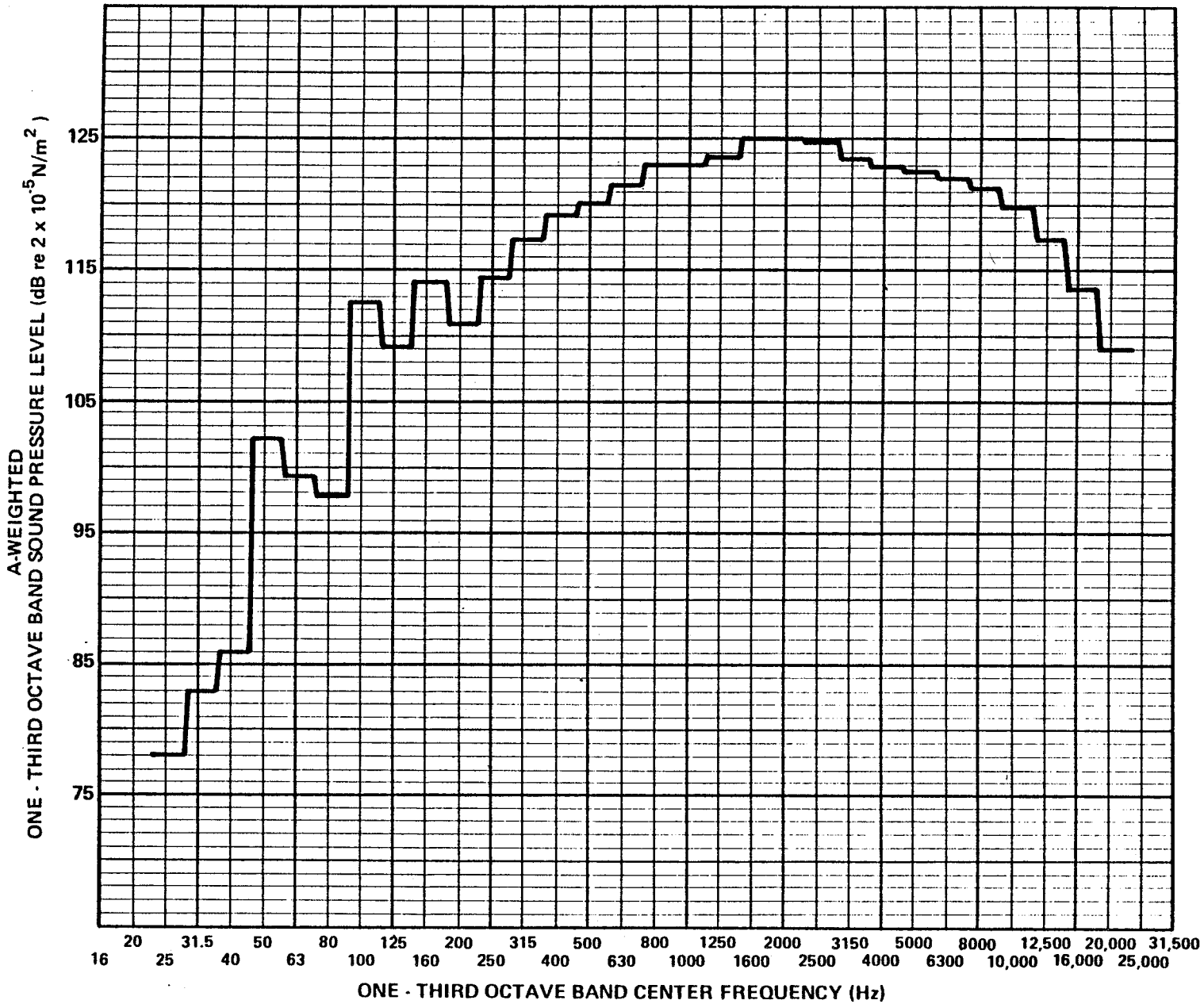

FIGURE D.11 NOISE SPECTRUM AT SURFACE MICROPHONE NEAR STARBOARD EXHAUST STACK. R182 WITH TWO BLADE PROPELLER, CRUISE AT 2100 RPM.

at "high" frequencies is apparently dominated by flow noise. Still this measurement provides a useful comparison to the results obtained with the probe microphone, as shown in the following sections.

D.4. Characterization of Paths by Which Exhaust Noise Reaches the Cabin

The major paths by which exhaust noise may enter the cabin are:

a) Through the lower firewall near the cowl flaps, particularly in the case of the R182 (compare Figs. D.3 and D.4);

b) Through the cabin sidewall skin forward of the cabin doors;

c) Through the cabin floor (a double panel structure).

The overall transfer function relating noise at or near the exhaust outlet to the resultant cabin noise was measured in free field conditions in the laboratory. Exhaust noise was simulated by connecting a sealed loudspeaker enclosure to a length of exhaust pipe of the proper size. The pipe outlet was placed as was shown in Fig. D.12 to correspond with the R182 geometry, and both exhaust sensors were mounted. Microphones were mounted in the cabin at positions where flight data were available. The sound field incident on the exterior of the fuselage caused by sound originating in the exhaust pipe was surveyed by a roving microphone. Transfer functions from noise received on the probe and surface microphones to noise in the cabin are shown in Figs. D.13 and D.14. The break in the data between 2000 Hz and 2500 Hz merely indicates that the sound source could not cover the entire frequency range at one time. The shape of the transfer function curves are identical out to a frequency of 500 Hz, above which in-pipe resonances interfered with that simulation.

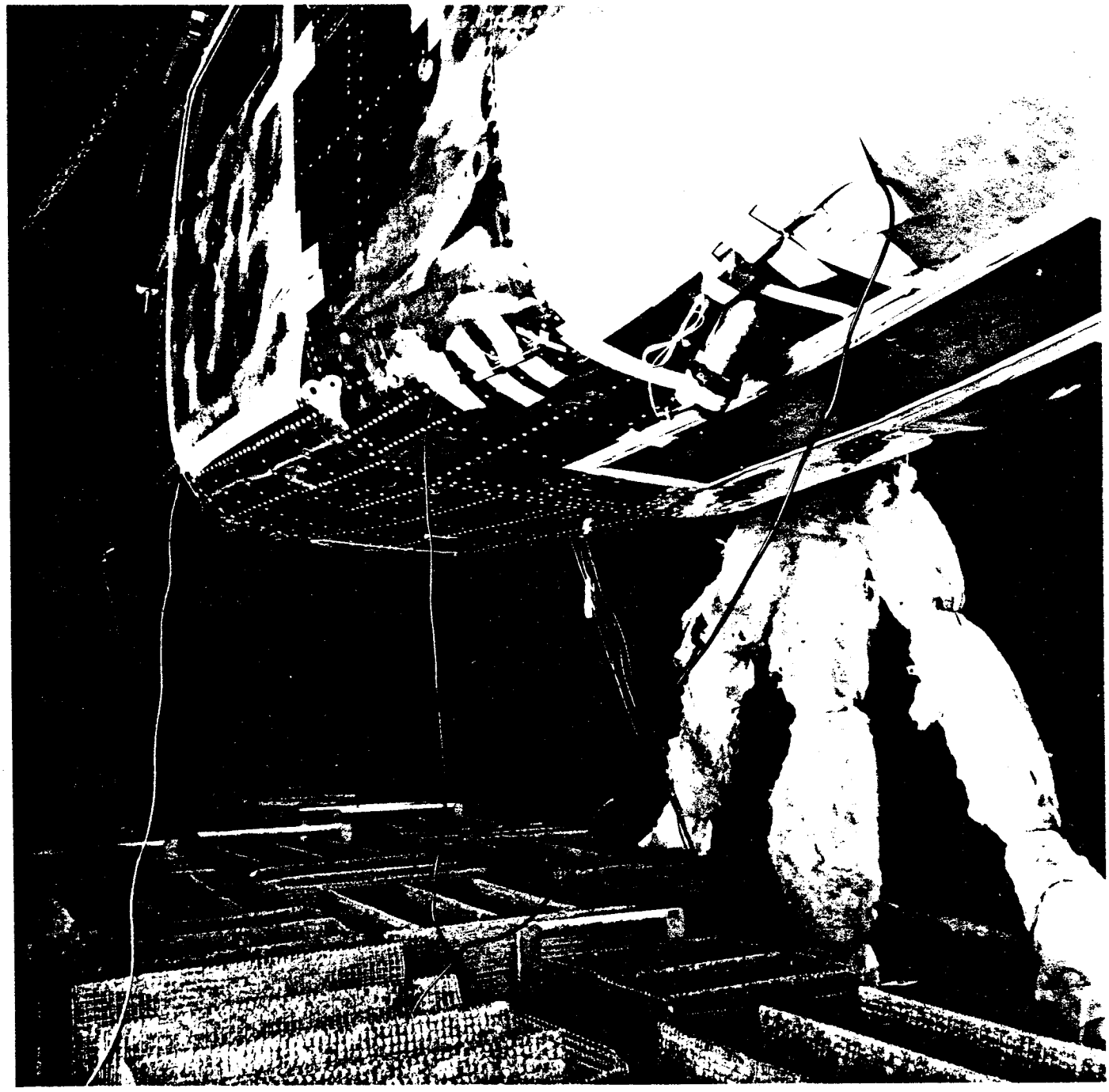

FIGURE D.12 EXHAUST NOISE SIMULATION IN LABORATORY.

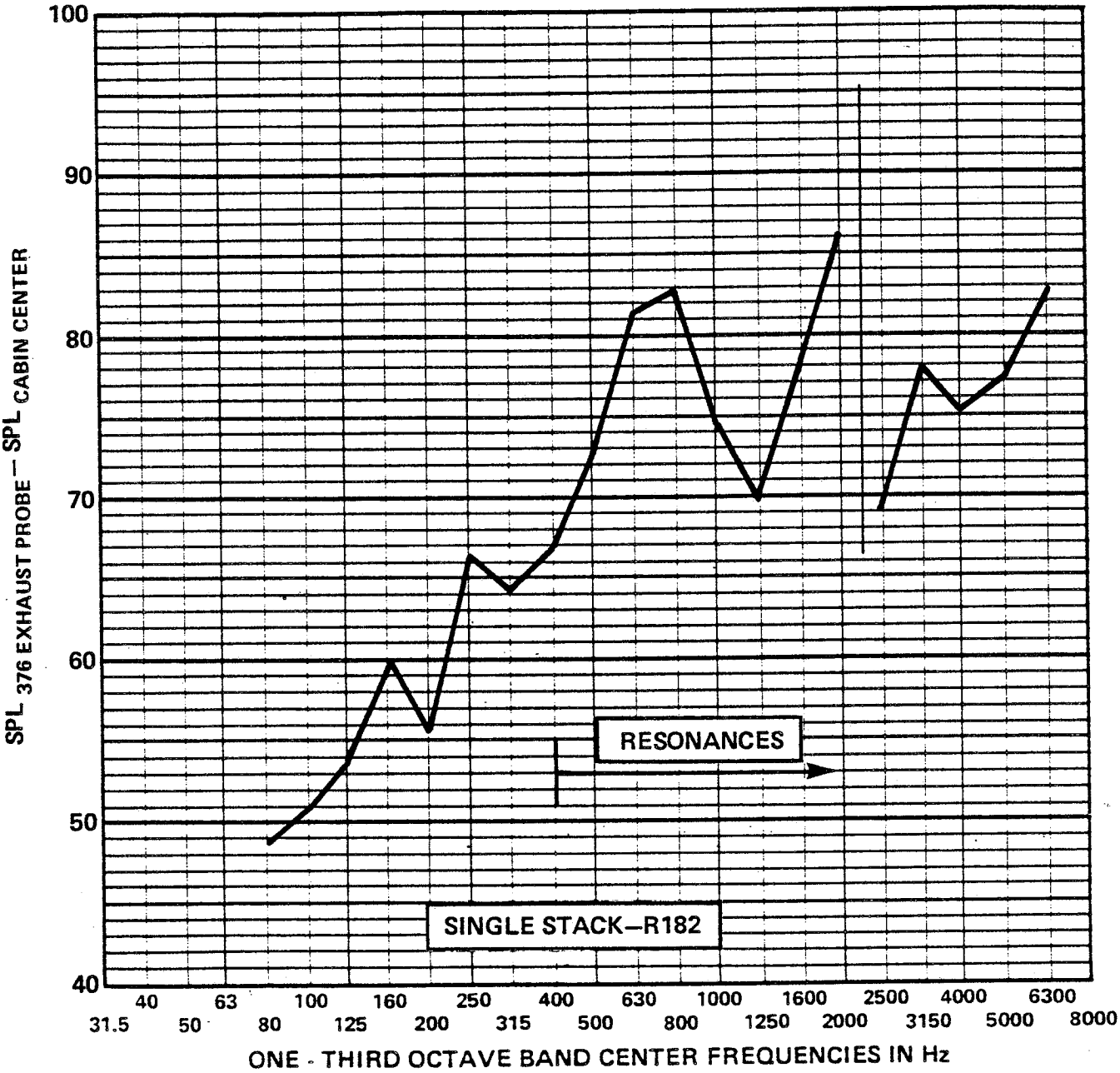

FIG. D.13. NO-FLOW TRANSFER FUNCTION BETWEEN PRESSURES AT END OF EXHAUST PIPE AND CABIN CENTER MICROPHONE.

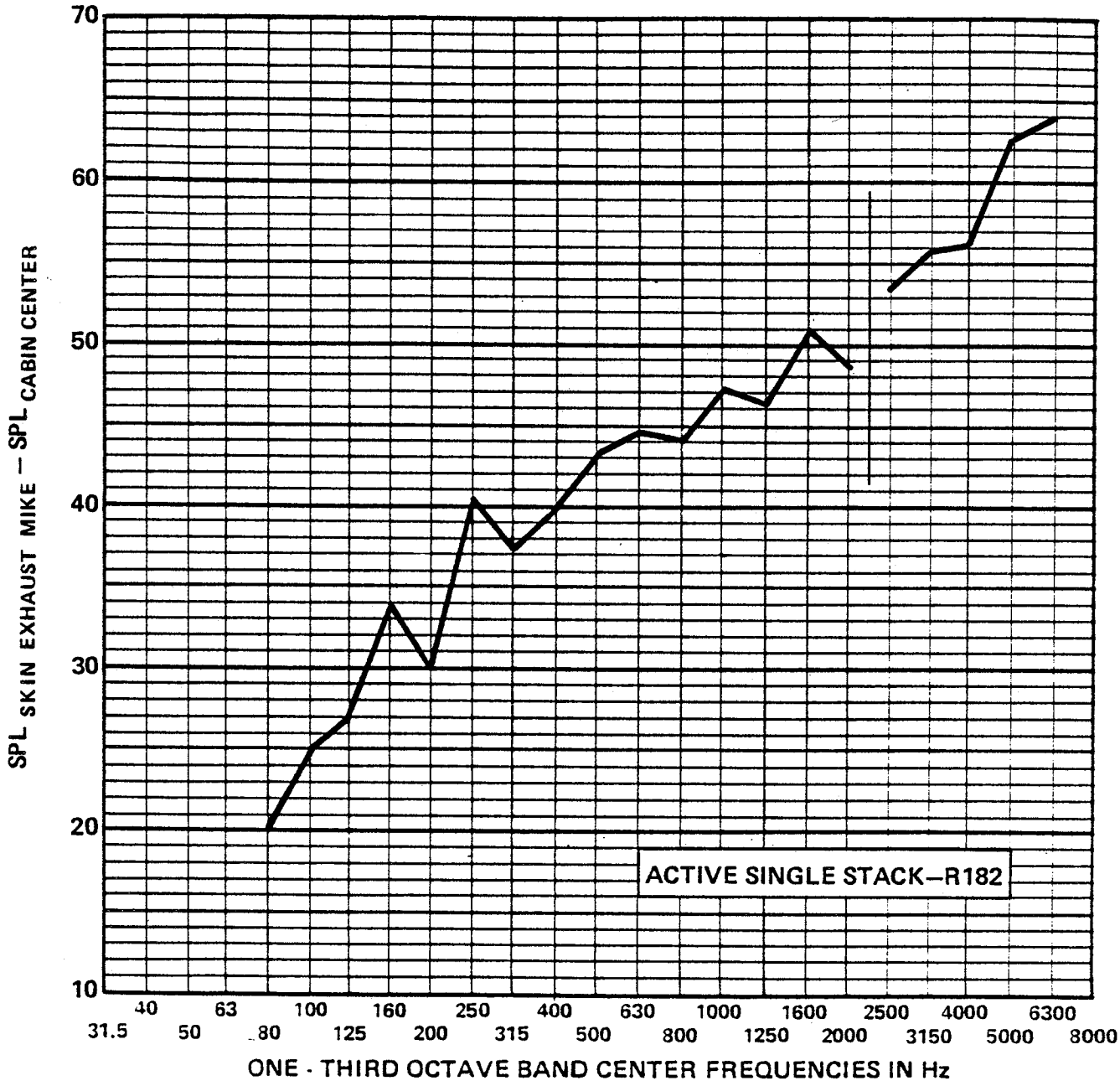

FIG. D.14. TRANSFER FUNCTION (NOISE REDUCTION) BETWEEN ACOUSTIC PRESSURES MEASURED ON SURFACE OF FUSELAGE NEAR EXHAUST PIPE EXIT AND CABIN CENTER.

D.5. Estimated Contribution of Exhaust Noise to Cabin Interior Noise

Two estimates for the contribution to cabin noise by the exhaust are plotted in Fig. D.15. The transfer function/source level pairs for the two exhaust noise transducers yield predictions differing by 6.5 dB at the 120 Hz firing frequency. In general, estimates derived from the in-stack measurements yield lower estimates. The high 80 Hz contribution shown by the surface microphone is clearly attributable to contamination by propeller noise. The surface microphone generally predicts levels higher than those measured in flight. Both transducers predict a strong component at 200 Hz that is not measured in the cabin center.

Refinement of the two predictions for exhaust noise contributions appears to require further flight testing. Particularly useful would be a simultaneous measurement of noise at both exhaust ports and at the surface microphone. The measurements discussed in this appendix were performed on two different airframes on different flights, so that aircraft-to-aircraft and flight-to-flight variations in cabin noise data as discussed in Ref. 1 may be significant.

The measurements of noise reduction of individual panels presented in App. C provide an indication that only a small area of the exterior surface is transmitting exhaust noise (see Figs. C.11 and C.12).

D.6. Treatments Applicable to Reducing Source/Path Contributions

The most direct means of reducing exhaust noise contributions is to reduce the levels emanating from the stack through use of an exhaust muffler. A muffler could be tuned to operate most effectively at a particular engine speed, e.g., cruise, thus avoiding bulky broadband mufflers.

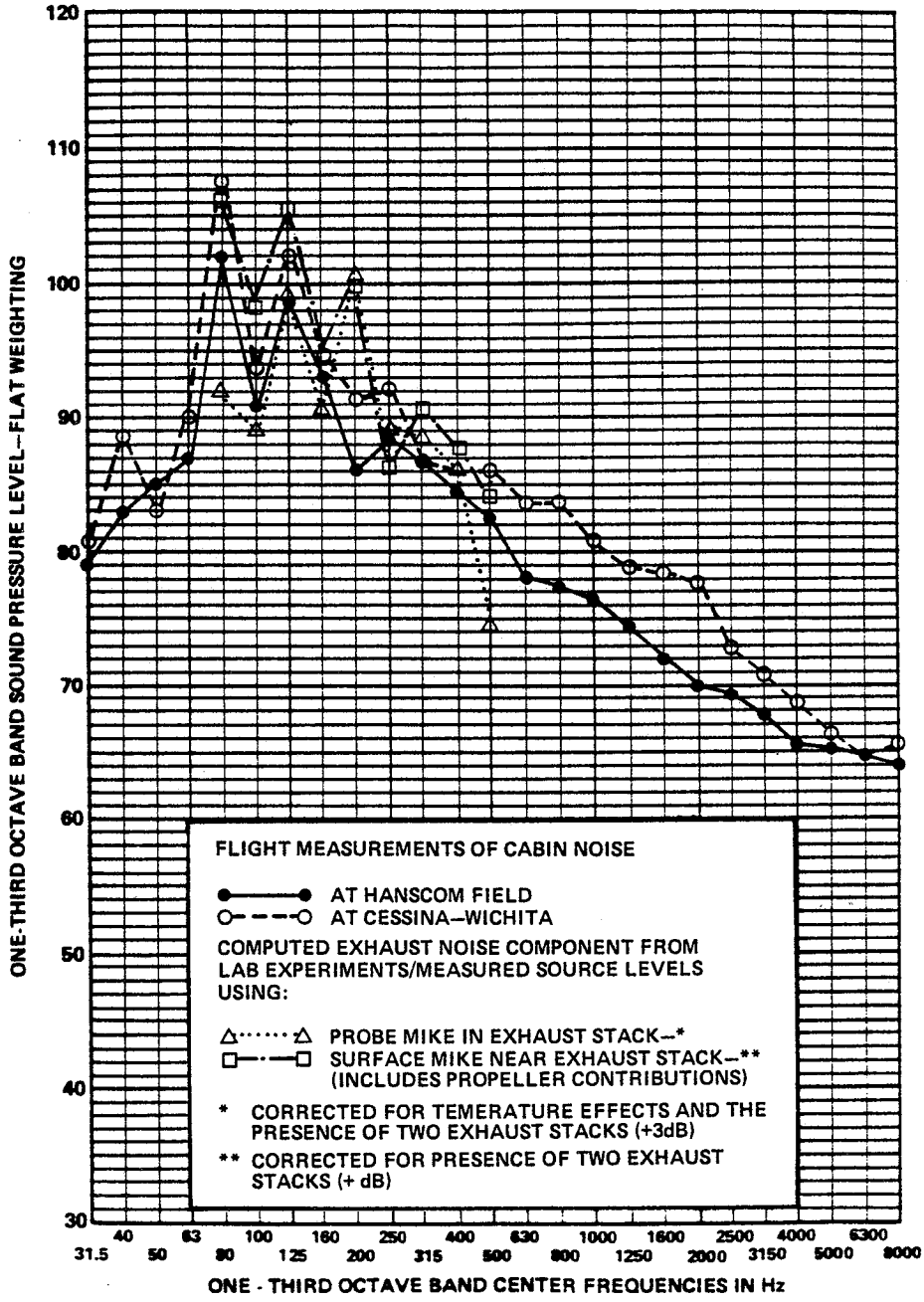

FIG. D.15 COMPUTED EXHAUST NOISE CONTRIBUTION TO CABIN NOISE: R182, 2-BLADE PROPELLER; CRUISE AT 2400 RPM.

Path reductions can be affected by:

a) Increasing the mass and/or stiffness of the skin of the sidewall or firewall by thicker material and/or honeycomb panels;

b) Double wall construction for the skin or firewall.

Either of these methods may also be required to reduce propeller and engine airborne and structureborne contributions, thus effectively reducing the contribution of all sources at once.

D.7. Applicability of Results to Other Aircraft

Practices within the general aviation industry suggest that the exhaust system for each aircraft model is unique. Engine manufacturers do not generally supply the exhaust ducting. Each airplane manufacturer tailors the exhaust system components for each model subject to cabin heating requirements, space limitations, and company preference. Thus, for example, aircraft in a given power range may have two or six exhaust stacks for normally aspirated models or one stack for turbocharged models. Exhaust mufflers are sometimes included. It is well known that exhaust noise from reciprocating engines is very sensitive to exhaust system design but is not easily predictable. Therefore, while the measurement techniques described here are certainly useful for other aircraft, no general conclusions can be drawn.

REFERENCES FOR APPENDIX D

1. Cessna Aircraft Company, "Information Manual: Model R182," published annually by Cessna Aircraft Company, Wichita, KS.

2. Howe, M.S., "Attenuation of Sound in a Low Mach Number Nozzle Flow," J. Fluid Mech., 91, 209-230, 1979.

APPENDIX E

CONTRIBUTION AND TREATMENT OF CABIN NOISE RESULTING FROM PROPELLER AIRBORNE NOISE

E. CONTRIBUTION AND TREATMENT OF CABIN NOISE RESULTING FROM PROPELLER AIRBORNE NOISE

E.1 Introduction

The propeller is a prime contributor to cabin interior noise levels, as evidenced by narrowband analyses of the cabin acoustic spectra. In this section, estimates are made of the contribution of propeller noise radiated into the cabin as a result of airborne acoustic excitation of exterior surfaces (windshields, windows, skin). Appendix F deals with propeller airborne noise which enters the cabin through the engine compartment/firewall path.

E.2 Geometry and Theoretical Considerations

The test aircraft is normally fitted with a single two- (or three-) bladed tractor propeller which is direct-driven by the engine driveshaft. The maximum diameter is 208 cm. Figure E.1 shows the position of the propeller relative to the airframe. Several aspects of the geometry are relevant in the context of propeller-generated noise:

1) The azimuthal and axial non-uniformity of the downstream "obstructions" (airframe) with respect to the propeller axis;

2) The close proximity of the propeller to key cabin sound-transmitting surfaces;

3) The location of engine air intakes immediately behind the propeller at approximately 3 o'clock and 9 o'clock.

These points are significant in attempting to calculate propeller noise levels on the exterior of the aircraft, in extrapolating measurements from one location to another, and in the context of design of noise control measures.

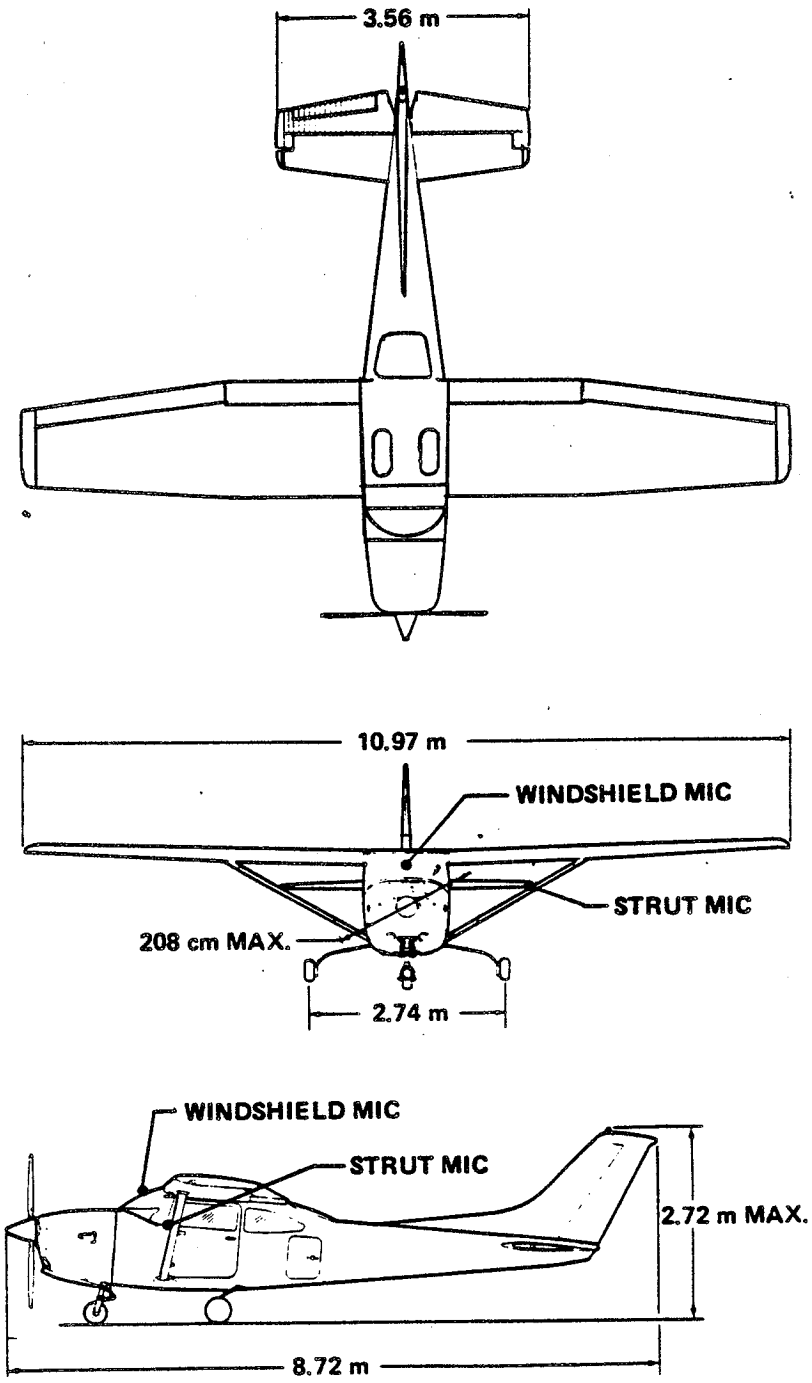

FIGURE E.1. RELATIONSHIP OF PROPELLER TO AIRFRAME AND APPROXIMATE MICROPHONE LOCATIONS.

The "downstream" variability in geometry as "seen" by the propeller creates several effects which are difficult to account for. First, the lack of azimuthal symmetry of surfaces close to the propeller creates periodic loading variations which result in sound generated at harmonics of blade passage frequency (as well as periodic loads which may create important structureborne sound - see Appendix H). Second, downstream surfaces reflect, diffract, and scatter propeller-generated sound, which may lead to large spatial variations in the distribution of propeller noise (particularly discrete frequency noise) over the aircraft surfaces; such spatial variations could have a major significance in the context of development of effective and optimally distributed noise control treatment, since both local "hot spots" and quiet spots may exist.

For example, at the propeller blade passage rate (80 Hz), the windshield is located at a distance approximately one-half an acoustic wavelength away from the propeller disc plane (axially); the wing chord at the root is also approximately one-half wavelength for sound at the blade passage frequency. Further, since the propeller sound generation processes are probably nonuniform in strength around the propeller disc, due to inflow distortion and the proximity of the engine cowling over part of the disc, phase interference between sound generated at different portions of the disc can be expected on the aircraft surfaces. The extent of the effects noted above was not fully quantified during the program. However, several exercises were carried out which provide a basis for estimating the distribution of propeller airborne levels. These are described below.

E.2.1 Calculation of propeller noise levels

Although extensive analytical and experimental efforts have been made in the area of propeller noise prediction, virtually no work has been reported which is applicable to calculating the spatial variation of sound levels in the geometric near-field of a tractor propeller in the space well away from the disc plane, e.g., between the prop axis about 45° from the axis. Extensive effort has gone into the calculation of propeller noise levels at locations which are more or less in the disc plane, but attempts at inclusion of airframe effects in these calculations is still leading to considerable difference between prediction and measurement. A sophisticated propeller noise prediction program [1] was used to estimate the noise measured at a wing-strut-mounted microphone. These calculations underestimated the measured levels by 4 dB at the blade passage rate - excellent agreement in view of the lack of detailed information describing the inflow and the effects of the airframe on propagation. However, we limited the use of these calculations to verifying the reasonableness of the measured data due to the lack of inflow data.

E.2.2 Extrapolation of measured data

In the geometric near field of the propeller, i.e., that region where the propeller does not appear to be effectively a point source, one can expect significant deviation from inverse square law variations in the sound field. Since most of the fuselage of the aircraft tested is located within a few diameters of the propeller, it is of interest to estimate the extent of the variation from inverse square law behavior. This can be done, in one limit, by representing the propeller as a uniform ring source having a dipole character, and ignoring the diffracting effects of the fuselage.

Assuming that the propeller can be replaced by a distribution of statistically independent dipole sources located at $x = a\cos\theta$, $y = a\sin\theta$, $z = 0$ (where a = propeller radius) and other parameters are defined by Figure E.2, and that a receiver is located at $x = r\sin\phi$, $y = 0$, $z = r\cos\phi$ in a freefield environment, the acoustic pressure is

$$p(r,\phi) = \text{const.} \times \frac{\cos\nu}{r'}\left(1 + \frac{i}{kr'}\right) e^{ikr'},$$

where $k = \frac{\omega}{c}$.

The distance, r', from the source location on the ring to the receiver is

$$r'^2 = (r\sin\phi - a\cos\theta)^2 + a^2\sin^2\theta + r^2\cos^2\phi$$

$$= r^2 - 2(ra)\sin\phi + a^2$$

$$= r^2\left(1 - 2\frac{a}{r}\sin\phi\cos\theta + \frac{a^2}{r^2}\right).$$

If we let $J = \left(1 - 2\frac{a}{r}\sin\phi\cos\theta + \frac{a^2}{r^2}\right)^{1/2}$,

then $r' = rJ$.

Defining ν as

$$\cos\nu = \frac{r\cos\phi}{r'} = \frac{\cos\phi}{J},$$

we then get

$$p(r,\phi) = \text{const} \times \frac{\cos\phi}{rJ^2}\left(1 + \frac{1}{krJ}\right).$$

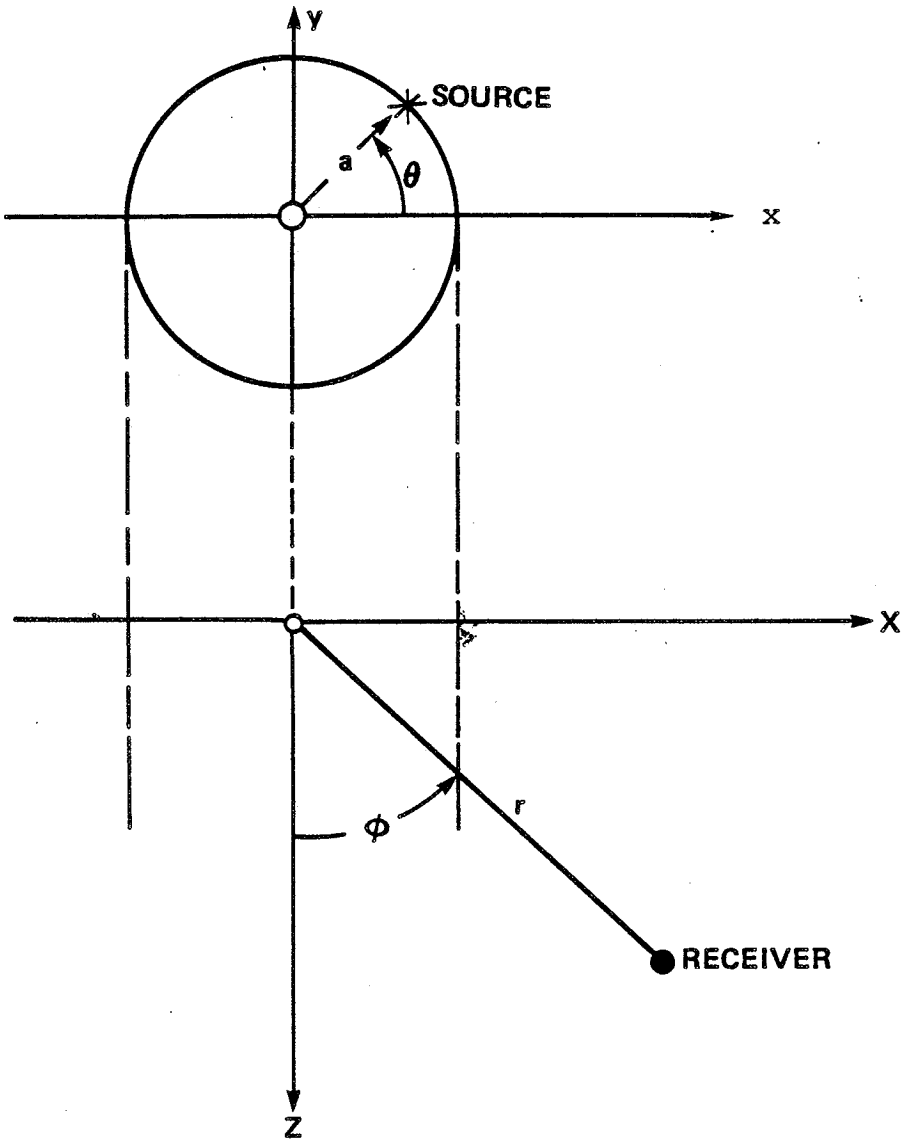

FIGURE E.2. GEOMETRY FOR "NEAR FIELD" CALCULATION.

For a distribution of statistically independent dipole sources located along a circle of radius a in the x-y plane,

$$|p(r,\phi)|^2 = \text{const} \times \int_0^{2\pi} \frac{\cos^2\phi}{r^2 J^4} \left(1 + \frac{1}{k^2 r^2 J^2}\right) a \, d\theta \quad . \tag{E.1}$$

For $r = R$ so large that $kR \gg 1$ (near field ignorable) and $\frac{a}{R} \ll 1$ (geometric field ignorable), we have $J \approx 1$, and we get from Eq. E.1

$$|p(R,\phi)|^2 = \text{const} \times \frac{2\pi a}{R^2} \cos^2\phi \quad . \tag{E.2}$$

Hence

$$\frac{|p(R,\phi)|^2}{|p(r,\phi)|^2} = \frac{2\pi a}{R^2} \cos^2\phi \; \frac{1}{\frac{a\cos^2\phi}{r^2} \int_0^{2\pi} \frac{1}{J^4} \left(1 + \frac{1}{(krJ)^2}\right) d\theta}$$

$$= \frac{r^2}{R^2} \left[\frac{1}{\pi} \int_0^{\pi} J^{-4} \left(1 + (ka)^{-2} \left(\frac{r}{a}\right)^{-2} J^{-2}\right) d\theta\right]^{-1} \quad . \tag{E.3}$$

(Note that J is even in θ.)

If $10 \log |p(R,\phi)|^2 = SPL(R,\phi)$, and

$10 \log |p(r,\phi)^2 = SPL(r,\phi)$,

then $$SPL(R,\phi) = SPL(r,\phi) + 20 \log \frac{r}{R} + CORR \quad , \tag{E.4}$$

where

$$CORR = -10 \log \left[\frac{1}{\pi} \int_0^{\pi} \frac{1}{J^4} \left(1 + \frac{1}{(ka)^2 \left(\frac{r}{a}\right)^2 J^2}\right) d\theta\right] \quad . \tag{E.5}$$

This CORR describes the average variation from inverse square law behavior which would be observed at distances close to a propeller in a free field, with an azimuthally uniform distribution of statistically independent dipole sources near the tips ("ring source").

Figures E.3 and E.4 present the CORR factor for several azimuthal directions, first for low values of ka (ka=1), in Fig. E.3, and then for all values of ka$\geq$10 (Fig. E.4). In practice, the periodic sources of propeller noise on a light aircraft are neither uniformly distributed nor statistically independent, due to the aforementioned variations in propeller environment. These effects could create periodic variations in the CORR factor (vs ka). However, we have insufficient information on the propeller environment to make such calculations at this point.

E.2.3 Lab data on spatial variations

The tests described in App. C also provided data on the spatial variations in exterior levels which might arise from concentrated sources. When a speaker was located ahead of the prop plane - on the prop axis - the spatial variations of exterior sound levels around the cabin were substantial, as shown in Figs. E.5 through E.8. Note that these data from a concentrated source only provide an indication of the extent of spatial variations; however, since the source was not located along the propeller tip path, the variations will differ somewhat from those that occur within an actual propeller.

When interpreting the data in Figs. E.5 through E.7 note that the windshield has essentially a line-of-sight to the speaker used in the tests, while other locations are fully or partially obstructed by the nose cowling.

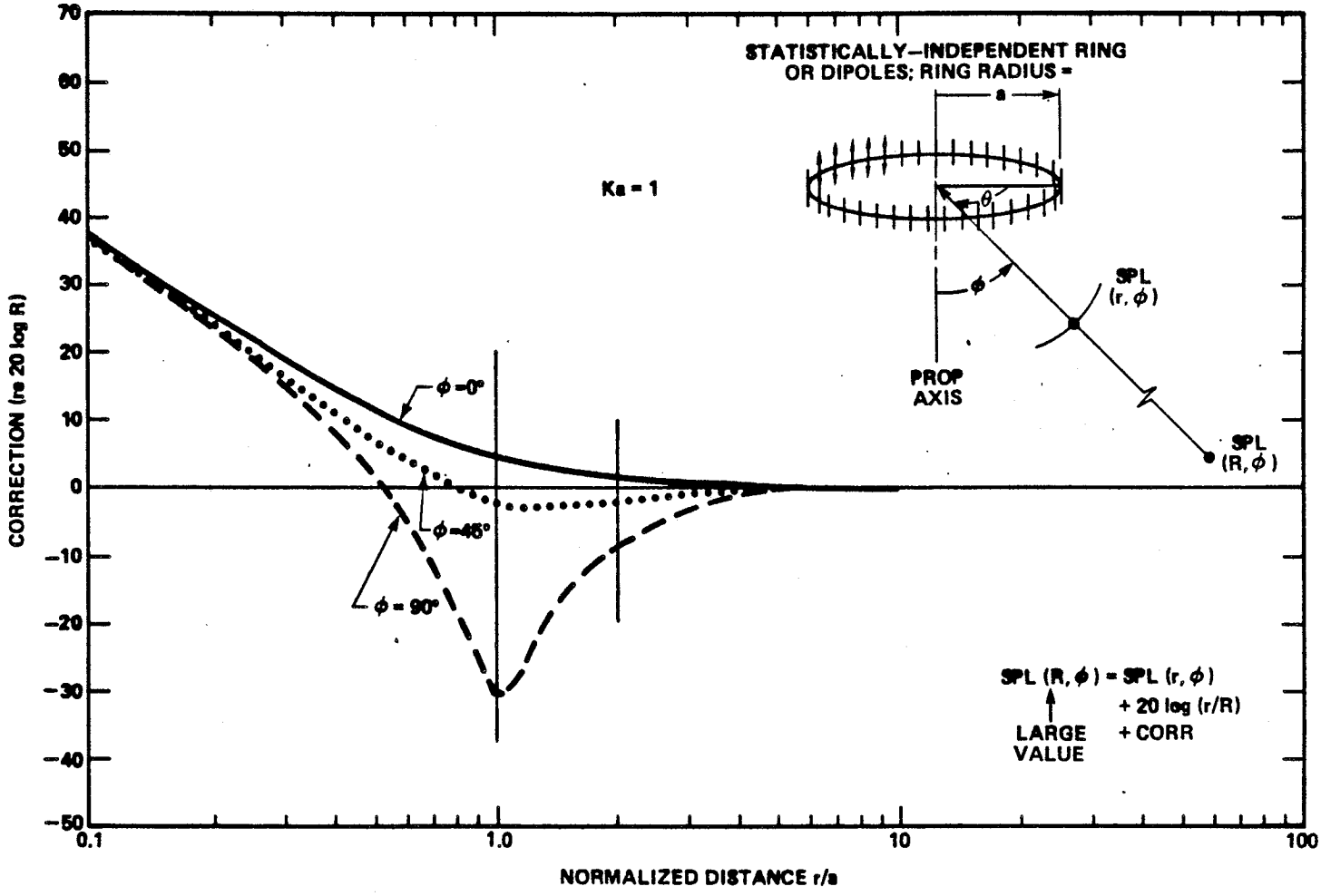

FIGURE E.3. DEVIATIONS FROM INVERSE SQUARE LAW BEHAVIOR NEAR A RING SOURCE OF DIPOLES (ka=1).

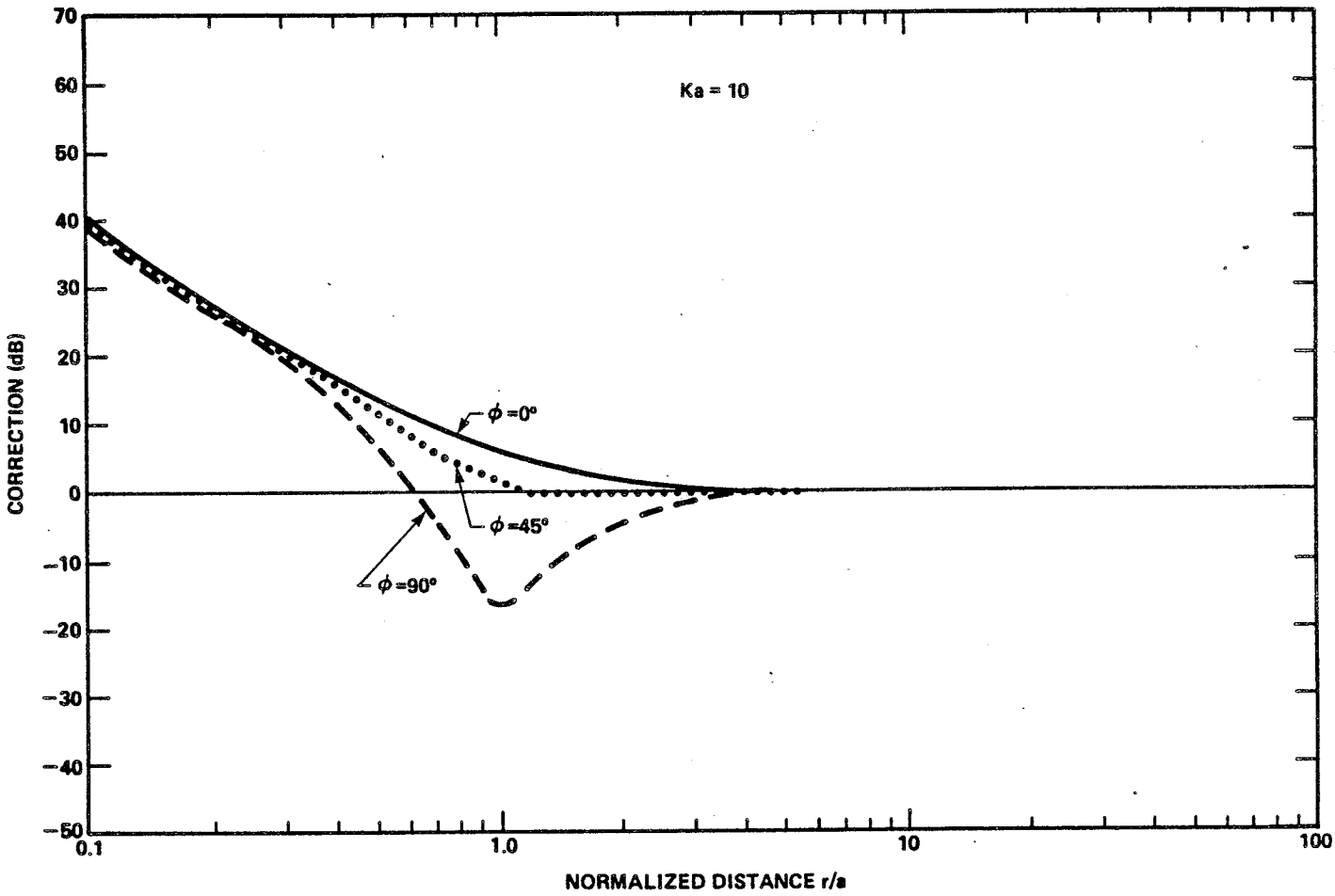

FIGURE E.4. DEVIATIONS FROM INVERSE SQUARE LAW BEHAVIOR NEAR A RING SOURCE OF DIPOLES ($ka \gtrsim 10$).

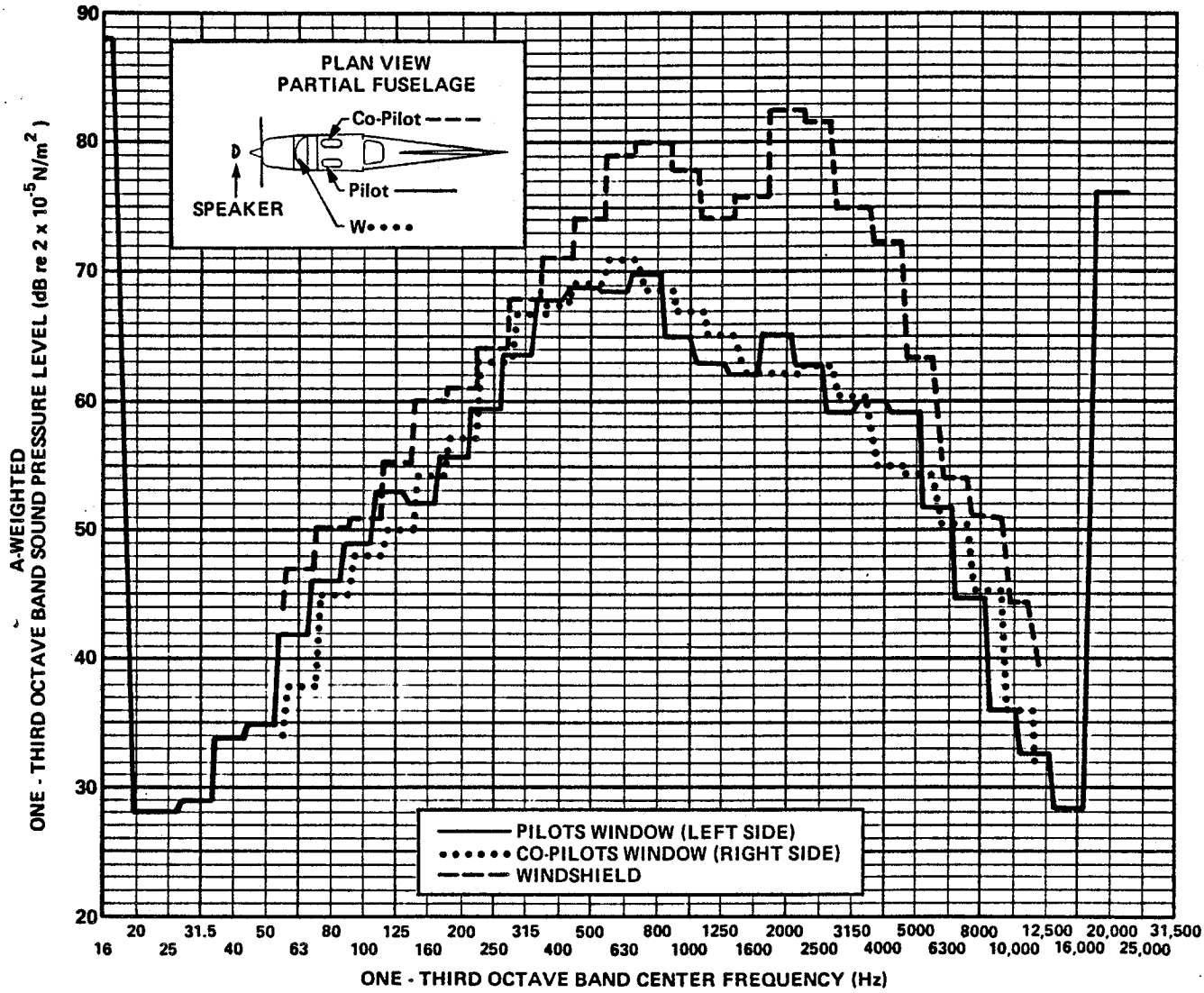

FIGURE E.5. DISTRIBUTION OF EXTERIOR SOUND LEVELS FOR BROADBAND LOUDSPEAKER SOURCE ON PROP AXIS.

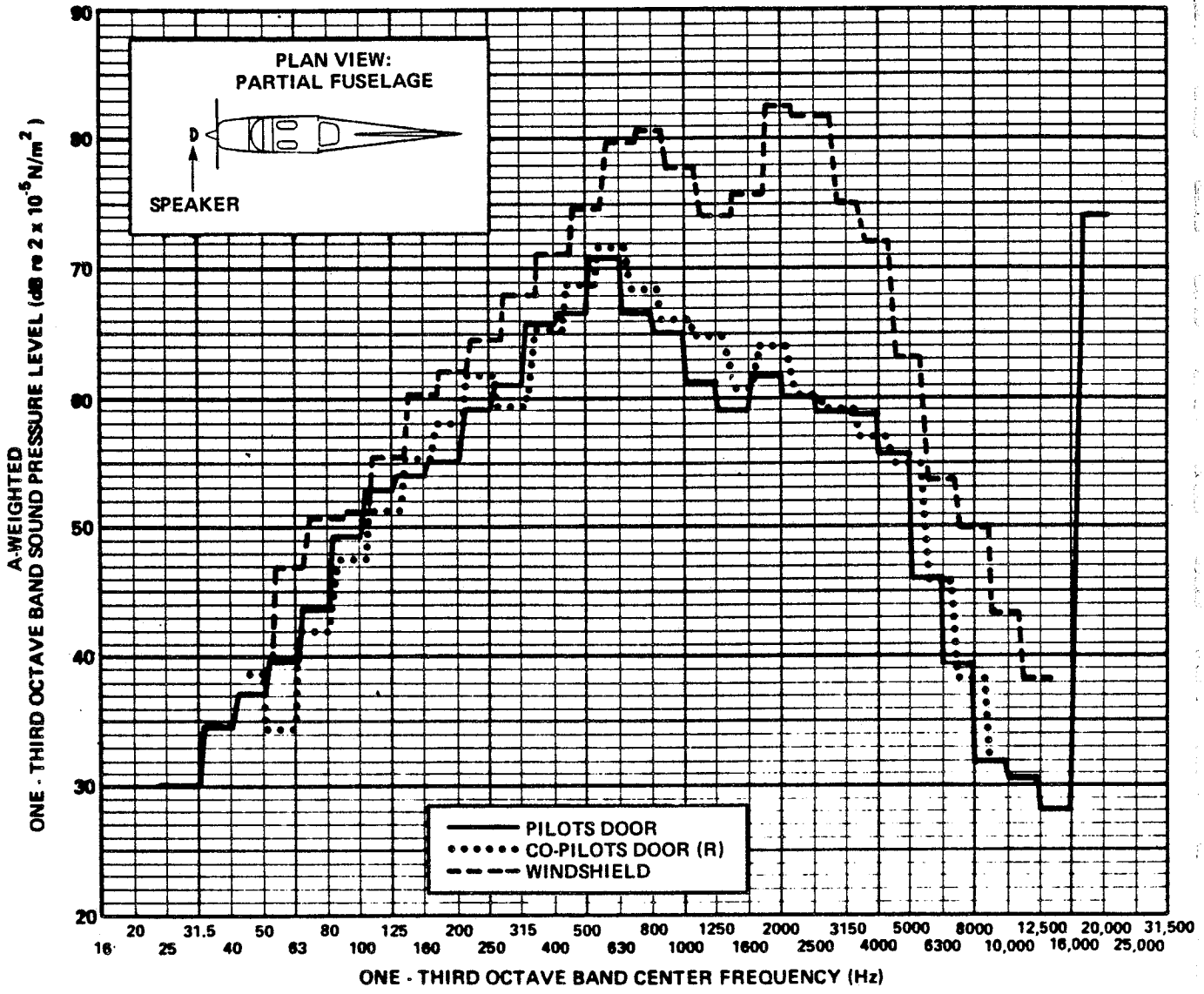

FIGURE E.6. DISTRIBUTION OF EXTERIOR SOUND LEVELS FOR BROADBAND SOURCE ON PROP AXIS.

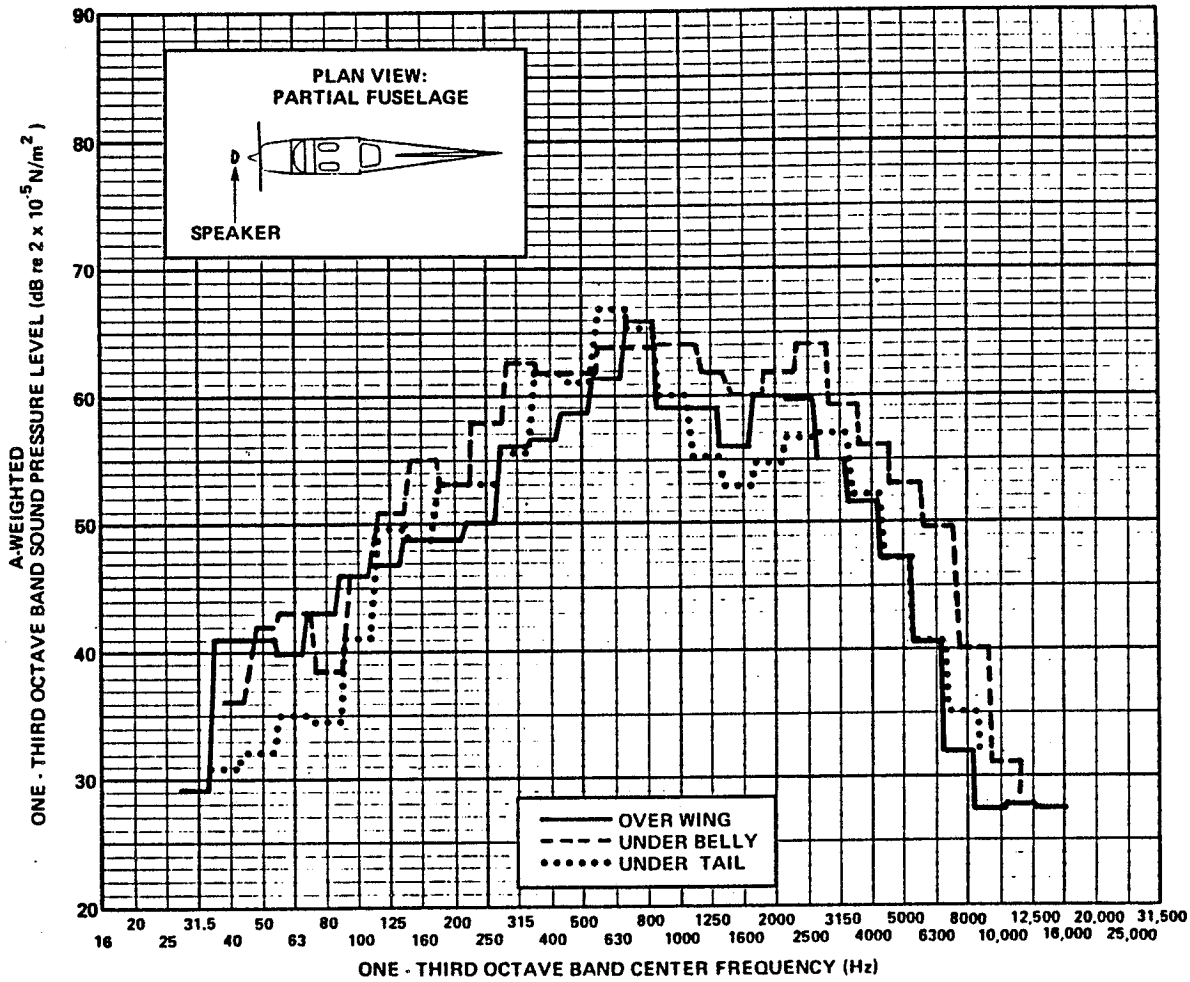

FIGURE E.7. DISTRIBUTION OF EXTERIOR SOUND LEVELS FOR BROADBAND SOURCE ON PROP AXIS.

Note also that complex paths exist through the engine compartment and that the wings consisted only of short stub extensions from the fuselage.

E.3 Flight Data

Data taken in Ref. 1 from a wing-strut-mounted microphone was supplemented with data from the windshield taken during the flight test described in App. B. The sensors used and their susceptibility to flow-induced pressures are described in App. I. Figure E.8 illustrates the location of the microphones used.

Figure E.9 shows the narrowband spectra measured at the wing strut microphone (from Ref. 1). Figure E.10 is data taken from the present study from the surface-mounted microphone on the windshield. Comparison of the data in Figs. E.9 and E.10 (when similarly weighted) show virtually identical levels at the propeller fundamental frequency but higher levels of the harmonics on the windshield. Figure E.11 shows data from the windshield location for the 2100 RPM condition. The level at the propeller fundamental frequency is comparable to that at 2400 RPM, but levels at the next few harmonics are lower than at 2400 RPM. Flight data is also available from microphones located in the engine compartment and for one located near the exhaust pipe opening; this data contains propeller source levels as well as data from other sources.

Flight data from other locations on the aircraft was not taken, because no flight test planned for such purposes took place.

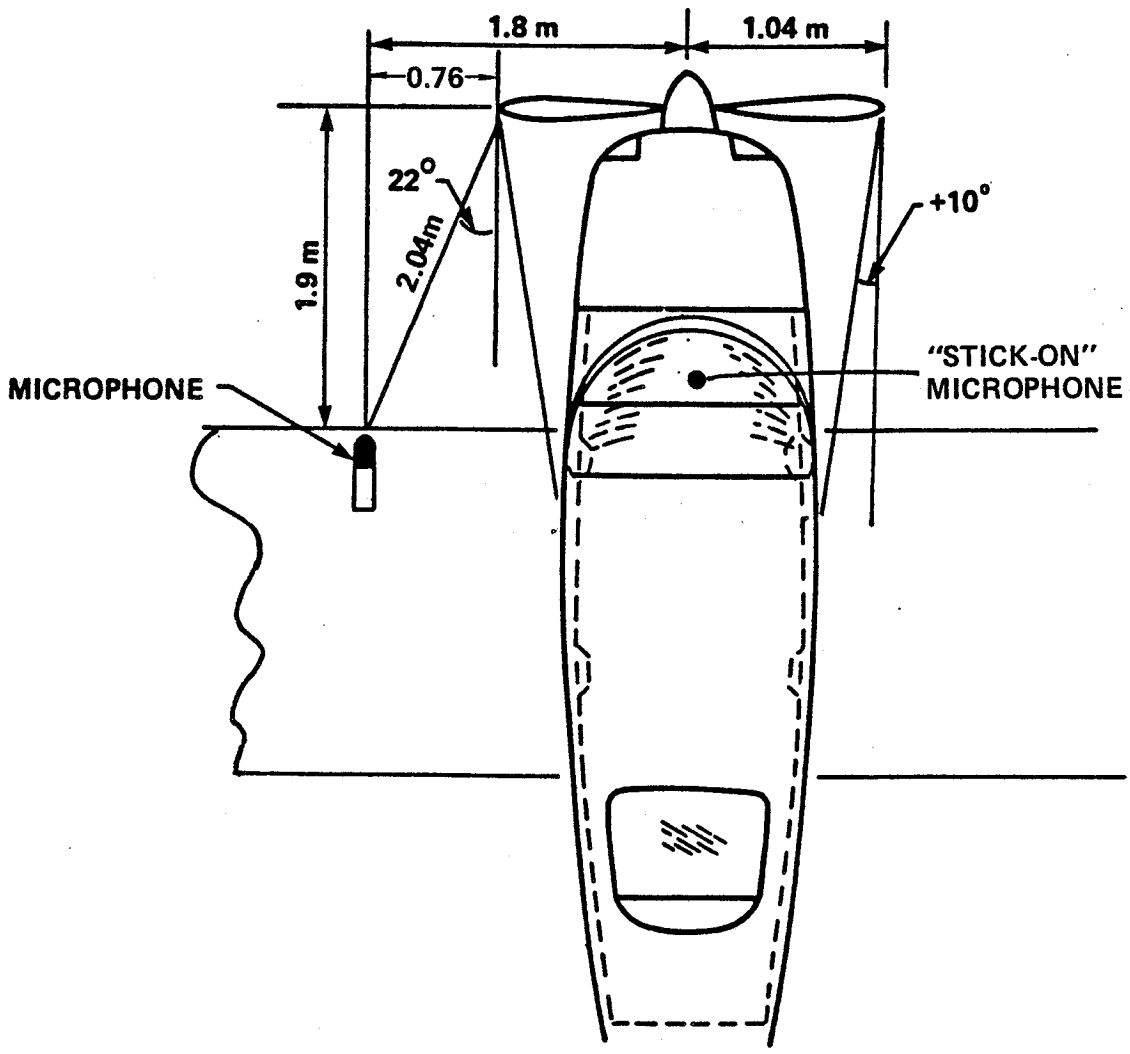

FIGURE E.8. LOCATION OF WING-STRUT AND WINDSHIELD MICROPHONES.

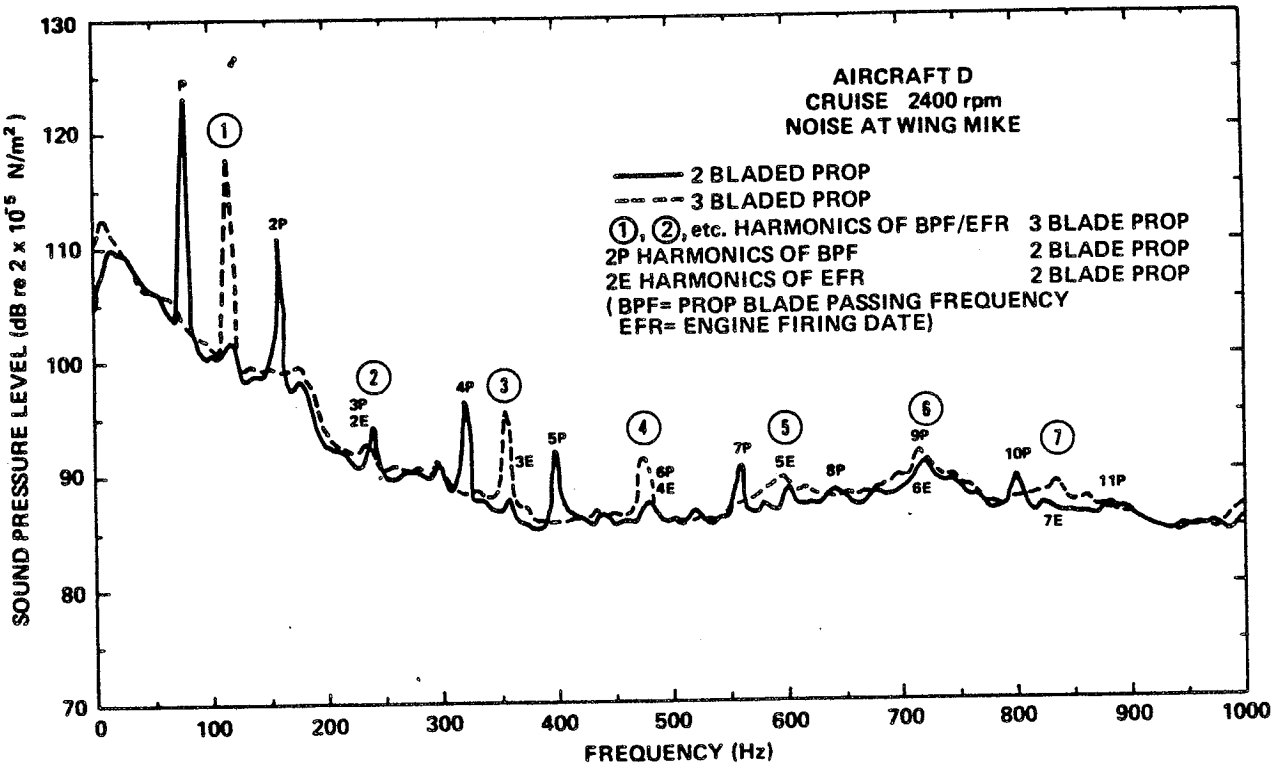

FIGURE E.9. MEASURED NOISE AT WING STRUT MICROPHONE (REF. 1).

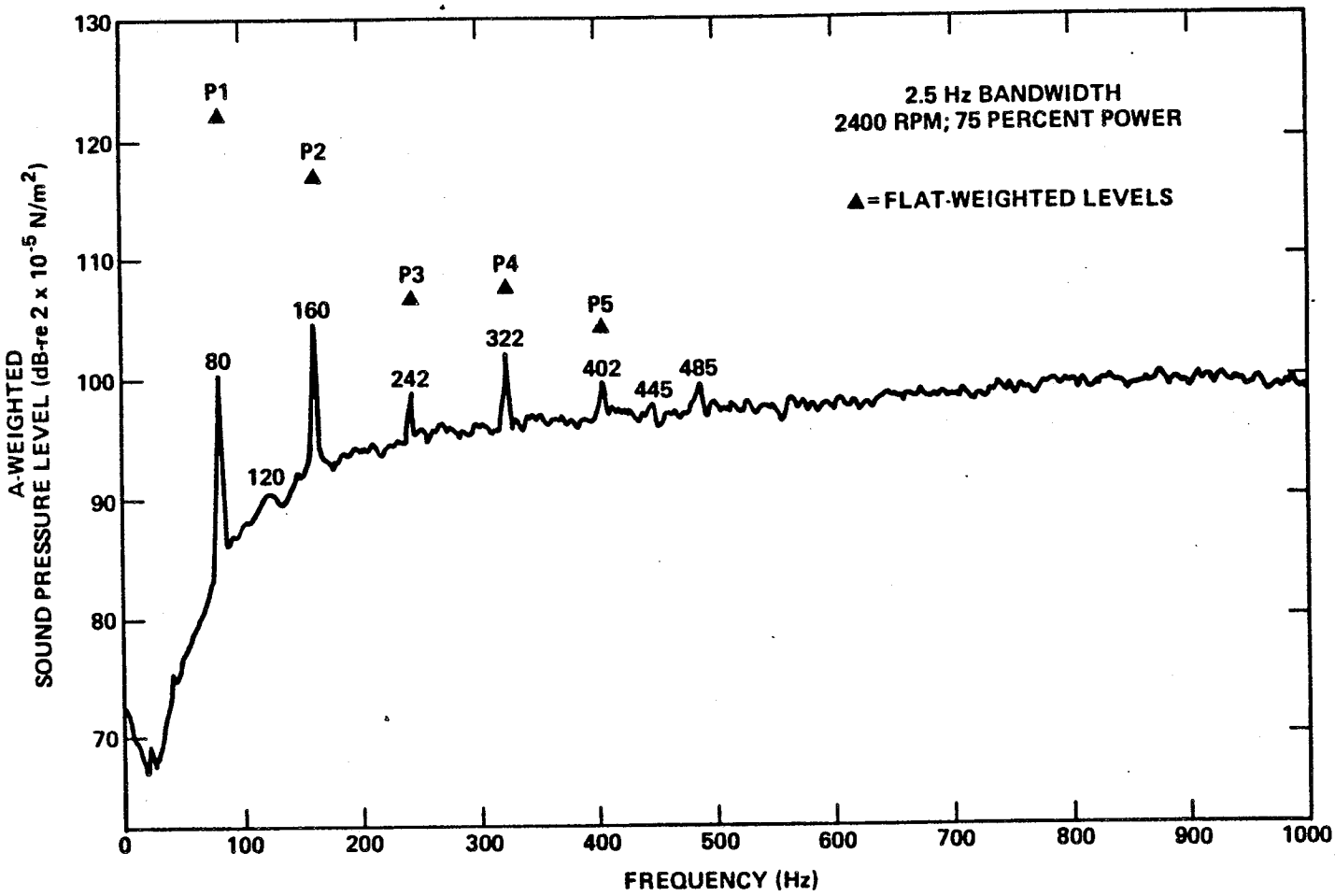

FIGURE E.10. MEASURED NOISE AT WINDSHIELD MICROPHONE (2400 RPM).

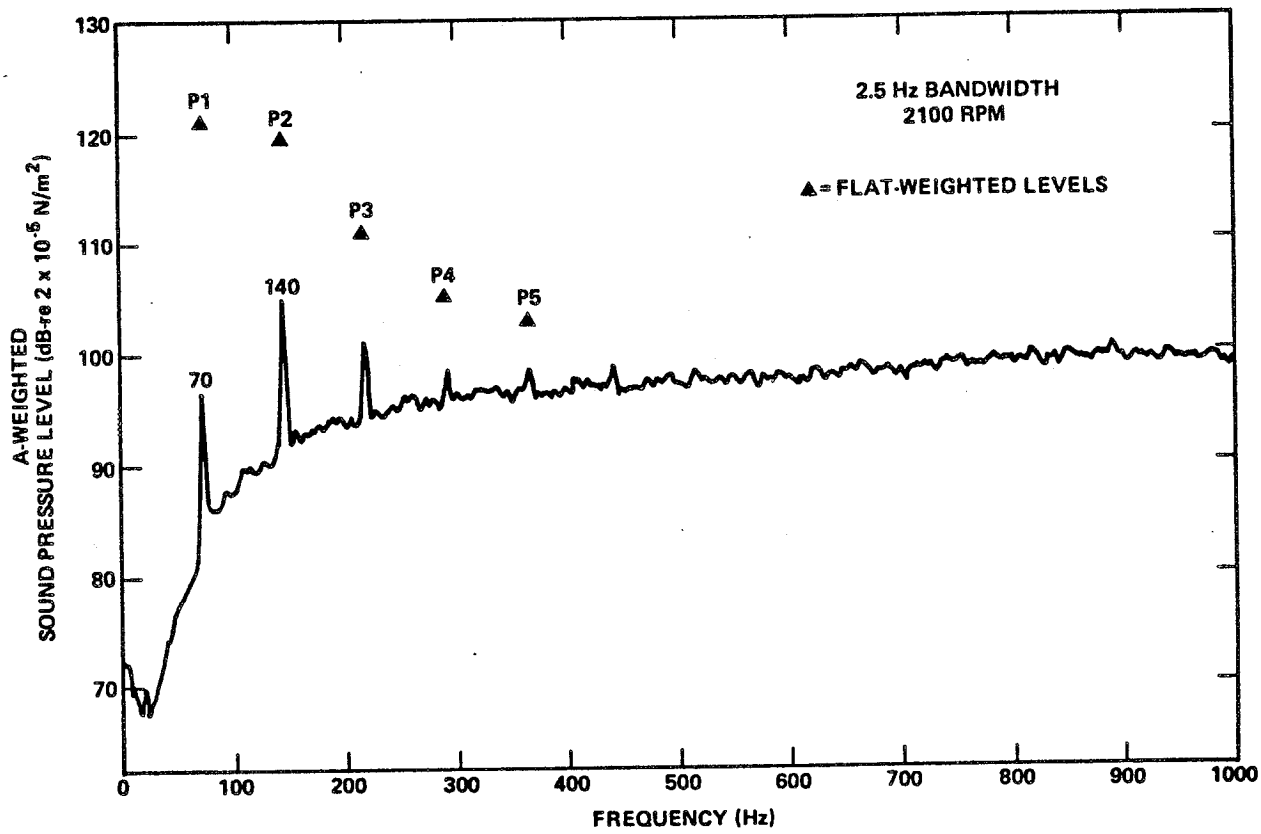

FIGURE E.11. MEASURED NOISE AT WINDSHIELD MICROPHONE (2100 RPM).

E.4 Predicted Contribution to Cabin Noise

For the purpose of estimating propeller airborne noise contributions to the cabin noise environment, the following source levels and transfer functions were used:

Path	Source Levels	Transfer Function
Windshield	Windshield Flight Data	Lab: Fig. C.9
Roof	Wing Strut Flight Data	Lab: Fig. C.8
Sidewall	Wing Strut Flight Data	Lab: Fig. C.11
Firewall	Engine Compartment Flight Data	Lab: Fig. C.7

Key results from this exercise are summarized in Fig. E.12, in which it can be seen that primary (and nearly equal) contributions are predicted for the roof, windshield, and engine compartment. Other paths may also be of importance once these primary paths have been treated.

E.5 Treatments Applicable to Reduction of Propeller Airborne Noise

E.5.1 Roof

Sound transmitted through the roof can be reduced by a combination of:

(a) Stiffening the roof to move the "dip" in the noise reduction spectrum (Fig. C.8) which occurs at the propeller blade passage frequency. (Such stiffening would be accomplished by replacing the roof structure with an integral aluminum or composite honeycomb sandwich, and/or through use of alternate structural members);

(b) Increasing the thickness of the roof to obtain mass law benefits (and some increase in stiffness), which might

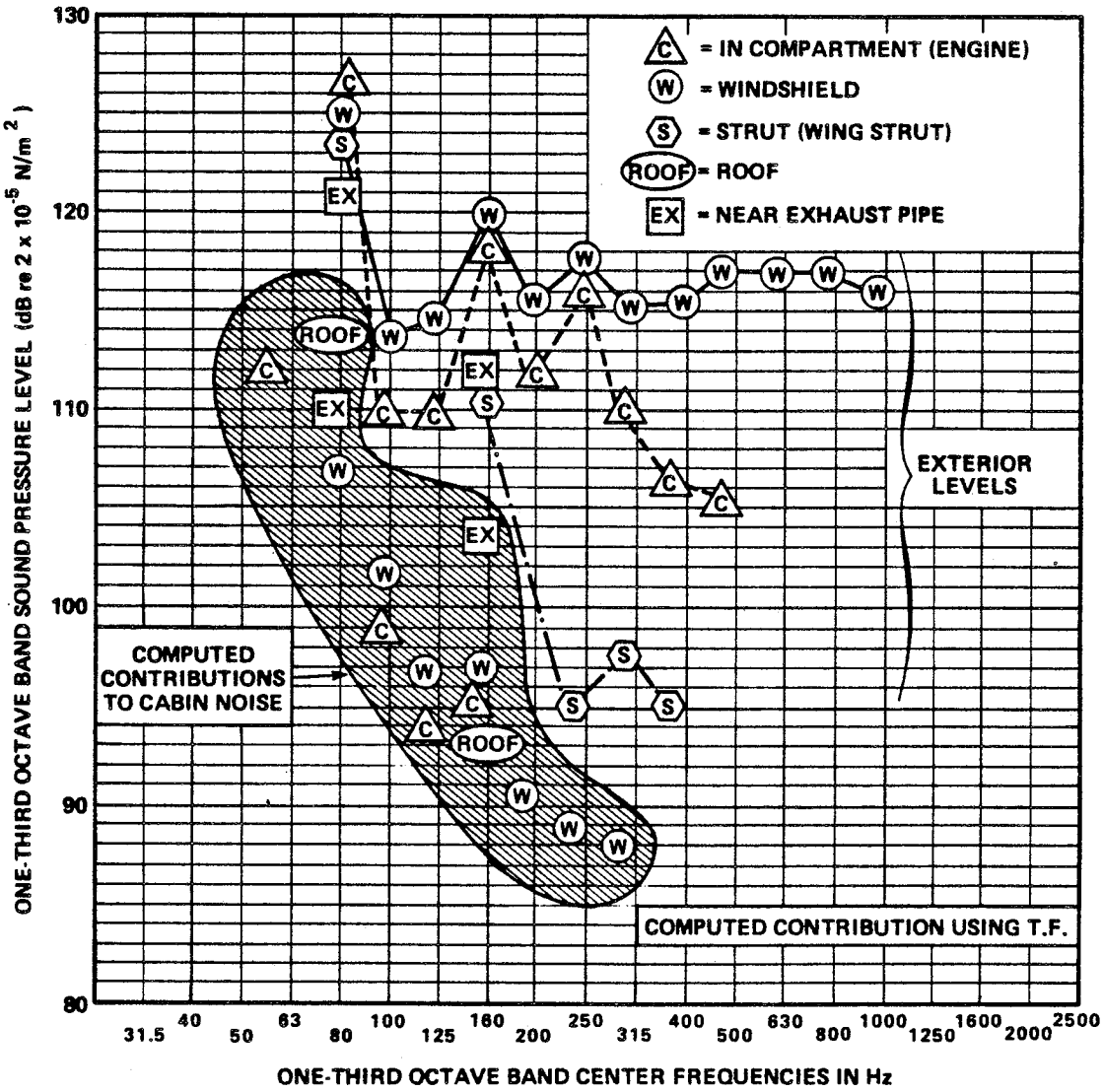

FIGURE E.12. PREDICTED CONTRIBUTIONS TO CABIN NOISE FOR PROPELLER AIRBORNE NOISE.

also shift the dip in the NR curve enough in frequency to realize benefits larger than the mass law effect at the propeller blade rate;

(c) Use of a double-wall structure in which the interior panel (trim) is made acoustically limp and suspended by isolators from the frame members, and the inner space is filled with fiberglass to avoid the low noise reduction (including "negative noise reduction") which occurs at the double-wall resonant frequency.

Stiffening the roof was not studied explicitly in this program since it was believed that important structural elements would have to be modified, and therefore such changes were outside the scope of the program. Also, the cause of the 80 Hz dip in noise reduction was not ascertained; if it was due either to radiation from structural members or to the resonance of the trim/roof combination, stiffening to move the resonance would be straightforward and most effective.

The applicability of a double-wall treatment to the roof was briefly studied. In the treatment envisioned, the trim panel would be limp, impervious, and suspended on isolators from structural elements, approximately 5 cm from the skin. The space between the trim panel and the skin would be filled with a fiberglass material having a flow resistance of approximately 35,000-50,000 mks Rayls. The trim panel would have an average surface mass density in the range of 2.7 kg/m^2. The proper covering of stringers and other structural elements and the isolation of the trim panel from them are critical aspects in achieving the noise reduction performance of a double-wall treatment. Figure E.13 shows the predicted performance of such a treatment. The performance predicted provides enough noise reduction to bring the propeller airborne noise contribution down to the desired spectral levels illustrated in Secs. 2 and 3.

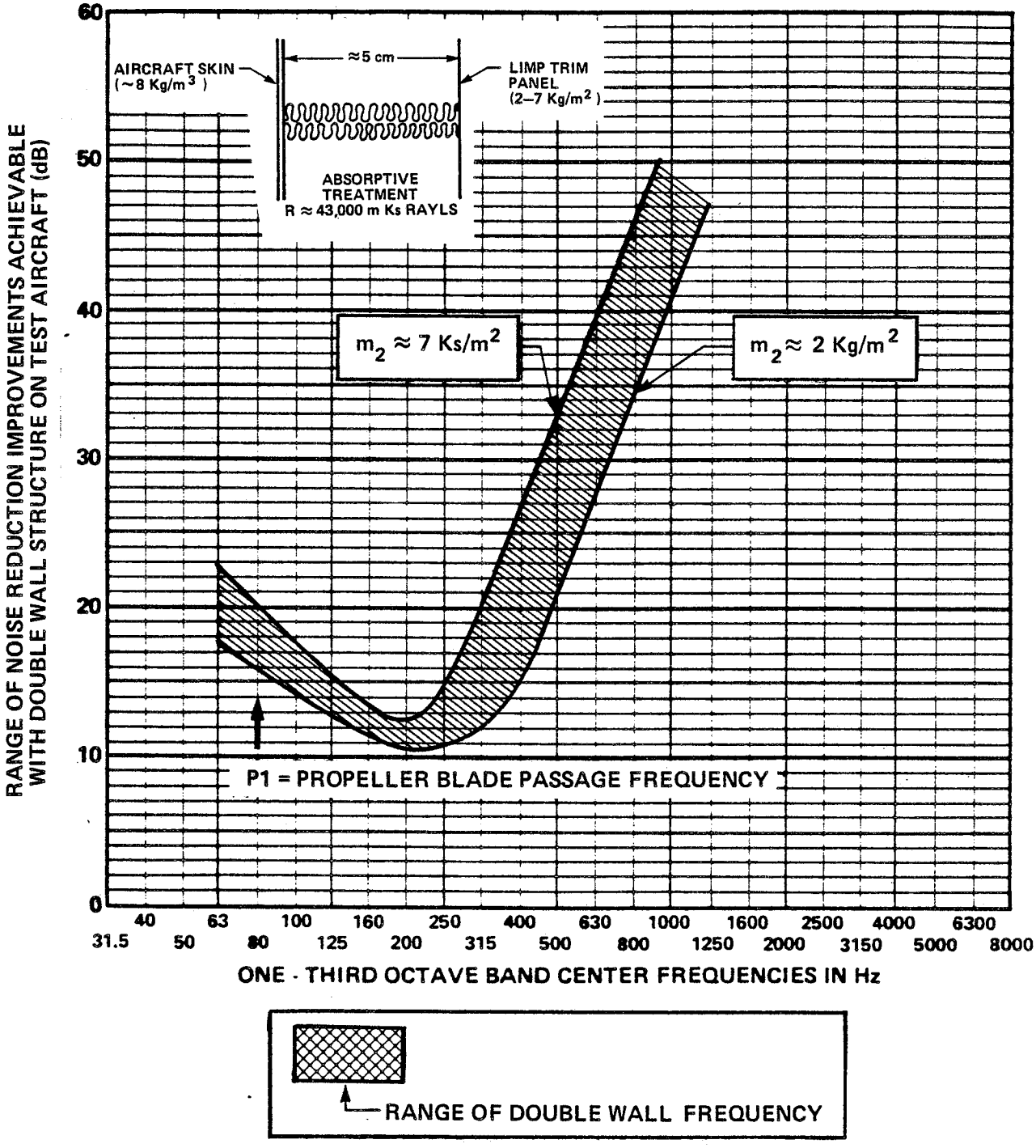

FIGURE E.13. THEORETICAL PERFORMANCE OF DOUBLE-WALL TREATMENT APPLIED TO ROOF (OR OTHER AREA WITH SIMILAR STRUCTURAL CHARACTERISTICS).

Note that this concept is compatible with thermal insulation and interior finishing requirements; and thus, the concept need not be penalizing in any significant way if the engineering effort can be applied to proper selection of materials and isolation of the trim from "short circuitry" effects caused by vibration of the stringers and other support structures. If the double-wall concept is applied to other parts of the cabin, the details of the design may change because of differing characteristics of the other wall elements, but in general, good noise reduction should be achievable within available space and weight constraints, and in concert with thermal and aesthetic requirements.

E.5.2 Windshield

The transmission through the windshield (and other windows) can best be improved by use of a thicker material, which will provide both mass law and stiffness benefits (see Sec. 3 for general discussion). The noise reduction curve shown in Fig. C.15 shows that over 6 dB difference in NR exists between the 63 Hz one-third octave band and the 80 Hz band, the latter having the lower noise reduction. This suggests that increased stiffness may cause the high NR achieved at 63 Hz to shift toward 80 Hz (with the rest of the spectrum also adjusting), which would produce over 6 dB noise reduction at the propeller blade passage rate. Because of the complex shape of the windshield, and the fact that there is a concentrated mass (compass) suspended on it (which may also be contributing to the "peaky" behavior of the noise reduction spectrum), the performance of an alternate windshield should be asessed experimentally (using methods similar to those described in App. C). It is possible that the mass or location of the compass might influence the low frequency behavior of the windshield, thus it could be used constructively to change the dynamic characteristics of the windshield assembly.

E.5.3 Firewall

A stiffened or double firewall is required to eliminate the strong blade-passage rate contribution from the propeller via the engine compartment. The double-wall concept may be difficult to implement effectively because of the number of penetrations, all of which would have to be isolated from the inner wall (a feasible but tedious exercise). A simpler but perhaps less effective approach is to stiffen the firewall to move its low frequency (80 Hz band) dip in the NR curve to a higher frequency (using the same materials as discussed above). Such a scheme was tested and is described in App. F.

E.5.4 Other parts of structure

As mentioned in App. C, the in situ noise reduction measurements made on the test aircraft did not readily reveal the airborne noise reduction characteristics of surfaces of the roof, firewall, and windshield. Low transmission loss characteristics of those elements resulted in flanking paths around other fuselage elements, in spite of efforts to block the flanking transmission. Consequently, successful treatment of the three major paths mentioned would provide most of the needed reduction of airborne noise; however, general experience would indicate that transmission through other fuselage elements would still contribute levels which could be in excess of the cabin noise goals set herein. Therefore, provisions should be made to treat the sidewalls and windows with an appropriate treatment selected from those described above and in Sec. 3 (to the same standard as the three major paths are treated). Alternatively, provisions should be made to quantify the transmission through those elements after the roof, firewall, and windshield have been treated, and treat the residual paths only to the level necessary to achieve the goal selected. We note in closing on this point that intensity measurement techniques would be useful in such a situation.

E.6 Applicability of these Results to Other Aircraft

The results shown herein have general applicability to single-engine propeller aircraft of construction similar to the aircraft tested. For different construction details, the details of the noise reduction requirements will be different than those discussed. However, the strategies for diagnosis and noise control discussed above are broadly applicable to both single- and twin-engine aircraft (the twin-engined aircraft having obvious differences in principal paths, etc.).

APPENDIX F

CONTRIBUTION AND TREATMENT OF CABIN NOISE RESULTING FROM AIRBORNE NOISE IN THE ENGINE COMPARTMENT

F. CONTRIBUTION AND TREATMENT OF CABIN NOISE RESULTING FROM AIRBORNE NOISE IN THE ENGINE COMPARTMENT

F.1. Introduction

This appendix analyzes the role of engine airborne noise as a contributor to noise in the cabin of the demonstrator aircraft. Engine airborne noise refers specifically to the noise radiated from the carburetor inlet, the engine block, and all engine accessories (magnetos, pumps, etc.) but excludes noise from the exhaust ports. It should be recognized that, in general, noise measured in an engine compartment could include contributions from the exhaust ports transmitted through the cowling.

F.2. Geometry and Theoretical Considerations

The engine of the R182 occupies a cavity with lightweight walls immediately adjacent to the aircraft's cabin. Figure F.1 shows several views of the engine and its mounts. Figure F.2 shows the cowling and nosecap elements which form the engine compartments. Figure F.3 shows a simplified schematic of the relationship of elements important to the cabin noise issue. The cavity is open to the external airflow in order to provide induction for the carburetor and cooling for the engine block. The internal flow is periodically interrupted by the propeller, leading to a situation where both hydrodynamic and acoustic disturbances are present in the engine cavity at the same frequencies (blade-passing frequency and multiples thereof). The six-cylinder, horizontally-opposed engine (Avco Lycoming Model 0-540-K3C5D) fills a significant portion of the volume of the cavity as shown in Figs. F.1 and F.2). Figures F.4 and F.5 show photographs of the aircraft with and without the engine in place. An appropriate acoustic model for the engine cavity is then that of a small (relative to the size of the noise source) unsealed enclosure, one wall of which (the firewall) also forms part of the aircraft cabin.

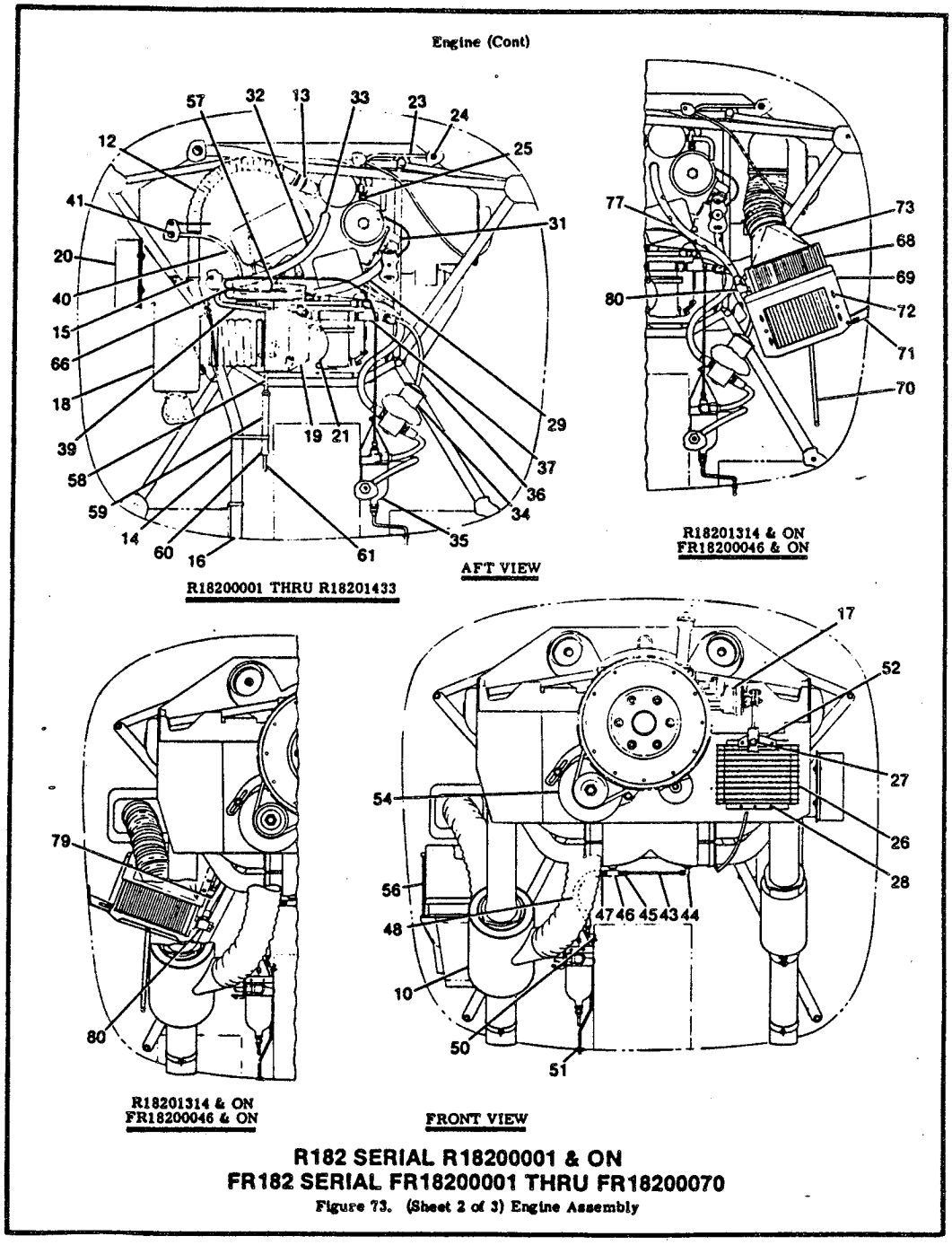

R182 SERIAL R18200001 & ON
FR182 SERIAL FR18200001 THRU FR18200070

Figure 73. (Sheet 2 of 3) Engine Assembly

FIGURE F.1(a) FRONT AND AFT VIEWS OF ENGINE ASSEMBLY

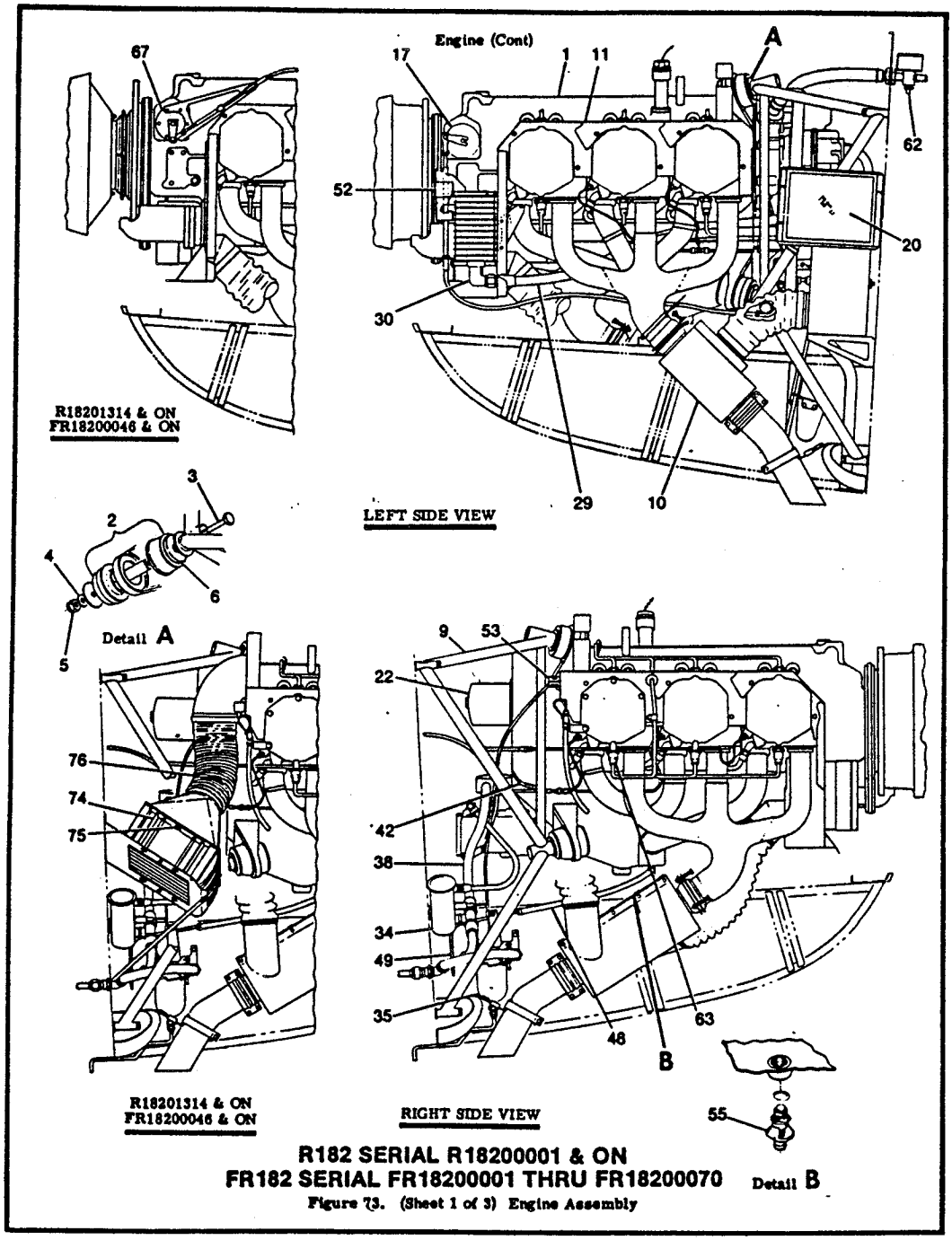

FIGURE F.1.(b) SIDE VIEW OF ENGINE ASSEMBLY

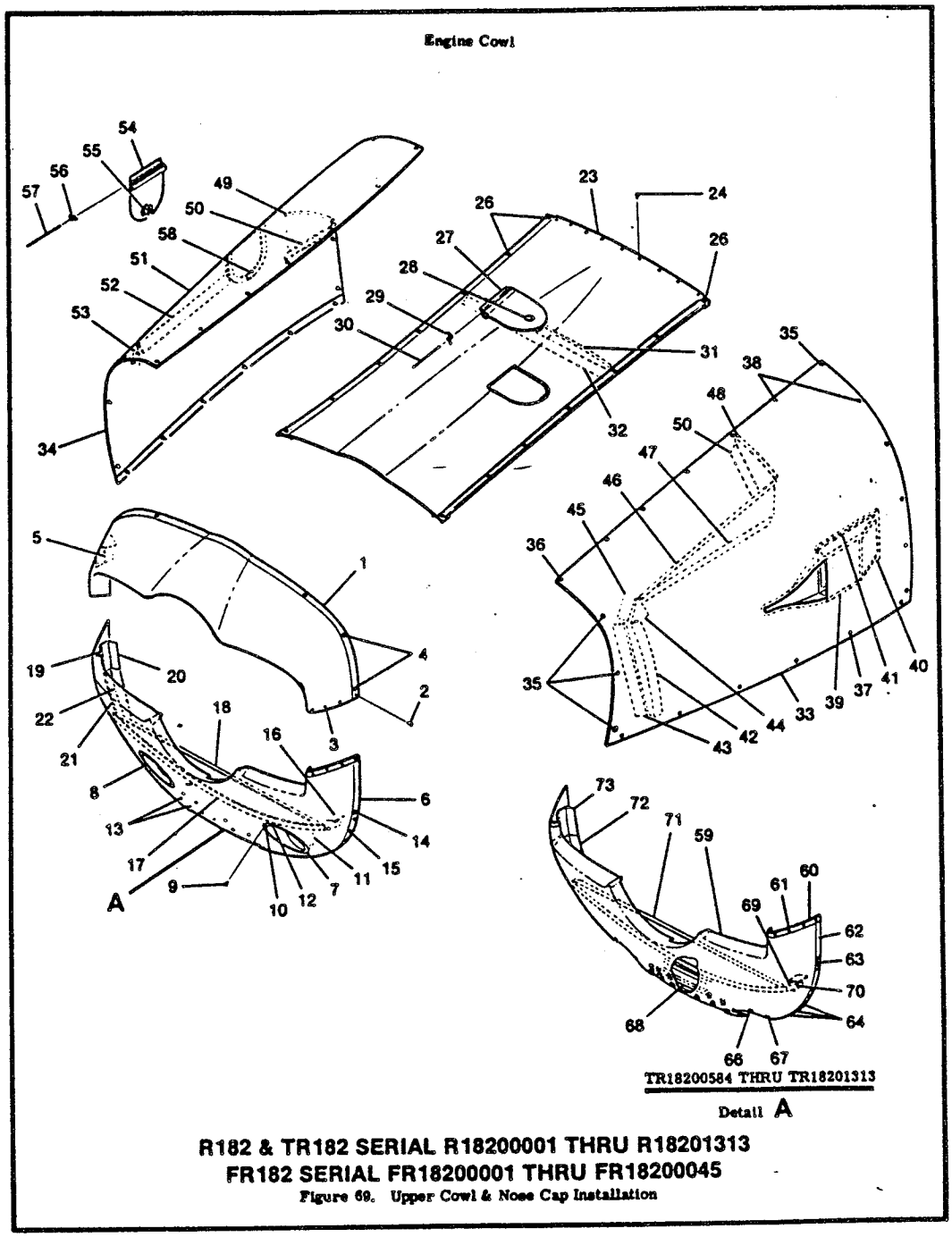

FIGURE F.2 FUSELAGE ELEMENTS FORMING ENGINE COMPARTMENT

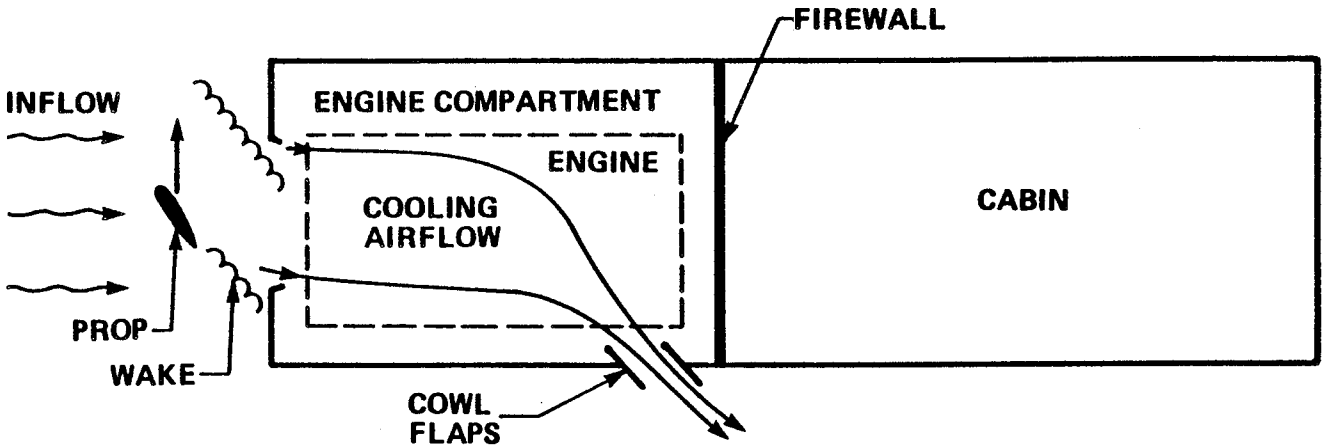

FIGURE F.3 CONCEPTUAL ARRANGEMENT OF ENGINE COMPARTMENT AND CABIN.

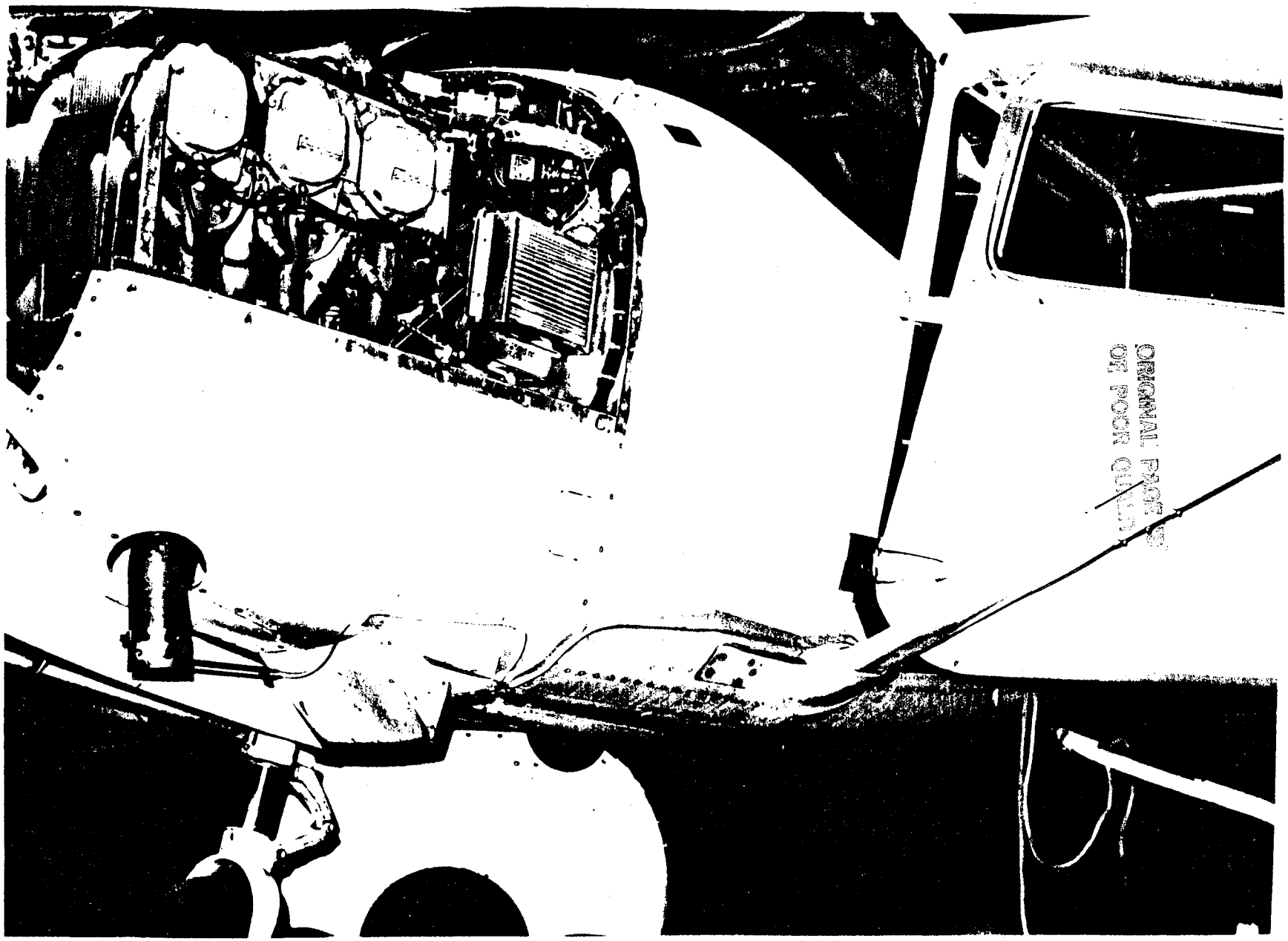

FIGURE F.4 ENGINE COMPARTMENT OF (T)R182 (COWLING REMOVED).

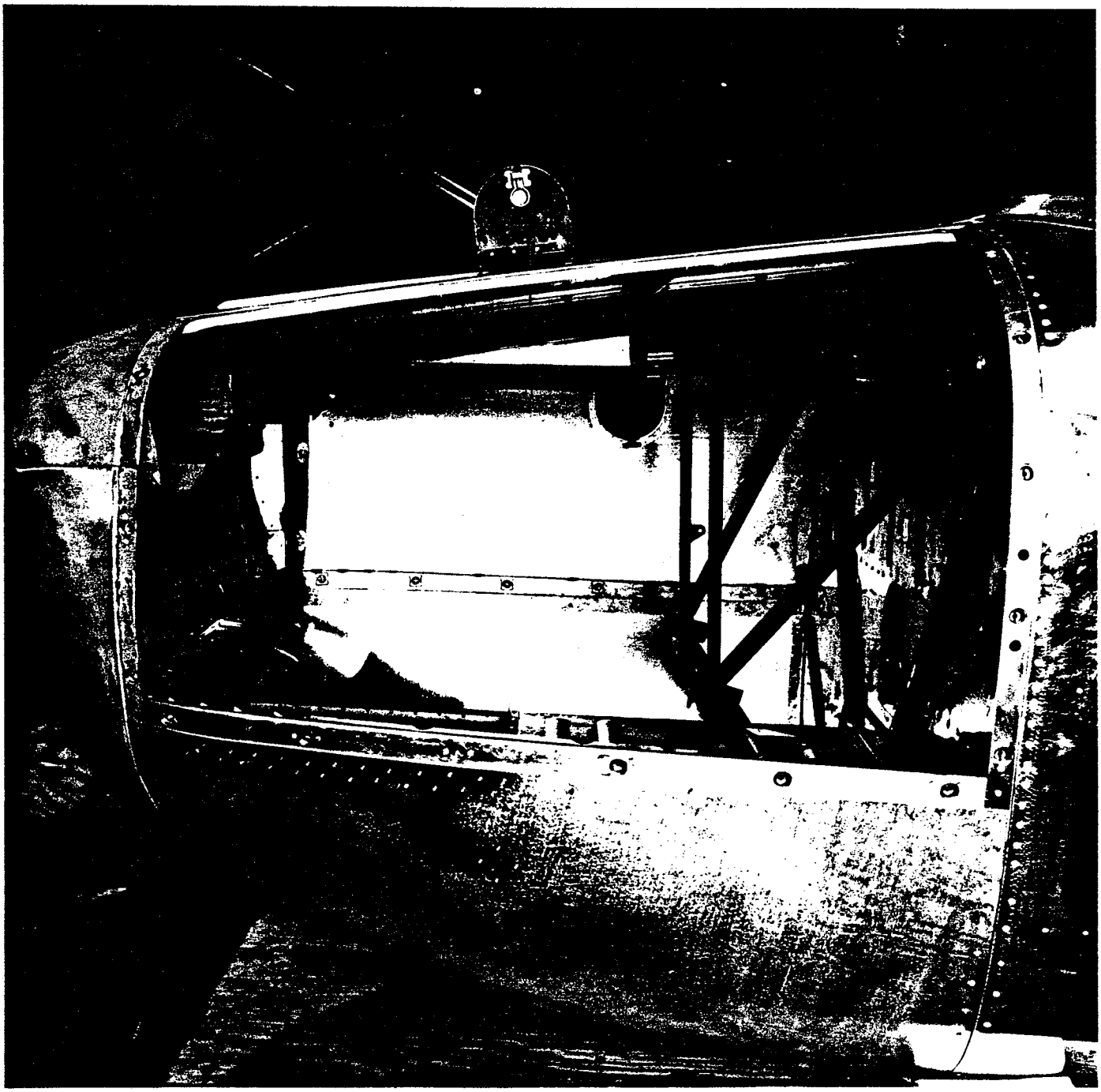

FIGURE F.5 ENGINE COMPARTMENT OF R182. ENGINE REMOVED

F.3 Review of Available Data on Source Levels and Spectra

All available data directly relating to engine compartment noise were recorded aboard a TR182 (turbocharged version of the R182) during tests reported in Ref. 1. For these tests, a microphone was mounted in the top of the engine compartment between the firewall and the rear of the engine block. The airplane was flown with both two- and three-bladed propellers at two engine speeds. One-third octave and narrowband spectra taken during these flights are included in Figs. F.6 through F.9. Note that engine and propeller tones are not separated in frequency when a three-bladed propeller was used. In cases where a two-bladed propeller was mounted, measured pressures in the engine cavity are dominated by propeller-related rather than engine-related pressures. One cannot immediately distinguish whether these are acoustic pressures from propeller noise or hydrodynamic "pumping" of the cavity as the internal airflow is periodically interrupted by the propeller passing the intake. The distinction between hydrodynamic and acoustic pressures is important when considering the excitation of the firewall and other structures. However, the present data are insufficient to clarify the nature of the pressure fluctuations at the propeller blade passing frequency.

F.4 Paths by which Noise Reaches the Cabin

The major paths by which engine airborne noise may enter the cabin are:

a) Acoustic transmission through the firewall;

b) Airborne transmission through the skin of the engine cavity and into the cabin through windows and cabin skin (acoustic flanking of the firewall);

c) Leakage through heating ducts and other penetrations of the firewall.

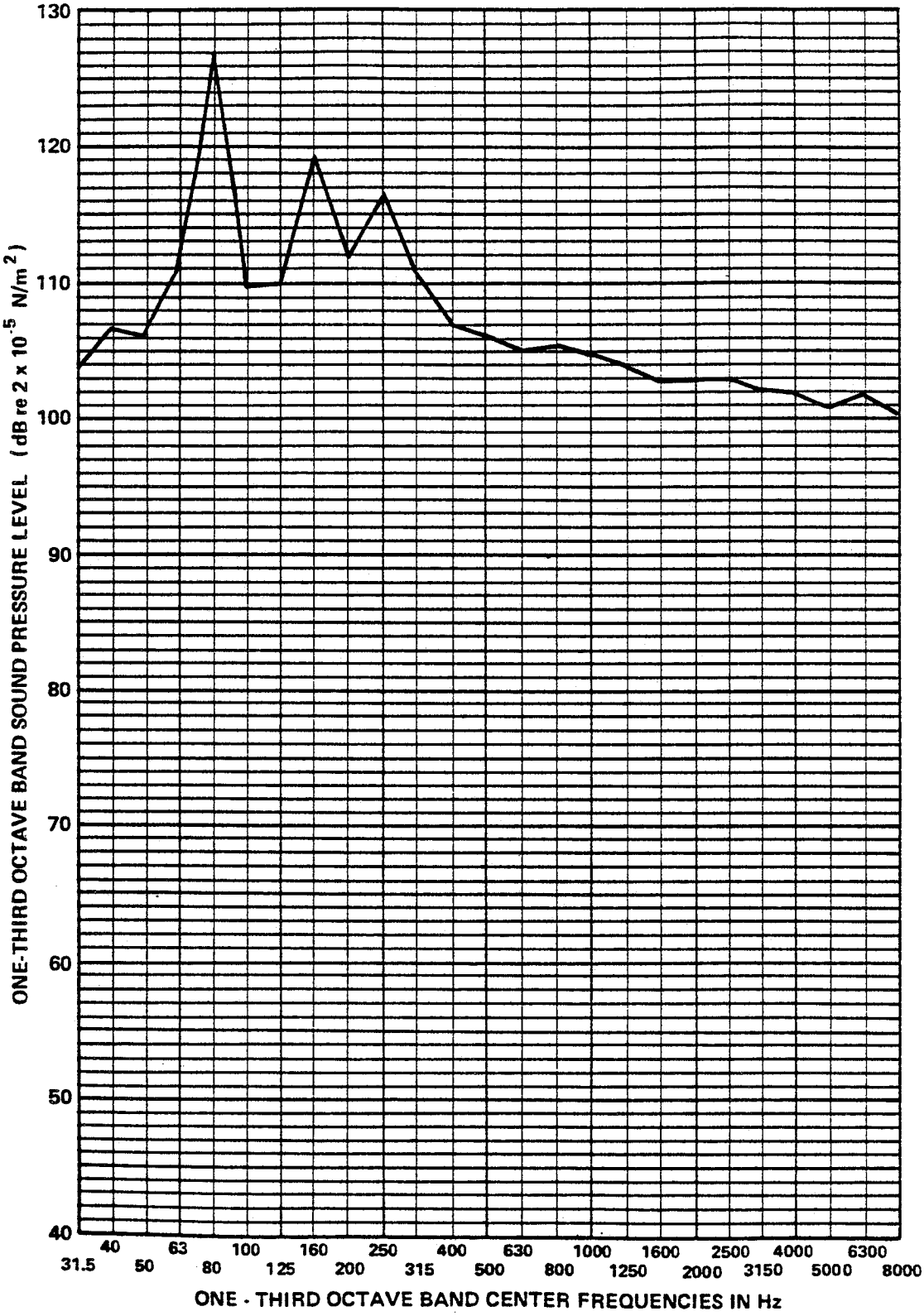

FIGURE F.6 NOISE IN ENGINE COMPARTMENT TR182 WITH TWO-BLADED PROPELLER. CRUISE AT 2400 RPM.

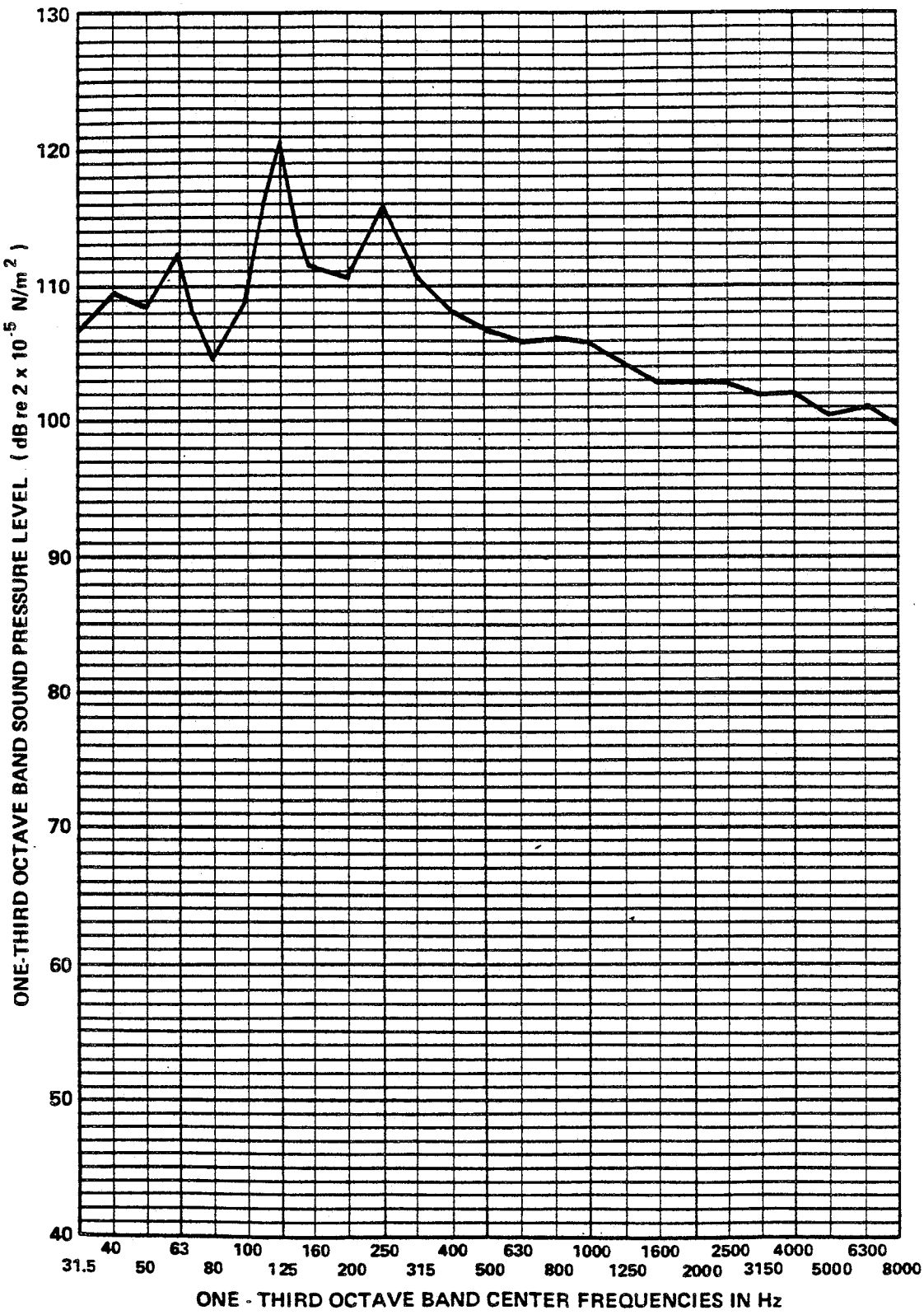

FIGURE F.7 NOISE IN ENGINE COMPARTMENT TR182 WITH THREE-BLADE PROPELLER. CRUISE AT 2400 RPM.

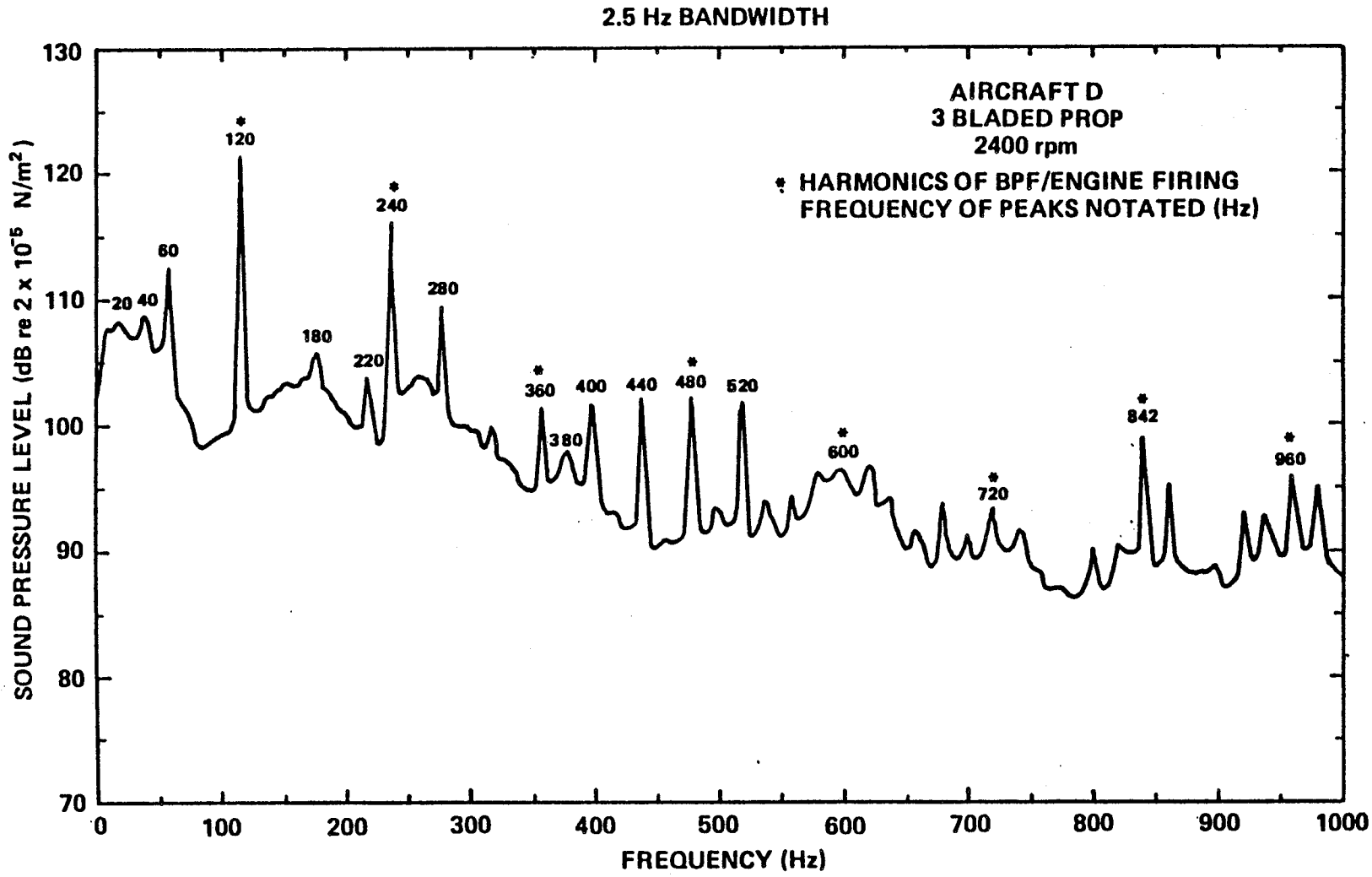

FIGURE F.8 NOISE IN ENGINE COMPARTMENT TR182 WITH THREE-BLADE PROPELLER. CRUISE AT 2400 RPM.

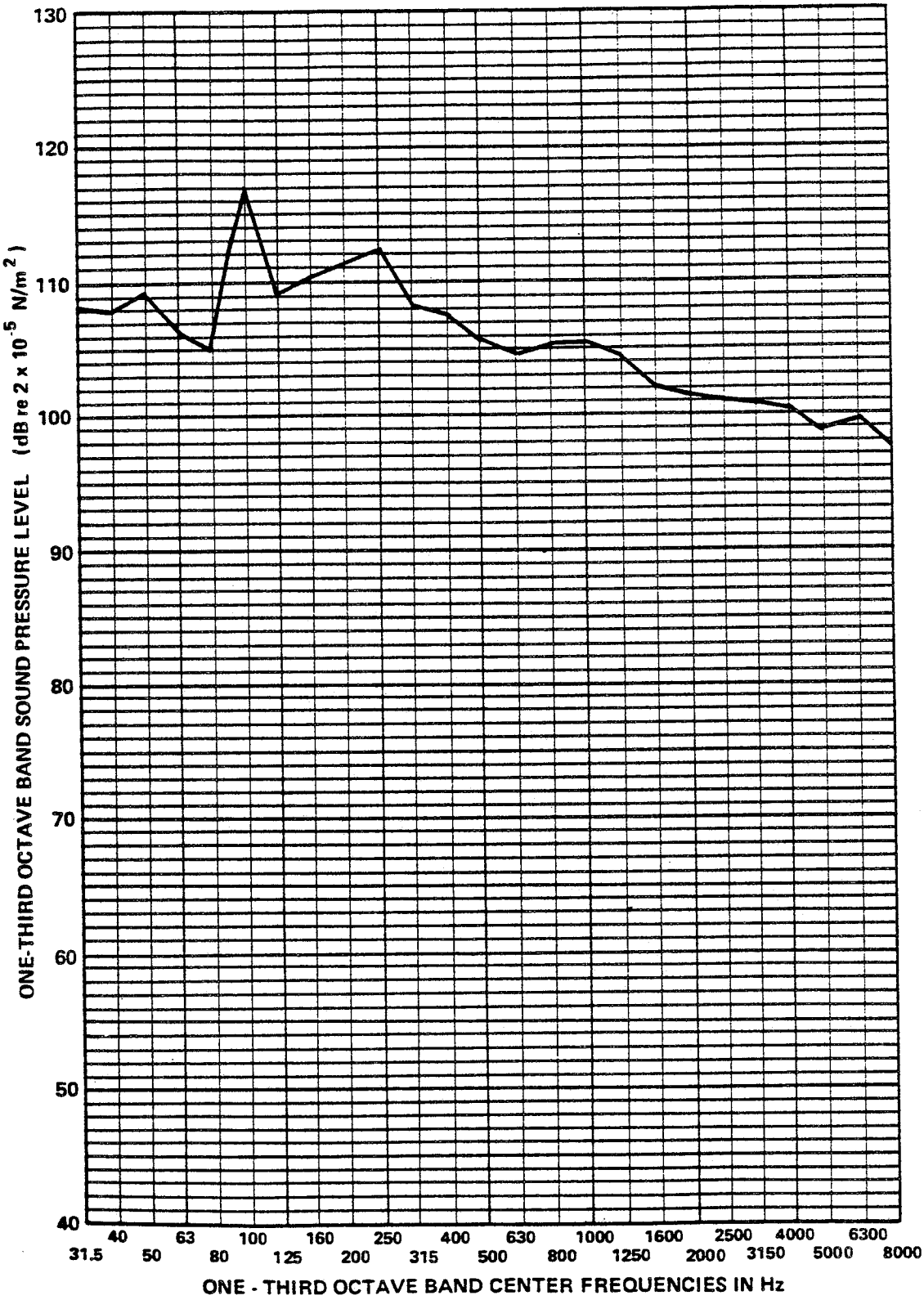

FIGURE F.9 NOISE IN ENGINE COMPARTMENT TR182 WITH THREE-BLADE PROPELLER. CRUISE AT 2100 RPM.

Before investigating individual paths, the overall transfer function relating noise in the engine cavity to cabin noise was measured in the laboratory setup which utilized the partial fuselage. This information, when combined with the flight source levels as reported, allows one to compute the engine compartment noise contribution to noise in the cabin. The laboratory measurement of the transfer function will now be described briefly.

The R182 fuselage was prepared for the engine noise tests by carefully sealing all firewall penetrations to conform with finished production models of the aircraft. The engine volume was simulated by means of a heavy-walled plywood box of the approximate dimensions of the engine as listed by the manufacturer. Two loudspeakers were mounted in the box to provide broadband noise in the engine cavity (See Fig. F.10). Two microphones were mounted in the engine cavity, one of which replicated the microphone position used during the flight tests. The spectra at these two positions are shown in Fig. F.11, in which some variation is apparent. Additional microphones were placed at positions in the cabin where flight noise measurements had been made. The spectra at these locations for the simulated engine source are shown in Fig. F.11. A final microphone was used to survey the exterior sound field of the airplane caused by noise in the engine cavity. It was found that relatively low levels on the fuselage are caused by the engine compartment airborne sound (Fig. F.12). The transfer function relating sound in the engine cavity to sound at the cabin center can be computed directly from these data, as shown in Fig. F.13, where the low noise reduction in the 80 and 100 Hz bands is very evident, apparently reflecting a firewall resonance and/or strong coupling with a cabin or engine compartment acoustic mode.

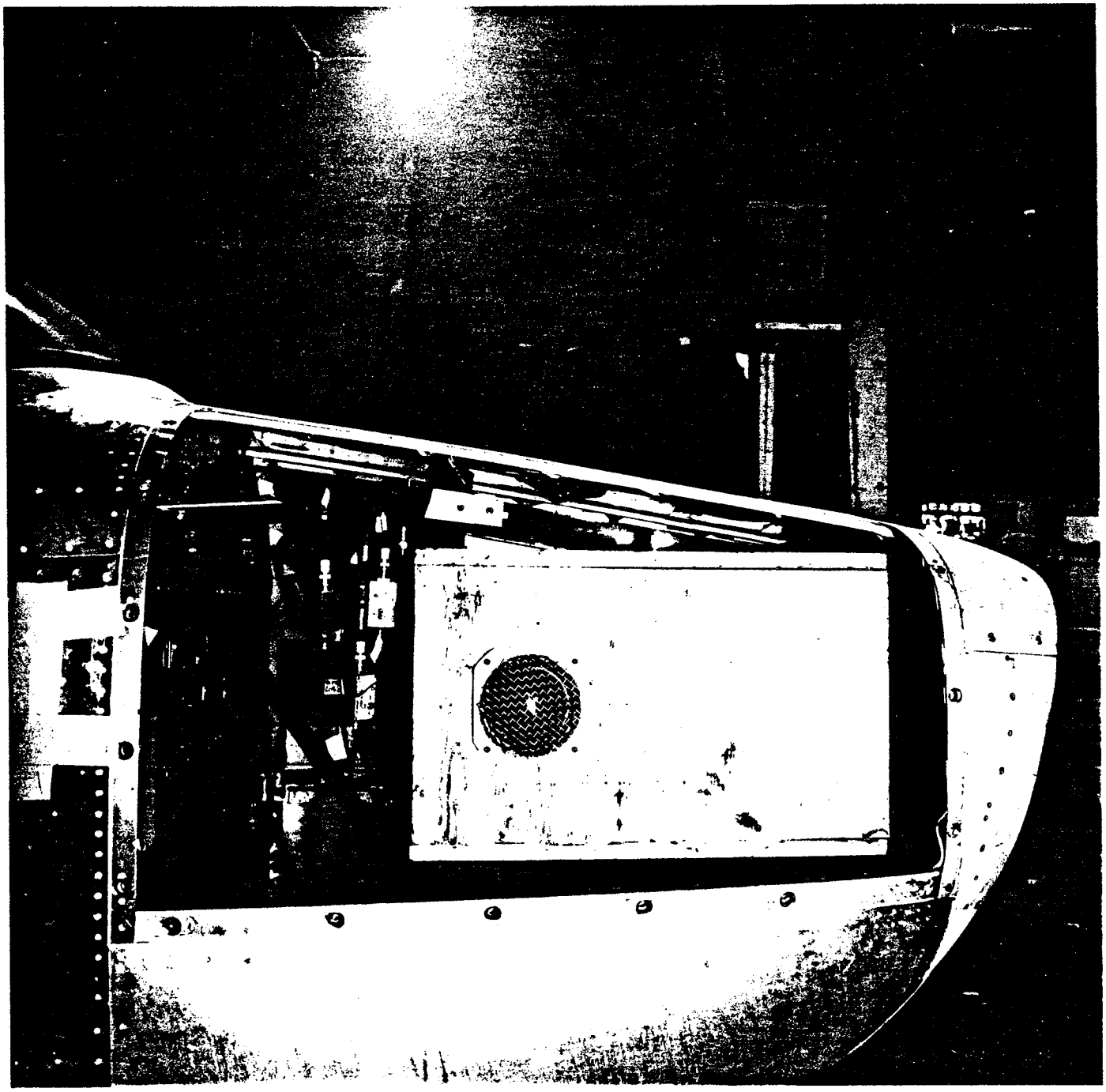

FIGURE F.10 NOISE SOURCE FOR LABORATORY SIMULATION OF AIRBORNE ENGINE NOISE.

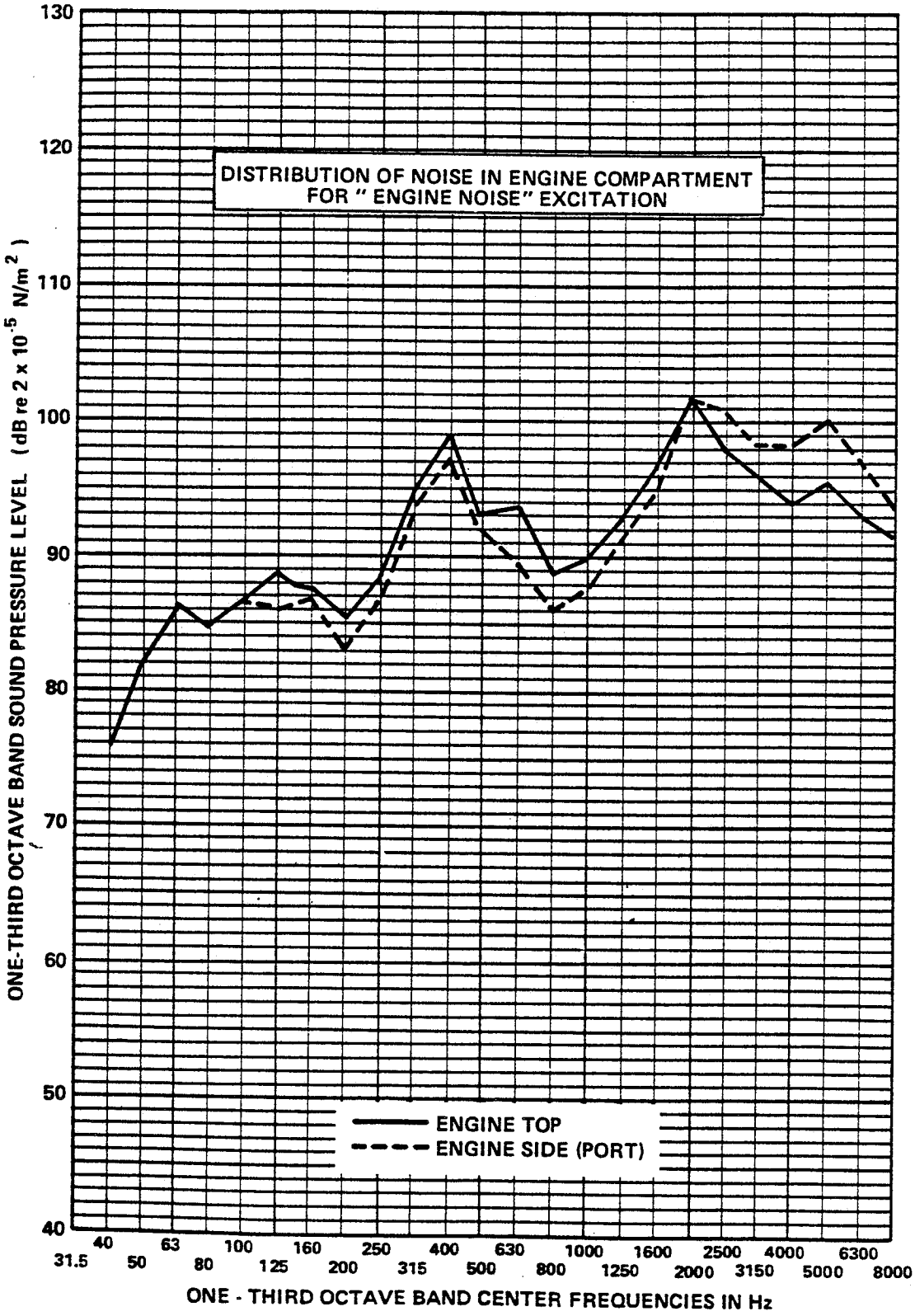

FIGURE F.11 ONE-THIRD OCTAVE SPL SPECTRA IN ENGINE COMPARTMENT CAUSED BY SIMULATED ENGINE SOURCE

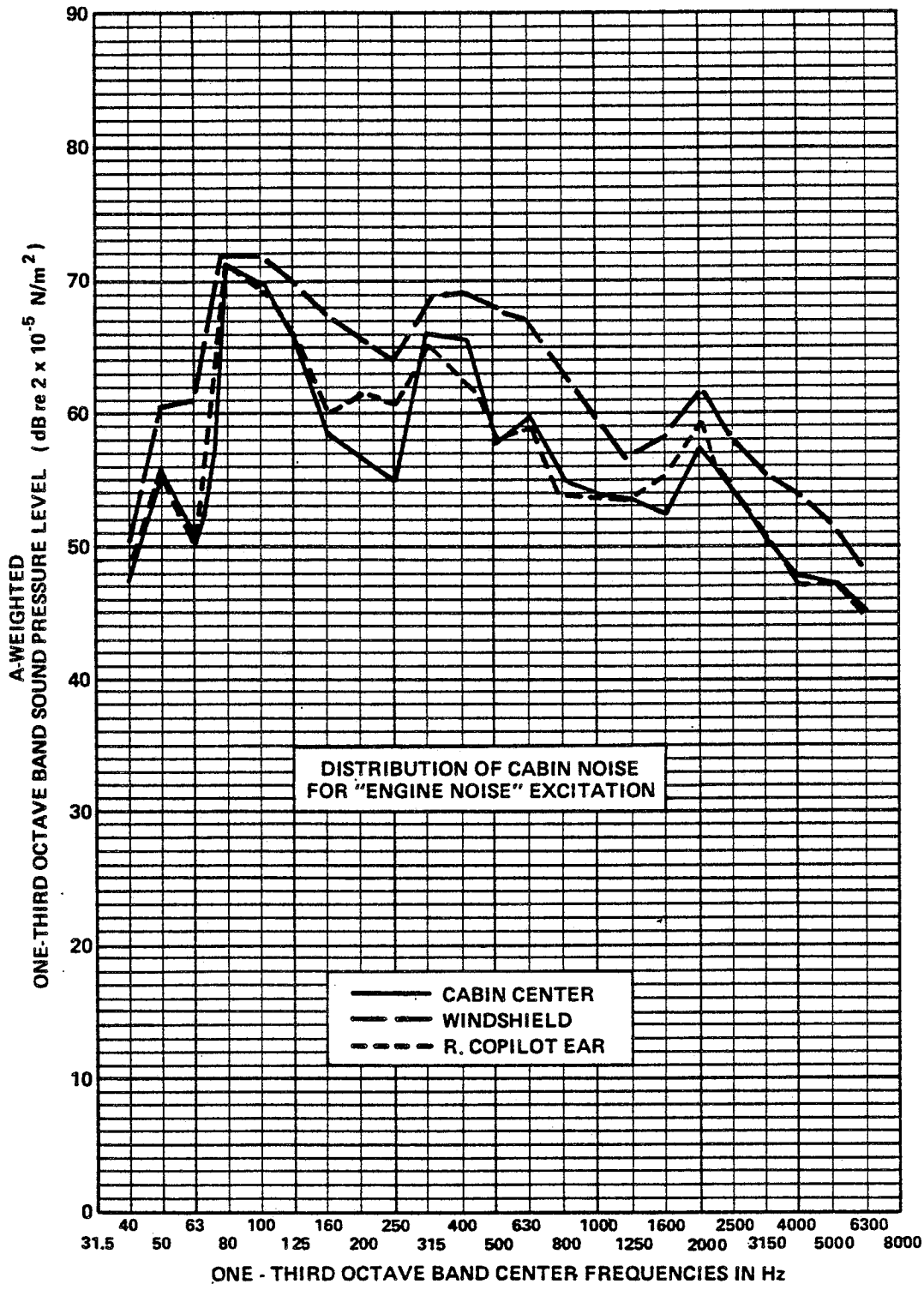

FIGURE F.12 CABIN NOISE SPECTRA CAUSED BY SIMULATED ENGINE COMPARTMENT NOISE SOURCE

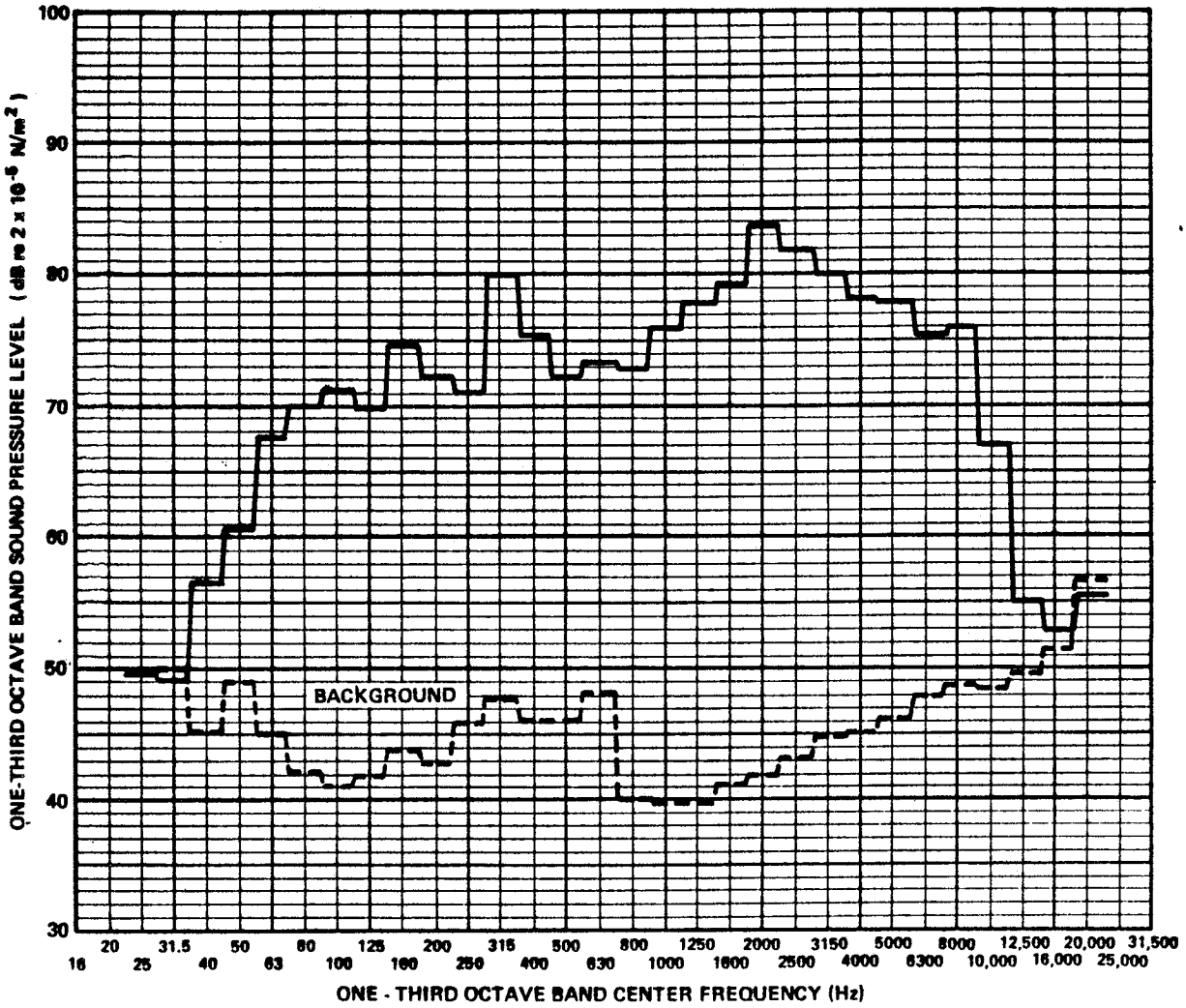

FIGIRE F.13. SHIN PANEL ACOUSTIC LEVELS CAUSED BY SIMULATED ENGINE COMPARTMENT NOISE.

F.5 Estimated Contribution to Cabin Noise

The estimated contribution to cabin noise by the airborne sound in the engine compartment is plotted in Fig. F.14. Two measurements of cabin noise (in flight - from all sources and paths) are plotted for comparison. The engine noise is seen to contribute to cabin noise at all frequencies of interest, but the prediction method appears to overpredict the noise at blade passage rate (80 Hz). The most plausible explanation for this overprediction is that the pressure sensed by the engine microphone is dominated at 80 Hz by hydrodynamic effects associated with the cooling airflow behind the propeller rather than propeller or engine acoustic pressures, or that the single microphone position used in flight was not representative of the spatial average at the firewall. In general it is clear that airborne sound in the engine compartment is a significant contributor to low frequency cabin noise when compared with contributions from other sources.

F.6 Treatments Applicable to Reducing Source/Path Contributions

The above data show that the dominant path by which engine compartment airborne noise enters the cabin is acoustic transmission through the firewall. In general, the treatments applicable to the firewall are the same as those by which airborne transmission through the cabin walls may be controlled. Possible treatments include:

a) Increasing the panel thickness (mass) of the firewall, which presently consists of one layer of stamped aluminum;

b) Increasing the firewall stiffness by means of a structural honeycomb panel or local stiffeners;

c) Using a double-wall construction for the firewall to decouple the panels in the engine compartment and cabin.

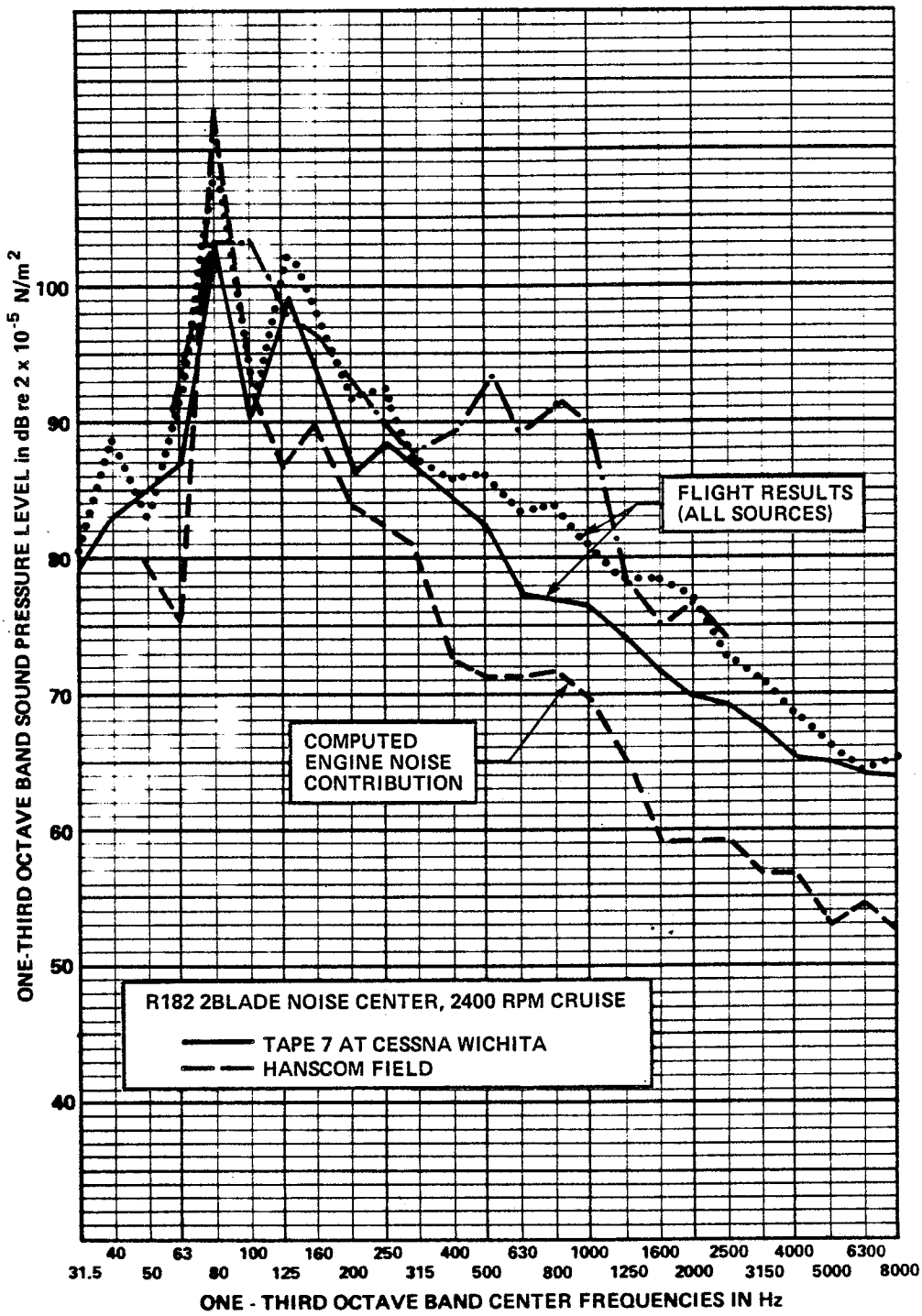

FIGURE F.14 CABIN NOISE CONTRIBUTION RESULTING FROM ENGINE COMPARTMENT NOISE.

Since the predominant characteristic of the firewall transmission is a narrow band of low transmission loss which coincides with strong periodic excitation from the propeller, the major priority is to shift the frequency of high response (transmission) to a different frequency. Increasing the firewall mass without stiffening would shift the response peak to a lower frequency and at the same time improve high frequency noise reduction. However, considerable mass addition would be required to achieve a significant frequency shift; also if the engine speed was maintained somewhat below the normal cruise rpm, at the discretion of a given pilot, the excitation could coincide with the modified response peak. Therefore, the approach pursued was to stiffen the firewall.

The first approach used to stiffen the firewall was to add stiffening elements locally. These elements, as described in App. C (Sec. C.5), show that up to 8 dB reduction in the 80 Hz third octave band was achieved (Fig. C.18). Some benefit was also realized at higher frequencies.

As an approach to increase the high frequency noise reduction and move the frequency of low noise reduction below the excitation frequency, a double-wall construction was considered. In making a preliminary assessment of the double-walled firewall, we found that for reasonable wall thicknesses, it is virtually impossible to take advantage of the improved transmission loss of the double-walled design. This is because the real transmission loss benefits of a double-walled panel are not realized until well above the frequency at which the mass of the two walls resonates on the stiffness of the air space between time. That frequency is given by

$$f_o = \frac{1}{2\pi} \frac{\rho c^2}{d} \left\{ \frac{M_1 + M_2}{M_1 M_2} \right\} ,$$

C-3

where ρ is the air density, c the acoustic wave speed, d the panel spacing, and M_1 and M_2 the mass per unit area of the panels. For two 60-mil panels separated by 2.54 cm (1 in.), the resonance frequency is 250 Hz. To move the frequency to below 10 Hz would be impossible with realistic panel masses and the spacing available.

As an alternative to the above approach, one could attach a honeycomb panel to the current firewall to increase the stiffness, and obtaining improved transmission loss that way. This panel would need to conform to the shape of the firewall and provide for a sealed gap around its perimeter. Unfortunately, limited resources prevented our examining this approach in any detail.

F.7 Applicability of Results to Other Aircraft

The measured transfer function relating engine compartment airborne noise to cabin noise in the R182 should be applicable to other single engine, nonpressurized aircraft in the Cessna fleet. Given the similarity of construction methods used in the general aviation industry, the transfer function should be approximately correct for single engine, nonpressurized aircraft built by other manufacturers. The distribution of engine compartment airborne noise around the exterior of the aircraft is also likely to be typical of a general trend for aircraft with similar cooling vent arrangements and cowling construction. The relative importance of engine compartment noise as a contributor to cabin noise for non-Cessna aircraft is probably not typical because of differences in engine mounting methods, exhaust systems, airframe and windshield construction, etc., which could alter the relationship between competing noise sources and paths.

The results generated for the test aircraft are expected to be of no direct value in assessing noise contributions in light, twin-engine aircraft because engine noise is decoupled from the cabin by relatively large distances. However, the engine compartment airborne levels measured would be typical for similar engines in similar confines.

APPENDIX G

NOISE DUE TO AIRFLOW

G. NOISE DUE TO AIRFLOW

G.1 Introduction

It is common experience in transport aircraft for broadband noise to be dominant in the cabin area during high speed flight, and landing approach when high lift surfaces and landing gear are deployed. The cabin noise in such cases results from a complex combination of acoustic radiation from flow interaction with surface discontinuities ("airframe noise"), hydrodynamically-induced wave motion in the cabin wall ("boundary layer noise"), and structureborne vibration caused by unsteady aerodynamic loads on wing and tail surfaces, landing gear and landing gear door covers, and control surfaces. The most extensively studied of these sources has been the excitation of the skin by attached turbulent boundary layers; for this source, extensive analytical models and flight test data bases are available. Noise created by deployed airframe surfaces and landing gear during final approach is recognized but, due to the short duration of this phase of flight, relatively little attention has been given to modeling or measuring the relevant sources and paths related.

Airflow-induced noise in light propeller-driven aircraft arises from similar mechanisms, although little attention has been given to the entire subject in the context of these aircraft. However, the flight survey phase of this study [1] provided conclusive evidence that airflow-induced noise was a significant contributor to the overall acoustic environment in the cabin of the test aircraft selected (as well as in others). Therefore, in the present study, analytical and experimental efforts were devoted to improving the understanding of sources and paths of airflow-related mechanisms on the test aircraft. Analytical efforts included modeling the response of the skin to the turbulent boundary layer excitation. A wind tunnel test of the specially constructed fuselage was also carried out to

provide data on the excitation pressure field and typical response levels as well as data for noise induced by flow over the landing gear cutouts. Structureborne noise caused by separated flow interaction with wing and tail surfaces was not explicitly studied, although it is clear that significant low frequency sound may be caused by those mechanisms. The sections below describe (1) analytical considerations related to flow excitation of the structure and the resultant response and radiation (Secs. G.2 through G.4), (2) the wind tunnel experiments (Secs. G.5 and G.6), (3) methods to reduce airflow-induced noise (Section G.7).

G.2 Outline of Analytical Procedure

One likely source of the broadband noise is the aerodynamic pressure field on the exterior of the cabin. This pressure field could be generated by the attached turbulent boundary layer and by any disturbed-flow components associated with flow separation around the windshield and with flow around protuberances. For this reason a simplified analysis has been performed to estimate the role played by the attached turbulent boundary layer. Additional factors associated with disturbed flow have been excluded since details of the flow field around the cabin are not well known. Inclusion of these factors would be highly speculative. In any case, the analysis was performed just to obtain an indication of the magnitude of the contribution.

G.2.1 Structural response

Several methods are available to estimate the response of the cabin structure to boundary layer excitation. These methods include closed-form modal analyses, finite element representations, wave approach, and statistical energy analysis methods. The different methods require different degrees of detail in

representing the structure and different amounts of computation. Since the objective of the present overall program is to explore a number of possible noise sources and transmission paths, it was decided to use one of the simplified analytical models for the response to boundary layer excitation. This model is based on the wave propagation approach.

Using this approach the linear response of a structure to a stationary, homogeneous, random excitation can be expressed in terms of the acceleration spectrum $G_a(\omega)$ at any point

$$G_a(\omega) = \iint \frac{\omega^2 G_p(\underline{k},\omega)\, d\underline{k}}{|Z_s(\underline{k},\omega) + 2Z_a(\underline{k},\omega)|^2} \qquad (G.1)$$

where $G_p(\underline{k},\omega)$ is the wavenumber-frequency spectrum for the excitation pressure field, $Z_s(\underline{k},\omega)$ is the normal impedance of the structure, and $Z_a(\underline{k},\omega)$ the normal impedance of the surrounding fluid. The excitation cross-spectral density function can be written in the form

$$G_p(\underline{\xi},\omega) = G_0(\omega)\, e^{-c_1\left|\frac{\omega\xi_1}{U_c}\right|}\, e^{-c_2\left|\frac{\omega\xi_2}{U_c}\right|}\, e^{-i\,\frac{\omega\xi_1}{U_c}} \qquad (G.2)$$

where U_c is the convection velocity of the pressure field. Then

$$G_p(\underline{k},\omega) = \frac{1}{(2\pi)^2} \iint G_p(\underline{\xi},\omega)\, e^{-i\underline{k}\cdot\underline{\xi}}\, d\underline{\xi}$$

$$= \frac{4c_1c_2(\omega/U_c)^2\, G_0(\omega)}{(2\pi)^2\, [c_1^2(\omega/U_c)^2 + (k_1+\omega/U_c)^2]\, [c_2^2(\omega/U_c)^2 + k_2^2]} \quad . \qquad (G.3)$$

The integrand in Eq. G.3 has two major regions which contribute significant parts of the integral. These occur at $|k| = k_b$ and $k_1 = \omega/U_c$. The first region is associated with resonant response of the structure and the second with convection of the excitation pressure field. Thus,

$$G_{a,res}(\omega) = G_p(k_b,\omega) \int \frac{\omega^2 d\underline{k}}{|Z_s(\underline{k},\omega) + 2Z_a(\underline{k},\omega)|^2}$$

$$= \frac{\pi^2\omega^2 G(\underline{k}_b,\omega)}{2\omega\eta c_L \kappa m_s^2} \tag{G.4}$$

and

$$G_{a,conv}(\omega) = \frac{\omega^2}{\left|Z_s\left(\frac{\omega}{U_c},\ \omega\right) + 2Z_a\left(\frac{\omega}{U_c},\ \omega\right)\right|^2} \int G_p(\underline{k},\omega)\, d\underline{k}$$

$$= \frac{G_0(\omega)\omega^2}{(m_s\omega)^2} \left|\frac{k_b^4}{(\omega/U_c)^4}\right|^2 \tag{G.5}$$

where m_s = surface mass density

$\kappa = h/\sqrt{12}$ = radius of gyration

c_L = longitudinal wavespeed in structure

h = plate thickness

k_b = resonant wavenumber

η = structural loss factor.

An estimate of $G(k_b,\omega)$ can be obtained from the low wavenumber approximation for Eq. G.3. When $k_1 << \omega/U_c$ and $k_2 << \omega/U_c$, then

$$G(k_b,\omega) \approx \frac{(c_1/c_2)G_0(\omega)}{\pi^2(\omega/U_c)^2} \quad . \tag{G.6}$$

Typical values of c_1 and c_2 are $c_1 = 0.1$ and $c_2 = 0.7$. The procedure followed for predicting the excitation pressure power spectral density function $G_0(\omega)$ is described in the next section. Empirical values for the structural loss factor η are given in Sec. G.3.2.

The preceding equations are valid only in the mid- and high-frequency regimes where the panel boundaries are not too important in determining the structural response. At low frequencies the individual modal response is more important. This low frequency dependency can be approached from the general modal equation for acceleration power spectral density $G_a(f)$. This can be written in the form, excluding cross terms,

$$G_a(f) = G_p(f) \frac{A^2}{4} \omega^4 \sum \Psi_a^2(\underline{x}) \, |H_\alpha(\omega)|^2 \, J_{mm}(\omega) J'_{nn}(\omega) \qquad (G.7)$$

where A is the panel area, $\Psi_\alpha(\underline{x})$ is the mode shape for mode $\alpha \equiv (m,n)$, $H_\alpha(\omega)$ is the response function and $J_{mm}(\omega)$, $J'_{nn}(\omega)$ are the panel joint acceptance functions in the directions parallel and perpendicular to the flow direction.

$$|H_\alpha(\omega)|^2 = 1/\{M_\alpha^2 \omega_\alpha^4 \, [(1 - \frac{\omega^2}{\omega_\alpha^2})^2 + \eta_\alpha^2]\} \qquad (G.8)$$

$$\rightarrow 1/M_\alpha^2 \omega_\alpha^4 \quad \text{as} \quad \omega \rightarrow 0 \quad .$$

If $G_p(f)$, $J_{mm}(\omega)$ and $J_{nn}(\omega)$ are constant as $\omega \rightarrow 0$, which is a reasonable assumption when $\alpha = (1,1)$ is the dominant mode, then $G_a(f) \sim f^4$ at small f and the one-third octave band acceleration level $\sim 10 \log f^5$. The simplified method given in Eqs. G.5 and G.6 is not valid when $f \sim f_{11}$, and the prediction procedure has to incorporate the preceding low frequency asymptotic approximation.

G.2.2 Boundary layer pressure fluctuations

Measurement of turbulent boundary layer pressure fluctuations in the wind tunnel and on commercial airliners have provided empirical prediction methods which usually involve the calculation of the broadband mean square pressure $\overline{p}^2$ followed by the calculation of the pressure power spectral density. The aerodynamic parameters used in the analysis are the free stream flow velocity (airplane speed), the wall shear stress (or skin friction) and the boundary layer thickness. For larger aircraft it has been found that the alternating adverse and favorable pressure gradients along the fuselage have no significant effect on the boundary layer growth. Consequently, the boundary layer thickness can be calculated with reasonable accuracy under the assumption of a zero pressure gradient. It is probably that the accuracy of this assumption is less good for the present airplane configuration but, in the absence of more detailed information, the assumption will still be applied.

Based on empirical data, the root mean square pressure $\sqrt{\overline{p}^2}$ is assumed to be proportional to the wall shear stress τ_w with the relationship

$$\sqrt{\overline{p}^2} = 2.6\ \tau_w \qquad \text{(G.9)}$$

where the wall shear stress is given by

$$\tau_w = c_f q_0 \quad . \qquad \text{(G.10)}$$

While the precise value of the constant of proportionality in Eq. G.9 is open to debate, the range of possible values is small and 2.6 is a reasonable compromise.

The pressure spectrum is obtained from the non-dimensional model spectrum based on Boeing 737 data, which is shown in Fig. 5(c) of [G.1]. In [G.1], the nondimensional frequency is given in terms of the Strouhal number $2\pi f\delta/U_0$ and the nondimensional power spectral density is given by $G_0(f)U_0/2\pi\bar{p}^2\delta$.

G.2.3 Acoustic radiation

The preceding discussion has concentrated on the vibration of skin panels and window panes exposed to broadband aerodynamic excitation. The final interest, however, lies in the cabin sound levels rather than structural vibration. Thus, the discussion should be extended to include acoustic radiation into the cabin. Detailed analysis of the coupling between the vibration modes of the structure and the acoustic modes of the cabin is a complicated procedure [G.2, G.3] and it is outside the scope of the present study. A simpler approach, which is valid only when there are several structural and acoustic modes in the frequency band of interest, is that of statistical energy analysis.

If $\langle p_i^2 \rangle$ denotes the space-average, mean square acoustic pressure in the cabin, then (see for example [G.4])

$$\langle p_i^2 \rangle = \frac{\rho_i c_i^2 \sigma}{\pi^2 f^2 \bar{\alpha}} \cdot \frac{S_t}{S_\alpha} \langle a^2 \rangle \qquad \text{(G.11)}$$

where ρ_i and c_i are, respectively, the ambient density and speed of sound in the cabin; S_t and S_α are the transmitting (or radiating) and absorbing areas, respectively; $\bar{\alpha}$ is the average acoustic absorption coefficient for the cabin interior; $\langle a^2 \rangle$ is the space-average, mean square acceleration of the radiating panel; and f is the center frequency of the band of interest. In general, the radiation efficiency coefficient σ is given by [G.4]

$$\sigma = \frac{\sigma_{AF} n_{AF} + \sigma_{AS} n_{AS}}{n_{AF} + n_{AS}} \qquad (G.12)$$

where n represents structural modal density and subscripts AF and AS refer to acoustically fast and acoustically slow modes, respectively. For the present case where the structure consists essentially of flat panels with critical frequencies above the range of interest.

$$\sigma = \sigma_{AS}$$

where σ_{AS} is a function of panel perimeter P, area S, and thickness h, as indicated in Fig. G.1. An upper bound estimate for σ can be taken as unity.

G.3 Cabin Structure

G.3.1 Resonance frequencies

The structure of the Model 182 cabin is of riveted skin/stringer/frame construction, the skin thickness being 0.64 mm (0.025 in.) except for three areas (cabin top forward of the rear spar, cabin doors, and baggage door) where the thickness is 0.81 mm (0.032 in.). The panel dimensions vary from panel to panel, unlike larger aircraft where there is extensive repeatability in panel size. Because of this variation in panel dimensions, a detailed analysis of all individual panels is time-consuming, and probably not necessary. What is necessary is an indication of the dynamic characteristics of representative panels, particularly those for which vibration data are available, and reported in [G.5]. Structural items selected for consideration are the window pane in the cabin door, side panels in the cabin structure, and bottom panels. Dimensions for a number of the skin panels and the door window are listed in Table G.1.

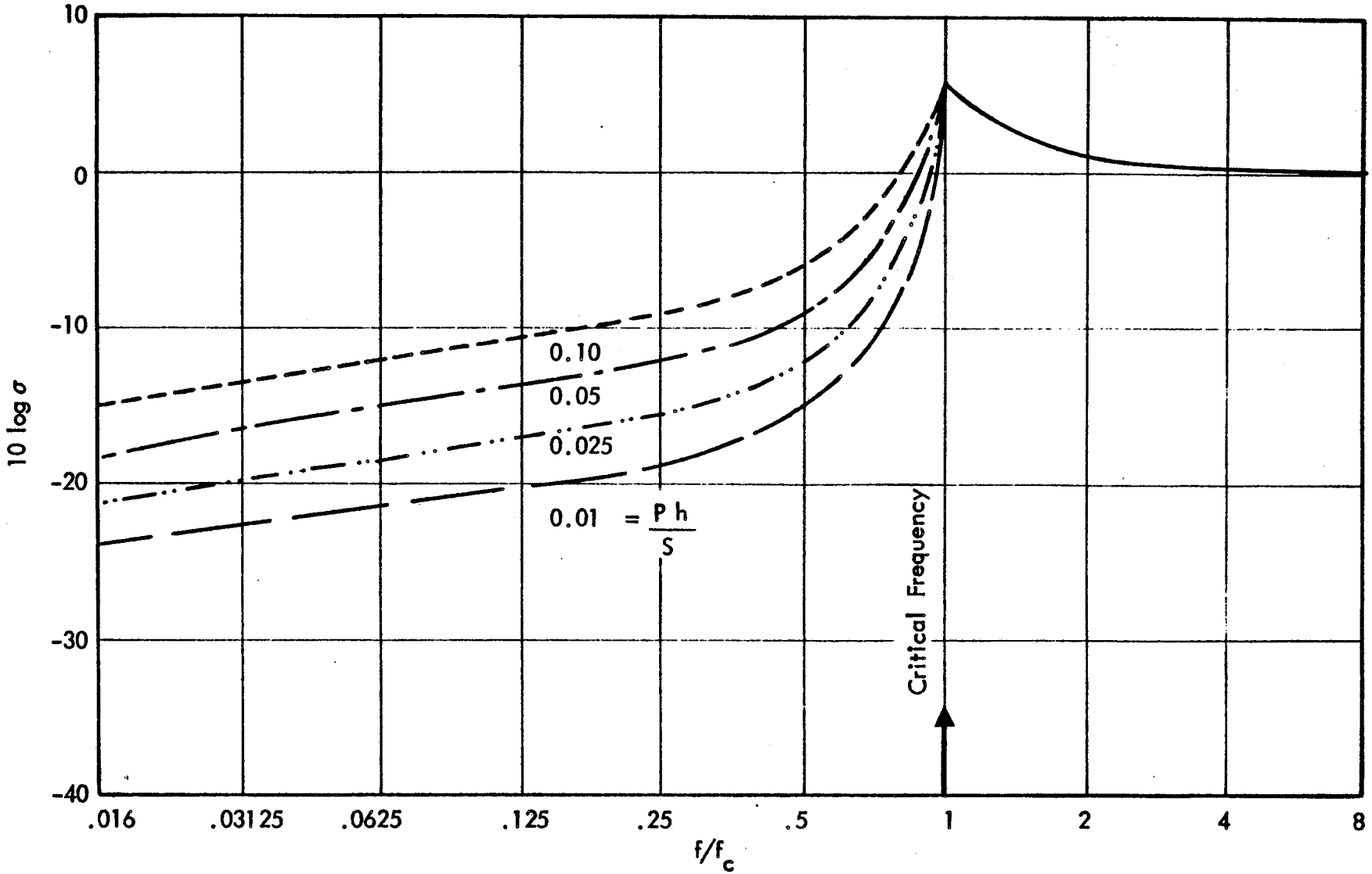

FIGURE G.1. RADIATION EFFICIENCY OF FLAT PANELS (SIMPLE SUPPORTED EDGES).

TABLE G.1

PANEL DIMENSIONS

Panel Description	Panel Dimensions*		
	L_x m (in.)	L_y m (in.)	h mm (in.)
Cabin Sidewall	0.46(18)	0.17(6.5)	0.64(0.025)
	0.46(18)	0.25(10)	0.64(0.025)
	0.60(23.5)	0.17(6.5)	0.64(0.025)
	0.48(19)	0.27(10.5)	0.64(0.025)
Floor Panel	0.28(11)	0.10(3.9)	0.64(0.025)
Tail Cone Panel	0.36(14)	0.11(4.35)	0.64(0.025)
	0.41(16)	0.13(5.25)	0.64(0.025)
	0.41(16)	0.22(8.5)	0.64(0.025)
Cabin Door Window	0.76(30)	0.32(12.75)	3.18(0.125)

*L_x is dimension in longitudional (flow) direction
L_y is dimension in circumferential direction
h is thickness.

Estimates of the lower and upper bounds for the panel resonance frequencies can be obtained assuming simply-supported or clamped boundary conditions, respectively. Values of resonance frequencies for simply-supported modes of order (m,1) are given in Table G.2 for the panels listed in Table G.1. Resonance frequencies for other modes of the bottom skin panel are given in Table G.3.

TABLE G.2

PANEL RESONANCE FREQUENCY FOR MODE ORDERS (m,1) AND SIMPLY-SUPPORTED BOUNDARY CONDITIONS

Panel Description	Resonance Frequency (Hz)											
	m=1	2	3	4	5	6	7	8	9	10	11	12
Sidewall Panel	63.7	85.8	122.5	174.0	240.2	321.0	416.6	526.8	651.8	791.5	945.9	2225.9
	31.2	53.2	90.0	141.4	207.6	288.5	384.0	494.3	619.3	758.9	913.3	1082.4
	60.7	73.6	95.2	125.4	164.2	211.6	267.7	332.4	405.7	487.7	578.2	677.4
	28.2	48.0	81.0	127.2	186.5	259.1	344.9	443.9	556.0	681.4	819.9	971.7
Floor Panel	176.3	235.3	333.8	471.5	648.7	865.2	1121.1	1416.4	1751.0	2125.0	-	-
Tail Cone Panel	138.0	174.5	235.2	320.3	429.7	563.3	721.3	903.6	1110.2	1341.1	-	-
	95.7	123.6	170.1	235.3	319.0	421.4	542.3	681.9	840.0	1016.8	1212.2	1426.2
	42.3	70.2	116.7	181.8	256.6	367.9	488.9	628.4	786.6	963.3	1158.7	1372.7
Door Windows	28.3	41.3	63.0	93.3	132.2	180.0	236.3	301.3	375.0	457.4	548.4	648.0

TABLE G.3

PREDICTED RESONANCE FREQUENCIES FOR FLOOR PANEL

Mode Order m	Simply Supported Boundaries		Clamped Boundaries
	Resonance Frequencies (Hz)		
	n = 1	n = 2	n = 1
1	176.3	646.1	371.6
2	235.3	705.1	420.8
3	333.8	803.5	511.3
4	471.5	941.3	647.1
5	648.7	1118.3	828.5
6	865.2	1335.0	1054.0
7	1121.1	1590.9	1322.2
8	1416.4	1886.2	1631.9
9	1751.0	2220.8	1982.4
10	2125.0	2594.8	2373.3

G.3.2 Panel Damping

Typical values of panel damping have been measured for three structural items on the test airplane. The measurements were made on a cabin sidewall panel, a tailcone panel, and a door window panel. The data are shown in Fig. G.2, and smoothed curves (for use in the analysis) are drawn through each set of data. Lowest damping was measured on the untreated tailcone structure, with higher damping on the cabin walls being due to the sidewall treatments.

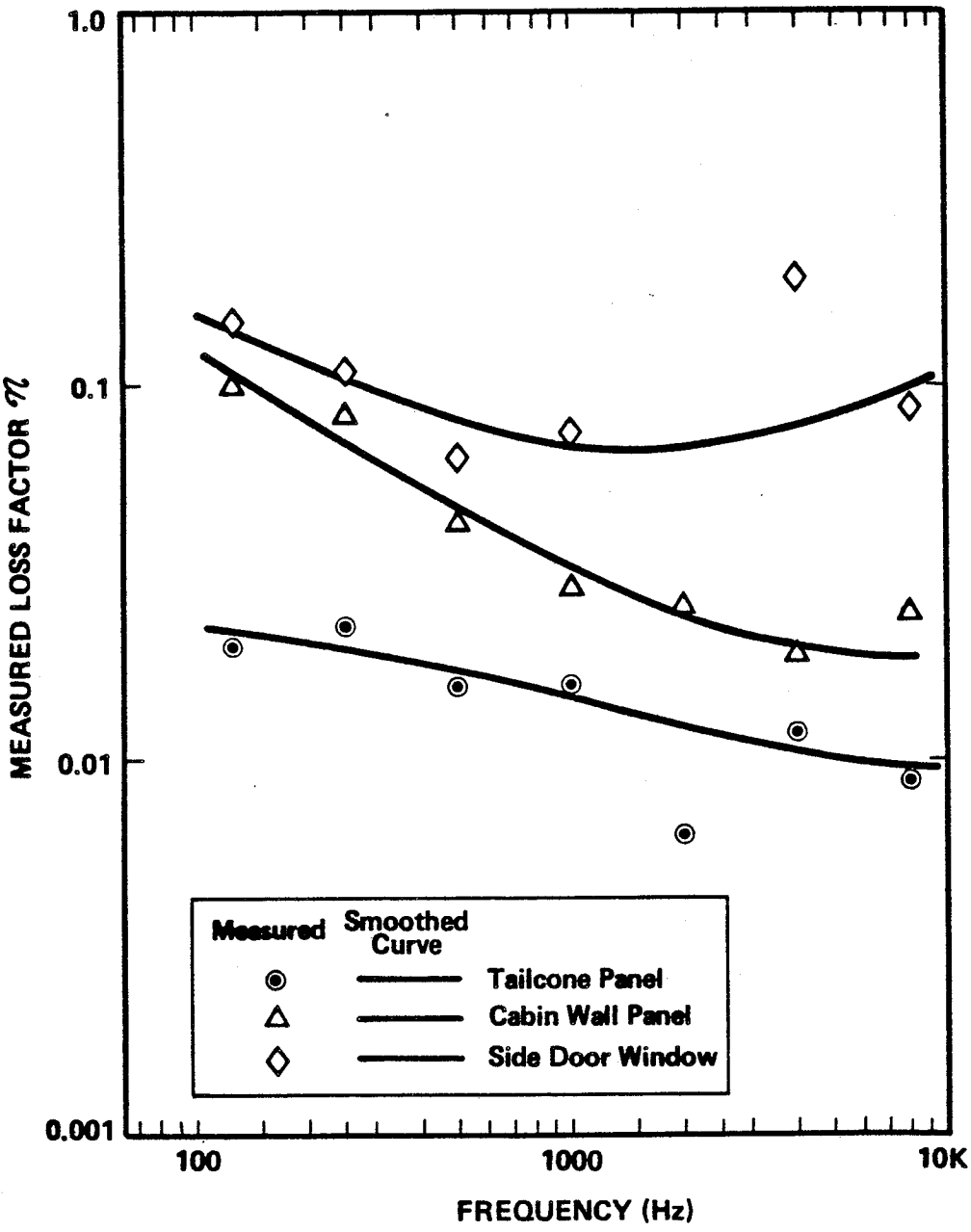

FIGURE G.2. DAMPING LOSS FACTORS.

G.4 Analysis of Flight Test Data

G.4.1 Boundary layer pressure spectrum

The flight conditions selected for study are those associated with one of the tests on a Model 182 airplane. They are:

Airplane speed U_0 = 266 km/hr = 242 ft/sec = 143 kts

Airplane Altitude = 1520 m = 5000 ft

Airplane Mach number M_o = 0.22

Flight dynamic pressure q_0 = 2.87 kN/m^2 = 60 lb/ft^2.

A typical location at the center of the cabin sidewall was selected as a reference, the distance from the airplane nose being 2.96 m (9.4 ft). The estimated boundary layer thickness δ is 38 mm (1.5 in.) and the skin friction coefficient c_f is 0.198. An associated pressure spectrum can now be calculated using the method outlined in Sec. G.2.2. The resulting spectrum is plotted in Fig. G.3. It is interesting to compare this prediction with measurements made on the test fuselage in the BBN wind tunnel. The measurements were on the bottom surface of the fuselage at a longitudinal station roughly equivalent to the location used for the prediction. The boundary layer thickness measured in the wind tunnel test is 15.2 mm (0.6 in.), which is approximately 40% of the value predicted above. The measured one-third octave band pressure levels are about 3 dB higher than those predicted for the turbulent boundary layer. Thus, although the prediction procedure is being used for rather extreme conditions, it appears to be reasonably accurate. Obviously, in-flight measurements are highly desirable.

G.4.2 Aerodynamic coincidence

Characteristic frequencies for infinite panels are the critical or coincidence frequencies associated with acoustic and aerodynamic excitation. The acoustic coincidence frequencies for the sidewall panel and the window of the test airplane are about 18,000 Hz and 9,800 Hz, respectively, well above the frequency range of interest. Coincidence frequencies associated with turbulent boundary layer excitation are much lower. Assuming that the convection speed U_c of the pressure field over the structure is 0.8 U_0, the infinite panel coincidence frequencies are approximately 570 Hz and 150 Hz for the skin and window, respectively.

The effective coincidence frequencies for finite panels may be different from the infinite panel values. However, in the case of acoustic excitation the critical frequencies are so high, and the corresponding flexural wavelengths so short, that the panels can be considered as infinite. This is not the case for boundary layer excitation, and the approach outlined in [G.6] was used to estimate typical coincidence frequencies. In this approach, modal frequencies are calculated for modes of varying order m and unit order n, where (m,n) are mode orders for panel axes parallel and perpendicular to the flow direction. The longitudinal component U_x of the flexural wave velocity is then determined by

$$U_x = f_{m1} \lambda_m \qquad \text{(G.13)}$$

where λ_m is the modal wavelength in the longitudinal direction

$$\lambda_m = 2L_x/m \quad . \qquad \text{(G.14)}$$

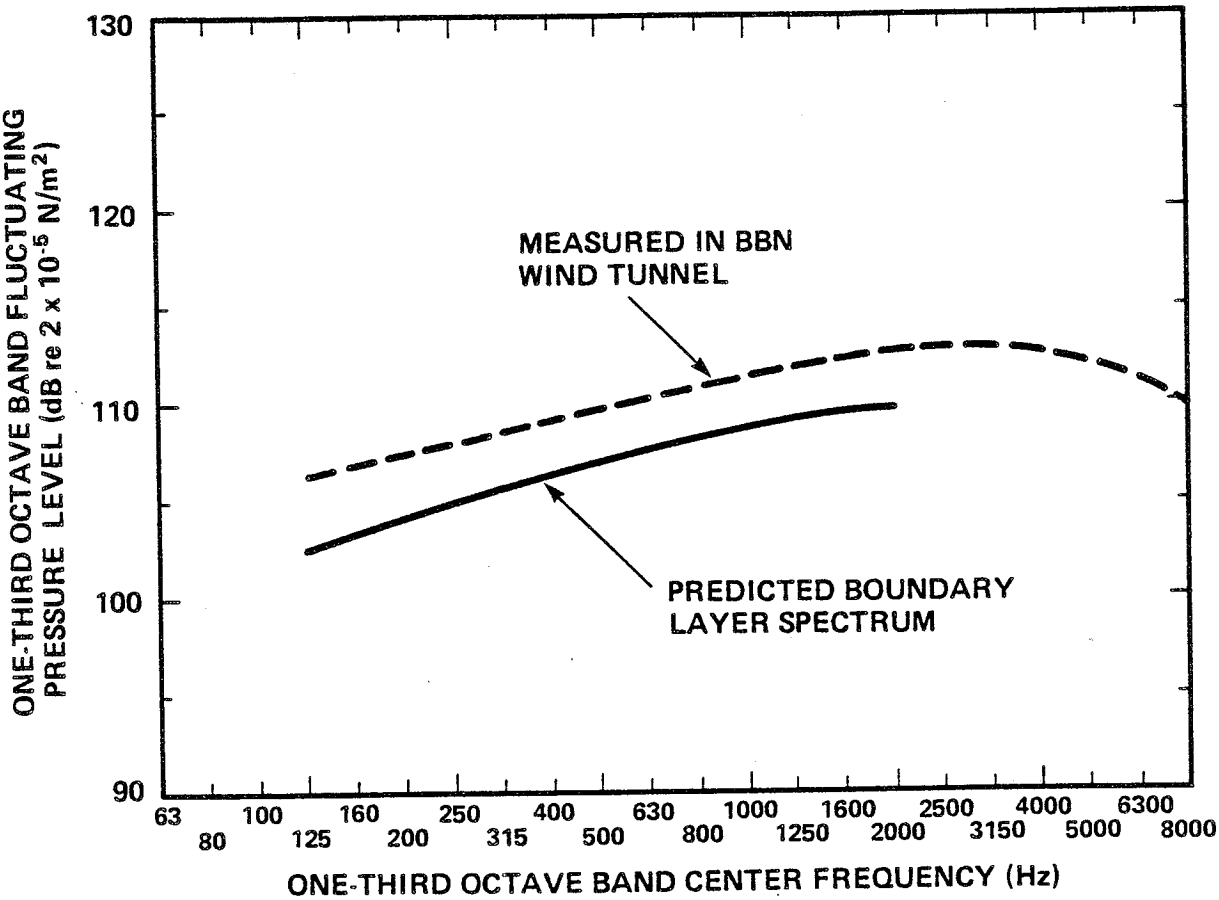

FIGURE G.3. EXTERIOR PRESSURE SPECTRA FOR CABIN.

Finally, U_x and the pressure field convection velocity U_c are compared graphically and the intersection points of the corresponding curves define coincidence frequencies. Sample comparisons for these panels are shown in Figs. G.4 through G.6. Two values of U_c are plotted in the figures, the value of $0.8\ U_0$ being that associated with the turbulent boundary layer, and the higher value of $1.1\ U_0$ being included to show the influence of changes in local flow velocity. In several cases there are two intersection points for the flexural wave and excitation convection speed curves. The higher frequency is found to be similar to, but lower than, the condition for coincidence in an infinite panel. The lower frequency is dependent on the panel aspect ratio, defined as the ratio of panel length in the flow direction to panel width. The higher the aspect ratio, the higher the associated coincidence frequency.

The main conclusions to be drawn from Figs. G.4 through G.6 are that, although aerodynamic coincidence frequencies for the finite-size panels lie below the corresponding frequencies for infinite panels, the differences are not large. The coincidence frequencies generally lie below 500 Hz, which is in the frequency range of interest in this study and in a range in which engine-off tests showed significant noise in the cabin.

G.4.3 Panel vibration

Vibration induced by the turbulent boundary layer has been predicted for two structural regions of the Model 182 cabin. One structural region contains the skin panels on the cabin sidewall and the other structure is the window panel on the cabin door. The predicted space-average, one-third octave band acceleration spectra are compared in Figs. G.7 and G.8 with spectra measured, during flight, at the center of the respective panels.

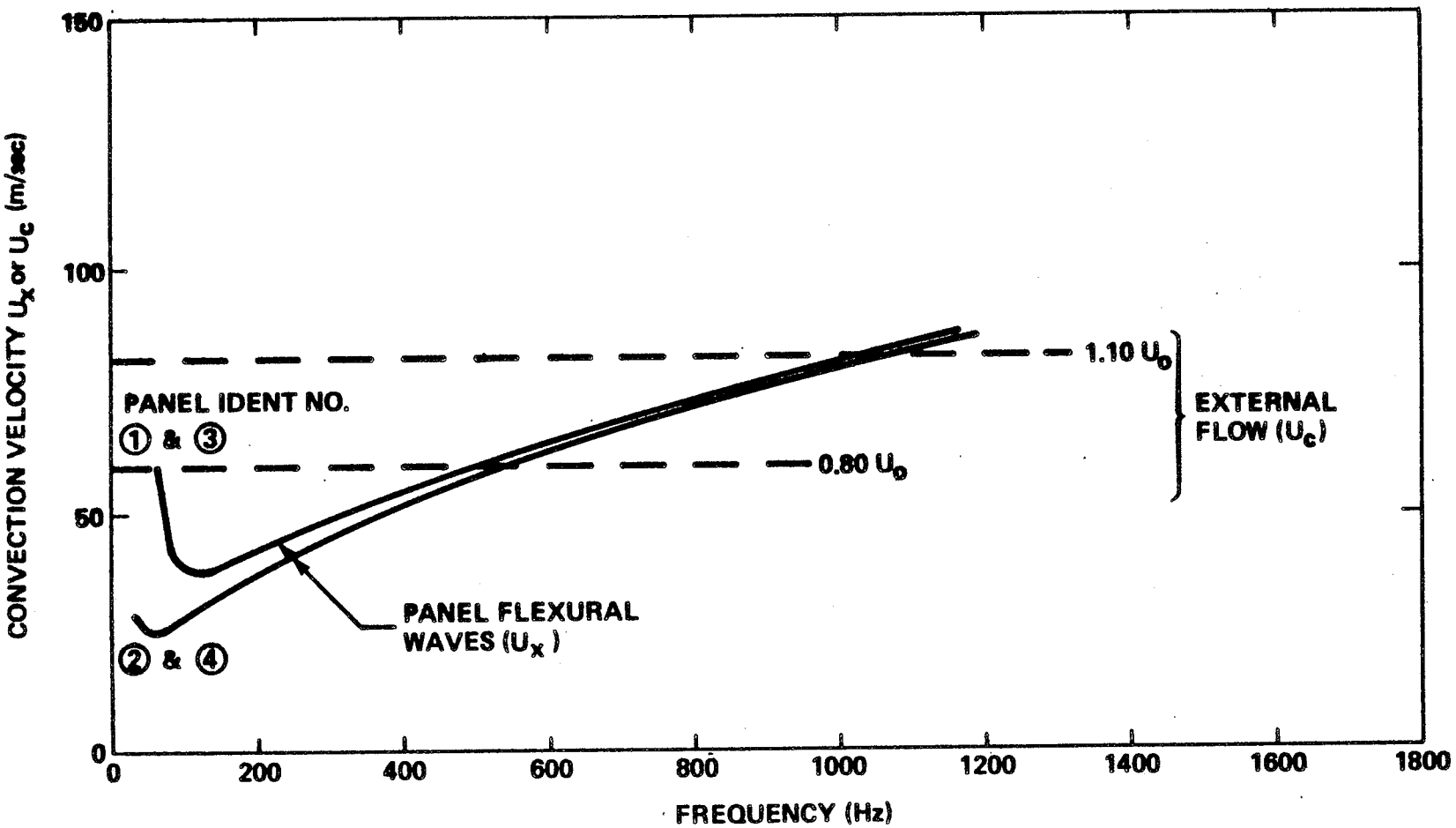

FIGURE G.4 CONVECTION SPEEDS: CABIN SIDEWALL (REAR).

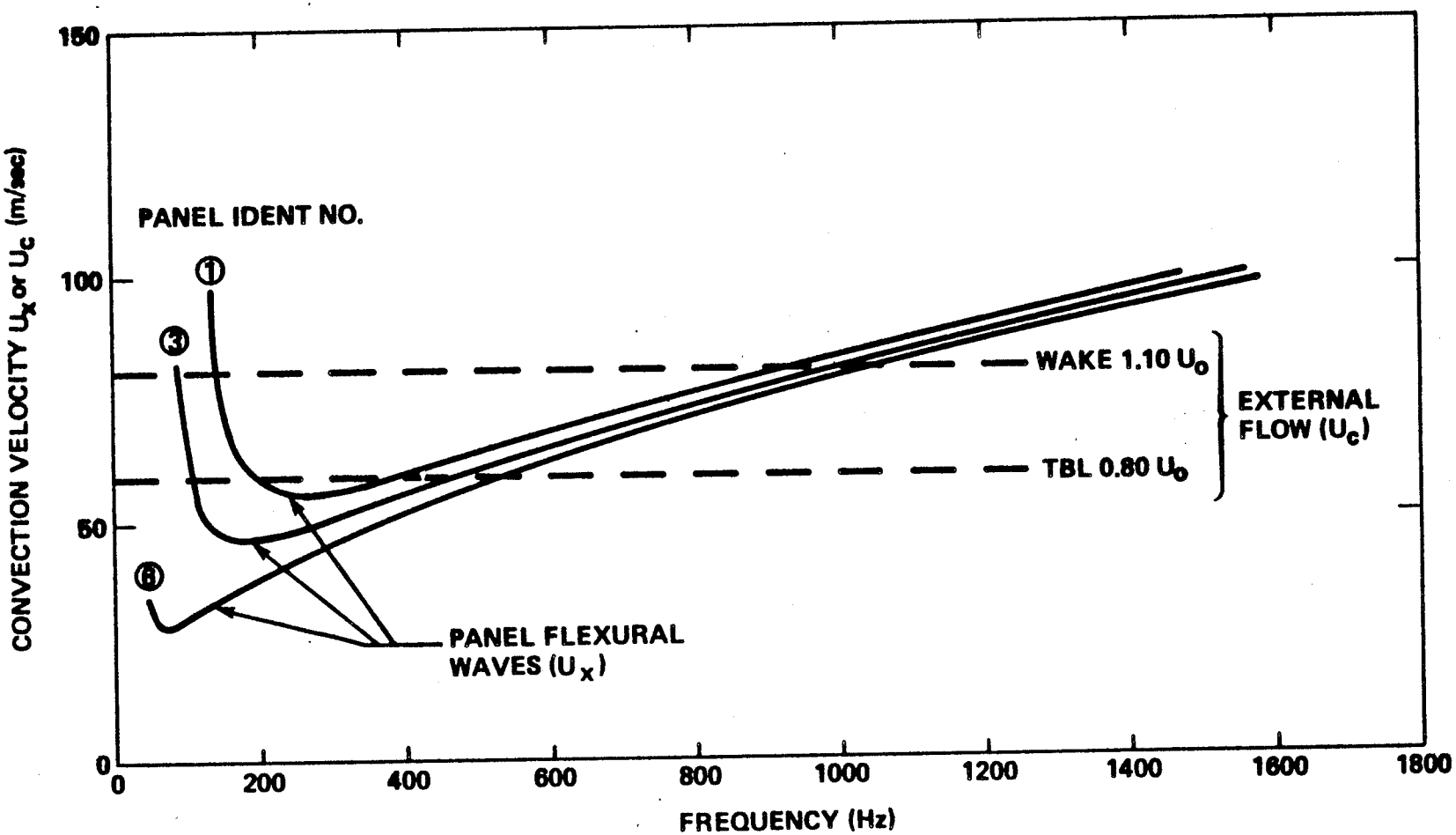

FIGURE G.5. CONVECTION SPEEDS: TAILCONE PANELS.

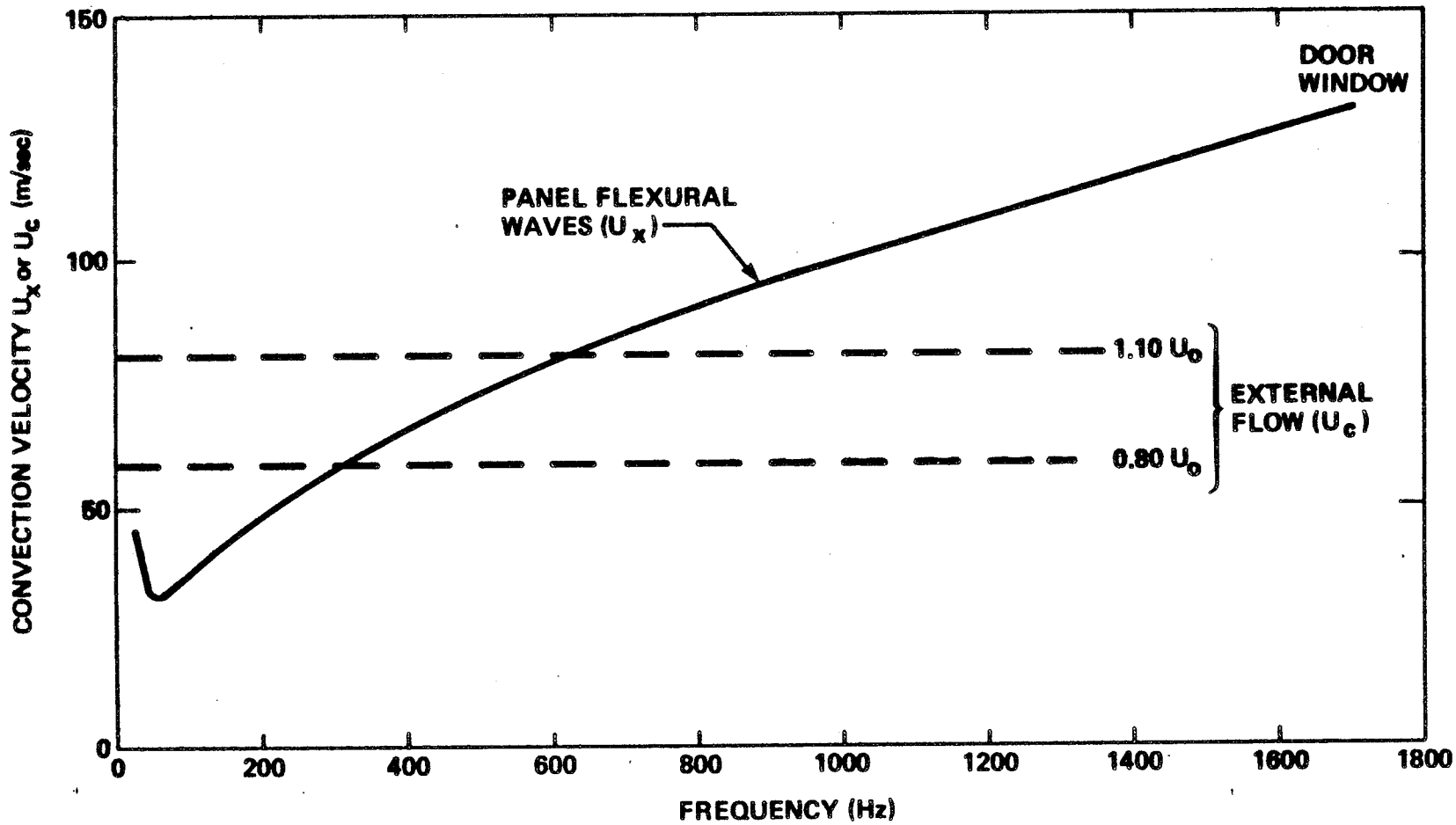

FIGURE G.6 CONVECTION SPEEDS: WINDOWS.

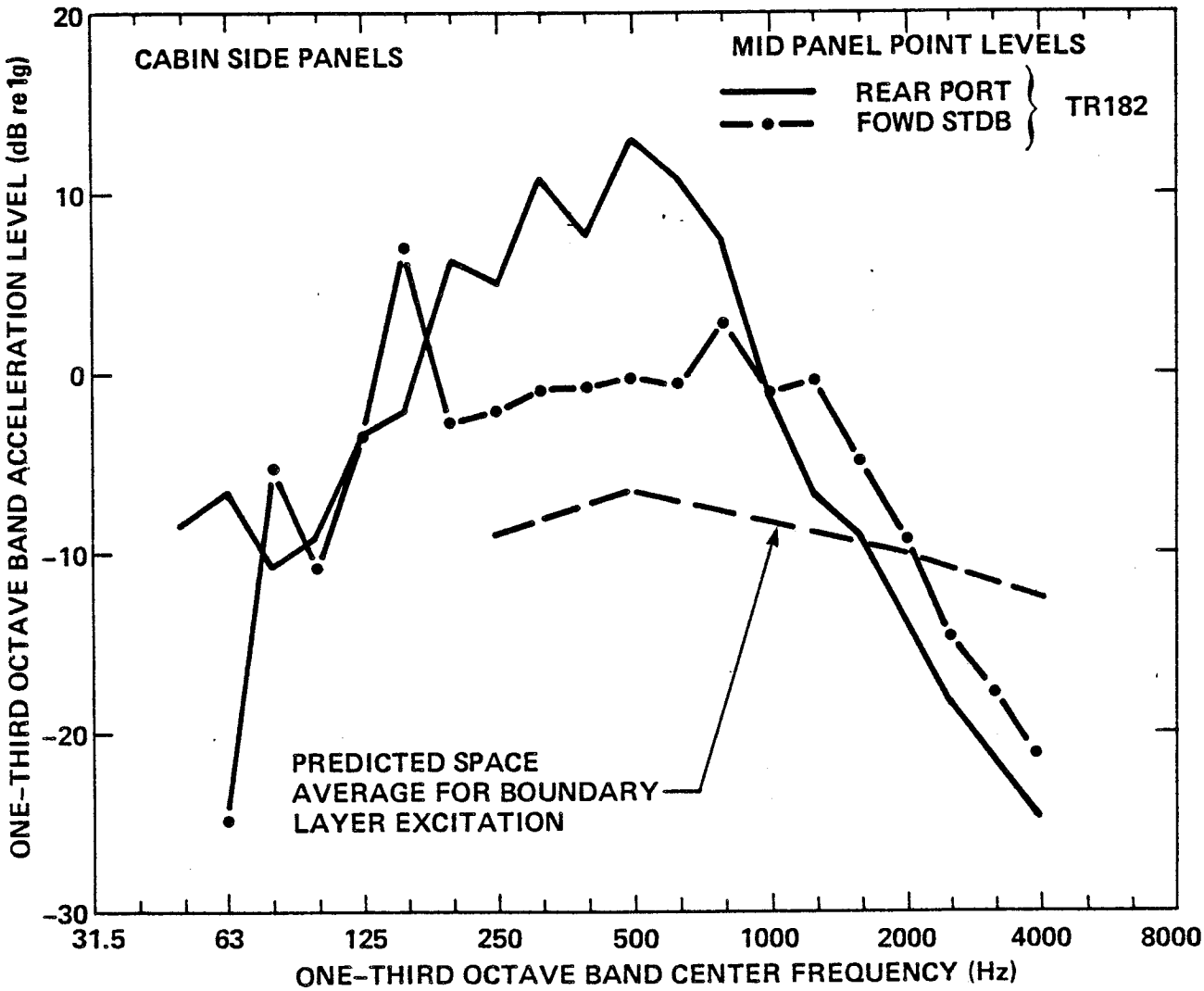

FIGURE G.7 COMPARISON OF MEASURED SIDE PANEL VIBRATION AND PREDICTED RESPONSE TO BOUNDARY LAYER EXCITATION.

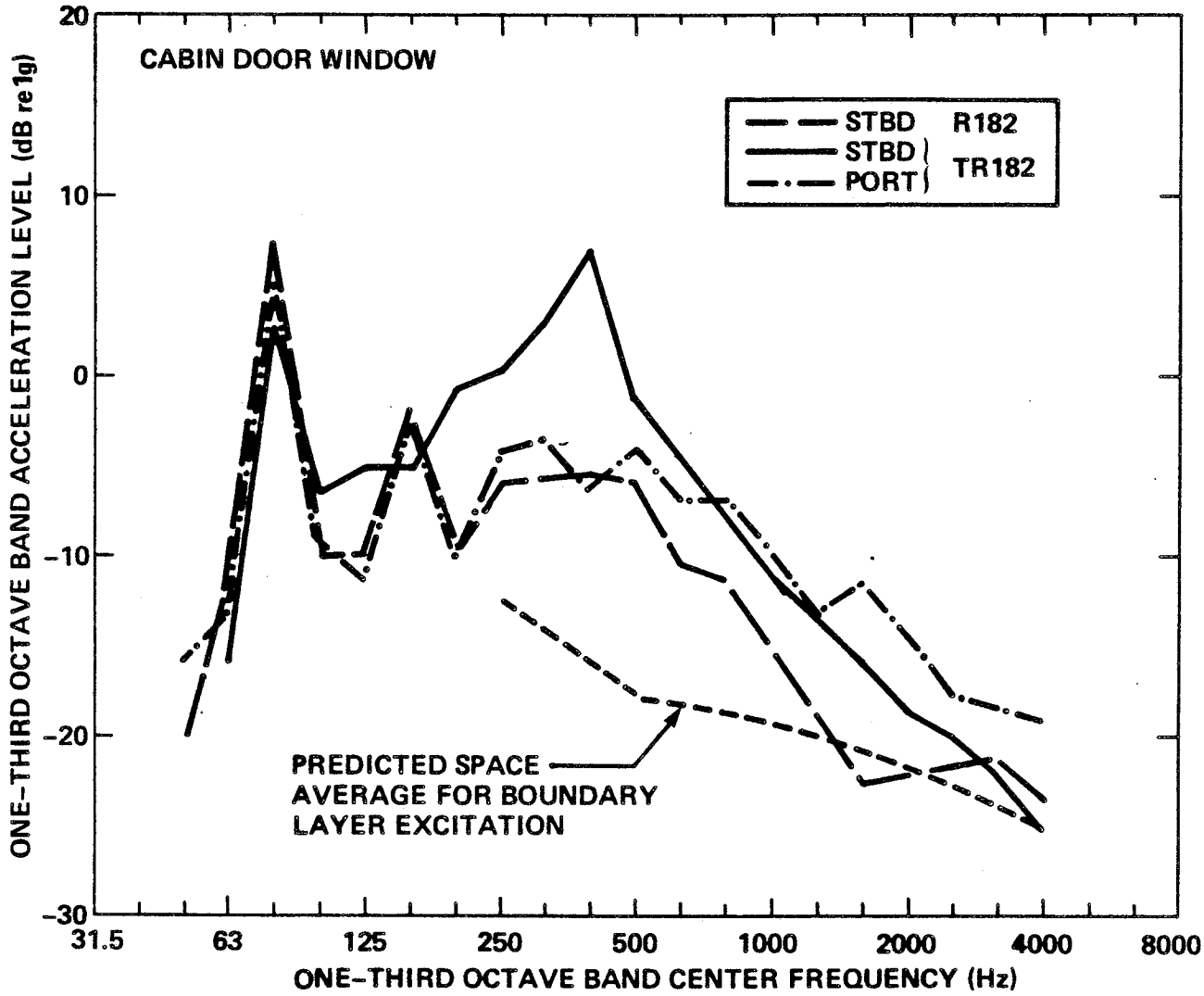

FIGURE G.8 COMPARISON OF MEASURED WINDOW RESPONSE VIBRATION AND PREDICTED RESPONSE TO BOUNDARY LAYER EXCITATION.

Predicted acceleration levels are presented for the frequency range from 250 to 4000 Hz. Data are not given for lower frequencies since the assumptions implicit in the analytical model are not valid in that frequency range. In any case, the panel response at low frequencies is dominated by excitation at harmonics of the propeller blade passage frequency - a situation which is not of interest in this present discussion.

In the mid-frequency regime, defined here as extending from 125 to 1000 Hz, the predicted response to attached turbulent boundary layer excitation is 10 to 20 dB lower than that measured. However, in this frequency range the measured spectra show a wide variation (up to ±7 dB) in acceleration level from panel to panel. Not only does this large variation in level make comparisons with predictions difficult, it also raises the implication that the dominant excitation is not the general attached turbulent boundary layer but is a local acoustic or flow condition. At frequencies above 1000 Hz, the measured vibration levels show less variation from panel to panel, and the predicted levels are in closer agreement with measurements. Thus, it seems likely that the attached turbulent boundary layer is a significant excitation only at frequencies above about 1000 Hz.

It is interesting, as an aside, to observe the relative response of the side panels and window panes at frequencies corresponding to the first and second harmonics of the propeller blade passage frequency. On the skin panel the vibration is much higher at the second harmonic than at the first, whereas the converse is true for the window pane. This relation is consistent with the predicted trend in the structural resonance frequencies in that the fundamental mode of the window pane has a lower resonance frequency than does the corresponding mode of the skin panel. Continuing this comparison further, the data suggest

that the resonance frequencies (Table G.3) predicted on the basis of simply-supported boundary conditions are lower than the actual values. This is expected since the assumption of simply-supported boundary conditions usually provides a lower bound on the actual resonance frequencies.

G.5 Wind Tunnel Tests

G.5.1 Arrangement

The special fuselage was merged with a specially formed channel in the BBN high speed acoustic wind tunnel to provide flow over the belly of the aircraft at representative flight speeds. The purposes of these tests were to (1) provide some data on the fluctuating pressure spectrum on the skin, and (2) investigate the effect of open wheel wells on the cabin noise spectrum; a third purpose was to simply investigate the feasibility of using low noise wind tunnels to study airflow noise on full size aircraft. Figure G.9 is a photograph of the aircraft (on its side) looking into the wind tunnel opening prior to installation of the channel. Figure G.10 shows a "plan" view of the same configuration. Figure G.11 shows a closeup of the wheel well area in which a surface-mounted pressure sensor was used to obtain local fluctuating pressure data. Figure G.12 shows the installation of the channel, the sides of which were contoured to fit the local shape of the aircraft (a 3 cm foam seal was used to prevent leaks and transmission of structureborne vibration to the fuselage from the channel or in the other direction). The area covered by the channel was shaped such that the flow velocities from the firewall station aft were roughly constant; the duct was terminated roughly at the forward location of the landing gear to prevent radiated noise from building up inside the duct and because it became difficult to create a flow channel which both followed the aircraft contours and maintained a constant cross-sectional area (for constant speed).

FIGURE G.9 SPECIAL FUSELAGE SUSPENDED IN FRONT OF WIND TUNNEL NOZZLE (AIRCRAFT ON ITS SIDE); VIEW LOOKING UPSTREAM.

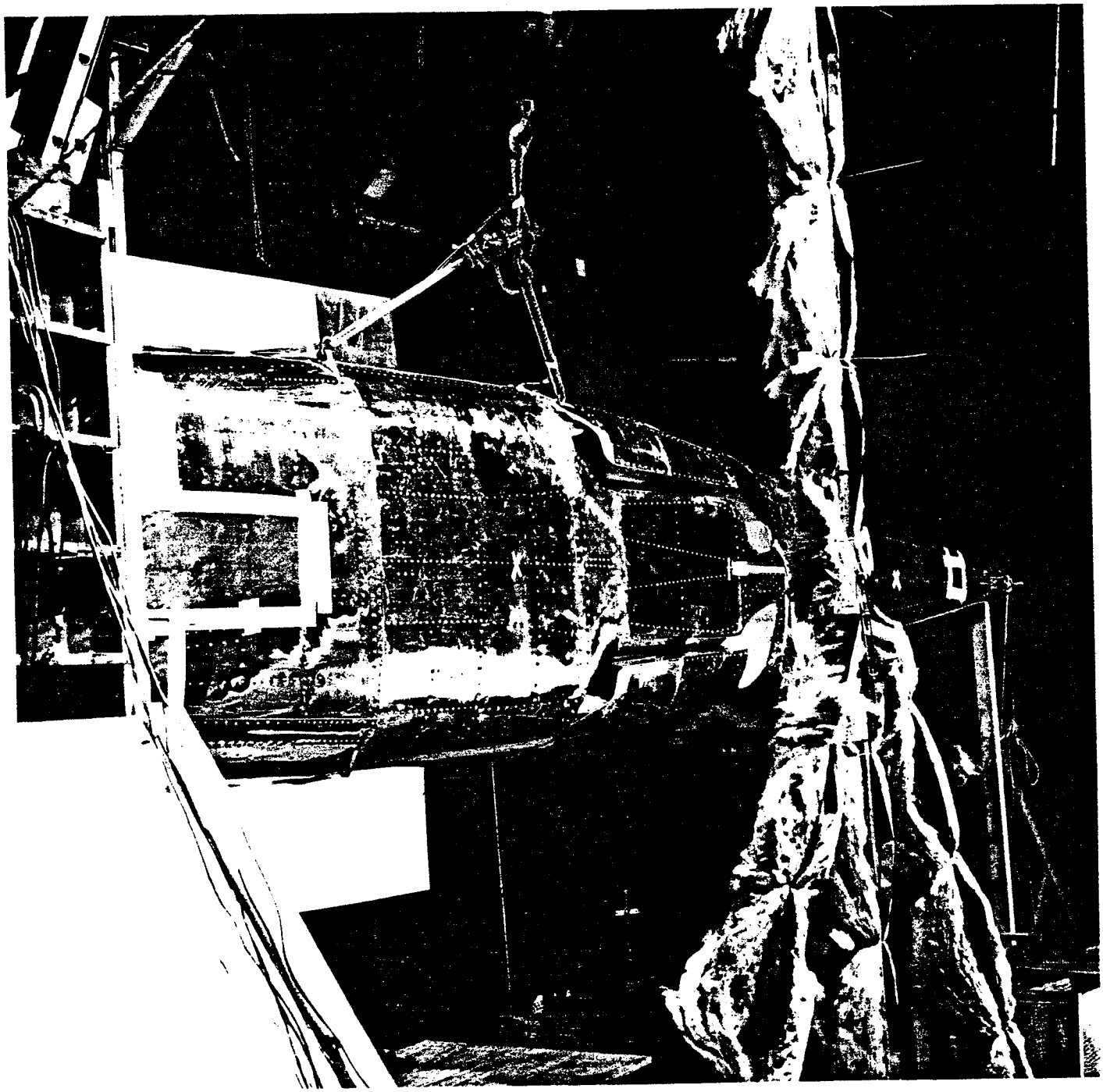

FIGURE G.10 SPECIAL FUSELAGE SUSPENDED IN FRONT OF WIND TUNNEL NOZZLE (AIRCRAFT ON ITS SIDE); VIEW OF BELLY LOOKING FROM UPSTREAM AND TO THE SIDE OF NOZZLE.

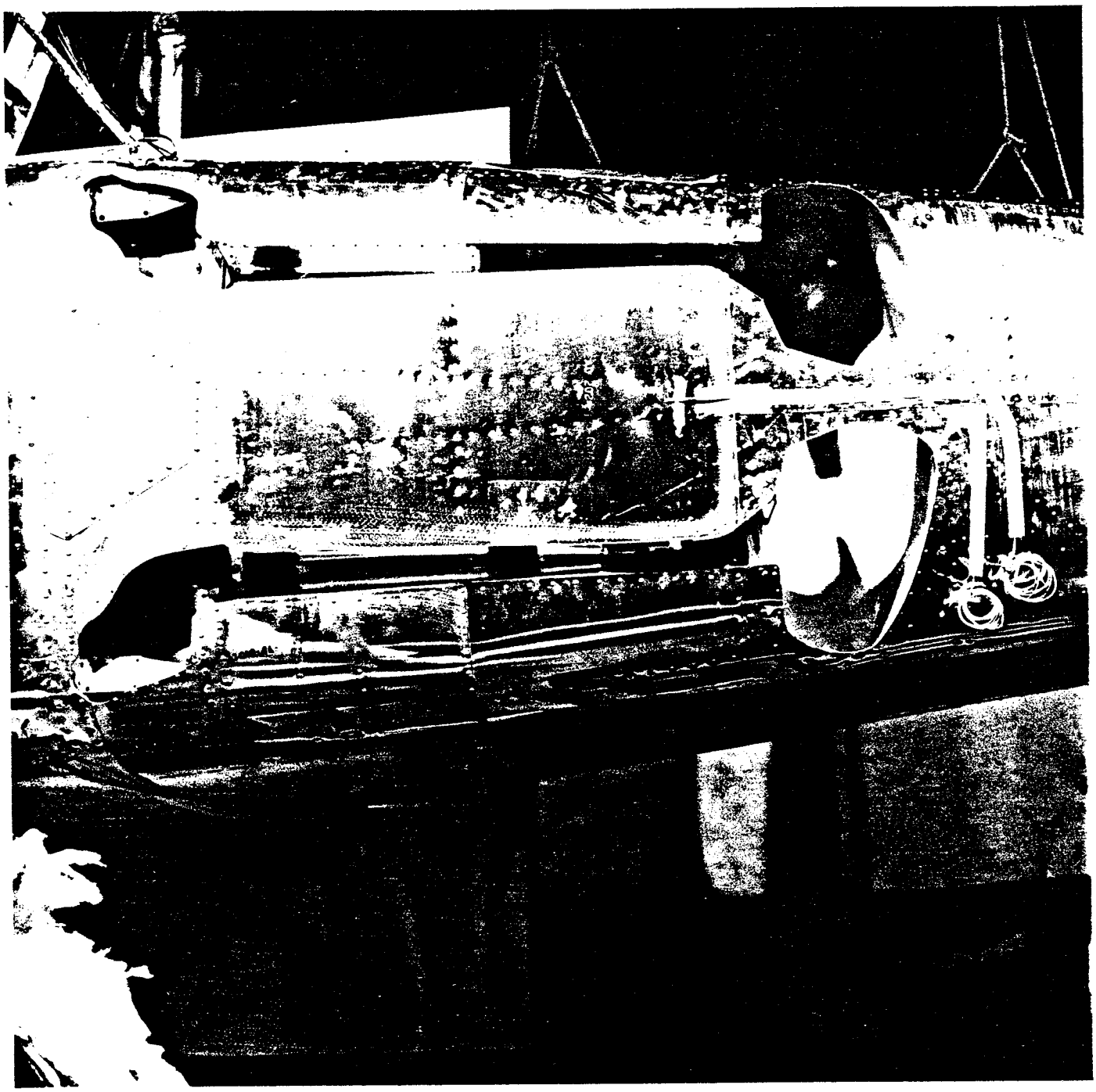

FIGURE G.11 SPECIAL FUSELAGE SUSPENDED IN FRONT OF WIND TUNNEL NOZZLE (AIRCRAFT ON ITS SIDE); CLOSEUP VIEW OF BELLY.

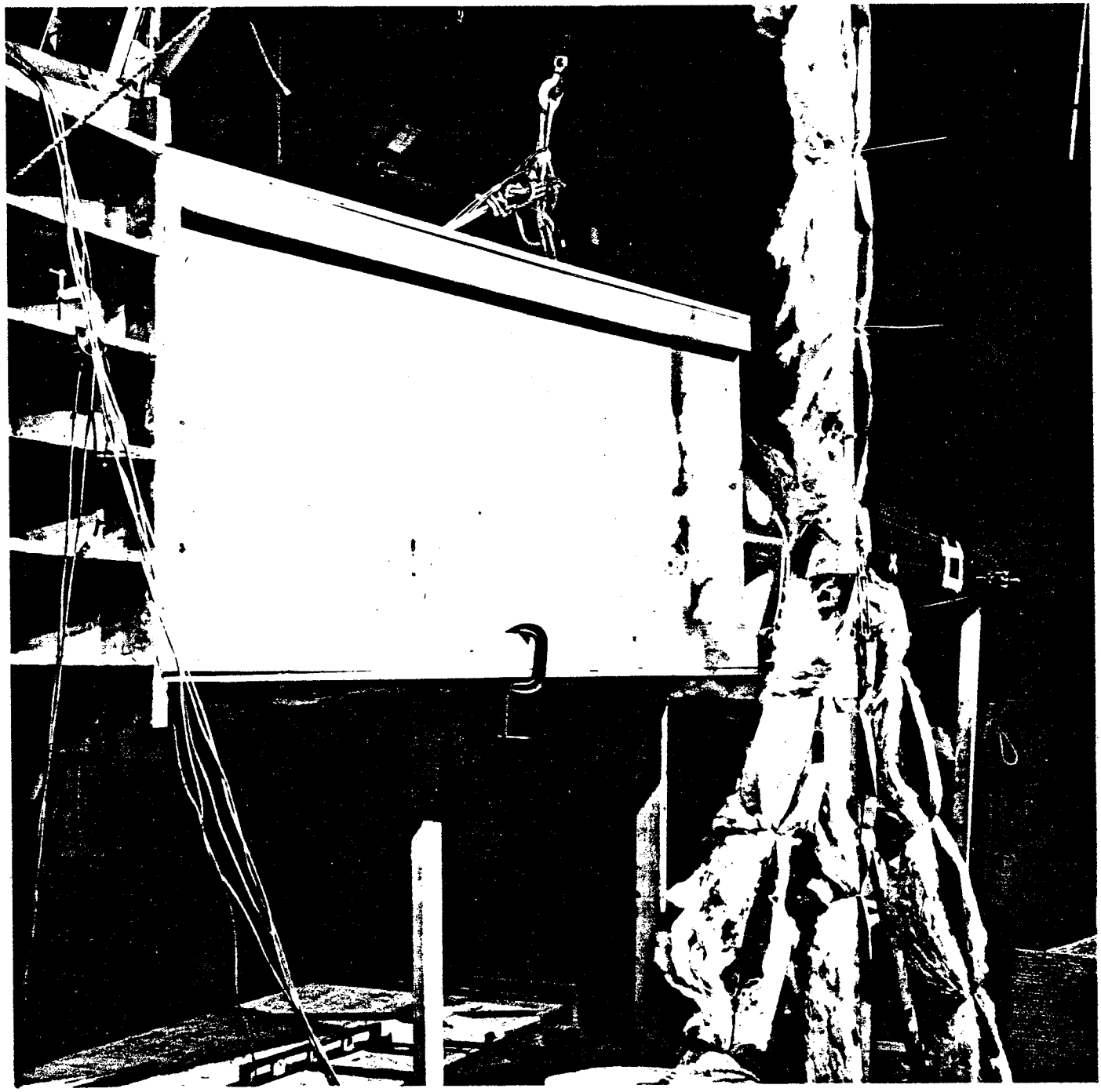

FIGURE G.12 SAME VIEW AS FIGURE G.10 WITH CHANNEL INSTALLED TO CREATE FLOW OVER BELLY AREA.

The test data were taken with and without the wheel wells covered (with an aluminum skin), with and without the tail cone wrapped in a double layer of fiberglass and lead vinyl, and with and without the exhaust pipe protruding. The results are described below.

G.5.2 Analysis of wind tunnel surface pressure data and vibration response

The wind tunnel tests provided an opportunity to perform measurements under controlled conditions such that the flow speed could be varied in the absence of engine and propeller noise. Also, the flow could be directed over specific regions of the fuselage, such as, for example, the belly of the cabin where flow disturbances are much smaller than on the sides and top, particularly when the wheel well cavities are covered over. The disadvantages of the belly area are that the skin panels are smaller than the sidewall panels (see Table G.1) and the presence of the floor above the skin may influence the response and acoustic radiation.

Tests were performed at two flow speeds of 38.5 and 75.9 m/s (126 and 249 ft/sec, respectively) and fluctuating pressure spectra were measured on the surface of the fuselage. Associated one-third octave band levels are shown in Fig. G.13. The fluctuating pressures were measured with "stick-on" (surface-mounted) rather than flush-mounted pressure transducers, with the result that the data may include aerodynamic self-noise of the sensor (see App. I). However, the comparison of measured and predicted spectra in Fig. G.3 gives some confidence in the test data. Vibration of the structure on the belly of the fuselage was measured at the center of one of the skin panels located at the aft end of the cabin. The panel had dimensions of 280 mm x 100 mm (11" x 3.9") with the longer dimension being parallel to

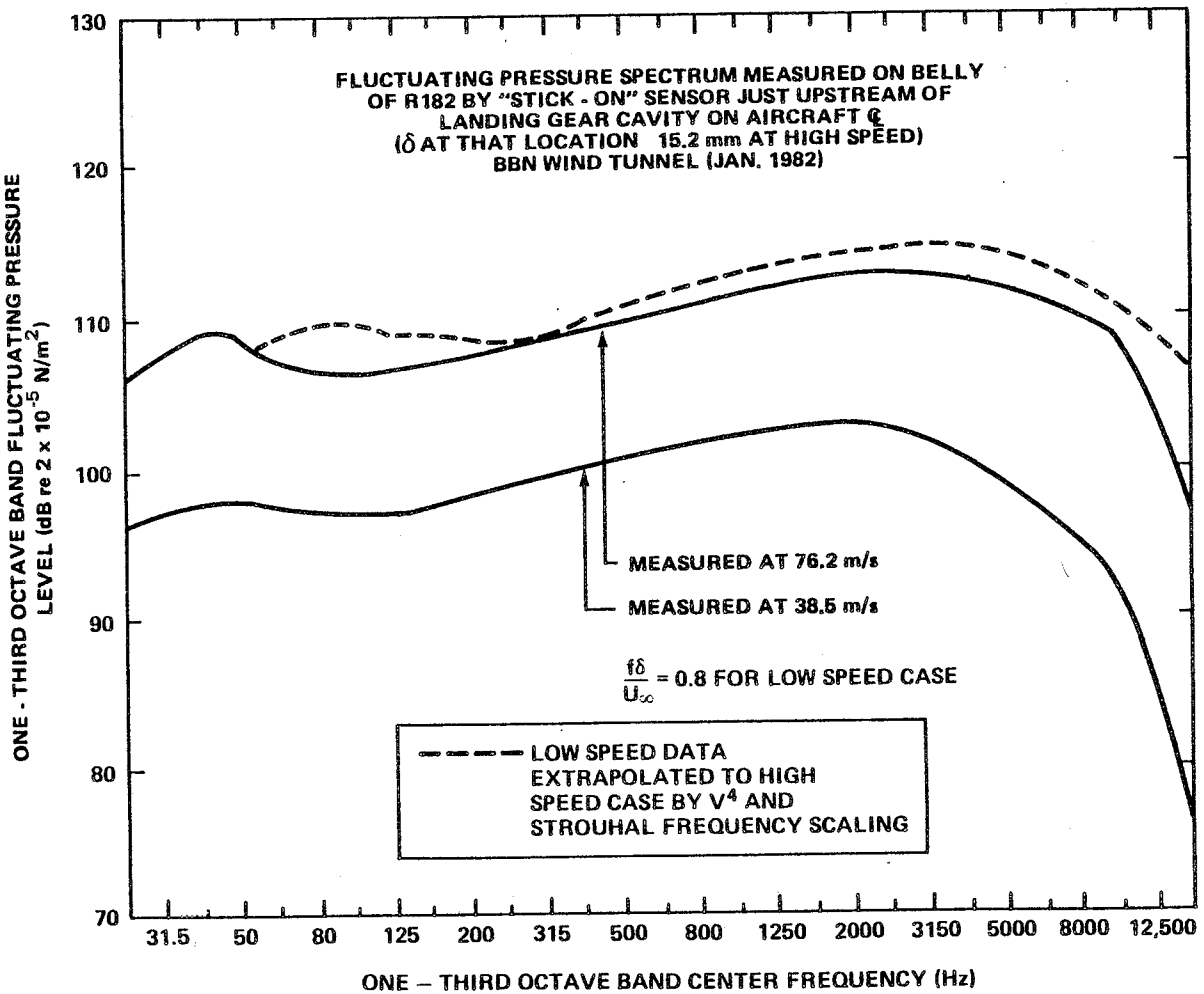

FIGURE G.13 FLUCTUATING PRESSURE SPECTRUM: BELLY OF R182.

the flow direction. Estimated resonance frequencies for some of the panel modes are given in Table G.3 and measured acceleration levels are plotted in Fig. G.14. The spectra in Figs. G.13 and G.14 show that, as flow speed doubles, the excitation pressures increase by 9 to 15 dB while the panel acceleration increases by 18 to 34 dB.

The predicted resonance frequencies listed in Table G.3 show that there are only four modes with resonance frequencies below 600 Hz if simply-supported boundary conditions are assumed, and only three if fixed boundaries are assumed. This sparsity of modes at low frequencies is in marked constrast to the cabin sidewall panels and window panes considered in Sec. G.4 with respect to flight test measurements. In those cases the panels have large number of modes with resonance frequencies below 600 Hz. The validity of the present analytical model at frequencies below 1000 Hz is thus in question for the test panel on the fuselage belly.

First, consider the aerodynamic coincidence regime for the test conditions. Modal wave speeds have been calculated for three panel conditions and the values are compared with the free stream flow speed U_o and the estimated boundary layer pressure field convected speed U_c ($U_c = 0.8\ U_o$) in Fig. G.15. The results indicated that the lower flow speed is well below aerodynamic coincidence conditions for the single panel whereas the higher flow speed is associated with a borderline coincidence condition.

Panel response has been estimated using the analytical procedures outlined in Sec. G.2.1. The resonant response contribution was estimated using Eqs. (G.5) and (G.7), and the convected response using Eq. (G.6). Values of the excitation pressure levels were obtained from the measured data shown in

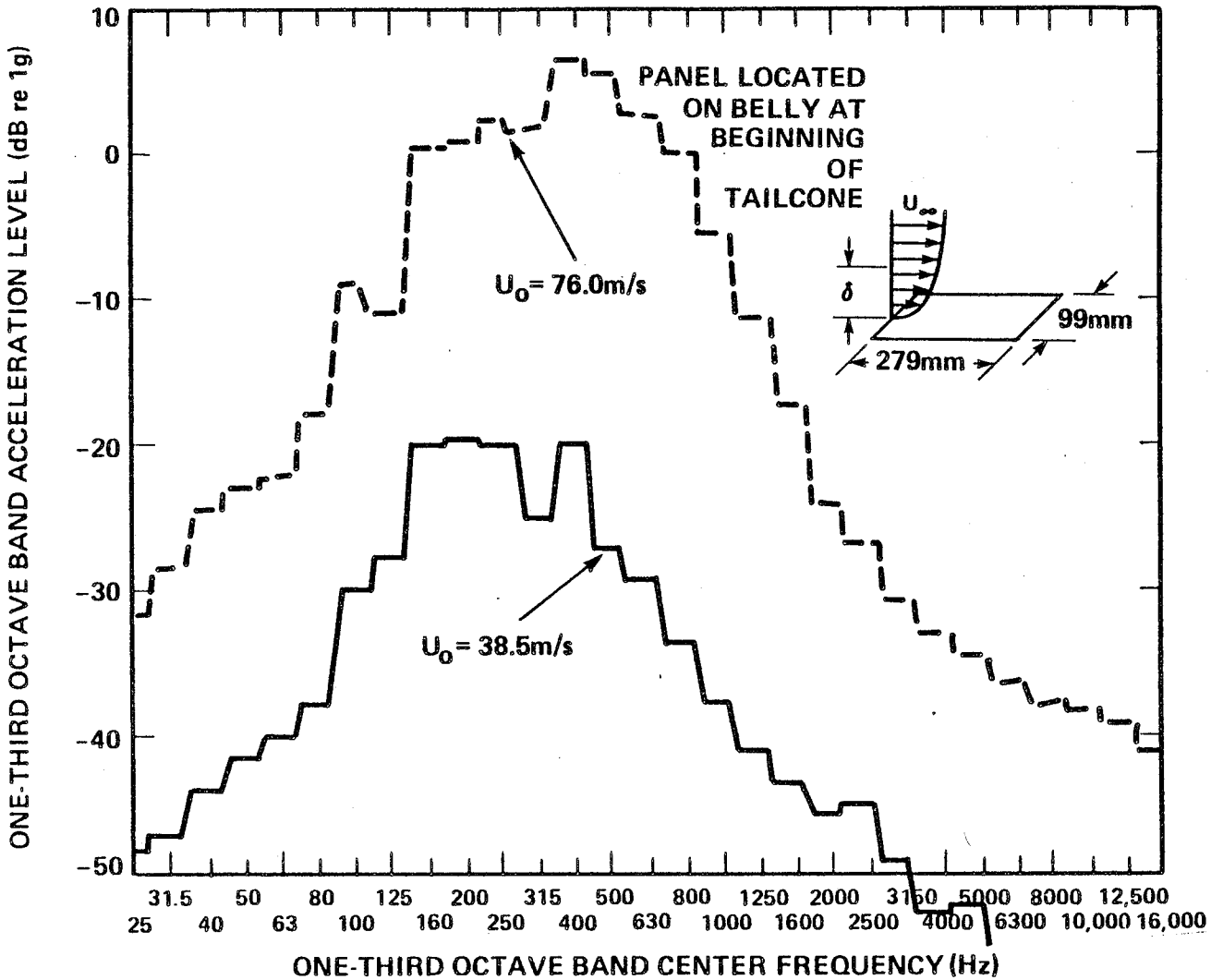

FIGURE G.14 VIBRATION RESPONSE OF 3.9 IN K11 IN. A1 PANEL CENTER R182 FUSELAGE IN BBN LOW NOISE WIND TUNNEL.

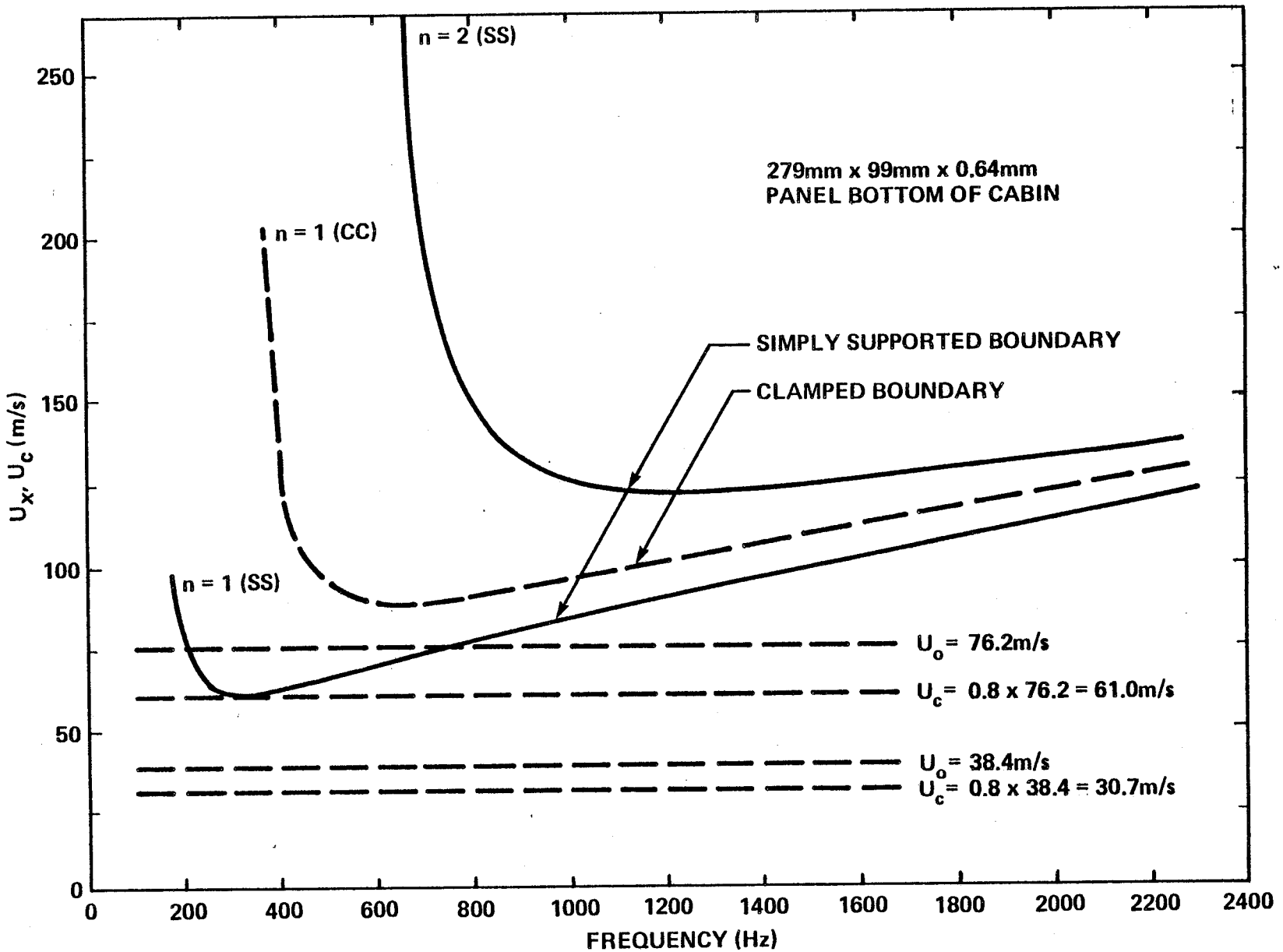

FIGURE G.15 CONVECTION SPEEDS FOR TEST PANEL ON BELLY.

Fig. G.13. At low frequencies, the response was assumed to be stiffness-controlled and to follow the asymptotic f^5 law. The resulting predicted spectra are plotted in Figs. G.16 and G.17 for the two test flow speeds. The low frequency asymptote was fitted to the measured data at 160 Hz - the one-third octave band containing the predicted fundamental resonance frequency for the panel when the boundaries are assumed to be simply supported. This low frequency asymptote is used here solely as an indicator of spectral slope.

The comparisons in Figs. G.16 and G.17 show quite good agreement between measured and predicted acceleration levels, particularly for the 75.9 m/s flow speed. At low frequencies, below the panel's lowest resonance frequency, the measured response spectra follow the predicted f^5 slope quite closely. Then, at high frequencies the slopes of the measured spectra are similar to those associated with the predicted convected term. Furthermore, the magnitude of the measured response varies with flow speed in a similar manner to that predicted for the convected contribution. The main divergence between measured and predicted acceleration levels is concerned with the resonant response contribution which shows a much flatter spectral shape than is measured. The reasons for this discrepancy have not been fully determined, but the validity of the pressure field model in Eq. (G.3) is open to question due to the thin boundary layer associated with the test.

In general, it is concluded from the comparisons in Figs. G.16 and G.17 that the simple analytical model presented in Sec. G.2 provides a reasonably good first-order estimate of the response of the cabin structure to excitation by an attached turbulent boundary layer. Thus, the conclusions drawn in Sec. G.4.3 regarding broadband response of the structure during flight should be valid.

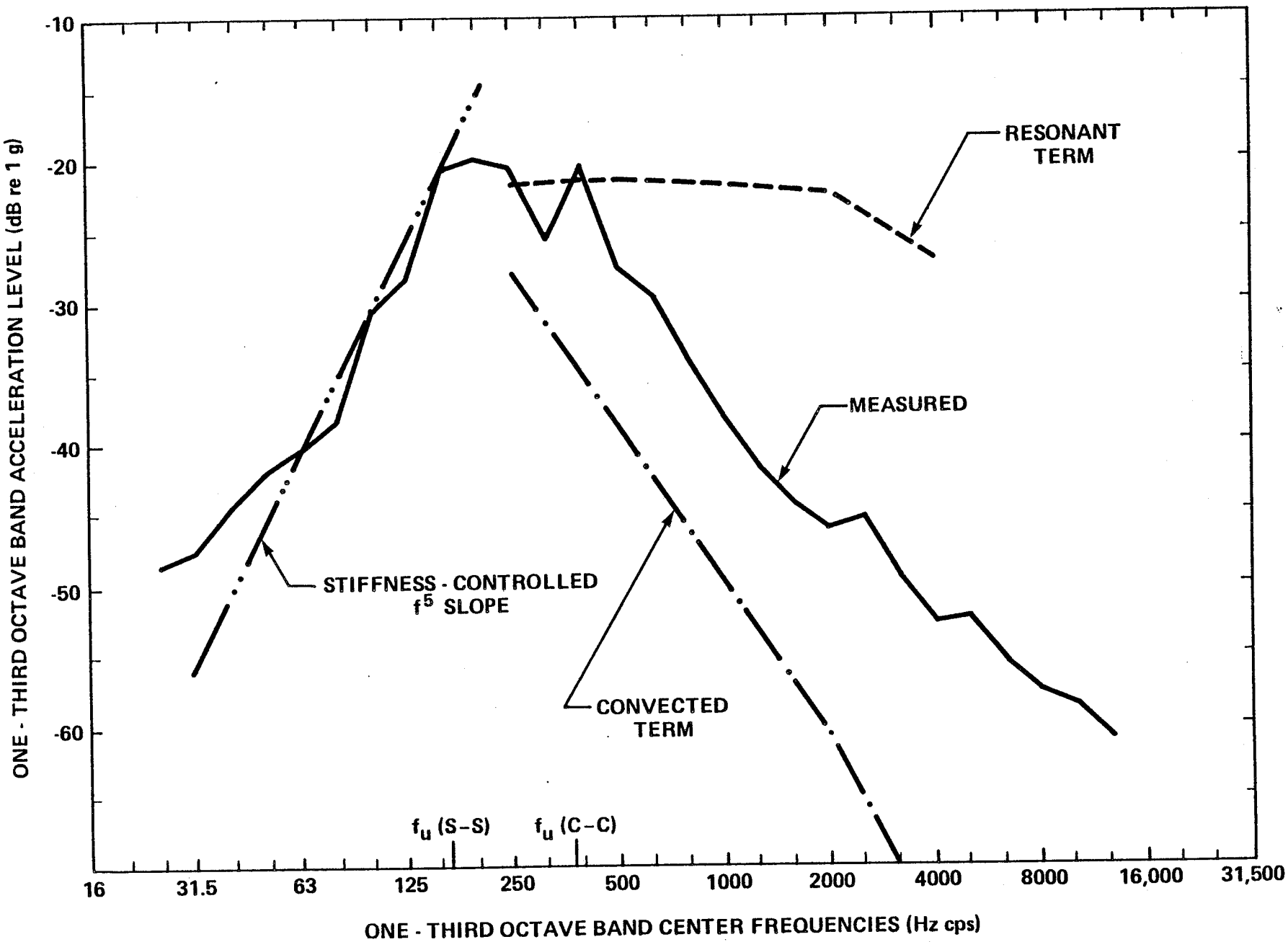

FIGURE G.16 COMPARISON OF MEASURED AND PREDICTED RESPONSE OF BOTTOM PANEL (U_o = 38.4 m/s)

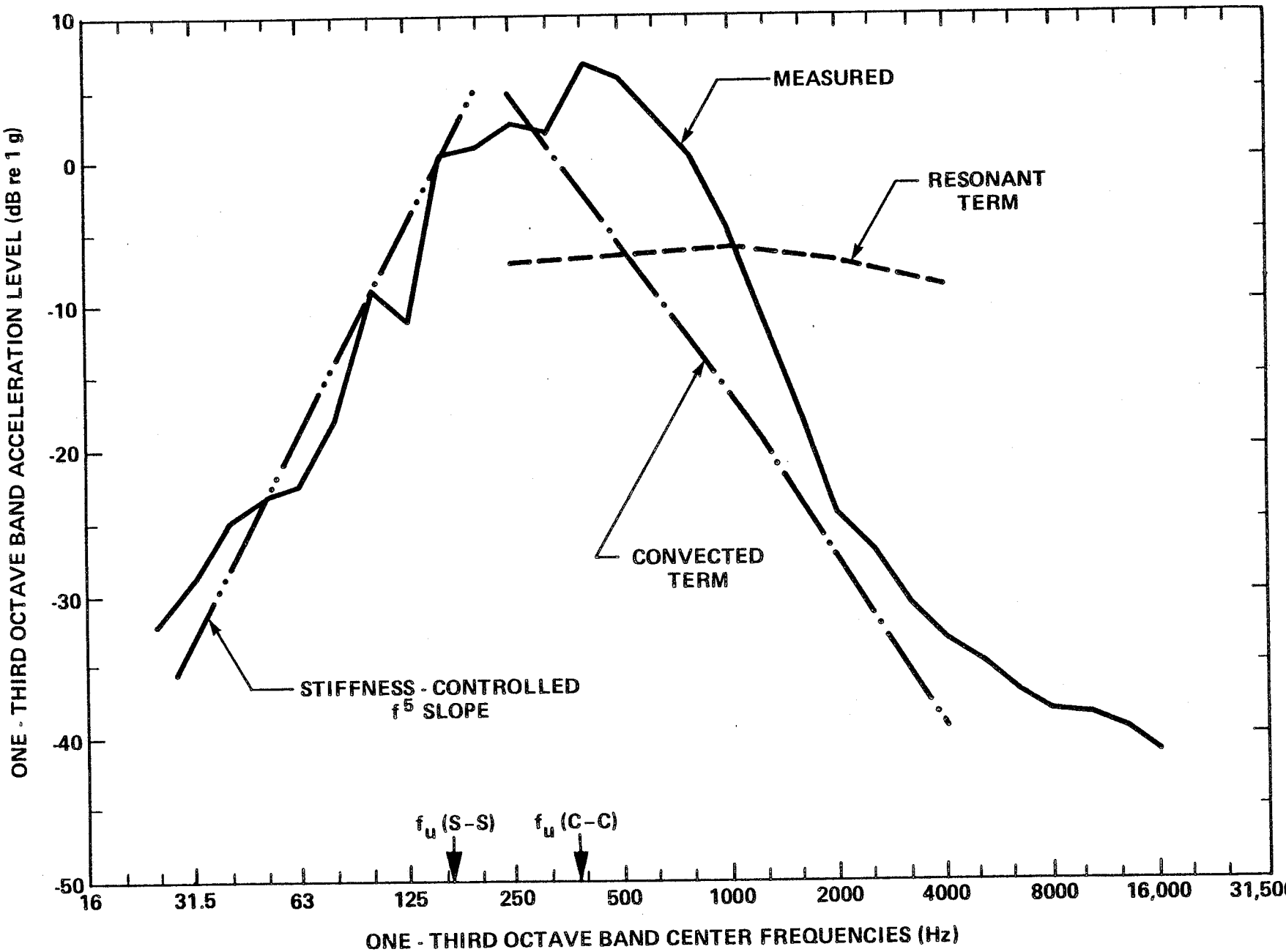

FIGURE G.17 COMPARISON OF MEASURED AND PREDICTED RESPONSE OF BOTTOM PANEL (U = 76.2 m/s)

G.5.3 Effect of wheel well openings

The above-described setup was used to investigate the effect of wheel well openings on cabin noise. The "open" wheel wells did not contain landing gear as they would in flight (note that in the stowed condition the cutout and cavity are still prominent). The covered wheel wells used a smooth sheet of aluminum with edges secured by double-backed tape and a single-layer of smooth tape on the outside to fair in the edges. Figure G.18 shows the dramatic result of opening the wheel wells for a typical cruise speed. The levels in the cabin center are increased by 12 dBA when the wheel wells are uncovered, and the level is within the range of interest in treating the cabin noise of this particular aircraft. It was of interest to ensure that the acoustic background noise in the facility - transmitted through the exposed parts of the aircraft (roof, windshield, sidewalls) - was not responsible for the levels in the "covered wheel well" case. Figure G.19 shows the levels calculated by using a typical measured background level in the facility and the noise reduction data for individual parts of the aircraft (as described in App. C.) The data in Fig. G.19 indicates that below 100 Hz, facility background noise may be responsible for the measured cabin noise levels, but at higher frequencies, the flow-induced mechanisms are responsible (note that for this case, the sound has to be transmitted through a double floor structure; thus, the levels in Fig. G.19 are below those which would be expected from a comparable test for the roof or sidewall sections of the aircraft). Figure G.19 also shows the resultant cabin sound at several locations within the cabin.

Figure G.20 shows the distribution of sound around the cabin for the case when the wheel wells are open and the exhaust pipe is simulated, the tail cone was uncovered in the case shown in Fig. G.20. Some minor reduction in levels had been observed

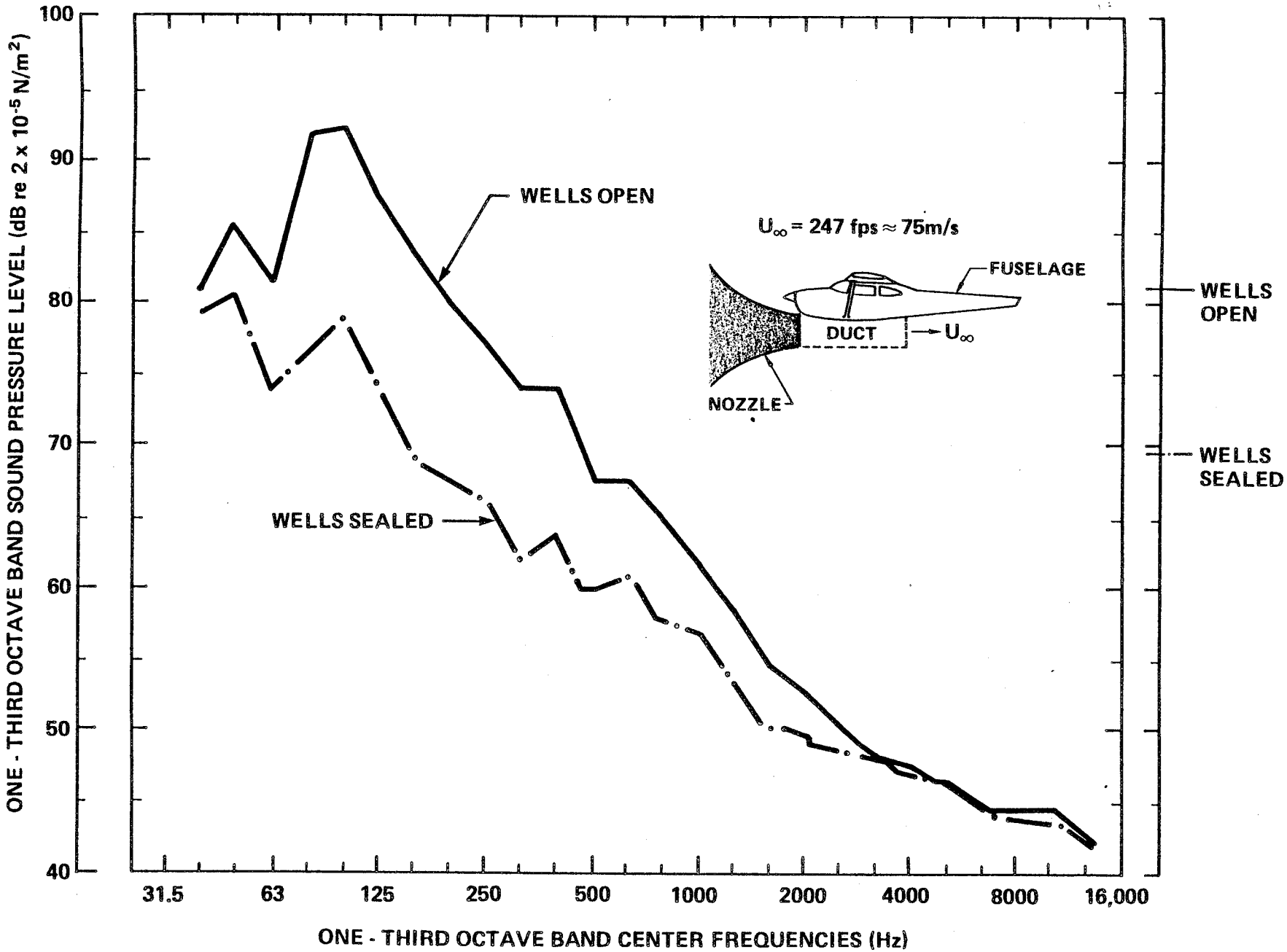

FIGURE G.18 NOISE AT CABIN CENTER DUE TO FLOW OVER AIRCRAFT BELLY WITH AND WITHOUT "WHEEL WELLS" EXPOSED - FURNISHED INTERIOR -R182 FUSELAGE.

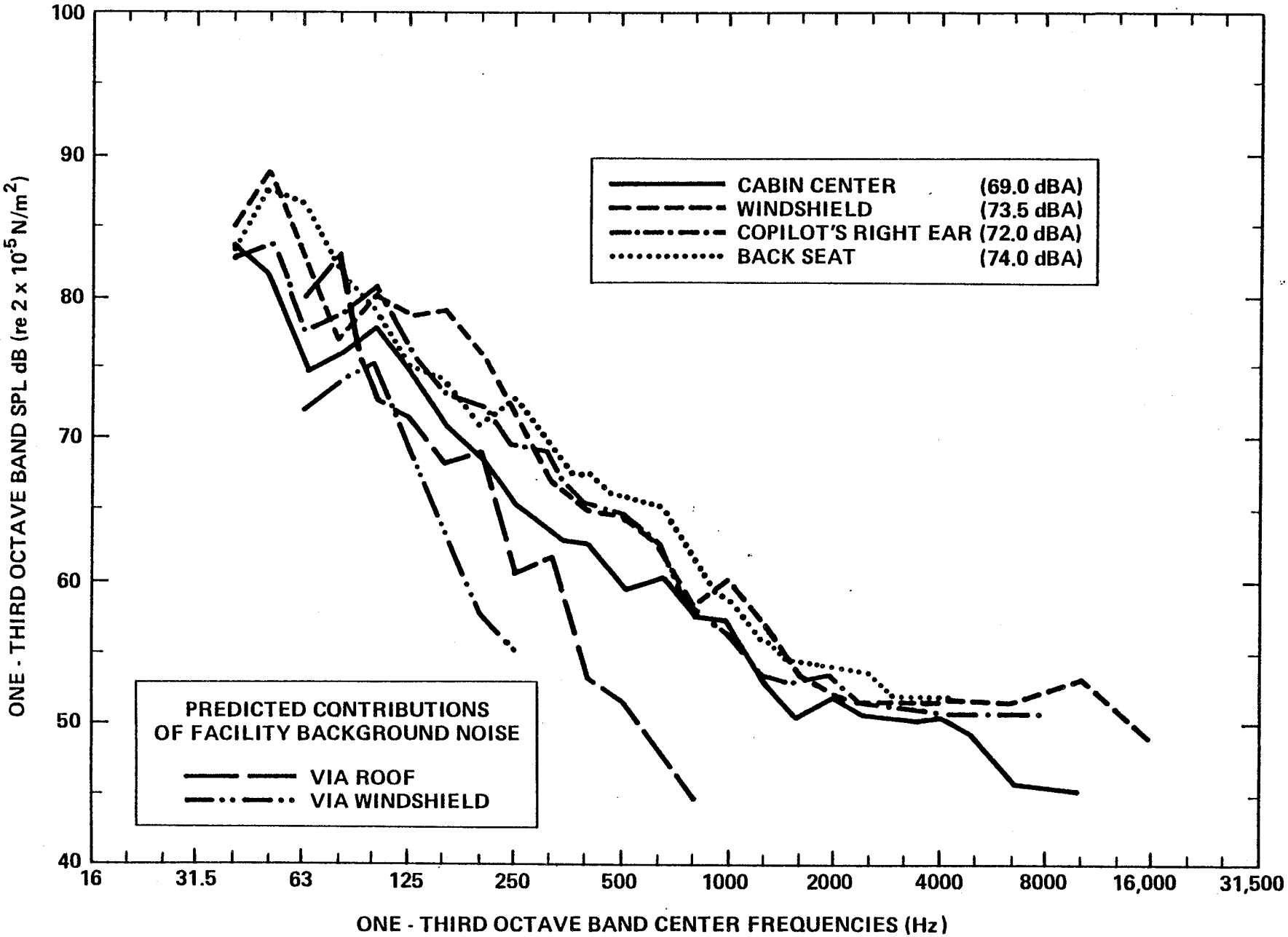

FIGURE G.19 EFFECT OF COVERING WHEEL WELLS.

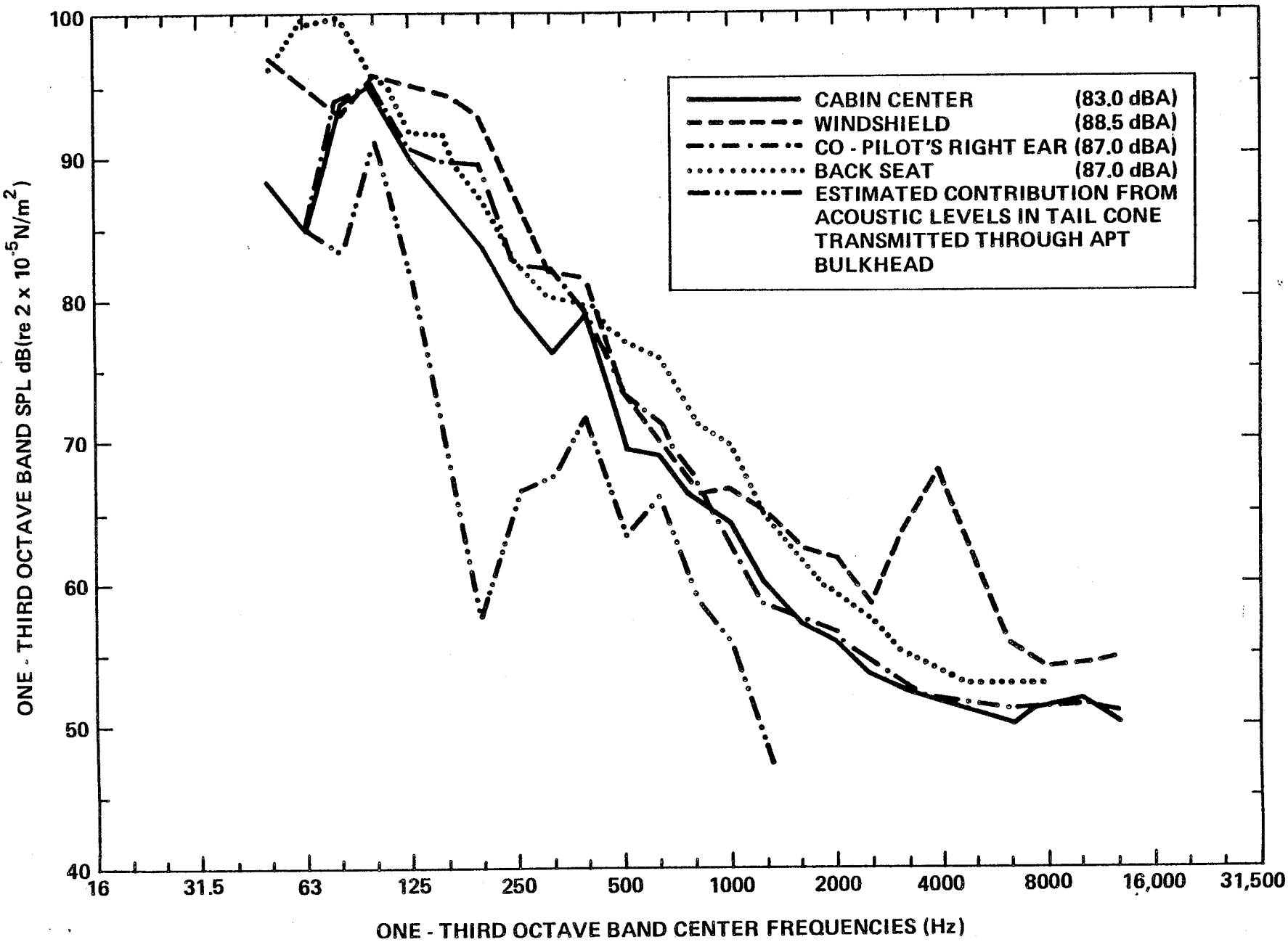

FIGURE G.20 DISTRIBUTION AROUND CABIN - TAIL SECTION UNCOVERD, WELLS OPEN, EXHAUST PIPE SIMULATED (147.5 kt).

when the tail cone was covered, therefore, it was of interest to determine the dominant mechanism associated with the tail cone.

Acoustic levels in the tail cone cavity were measured by a hanging microphone; these levels were then reduced by the noise reduction values measured in the controlled tests described in App. C, with the resultant prediction for acoustically-transmitted airborne noise shown in Fig. G.20 to be not dominant. Therefore, it was concluded that either radiation through the wheel well structure and/or tail cone structureborne noise is the dominant mechanism. However, when the wheel wells were covered, the tail cone vibration levels were not reduced significantly; therefore, it is concluded that the dominant mechanisms associated with the open wheel well condition are directly related to the cavity flow excitation of the surrounding structure and/or acoustic radiation from the edges of the cavity.

The "belly" flow effects were also studies as a function of speed, with the results shown in Figs. G.21 and G.22. As previously noted, the levels associated with the wheel well's open condition appear in the range of concern for achieving a quiet cabin environment.

G.7 Control of Airflow Induced Noise

Control of cabin noise associated with the aerodynamic flow over the cabin exterior can be achieved, in principle, by modification to the flow, reduction of the structural response to the aerodynamic excitation, or attenuation of the radiated sound.

Modification of the aerodynamic field on the exterior of the cabin is difficult for single-engine airplanes such as the one considered in this study because of the influence of the propeller wake. However, some improvement can be achieved by minimizing the number and size of protuberances and other

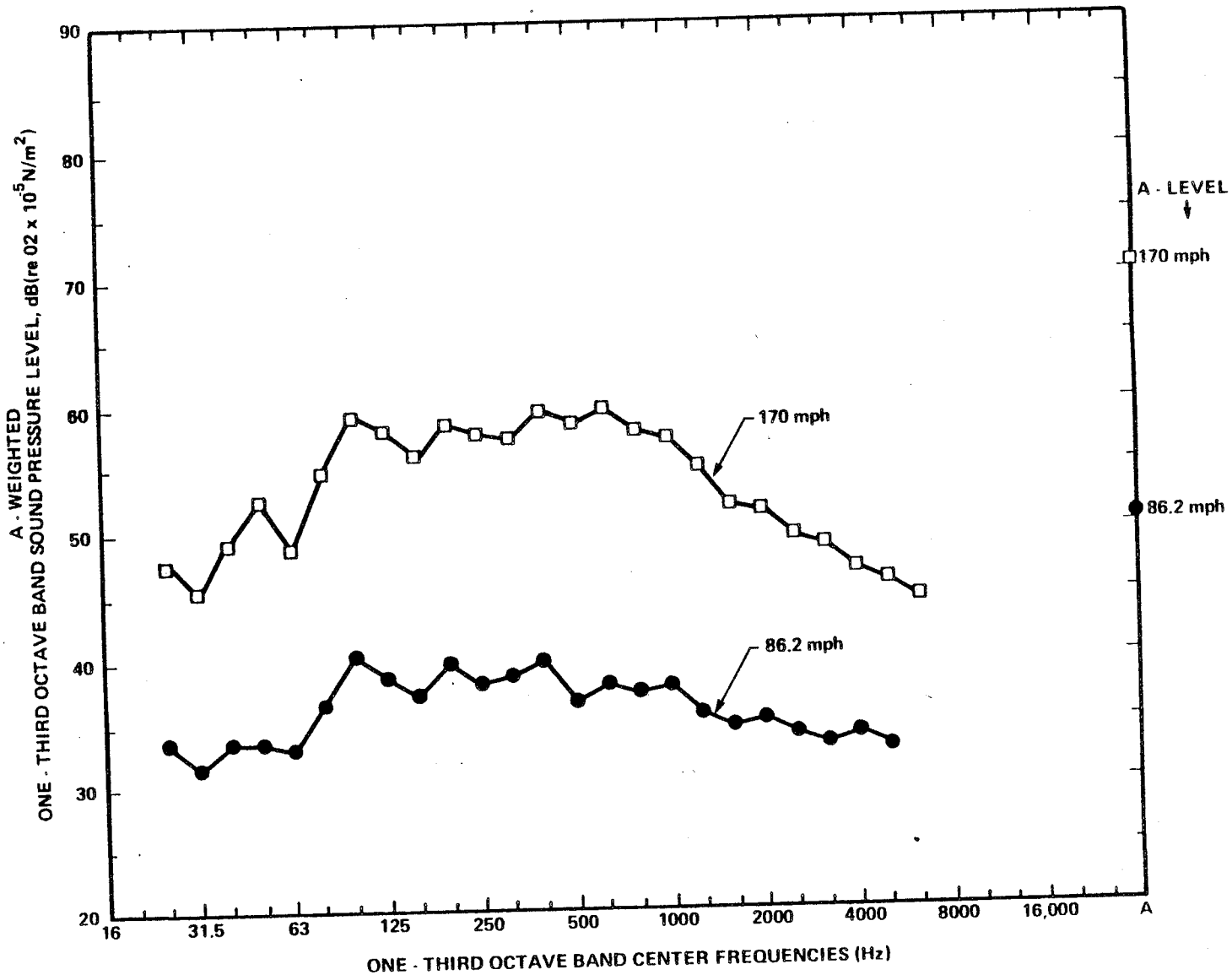

FIGURE G.21 A-WEIGHTED LEVELS AT CABIN CENTER - WHEEL WELLS COVERS, TAIL SECTION IN NOMINAL CONDITION.

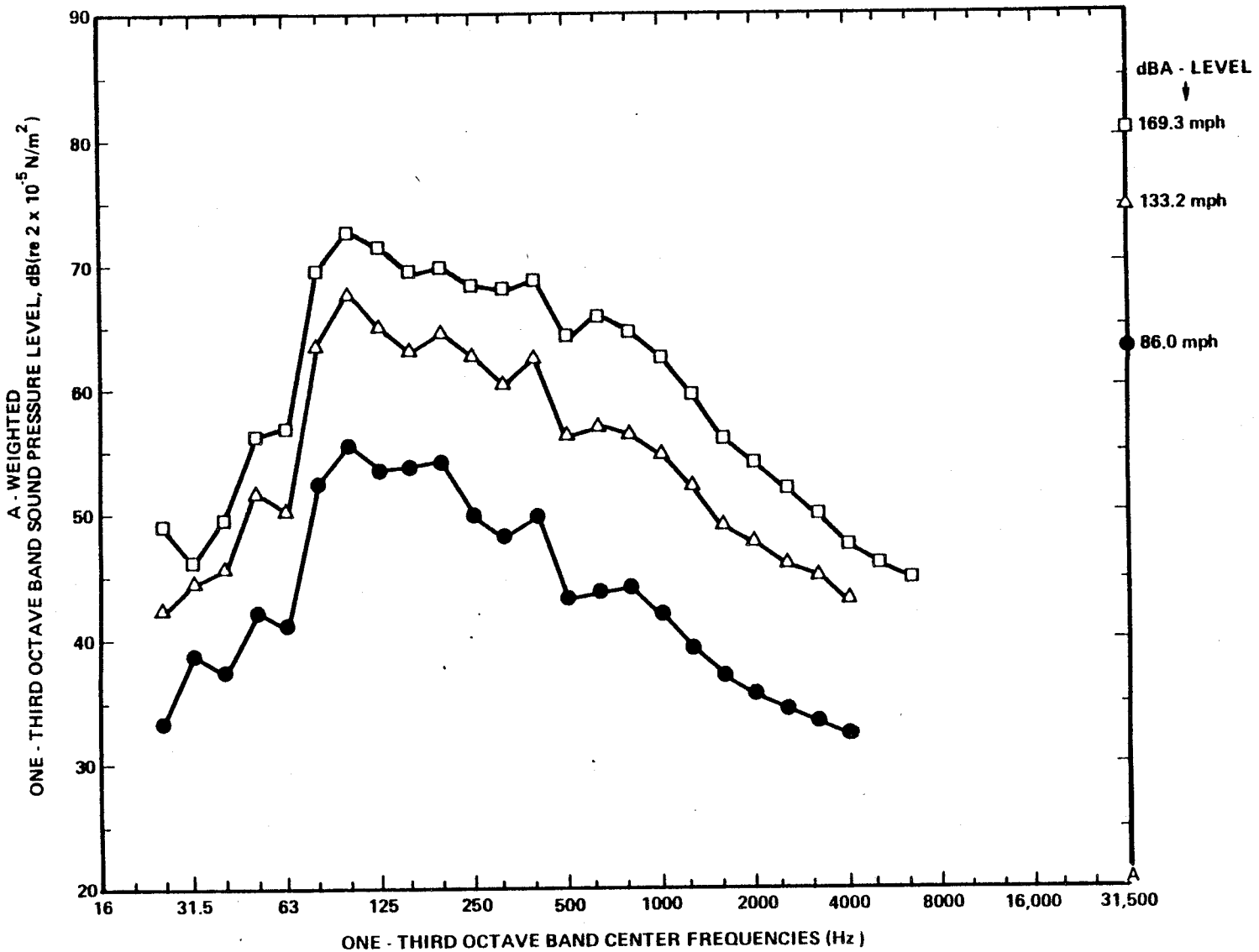

FIGURE G.22 A-WEIGHTED LEVELS AT CABIN CENTER - WHEEL WELLS OPEN, TAIL SECTION IN NOMINAL CONDITION.

obstructions to the flow ahead of, and over, the cabin. Also, it is important to insure that there is no flow separation, especially over transparent surfaces such as the windshield and cabin side windows. This means that transitions in fuselage cross-section should be achieved gradually rather than abruptly. It is possible that some beneficial "clean up" of the wheel well area could be effected on the test aircraft without any adverse effect on weight or aerodynamic performance.

Since the opportunity for improvement of the external flow is limited, the main potential for noise control will lie in the transmission path - that is in the structure and the sidewall treatment. Considering first the response of the structure, there are three general parameters available in the control of skin panel or window pane response to aerodynamic excitation. These parameters are mass, stiffness, and damping. The relative importance of these parameters can be estimated from Eqs. (G.5) and (G.6). The resonant response is inversely proportional to the damping loss factor and the square of the surface mass density. The convection response is inversely proportional to the square of the surface mass density and directly proportional to the eighth power of the resonant wavenumber (which is, in turn, inversely proportional to stiffness).

Increasing the mass of the structure is not an attractive approach from the aircraft designer's viewpoint but stiffness can be increased at minimal weight penalty by the addition of honeycomb material [G.7, G.8], or by designing the skin panels initially with non-load bearing honeycomb material. (Since the airplane under consideration is not pressurized there are no in-plane pressurization stresses to provide effective stiffness to the panels.) One disadvantage usually associated with increased stiffness is that the coincidence frequencies are reduced. However, in the case of aerodynamic excitation the coincidence frequencies already lie within the frequency range of interest.

The acoustic critical frequencies for the skin panels would decrease toward the frequency range of interest but their impact should be mitigated by the attenuation of high frequency sound by the sidewall insulation.

Damping treatments can provide reductions in panel response to turbulent boundary layer excitation at high frequencies [G.9] when coincidence conditions exist. In the reference [G.9] the additional damping was provided by damping tape applied to about 80% of the panel area. The effectiveness of additional damping will depend on the initial damping present in the cabin structure. Typical measured loss factors for the basic structure are shown in Fig. G.1. The data show fairly high values for the loss factor of cabin wall panels at low frequencies but fairly low values at frequencies above 1000 Hz. Consequently, additional damping could be of benefit at high frequencies.

In order for the sidewall treatment (such as fiberglass blankets) to be effective it must completely fill the regions between circumferential stiffeners; in fact, the material should be cut over-size to ensure a tight fit. Also, a continuous additional layer of acoustic treatment should be placed over the frame caps. The objective of this second layer is to prevent the frames from acting as flanking paths. Finally, the cabin trim panels which cover the insulation should be resiliently mounted to the fuselage structure. These resilient mounts should have low resonance frequencies - stiff shock mounts are not adequate isolators.

REFERENCES FOR APPENDIX G

G.1 Bhat, W.V., "Flight Test Measurement of Exterior Turbulent Boundary Layer Pressure Fluctuation on Boeing Model 737 Airplane," J. Sound Vib., 14, 4, 439-457, 1971.

G.2 Unruh, J.F, D.C. Scheidt, D.J. Pomerening, "Engine Induced Structural-Borne Noise in a General Aviation Aircraft," NASA CR-159099, August 1979.

G.3 Pope, L.D., E.G. Wilby, J.F. Wilby, "Propeller Aircraft Interior Noise Model," NASA CR-3813, July 1984.

G.4 Wilby, J.F., T.D. Scharton, "Acoustic Transmission Through a Fuselage Sidewall," NASA CR-132602, July 1974.

G.5 Hayden, R.E., B.S. Murray and M.A. Theobald, "A Study of Interior Noise Levels, Noise Sources and Transmission Paths in Light Aircraft," NASA CR-172152, July 1983.

G.6 Wilby, J.F., F.L. Gloyna, "Vibration Measurements of an Airplane Fuselage Structure, I. Turbulent Boundary Layer Excitation," J. Sound Vib., 23, 4, 443-466, 1972.

G.7 Barton, C.K., J.S. Mixson, "Noise Transmission and Control for a Light Twin-Engine Aircraft," J. Aircraft, **18**, 7, 570-575, 1981.

G.8 Vaicaitis, R., M. Slazak, "Cabin Noise Control for Twin Engine General Aviation Aircraft," NASA CR-165833, February 1982.

G.9 Bhat, W.V., J.F. Wilby, "Interior Noise Radiated by an Airplane Fuselage Subjected to Turbulent Boundary Layer Excitation and Evaluation of Noise Reduction Treatments," Journal of Sound and Vibration, **18**, 4, 449-464, 1971.

APPENDIX H

CONTRIBUTION AND TREATMENT OF CABIN NOISE RESULTING FROM ENGINE AND PROPELLER-INDUCED STRUCTUREBORNE NOISE

H. CONTRIBUTION AND TREATMENT OF CABIN NOISE RESULTING FROM ENGINE AND PROPELLER-INDUCED STRUCTUREBORNE NOISE

H.1 Introduction

This section summarizes the role of structureborne noise induced by engine and propeller forces as a contributor to noise in the cabin of the demonstration aircraft.

H.2 Geometry

The engine and propeller of the R182 are mounted via four elastomeric vibration isolators to a "spider" which combines and transfers loads carried by the isolators to structural members behind the firewall, as shown in Figs. H.1 through H.5. The spider is a welded steel tubular structure which bolts to the firewall at four points, and has four mounting points to the engine. The load transfer paths are complex and the relative loading (mean and dynamic) on each member is a function of flight conditions due to the variation of torque and thrust on the propeller.

H.3 Estimation of Structureborne Cabin Noise from Engine Mount Vibration Measurements

To estimate the structureborne contribution from the engine to light aircraft cabin interior noise, one has the option of two related transfer function approaches. The cabin noise can be estimated as a function of the forces applied to the engine mounts or as a function of a resulting response at the mounts. The former approach is especially advantageous for making laboratory measurements of the transfer functions, since in the lab one can selectively apply forces to the engine mounts one at a time. However, the measurement of the forces applied to the engine mounts in flight requires transducers that are currently

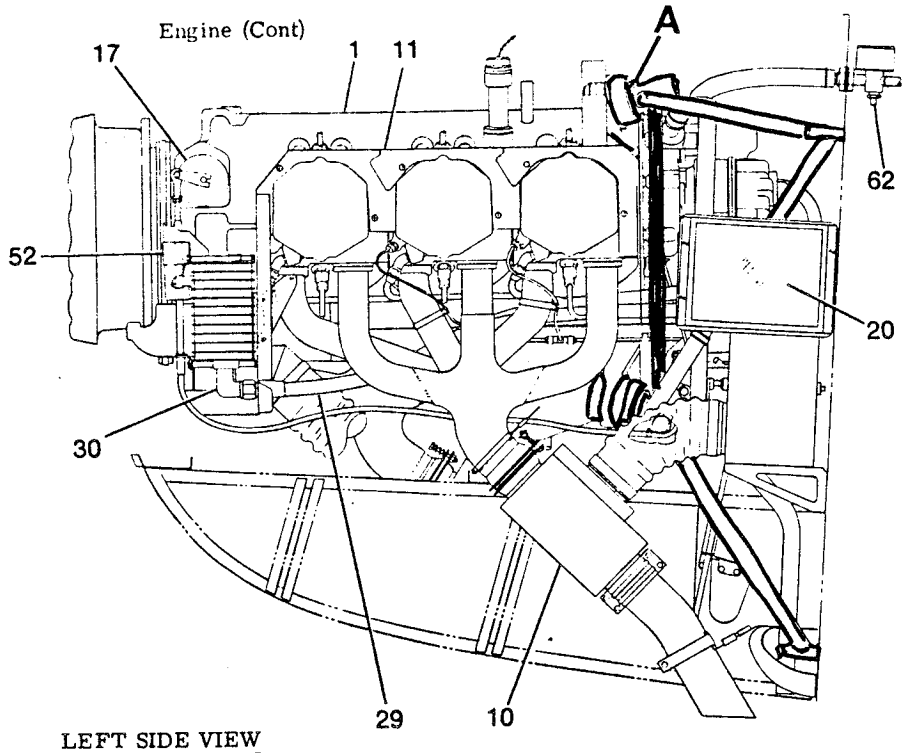

LEFT SIDE VIEW

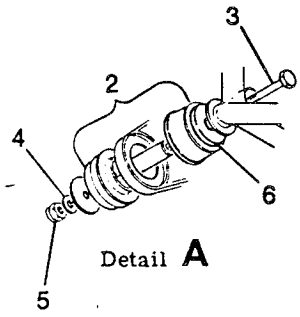

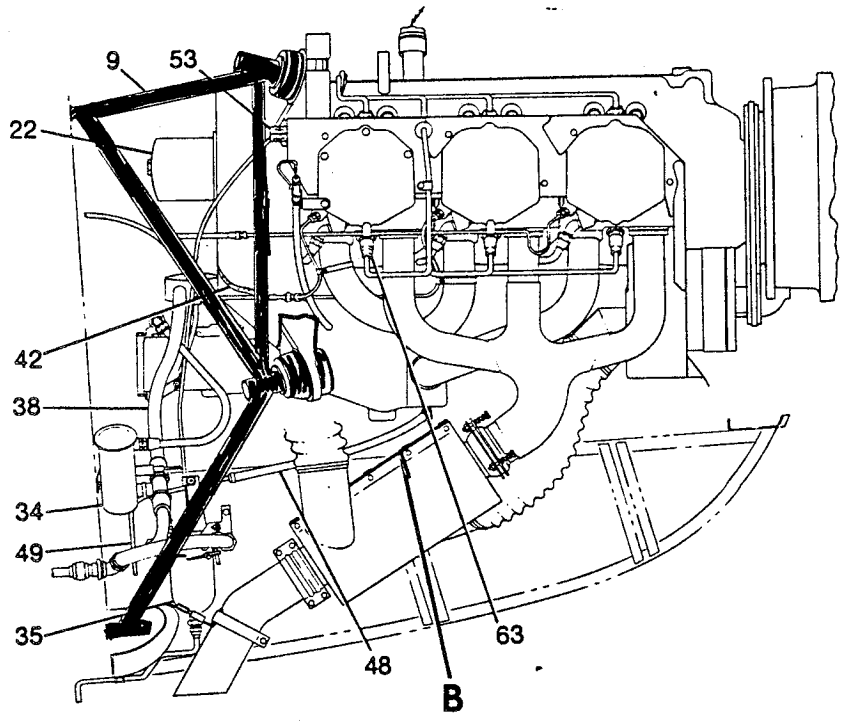

RIGHT SIDE VIEW

FIGURE H.1 DETAILS OF ENGINE MOUNTING.

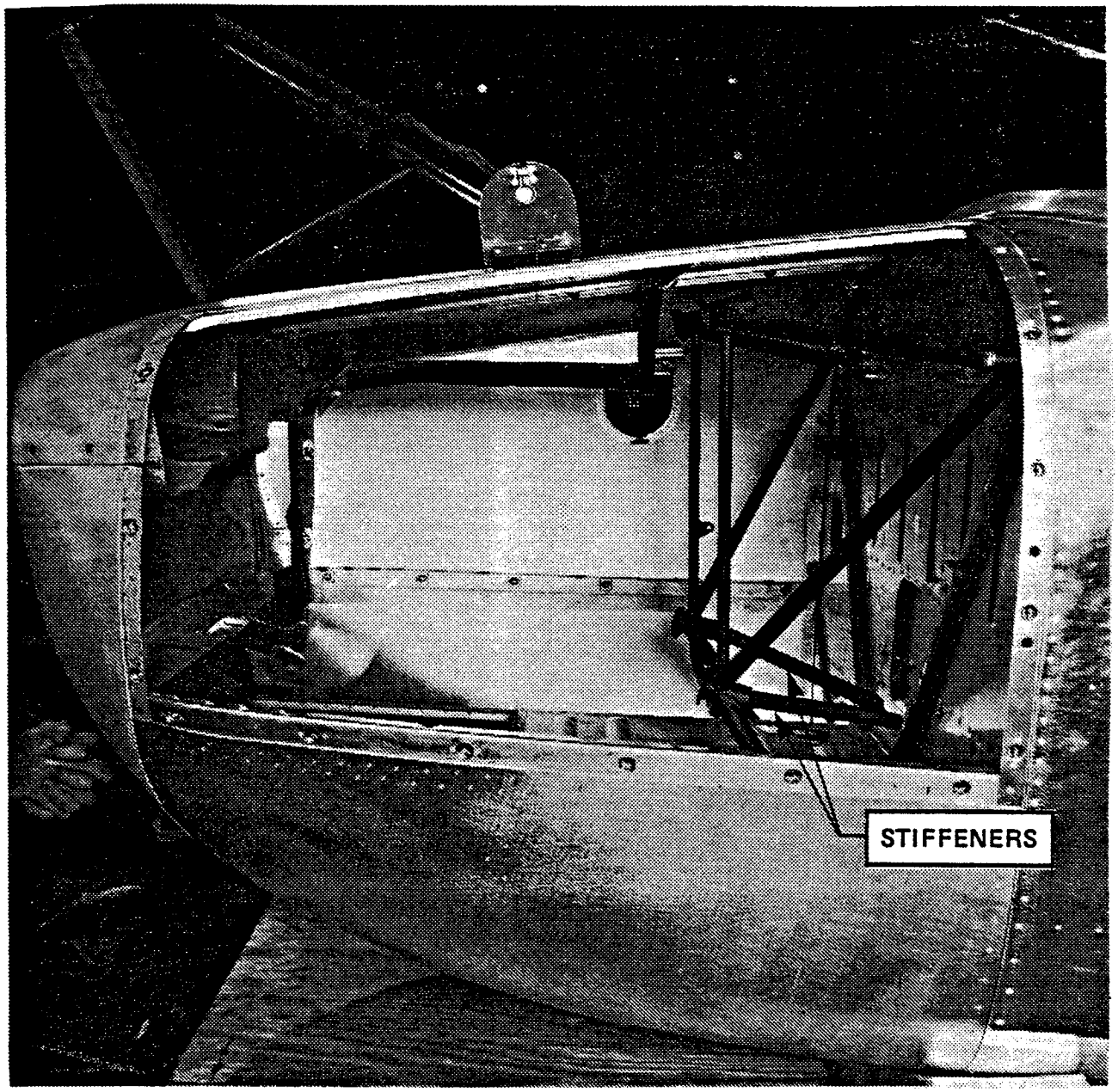

FIGURE H.2 SIDE VIEW OF ENGINE SUSPENSION WITH ENGINE REMOVED.

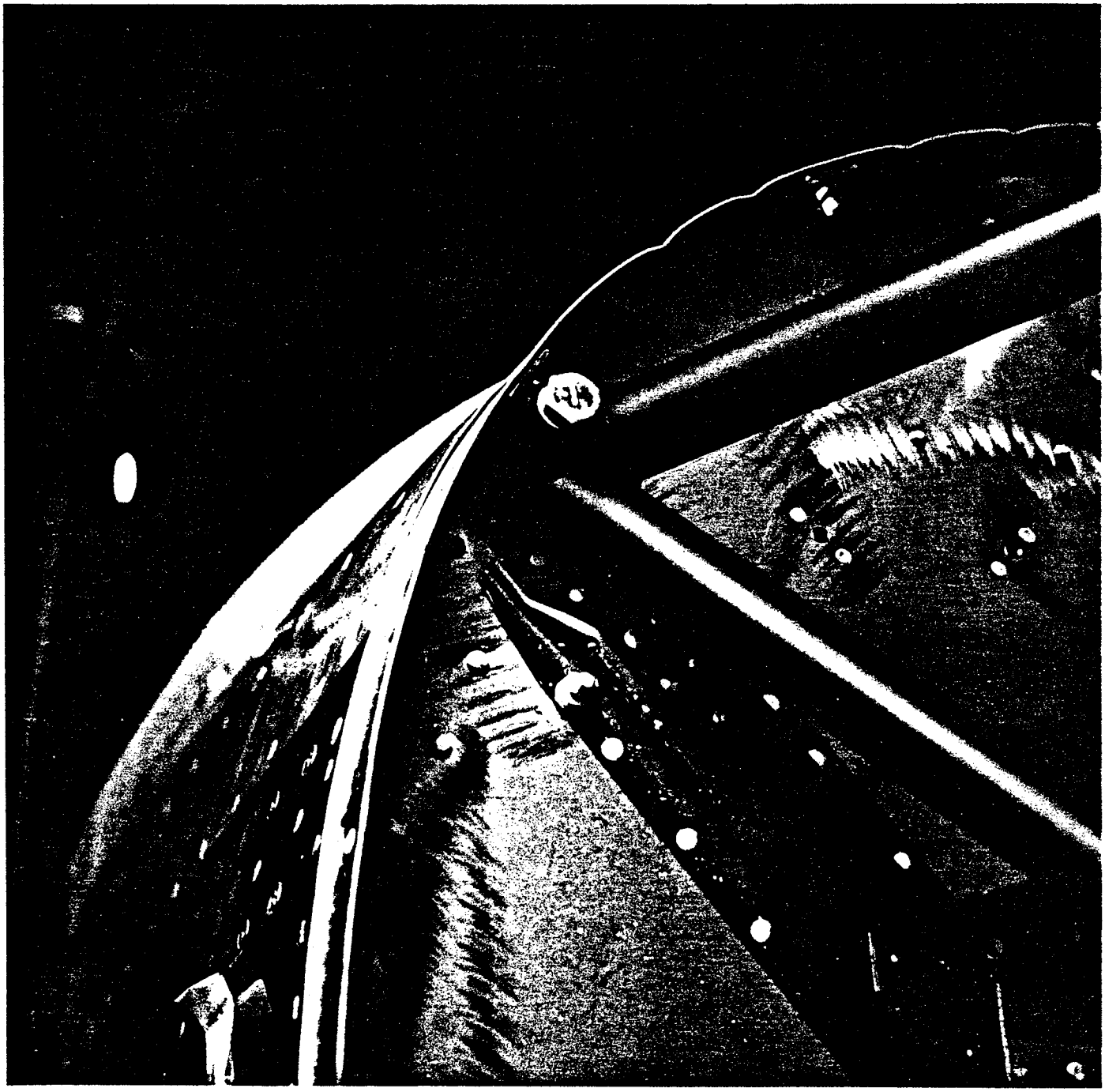

FIGURE H.3 TYPICAL UPPER ATTACHMENT OF ENGINE SUPPORT ASSEMBLY TO FIREWALL.

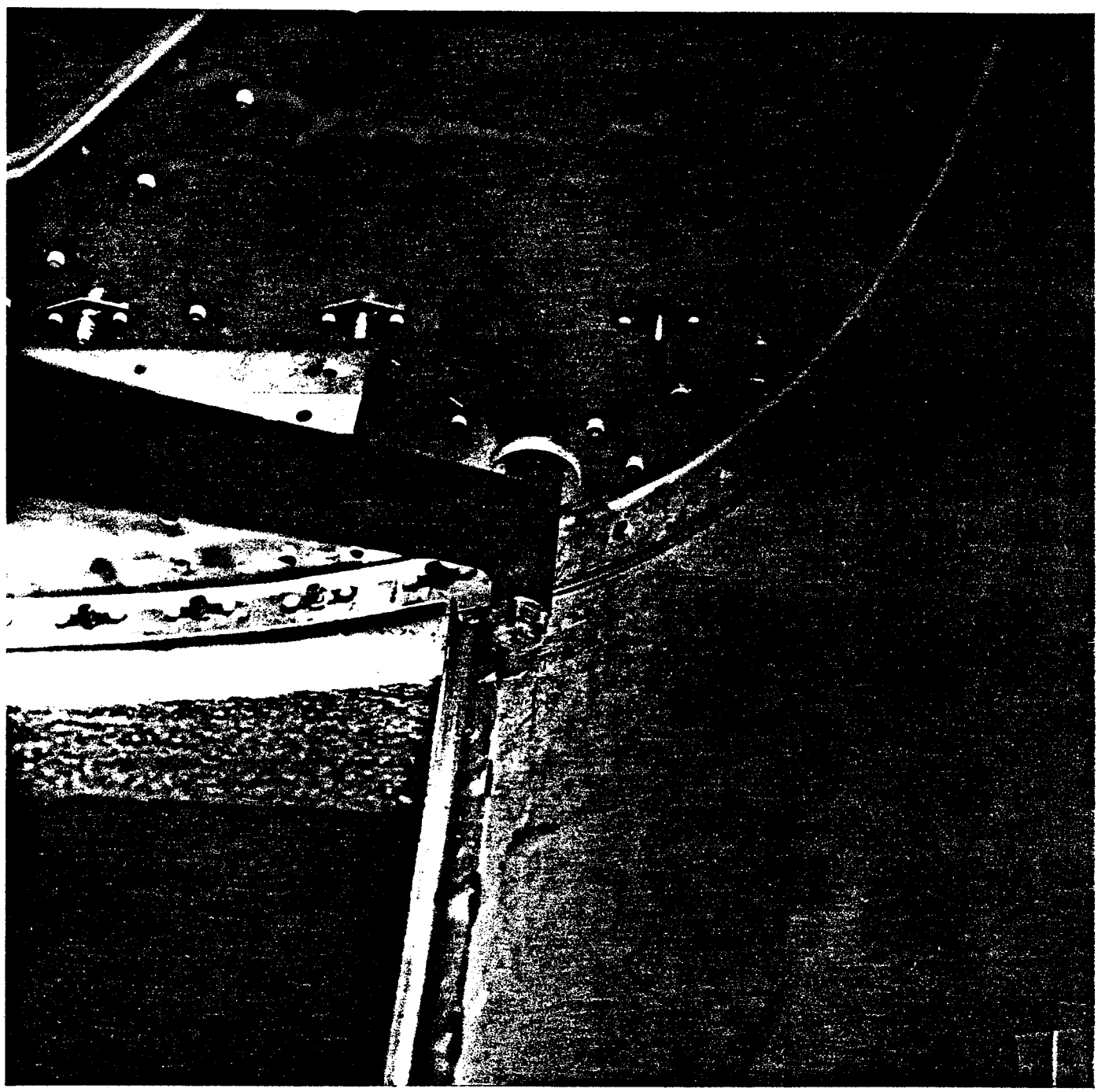

FIGURE H.4 TYPICAL LOWER ATTACHMENT OF ENGINE SUPPORT ASSEMBLY TO FIREWALL.

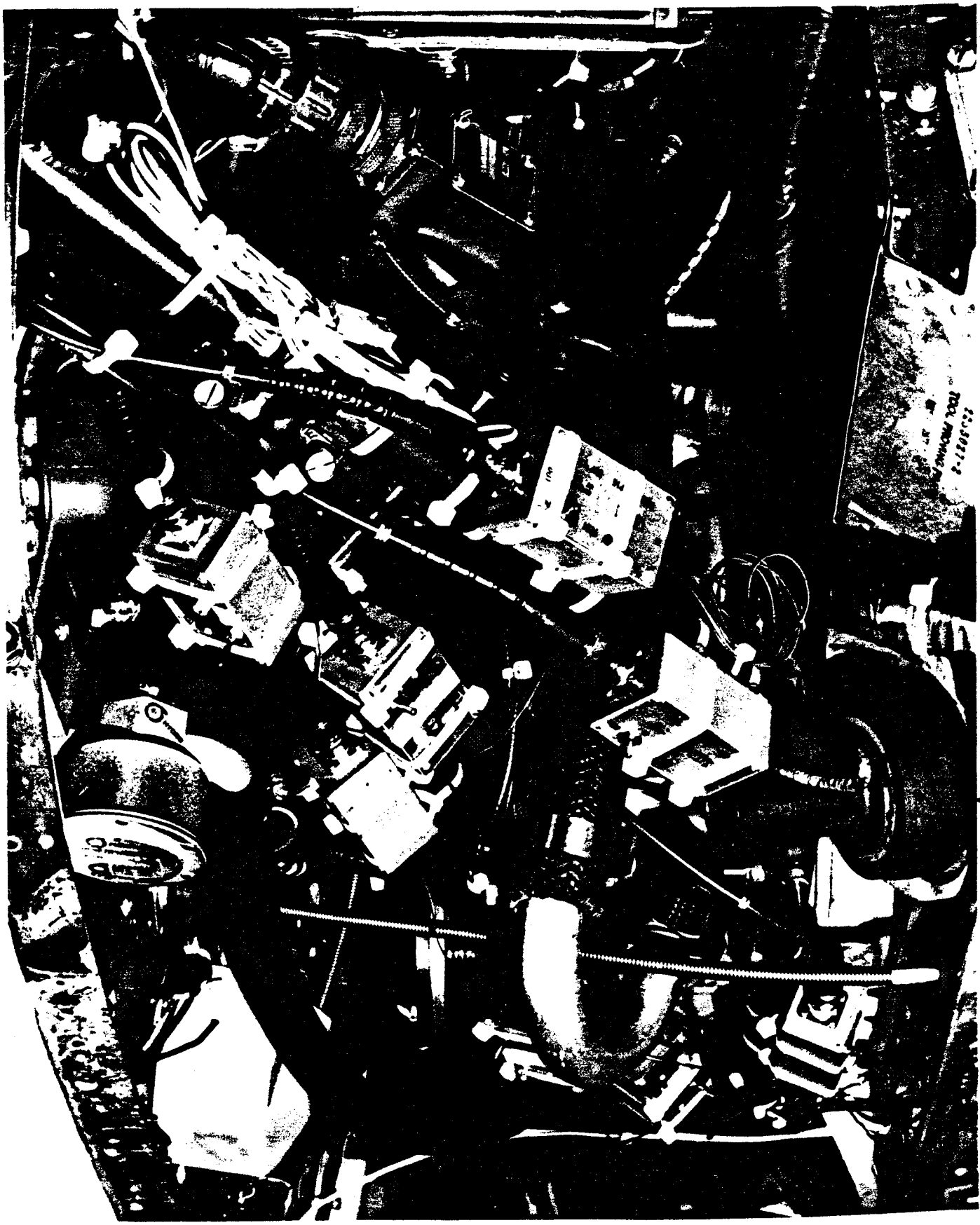

FIGURE H.5 UPPER PORT ENGINE MOUNT WITH ELASTOMERIC VIBRATION ISOLATOR IN PLACE.

unavailable and would require a significant program to develop. The latter approach presents difficulties in the lab when the transfer functions are to be measured. When one excites one mount in one direction, the other mounts all respond and it is nearly impossible to restrain them. Consequently, a "clean" transfer function cannot be measured. On the other hand, the measurement of mount response, in flight, presents no difficulties.

In this program, the use of the transfer function approach employing mount response was chosen rather than applied force, since the scope of this program did not contemplate the development of the required transducers. In this section, we discuss how to analyze the laboratory and flight measurements so as to obtain the best estimate of the structureborne contribution from the engine.

In the Cessna R182, there are four engine mounts, each of which responds in three orthogonal directions giving 12 mount response inputs. (In fact, there are three rotations associated with each mount that could also result in sound transmitted to the cabin.) The sound pressure in the cabin is then given by

$$P(\omega) = \sum_{J=1}^{N} H_j(\omega) V_j(\omega) \qquad (H.1)$$

where $P(\omega)$ is the cabin sound pressure amplitude at frequency ω; $V_j(\omega)$ is the amplitude of mount response j at ω; ("response" here means either displacement, velocity or acceleration.) $H_j(\omega)$ is the transfer function relating cabin sound pressure and mount response j at frequency ω; and N is the number of responses contributing to the cabin sound pressure. The mean square cabin response, $\langle p^2 \rangle$ can then be written

$$\langle p^2 \rangle = \sum_{i=1}^{N} |H_i^2| \langle v_i^2 \rangle + \mathrm{Re} \sum_{i=1}^{N} \sum_{j=1}^{N} H_i H_j^* \langle V_i V_j^* \rangle \qquad (H.2)$$

where we have neglected writing the frequency ω to simplify the notation, $\langle v_i^2 \rangle$ is the mean square engine mount response, i, and $(\ )^*$ means complex conjugate. The double summation in Eq. (H.2) accounts for the correlation between the various engine mount responses. In general, that term can be neglected relative to the single summation in the equation if the minimum frequency of interest is above the first few resonances of the engine mounting spider. In such a case, the phase shift between the various responses will be significant and the double summation in Eq. (H.2) will consist of the addition of terms of alternating sign. It is reasonable then to neglect the double summation if there are a sufficient number of terms as we have here with 12 input responses. Equation (H.2) then simplifies to

$$\langle p^2 \rangle = \sum_{i=1}^{N} |H_i^2| \langle v_i^2 \rangle \qquad \text{(H.3)}$$

In the laboratory, one would like to measure each H_i. To do so requires that one excite one response V_i and restrain all others.

If the mounts are essentially independent, then no restraint is required. All V_i's but the excited one will be zero and each $|H_i^2|$ can be measured quite easily. If, however, the mounts are well coupled together, as is the case in the Cessna R182, then all of the responses are excited nearly the same, even though only one mount in one direction is being forced. In general, it is not possible to restrain the other responses. Consequently, in the laboratory, one is left with a contaminated measure of the transfer functions which we can estimate as follows. The response v_i to forces applied to all the mounting points is given by

$$\langle v_i^2 \rangle = \sum_{j=1}^{N} |A_{ij}(\omega)|^2 \langle F_j^2 \rangle \qquad \text{(H.4)}$$

where A_{ij} are the admittances and cross-admittances relating an applied force to any of the 12 responses, $\langle F_j^2 \rangle$ is the mean square force applied at the location and direction of response v_j. Note that Eq. (H.4) assumes that the applied forces are uncorrelated; although that assumption is not necessary, it does simplify the mathematics.

If only one force F_k is applied, as would be done in the laboratory to measure a transfer function, the resulting responses are given by

$$\langle \tilde{v}_i^2 \rangle^k = |A_{ik}|^2 \langle F_k^2 \rangle \qquad (H.5)$$

where $\langle \tilde{v}_i^2 \rangle^k$ is the mean square response v_i due to a single force F_k. Using Eq. (H.5) in Eq. (H.3), the mean square cabin sound pressure due to force F_k is found to be

$$\langle p^2 \rangle^k = \{ |H_k^2| + \sum_{\substack{i=1 \\ i \neq k}}^{N} \left| \frac{A_{ik}}{A_{kk}} \right|^2 |H_i^2| \} \langle \tilde{v}_k^2 \rangle \qquad (H.6)$$

Normally, one estimates the transfer function $|H_k|^2$ by dividing the mean square cabin pressure by the mean square response at k. If the A_{ik}'s, the cross-admittances, are much less than the A_{kk}'s, the point admittances, then that procedure would yield a good estimate of $|H_k^2|$. If, however, the responses are all well coupled, then the A_{ik}'s and A_{kk}'s are of comparable magnitude and Eq. (H.6) shows that one will overestimate $|H_k^2|$ by a significant margin.

Since the engine mounts in the R182 are well coupled, one cannot use the traditional transfer function approach. If the responses are all well coupled, however, it is probably not unreasonable to assume that the $|H_k^2|$ are all of comparable magnitude. If that is the case, then when one excites response, k, in the lab with a single force, the cabin sound pressure can be written

$$\langle p^{\angle} \rangle^k \tilde{=} |H_k^{\angle}| \sum_{j=1}^{N} \langle \tilde{v}_j^{\angle} \rangle^k \qquad (H.7)$$

and the transfer function $|H_k{}^{\angle}|$ can be estimated by dividing the mean square cabin sound pressure by the sum of all the mean square responses. Each $|H_k|^{\angle}$ could then be substituted into Eq. (H.3) and multiplied by the appropriate response $\langle v_i^{\angle} \rangle$ measured during a flight tests. However, to be consistent with the assumption in Eq. (H.7) that all $|H_k^{\angle}|$ are equal, Eq. (H.3) can be rewritten

$$\langle p^{\angle} \rangle = |H^{\angle}|^A \sum_{j=1}^{N} \langle v_j^{\angle} \rangle \qquad (H.8)$$

and we use for $|H^{\angle}|^A$ the average of the transfer functions calculated to each exciation force, F_k

$$|H^{\angle}|^A = \frac{1}{N} \sum_{k=1}^{N} \frac{\langle p^{\angle} \rangle}{\sum_{j=1}^{N} \langle \tilde{v}_j^{\angle} \rangle} = \frac{1}{N} \sum_{k=1}^{N} |H_k^{\angle}| \qquad (H.9)$$

where the summation on k is over all the possible excitation forces, in this case three directions at each of the four mounting points for a total of 22. This average transfer function is then multiplied by the sum of the mean square engine mount responses measured during a flight test.

Equations (H.8) and (H.9) provide a calculation procedure for estimating the structureborne contribution from the engine in the R182 that should provide estimates that will be significantly in error only if a very small number of responses out of the total is solely responsible for the cabin sound pressure*.

---

* It is interesting to note that Eqs. (H.8) and (H.9) will also correct the structureborne noise even if the engine mounts are independent. The only requirement is that the $|H_k^{\angle}|$ be nearly the same for all the mount responses.

For the geometry of the engine mounting system, such a situation is very unlikely.

A special advantage of Eqs. (H.8) and (H.9) is that instrumentation is readily available that will take a number of signals (responses) and generate a one-third octave band spectrum of the sum of their mean squares. This is precisely what must be done with the 12 responses obtained in the laboratory transfer function measurements and with the 12 response measurements from the flight tests.

H.4 Review of Available Data on Source Levels and Spectra

The most comprehensive set of engine vibration data was acquired during preliminary diagnostic test flights described in Ref. 1. During those tests an R182 (with two-blade propeller) with 12 accelerometers was instrumented for extensive ground run-up tests and several flight tests. Each mount was fitted with three accelerometers to measure three orthogonal components of mount translation. Ideally, one would also measure the three orthogonal components of rotation as well, but such measurements were impractical in this study.

The engine vibration monitored during a ground run-up (energy averaged over all 12 accelerometers) is shown in Fig. H.6 for the R182 with stock vibration isolators. A clear response peak occurs at 80 Hz, the propeller blade passing rate. These and other similar data repeatedly show strong vibration components at harmonics of the blade passing rate which are presumably due to unbalance forces or unsteady air loads on the propeller. An important question associated with these experiments is whether ground run-up data are indeed representative of flight conditions. While this question cannot be answered definitively with the present data base, there are indications that average

structural vibration of the engine mounts is changed only slightly by flight loads, although the vibration of individual mounts may change substantially. Shown in Figs. H.6 through H.11 are comparisons for one engine mount location (in three directions) of flight and ground vibration data. At low to mid frequencies where structureborne noise is expected to be important, the variation between flight and ground run-up conditions is on the order of 0-5 dB on individual mounts.

A visit to Cessna's factory afforded an opportunity to make unique measurements of the insertion loss of the engine vibration isolators with the engine in place. These measurements were accomplished by measuring cabin noise and mount vibration with first the standard isolators in place and then with the isolators replaced by aluminum blocks (see Fig. H.12). The insertion loss of the vibration isolators is shown in Fig. H.13. Measurements at three engine operating conditions show very similar results indicating that the isolation is not a strong function of the static load on the mounts. Insertion loss at the important frequencies of 80 Hz (blade passing) and 120 Hz (engine firing) is negligible, pointing toward an area of possible improvement in the isolator design. Measurements of cabin noise in flight produced the results shown in Fig. H.14. The cabin noise under cruise conditions is seen to increase with the use of hard engine mounts, but above the 250 Hz third octave band, the increases are much less than the vibration increases. From this pragmatic experiment, one can infer that structureborne noise from the engine propeller system is one of several contributors to cabin noise in the frequency range from 25-63 Hz, and from 160 Hz to 4 kHz.

The increase in the cabin measured sound pressure level during the ground run-up in combination with the increase in vibration was used in Ref. 1, to compute an approximate transfer function relating engine vibration and cabin noise due to engine

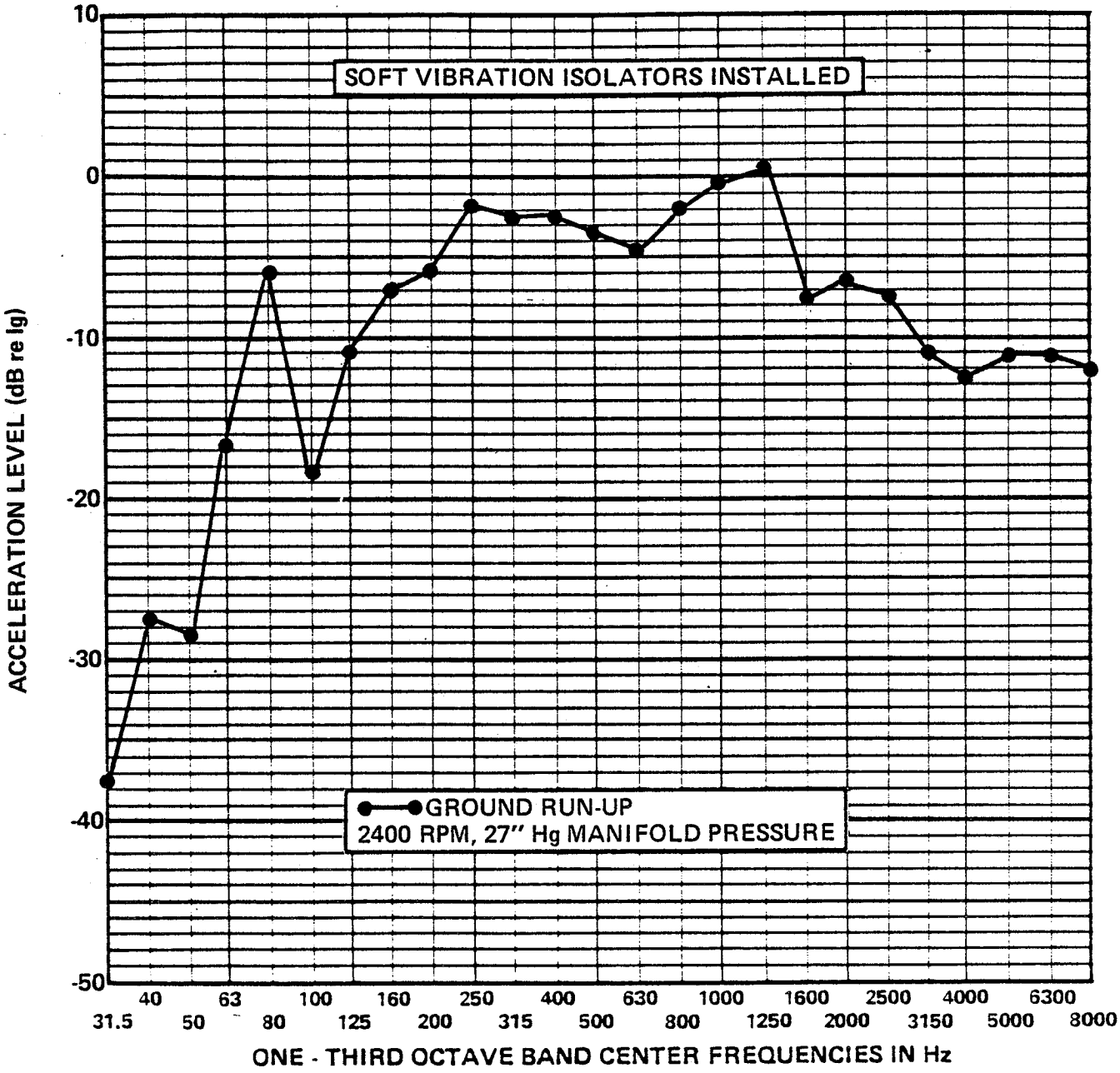

FIGURE H.6 ENERGY AVERAGE OF VIBRATION ON FOUR-MOUNT POINTS DURING GROUND RUN-UP (STOCK ISOLATION MOUNTS).

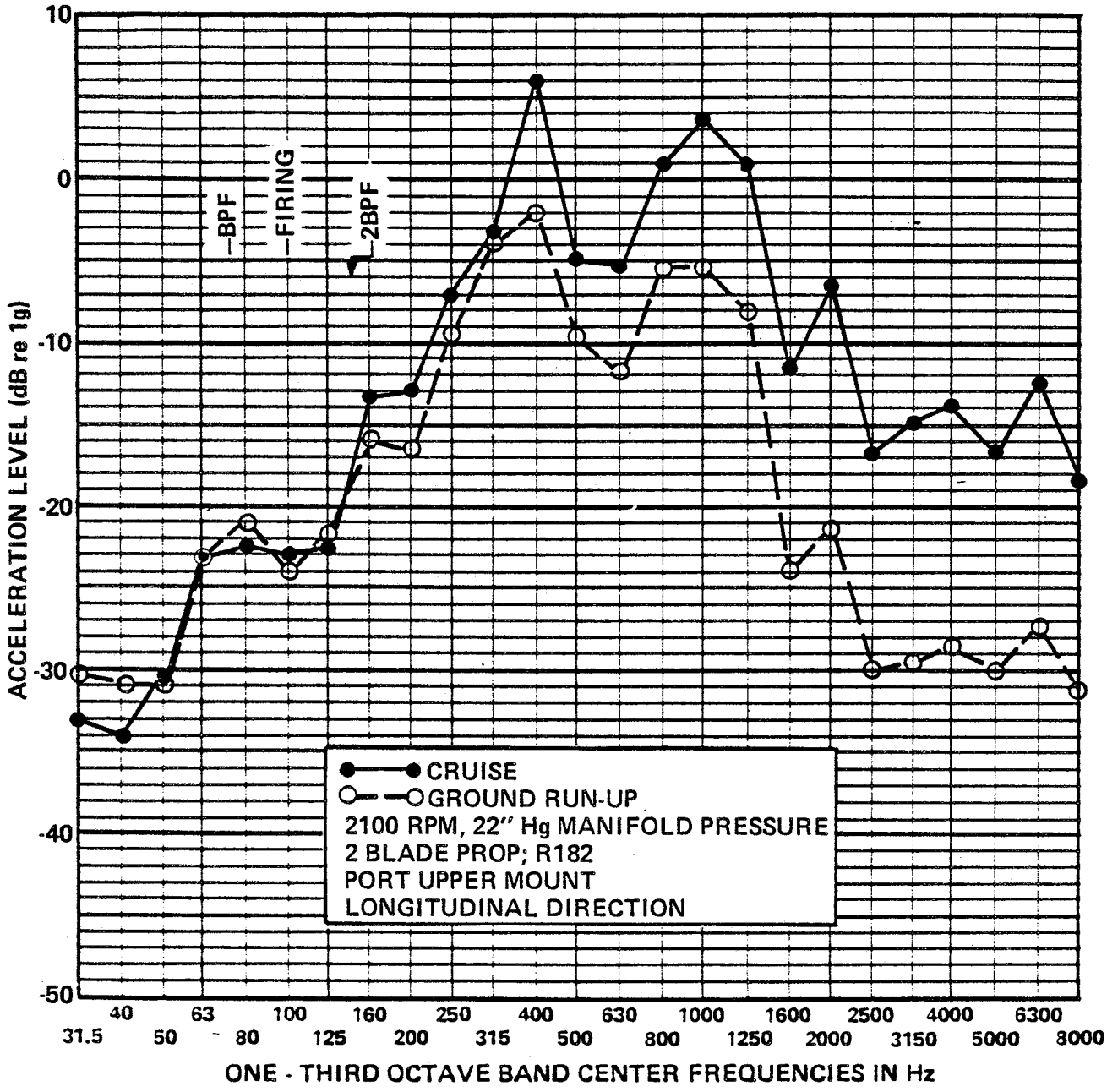

FIGURE H.7 COMPARISON OF MOUNT VIBRATION BETWEEN FLIGHT AND GROUND RUN-UP CONDITIONS (PORT UPPER-MOUNT LONGITUDINAL DIRECTION - 2100 RPM).

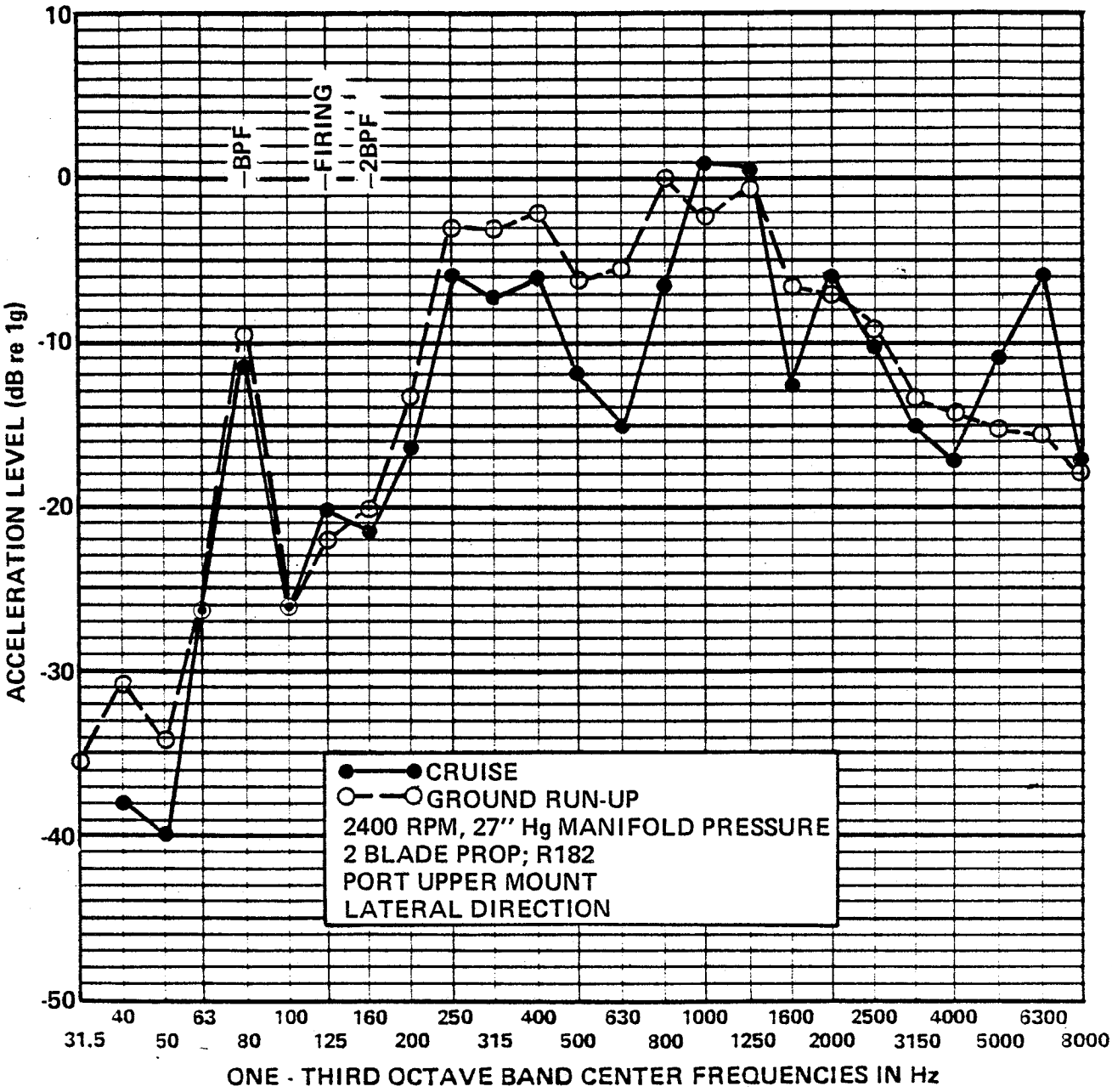

FIGURE H.8 COMPARISON OF MOUNT VIBRATION BETWEEN FLIGHT AND GROUND RUN-UP CONDITIONS (PORT UPPER MOUNT LATERAL DIRECTION - 2400 RPM).

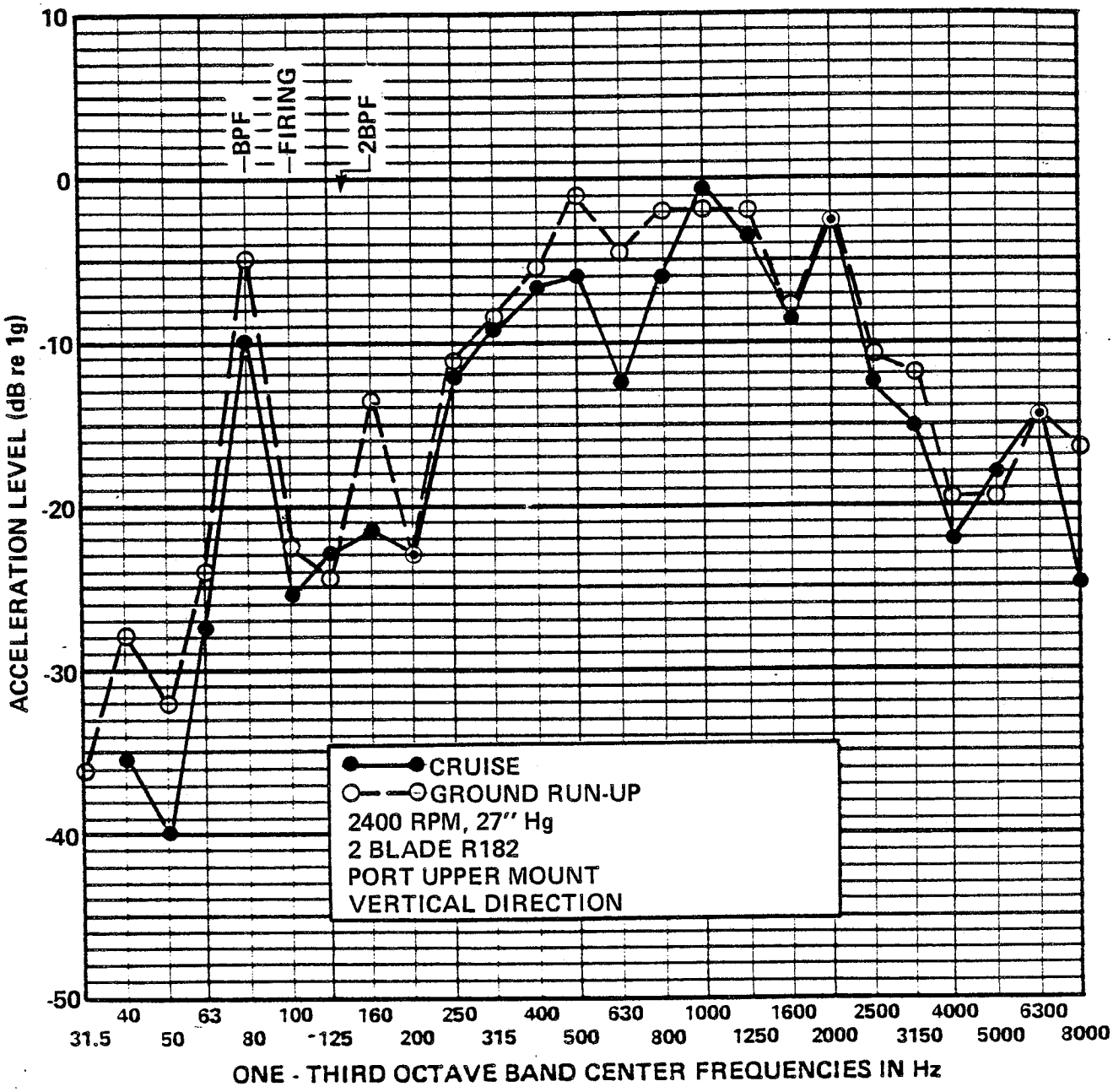

FIGURE H.9 COMPARISON OF MOUNT VIBRATION BETWEEN FLIGHT AND GROUND RUN-UP CONDITIONS (PORT UPPER MOUNT VERTICAL DIRECTION - 2400 RPM).

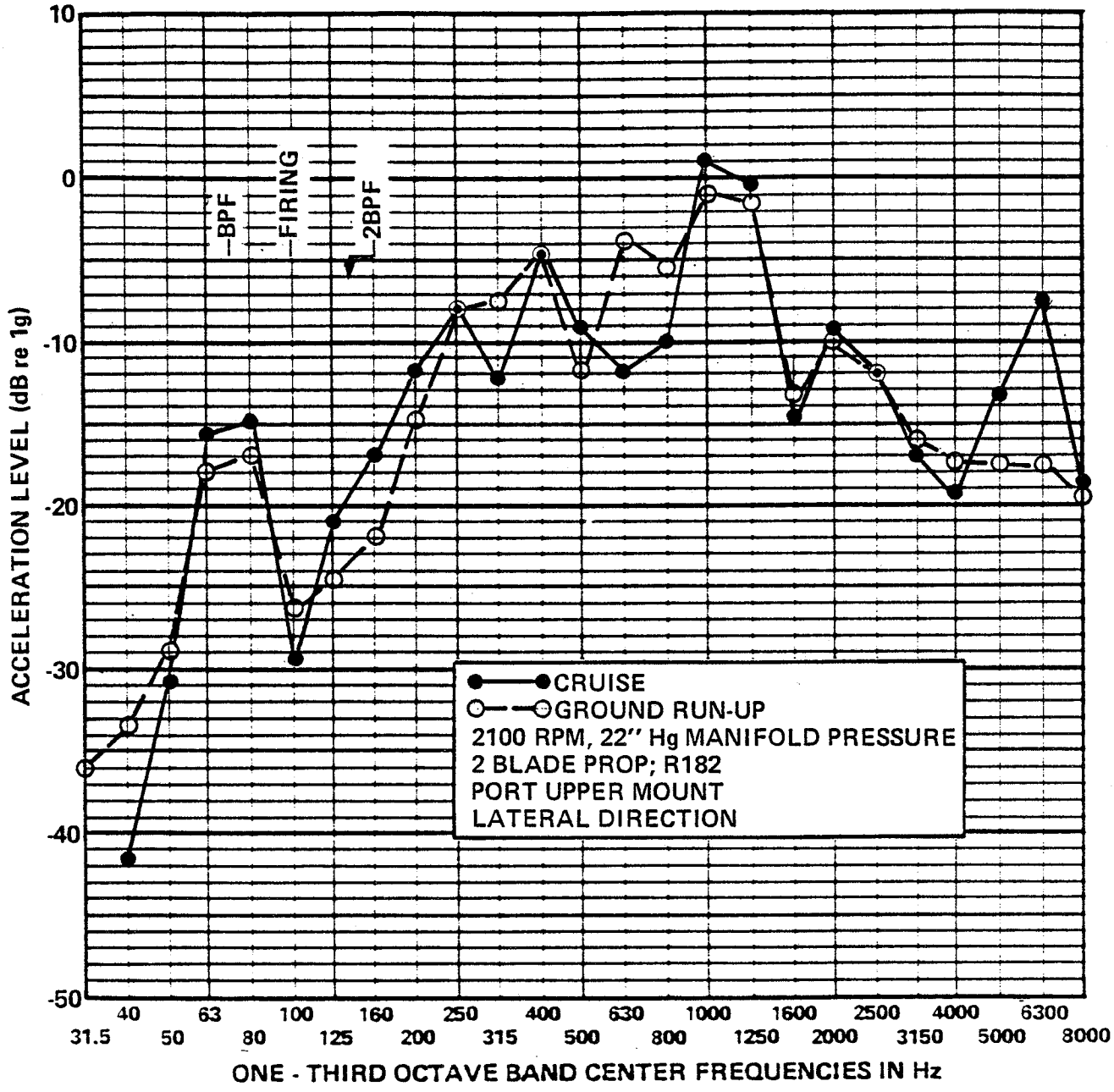

FIGURE H.10 COMPARISON OF MOUNT VIBRATION BETWEEN FLIGHT AND GROUND RUN-UP CONDITIONS (PORT UPPER MOUNT LATERAL DIRECTION - 2100 RPM).

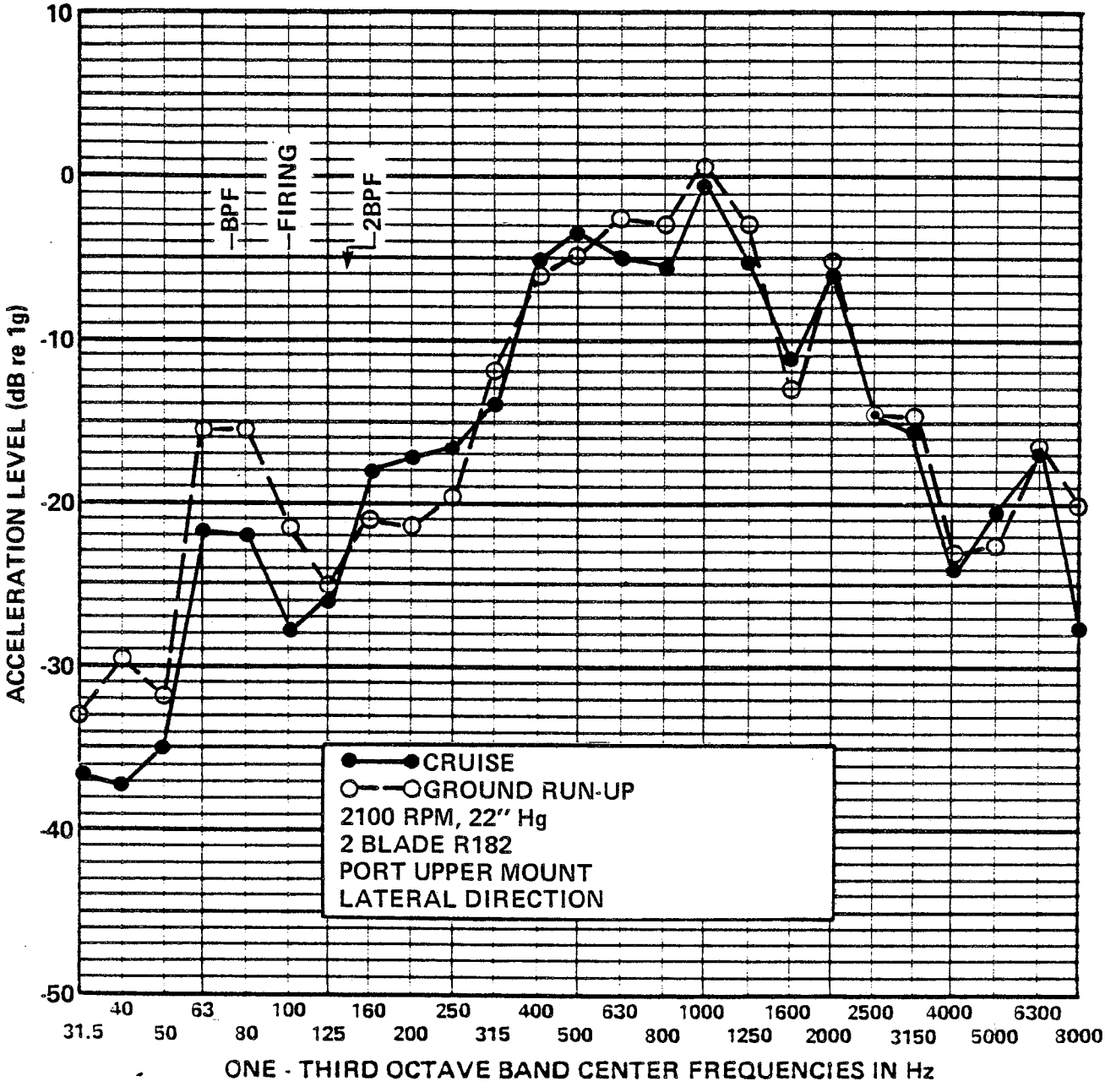

FIGURE H.11 COMPARISON OF MOUNT VIBRATION BETWEEN FLIGHT AND GROUND RUN-UP CONDITIONS (PORT UPPER MOUNT VERTICAL DIRECTION -2100 RPM).

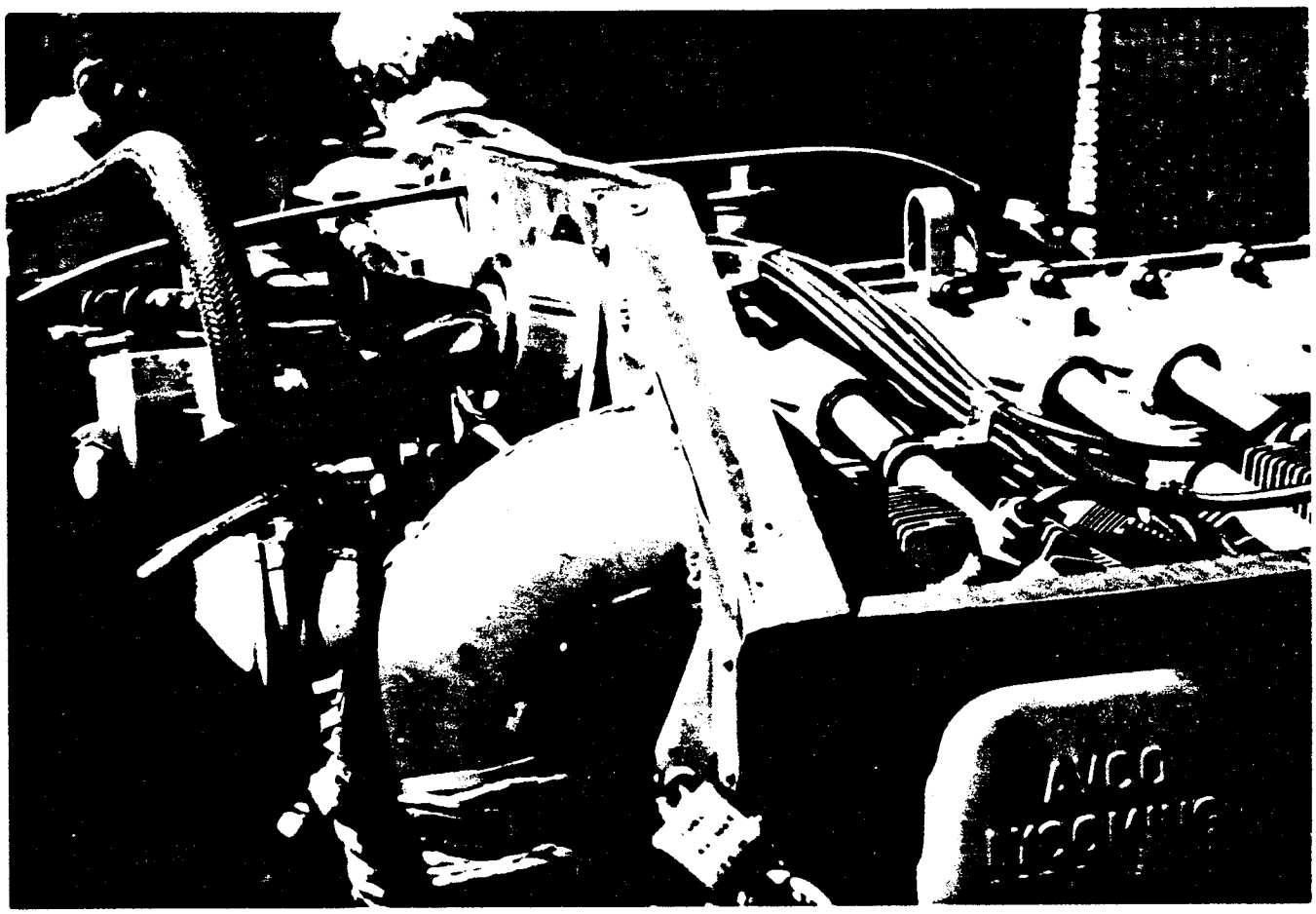

FIGURE H.12 UPPER STARBOARD ENGINE MOUNT OF R182 WITH ALUMINUM BLOCK INSTALLED IN PLACE OF ELASTOMERIC VIBRATION ISOLATOR.

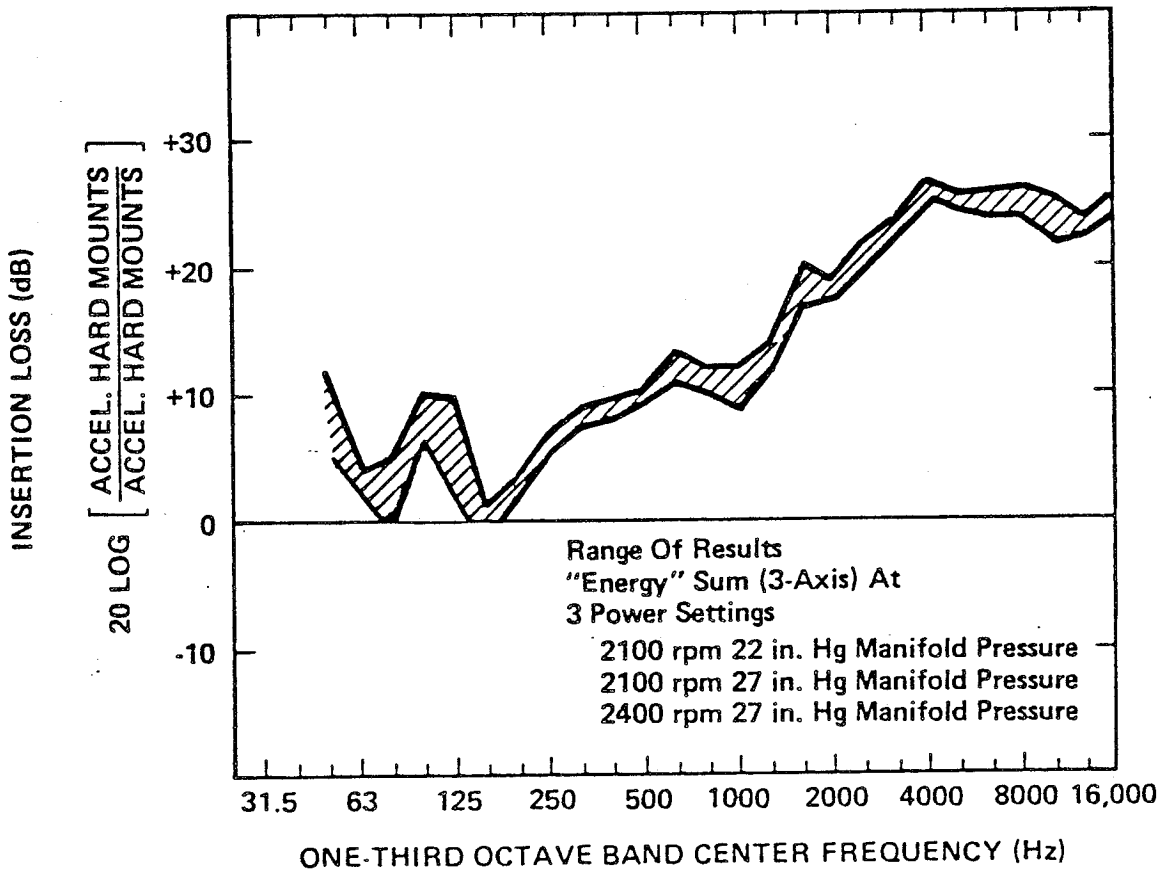

FIGURE H.13 INSERTION LOSS OF ENGINE MOUNTS (SEE REF. 1 FOR DETAILS)

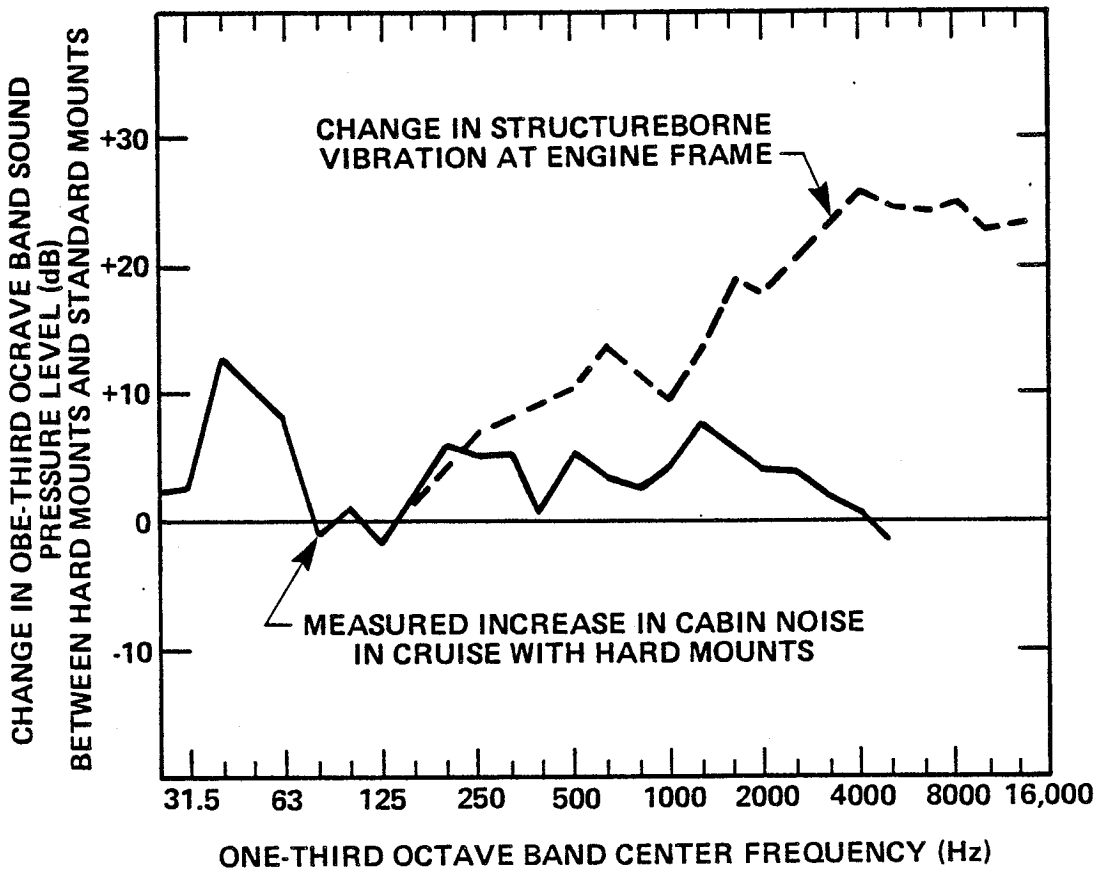

FIGURE H.14 CHANGE IN CABIN NOISE LEVELS WITH HARD MOUNTS (SEE REF. 1 FOR DETAILS).

vibration. This computation necessarily assumed that the relative contribution of other sources is the same between ground run-up and flight, an assumption which is not expected to be completely valid. The results of this computation are plotted in Fig. H.15. This transfer function will be compared with a transfer function derived from controlled laboratory measurements, which are described i the next section.

H.5 Characterization of Paths by which Noise Reaches the Cabin

The two major paths through which engine structureborne noise may be radiated to the cabin are presumed to be:

a) Vibration excitation of the lightweight firewall which then acts as a partially-stiffened membrane to radiate sound, and

b) Vibration excitation of the cabin sidewall and window surfaces through the main structural members, resulting in many large radiating surfaces in close proximity to the passengers' ears.

A controlled test in the laboratory was used to derive the transfer function relating vibration at the engine mount spider to noise in the cabin by both paths, i.e., separate transfer functions were not computed. This transfer function, when combined with the mount vibration spectra, allows one to compute structureborne noise produced by the engine/propeller combinations. The laboratory measurement of the transfer function is described below.

The engine mount spider was excited by a small inertia-type shaker at each engine mount point in each of three directions (12 experiments). (See Fig. H.16.) Twelve accelerometers were mounted in the same positions used during the ground run-up test

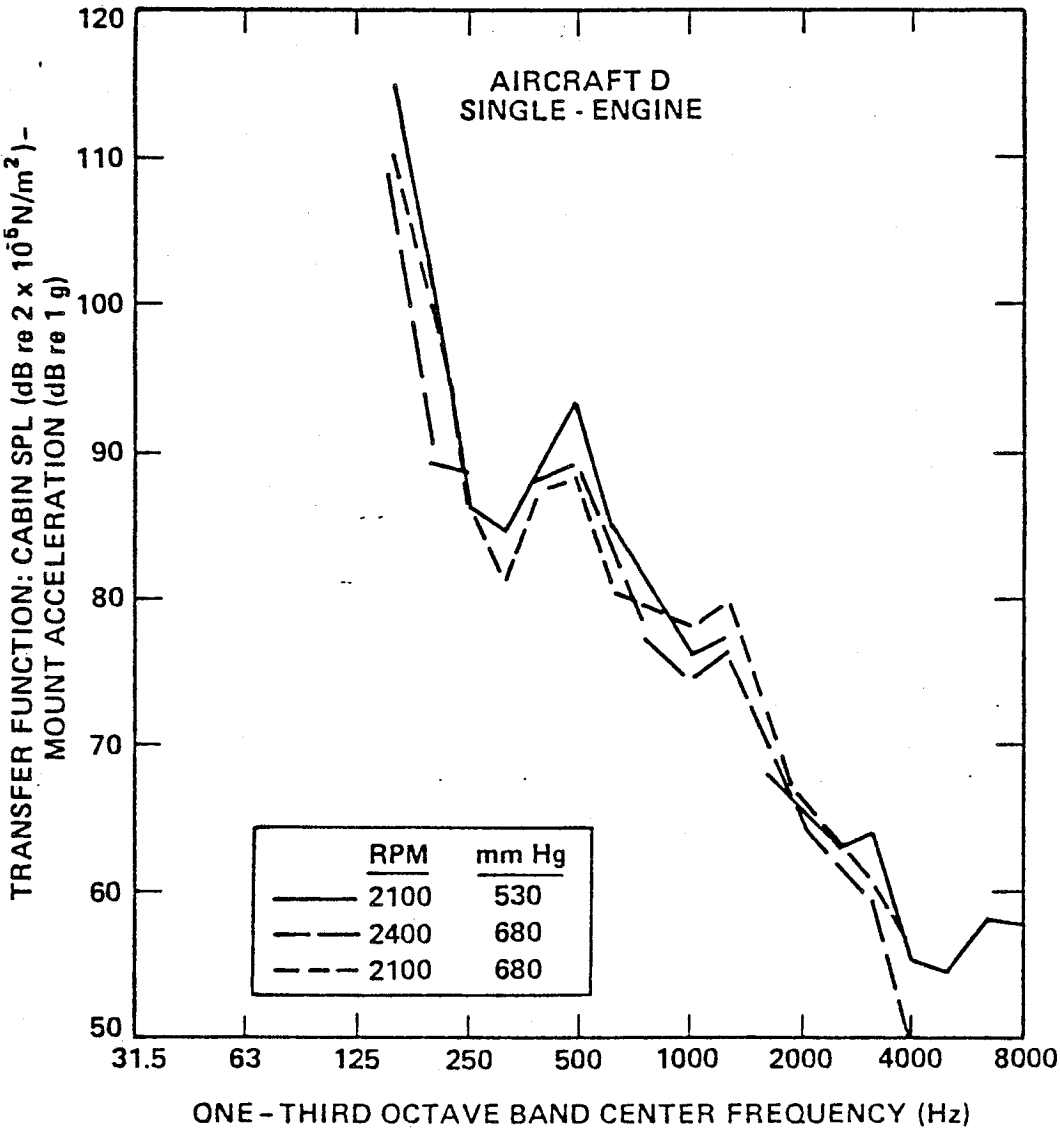

FIGURE H.15 TRANSFER FUNCTION BETWEEN AVERAGE MOUNT ACCELERATION AND CABIN NOISE (DERIVED IN REF. 1 FROM GROUND TESTS).

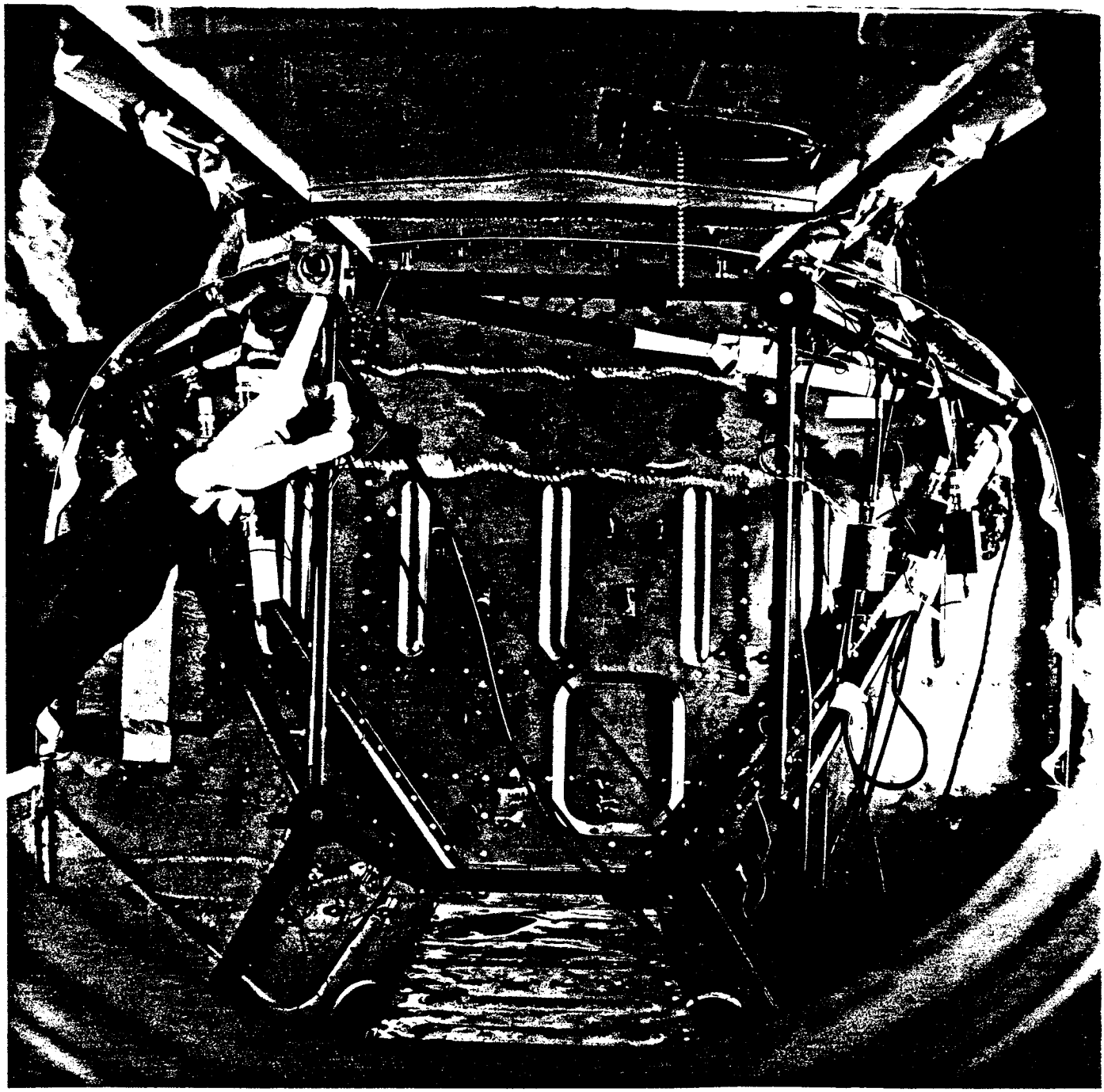

FIGURE H.16 ENGINE MOUNT SPIDER WITH MOUNTING BLOCK FOR SHAKER IN LABORATORY VIBRATION TEST. ACCELEROMETERS MONITORING VIBRATION LEVELS ARE VISIBLE IN PART.

described above. Microphones were installed in the engine cavity to monitor noise radiated by the shaker. Microphones were suspended in the cabin at positions where flight noise data were available (see App. B). It was verified that airborne noise radiated by the shaker and the engine mount struts made a negligible contribution to the noise in the cabin compared with the structureborne component. For each vibration direction, all twelve acceleration responses at the spider were measured. These vibration responses were averaged on a power basis using the method described in Sec. H.3. The resulting 12-component transfer functions, i.e. one for each forcing direction as monitored at twelve positions to cabin noise, were averaged on an energy basis to yield the space-averaged transfer function shown in Fig. H.17. Also shown in Fig. H.17 are the transfer functions computed using ground run-up data as discussed above and in Ref. 1. The general agreement between the two sets of data is quite good in light of the different conditions under which they were obtained. The laboratory-derived transfer function shown in Fig. H.17 yields generally lower values than the field experiment, presumably reflecting the improved ability of the lab experiment to clearly separate structureborne contributions from other sources. It is interesting and significant to note that each mount has a different transfer function for different directions of applied force (see Table H.1). The variations in these transfer functions suggest that each mount might contribute quite differently to the structureborne sound radiating into the cabin.

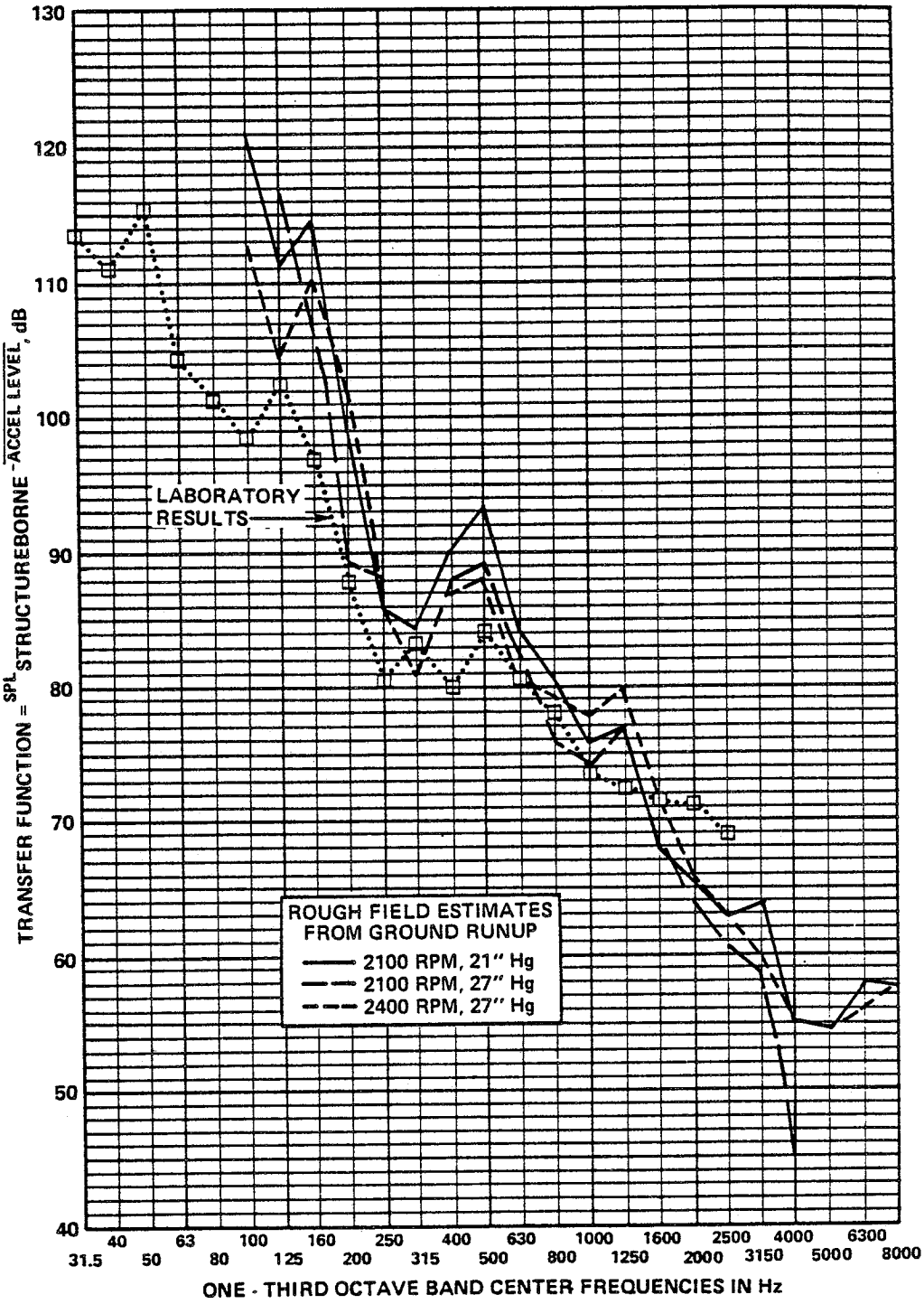

FIGURE H.17 LABORATORY TRANSFER FUNCTION RELATING CABIN NOISE (STRUCTURBORNE) TO ENGINE VIBRATION.

TABLE H.1

INDIVIDUAL TRANSFER FUNCTIONS FOR STRUCTUREBORNE NOISE
IN CABIN CAUSED BY ENGINE MOUNT VIBRATION

1/3 Octave Band Center Frequency (Hz)	RMS Average of Transfer Functions (SPL Cabin Center - AL Mount) (Mount-direction of force)													
	1-X	1-Y	1-Z	2-X	2-Y	2-Z	3-X	3-Y	3-Z	4-X	4-Y	4-Z	12 Forcing Positions Energy Avg	11 Forcing Positions Energy Avg
31	89.0	81.0	97.5	89.5	83.5	93.0	110.5	100.5	96.5	107.0	98.0	91.0	102.1	102.4
40	93.0	86.0	96.0	90.0	88.0	98.0	105.0	105.0	92.0	98.0	103.5	96.0	99.7	99.9
50	93.5	87.5	110.0	82.0	89.0	98.0	109.0	108.0	102.5	108.0	107.0	103.0	105.3	104.4
63	75.5	75.0	100.0	78.0	74.0	86.0	97.0	94.0	96.0	97.5	90.5	98.0	94.7	93.6
80	64.0	73.0	100.0	71.0	74.0	88.5	91.0	90.5	93.0	91.5	91.5	95.5	92.5	90.2
100	66.5	74.5	99.5	67.0	69.5	90.5	88.5	82.5	92.0	86.5	79.5	92.5	90.9	87.3
125	76.0	74.0	102.5	79.5	76.5	93.0	92.5	90.0	97.0	92.5	84.0	95.0	94.4	91.4
160	69.5	64.5	96.0	73.5	68.0	85.0	88.0	85.0	91.0	86.0	79.5	90.0	88.3	85.7
200	70.5	69.5	83.5	73.5	70.5	76.0	77.5	74.5	80.5	81.0	73.5	79.5	78.0	76.8
250	70.0	68.0	81.5	68.0	67.0	72.0	70.0	70.0	70.0	72.0	62.0	69.5	73.0	69.6
315	70.0	69.0	85.0	71.0	71.0	78.0	71.5	69.5	72.0	71.5	66.5	73.5	76.2	72.3
400	66.0	65.5	81.0	67.5	68.0	68.5	70.0	68.5	68.5	70.5	72.0	69.0	72.5	68.9
500	76.5	76.5	84.5	67.5	69.0	71.5	69.5	67.5	74.0	74.5	72.5	75.0	76.3	73.3
630	71.5	71.0	81.5	67.5	68.0	70.5	66.0	67.0	71.5	71.0	69.0	71.5	73.2	69.9
800	64.5	62.5	76.5	63.5	61.5	65.5	72.0	66.0	69.0	64.5	70.0	66.5	69.3	67.1
1000	60.5	62.0	72.5	63.0	61.5	63.5	61.0	63.0	65.0	62.5	63.5	61.5	65.0	62.6
1250	61.0	60.0	75.0	62.0	60.0	62.5	59.5	60.0	63.5	62.0	57.5	63.0	65.9	61.3
1600	61.0	58.5	72.0	59.5	58.0	58.5	59.0	58.5	67.0	59.5	52.5	59.0	63.7	60.6
2000	62.0	58.0	71.0	61.0	62.0	61.5	59.0	57.5	61.0	56.0	57.5	58.0	62.8	59.9
2500	57.5	57.0	68.0	61.5	59.5	57.0	58.0	54.5	59.0	59.0	57.5	57.0	60.6	58.1

Note: (1) Mount #1 = lower port side
2 = lower starboard side
3 = upper starboard side
4 = upper port side
(2) Directions of driving mounts are with respect to aircraft x-axis

H.6 Estimated Contribution to Cabin Noise

The estimated contribution to cabin noise by structureborne noise from the propeller/engine is plotted in Fig. H.18. The contribution was computed using vibration data taken during the ground test (described earlier) in combination with the 11-point transfer function measured in the laboratory (see above). Two measurements of in-flight cabin noise are also plotted in Fig. H.18 for comparison. The structureborne noise appears to contribute significantly over the entire frequency range of interest. Due to mount-to-mount variations in vibration level, and in transfer functions, the predicted contributions could be in error. One could utilize the different transfer function shown in Table H.1 and the individual vibration spectra presented in Figs. H.7 to H.11 to refine this calculation. However, a full set of vibration data is not available for in-flight conditions, and such an exercise will not yield accurate noise predictions without such data.

H.7 Treatments Applicable to Reducing Source/Path Contributions

Vibrational energy is transfered from the propeller/engine source through paths which include the vibration isolators, engine mount spider, and finally the cabin side panels and firewall. Possible modifications which could reduce the vibration producing cabin noise then include:

a) Vibration reduction at the source by improving the balance of rotating engine and propeller components. This modification would entail major redesign which is outside the scope of this program.

b) Use of improved vibration isolators. Two-stage isolators or vibration absorbers at the engine mounts offer increased vibration transmission loss at mid to

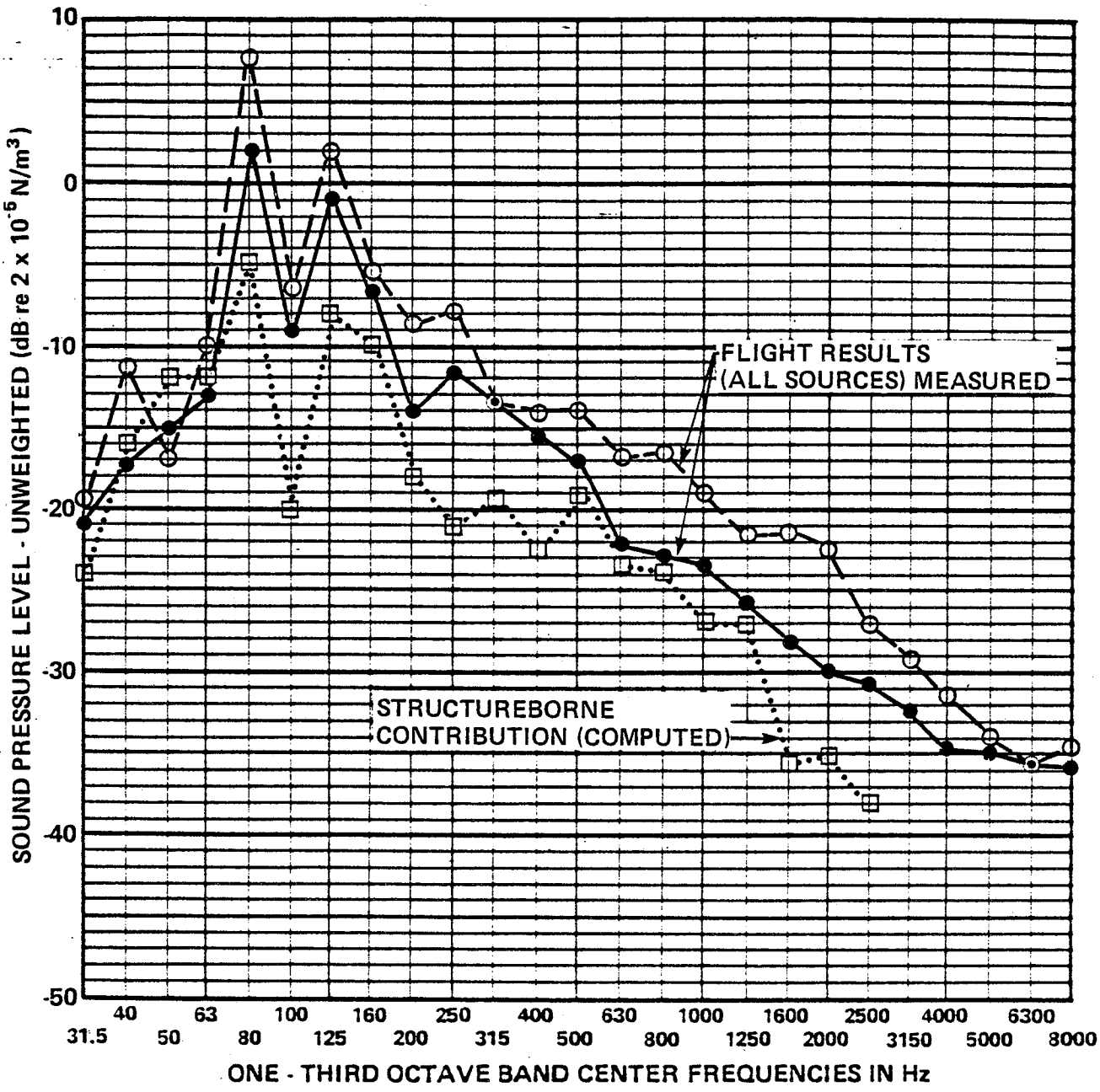

FIGURE H.18 COMPUTED STRUCTUREBORNE ENGINE NOISE CONTRIBUTION TO CABIN NOISE

high frequencies without the need for major modifications to the aircraft structure. Complications may include allocating additional volume to the isolators in a cramped space, achieving desired stiffness rates with suitable materials, and a possible requirement to recertify the airplane.

c) Modifications to the engine mount spider. Changes in stiffness or the addition of mass at mounting points is sometimes useful to alter the mechanical impedance and hence the power flow into lightweight structures. Mechanical impedance measurements of the particular structure will be required to evaluate this option.

d) Increases in panel mass, stiffness, or the use of double panels for both the firewall and cabin side walls.

For a single-stage isolator to work effectively, its admittance must be greater than the admittance of the structure to which it is being attached. For the R182, the current engine mounts are much too stiff. Data from Lord Manufacturing Company indicate the following for the R182 stock mounts:

Axial stiffness - approximately 9000 lb/in
Radial stiffness - approximately 840 lb/in

Figure H.19 shows a measurement of the acceleration of the lower left spider mounting point when driven by a sinusoidal force of constant amplitude (-10 dB re 1 lb). The result shown in the figure (the acceleration amplitude divided by the force amplitude) is simply the product of the admittance and the frequency. Also shown in Fig. H.19 is the admittance times the frequency for the engine mounts in the radial and axial direction. These results show a serious problem in the vicinity of 100 Hz, the region where structureborne noise from the engine/propeller combination is expected to be one of the major

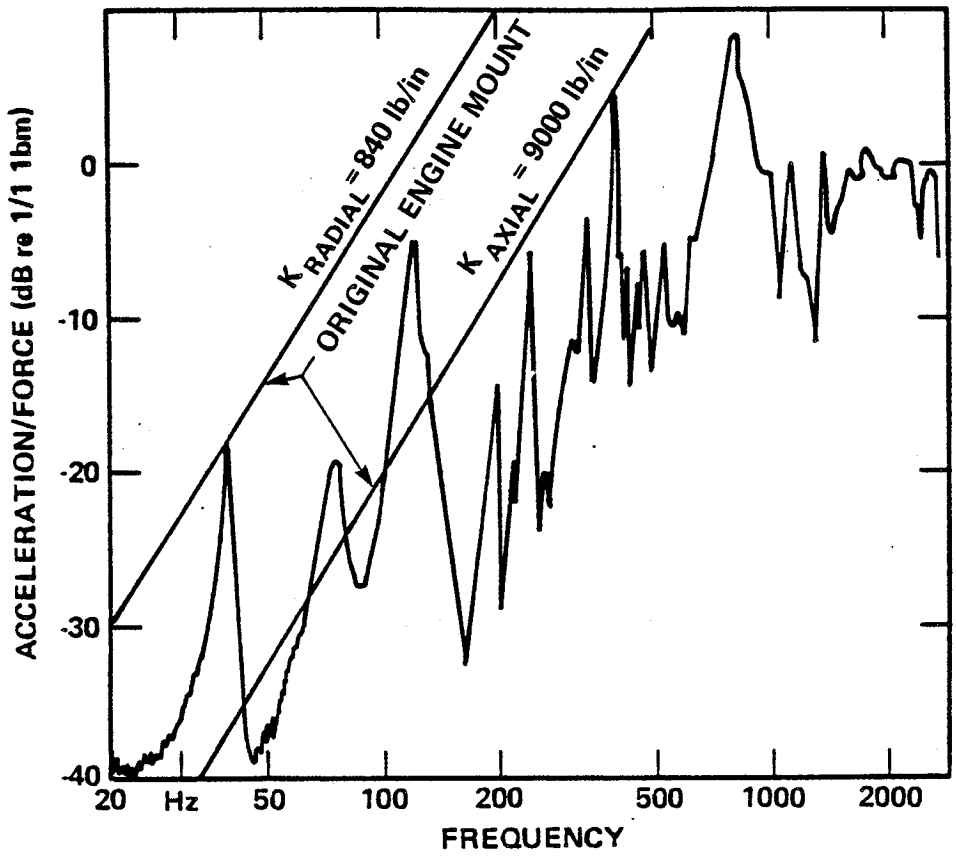

FIGURE H.19 THE ACCELERATION DIVIDED BY THE FORCE FOR THE LOWER MOUNTING POINT PILOT'S SIDE ON THE SPIDER IN THE DIRECTION OF THE AIRCRAFT AXIS.

contributors to the cabin noise. It is interesting to note that the upper mounting point on the spider, as illustrated in Fig. H.20, does not seem to have this problem. Thus, we have yet another piece of data illustrating the complexity of the engine isolator issue.

Before developing more complex mounting configurations, we first examined what could be done by stiffening the firewall and spider to raise the impedance at the spider mounting point.

In our attempts to improve the transmission loss through the firewall, a number of stiffening beams were attached (as described in App. C). Those stiffeners affected the impedance as illustrated in Fig. H.21. Unfortunately, they may also have exacerbated the vibration isolation problem since the strong peak in the admittance at approximately 100 Hz is higher than the admittance peaks before stiffening at 75 and 120 Hz (see Fig. H.19) that existed before stiffening.

A second stiffening approach, illustrated in Fig. H.22, was also tried with somewhat more success. An adjustable beam was intalled between the lower spider mounting points and the point where the firewall meets the landing gear box. That location is especially stiff because the OEM channel stiffener on the firewall also passes through that point. Figure H.23 shows the change in the acceleration divided by the force due to the addition of this stiffener. The measurements indicate that the mount should now work quite well throughout the frequency range of interest.

To examine the potential reduction in structureborne noise into the cabin due to the stiffeners, we excited the lower spider mounting point with the resilient mount in place. We then measured the change in cabin noise level with and without the stiffener in place keeping the acceleration level on the engine

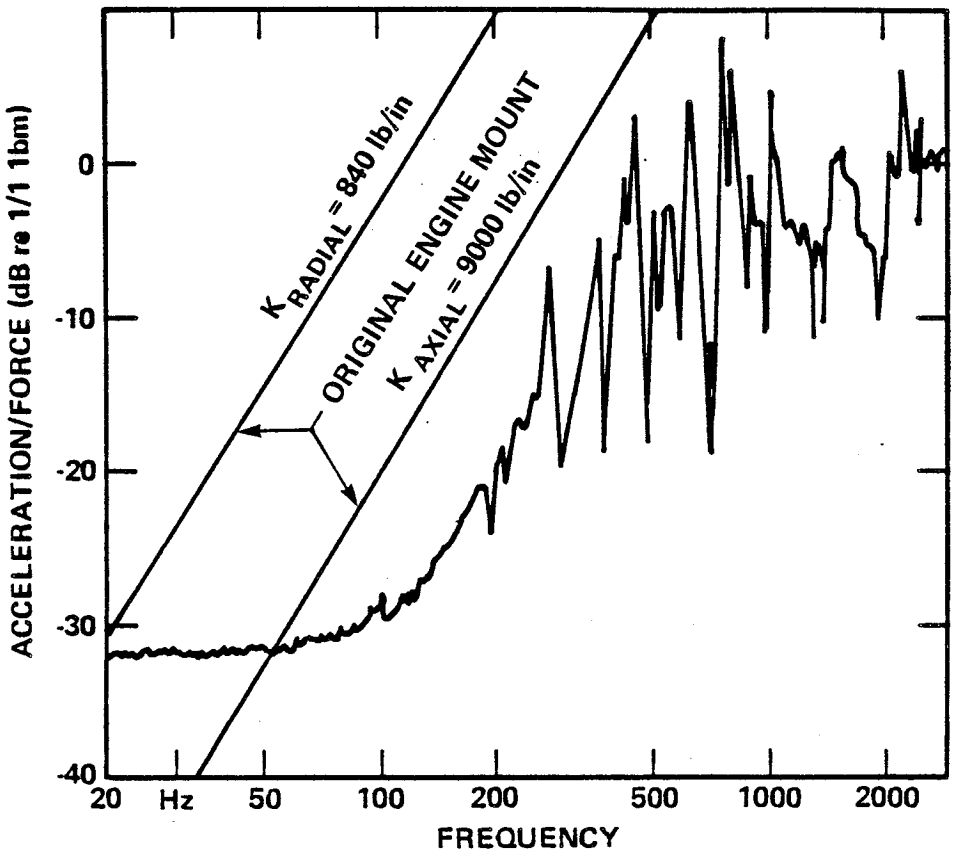

FIGURE H.20 THE ACCELERATION DIVIDED BY THE FORCE FOR THE UPPER MOUNTING POINT, PILOT SIDE ON THE SPIDER IN THE DIRECTION OF THE AIRCRAFT AXIS.

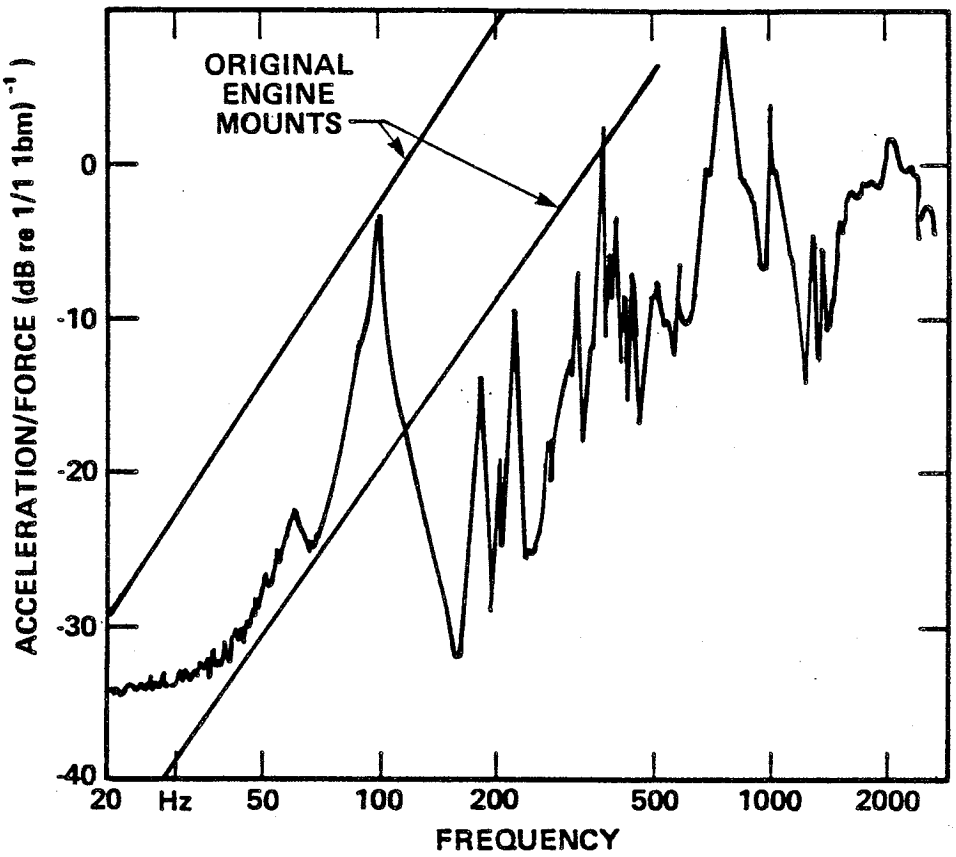

FIGURE H.21 ACCELERATION DIVIDED BY FORCE FOR THE LOWER MOUNTING POINT, PILOT'S SIDE ON THE SPIDER IN THE AXIAL DIRECTION WITH THE FIREWALL STIFFENED.

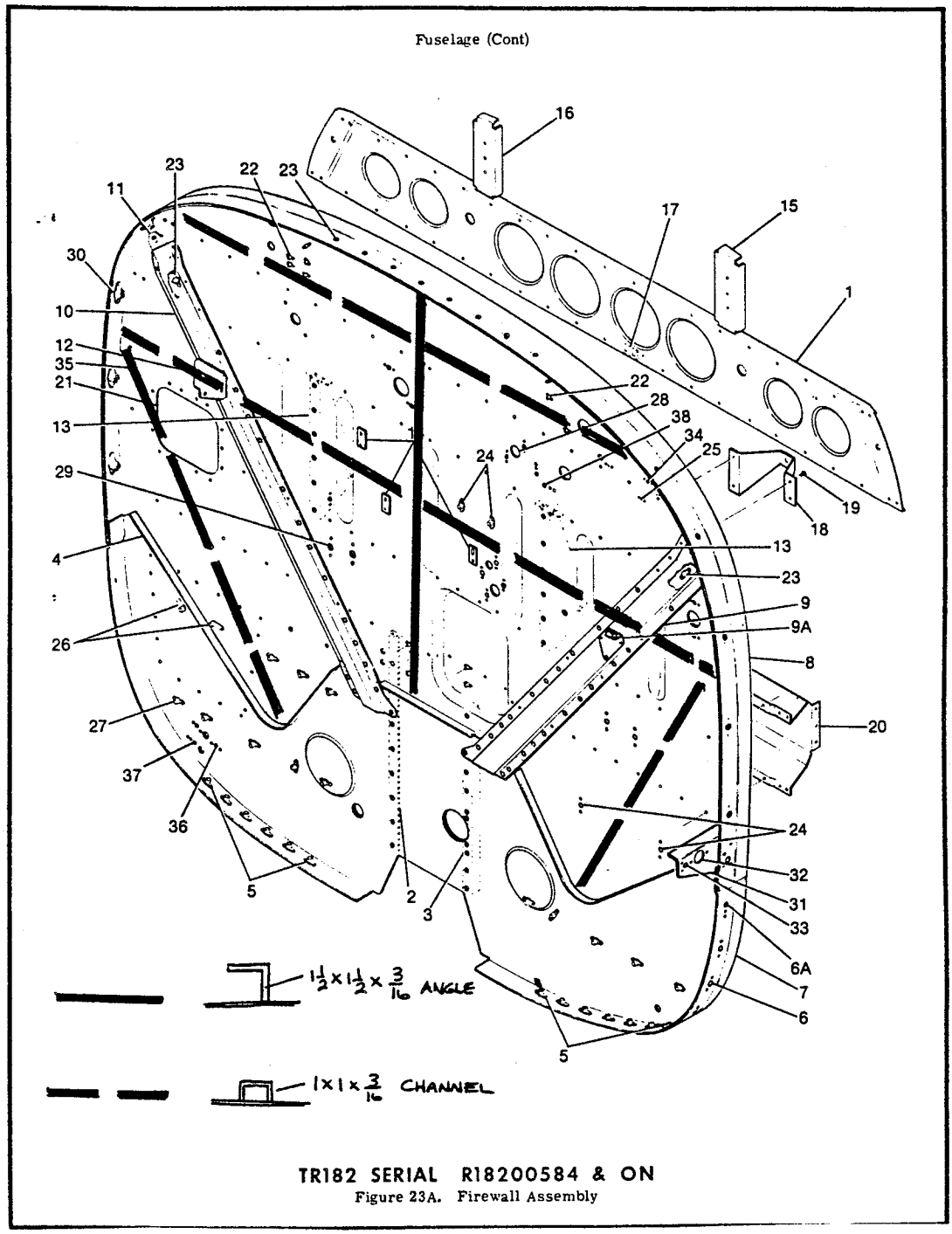

Figure 23A. Firewall Assembly

FIGURE H.22 SPIDER-TO-FIREWALL STIFFENER LOCATION.

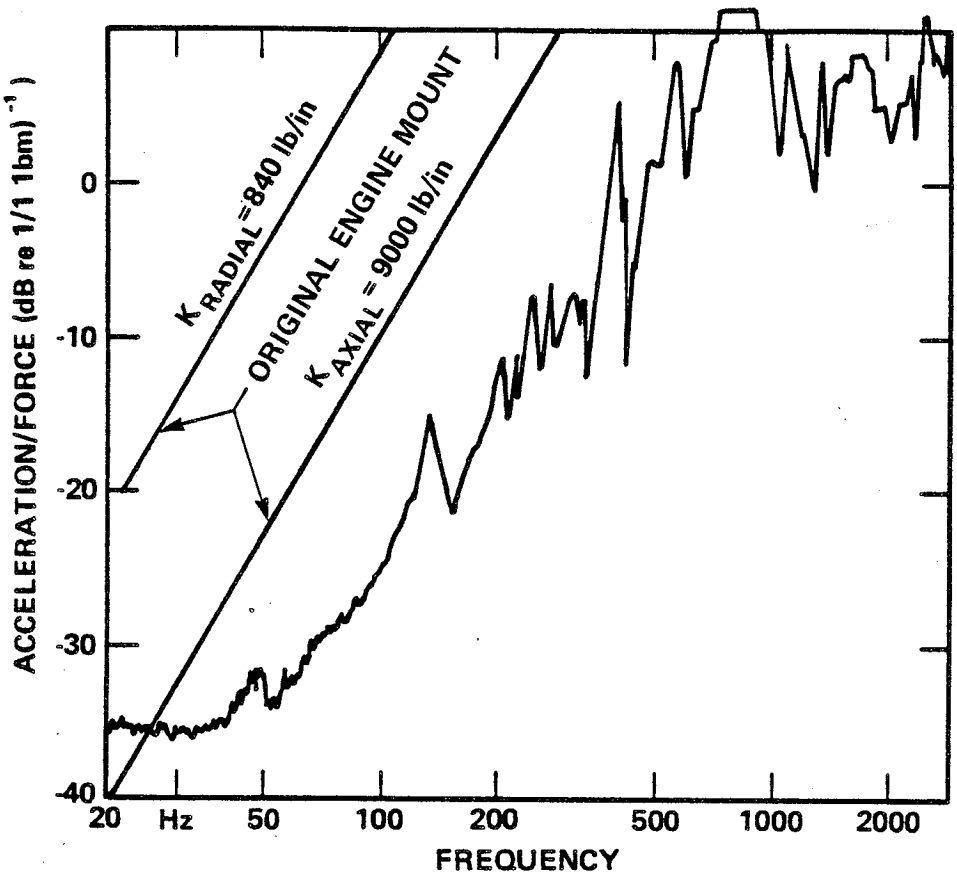

FIGURE H.23 THE ACCELERATION DIVIDED BY THE FORCE FOR THE LOWER MOUNTING POINT, PILOT'S SIDE ON THE SPIDER IN THE DIRECTION OF THE AIRCRAFT AXIS WITH THE STIFFENER BETWEEN THE SPIDER AND THE FIREWALL IN PLACE.

side of the mount the same for the two conditions. Figure H.24 shows the change in cabin noise level versus frequency due to the stiffener. Stiffening the spider clearly has some benefits especially for vibration in the axial direction of the aircraft. Unfortunately, the benefits do not extend below 100 Hz. Since there is significant engine vibration down to at least 80 Hz, the results in Fig. H.24 indicate that the stiffener may in fact increase structureborne noise in the lower frequency bands due most likely to improved coupling between the spider and the firewall at low frequency.

Although stiffening may, with additional effort, lead to greater improvements than shown here, limited resources prevented us from pursuing this course any further. Instead we investigated the use of two-stage isolators to try and deal with the high admittance of the spider mounting points.

A schematic drawing of a single- and a two-stage vibration isolator is shown in Fig. H.25. Also shown is its performance, i.e., its vibration reduction, relative to the vibration reduction of the single stage isolator. Although the static stiffnesses of the two-stage and single-stage isolators are the same, the two stage isolator provides suspension vibration reduction well above ω_o ($\omega_o = \sqrt{\frac{2\kappa}{m}}$). If $j\omega/\kappa >> A_s$ where A_s is the admittance of the spider then

$$VR_2 - VR_1 = 20 \log \; 1/2 \; (\frac{\omega}{\omega_o})^2 \quad ; \; \omega >> \sqrt{2}\omega_o$$

where κ is the single-stage isolator stiffness, m is the seismic mass, VR_2 is the vibration reduction in decibels of the two-stage isolator, and VR_1 is the vibration reduction in decibels of a single-stage isolator.

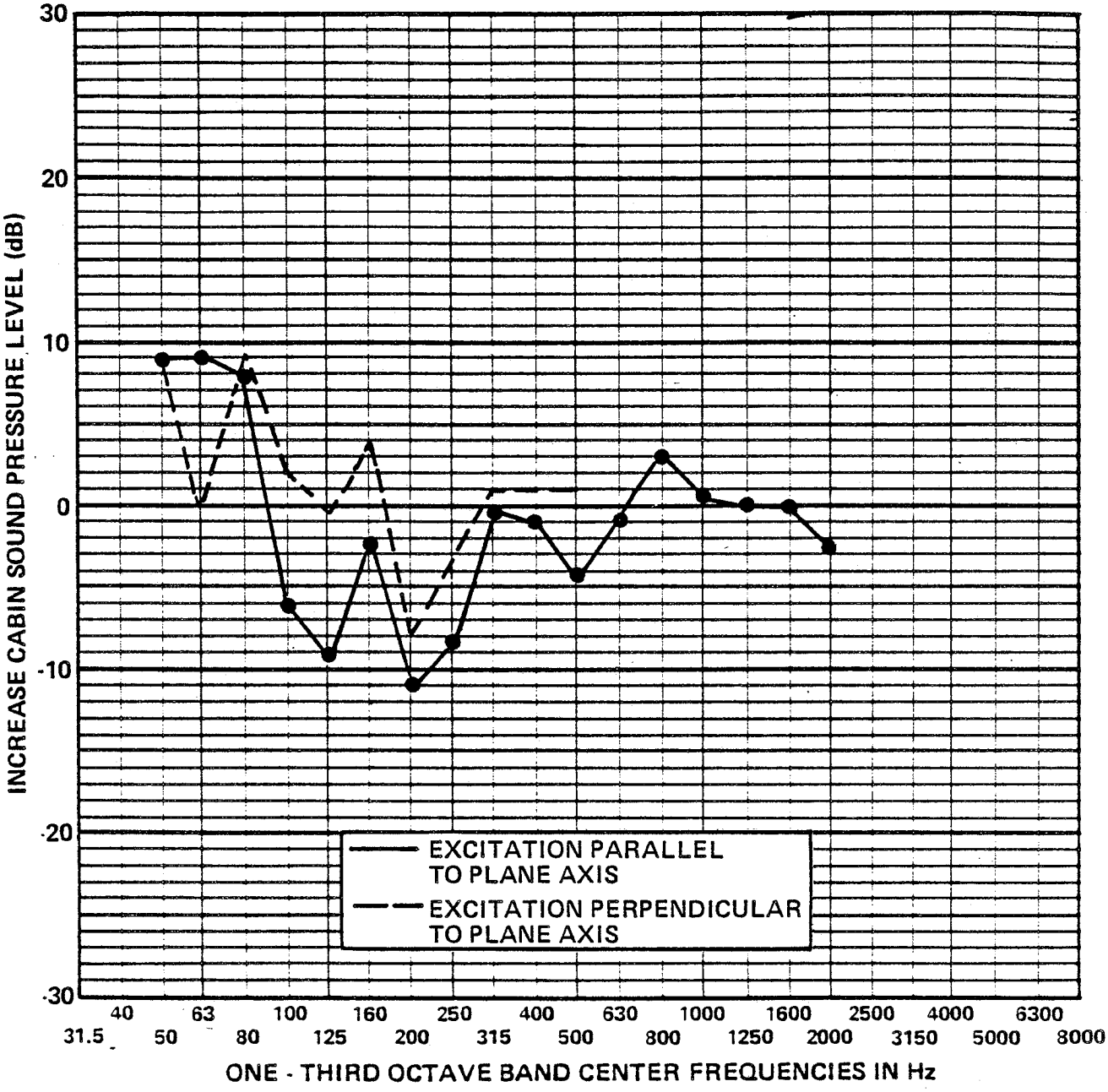

FIGURE H.24. CHANGE IN CABIN STRUCTUREBORNE NOISE DUE TO SPIDER STIFFENER.

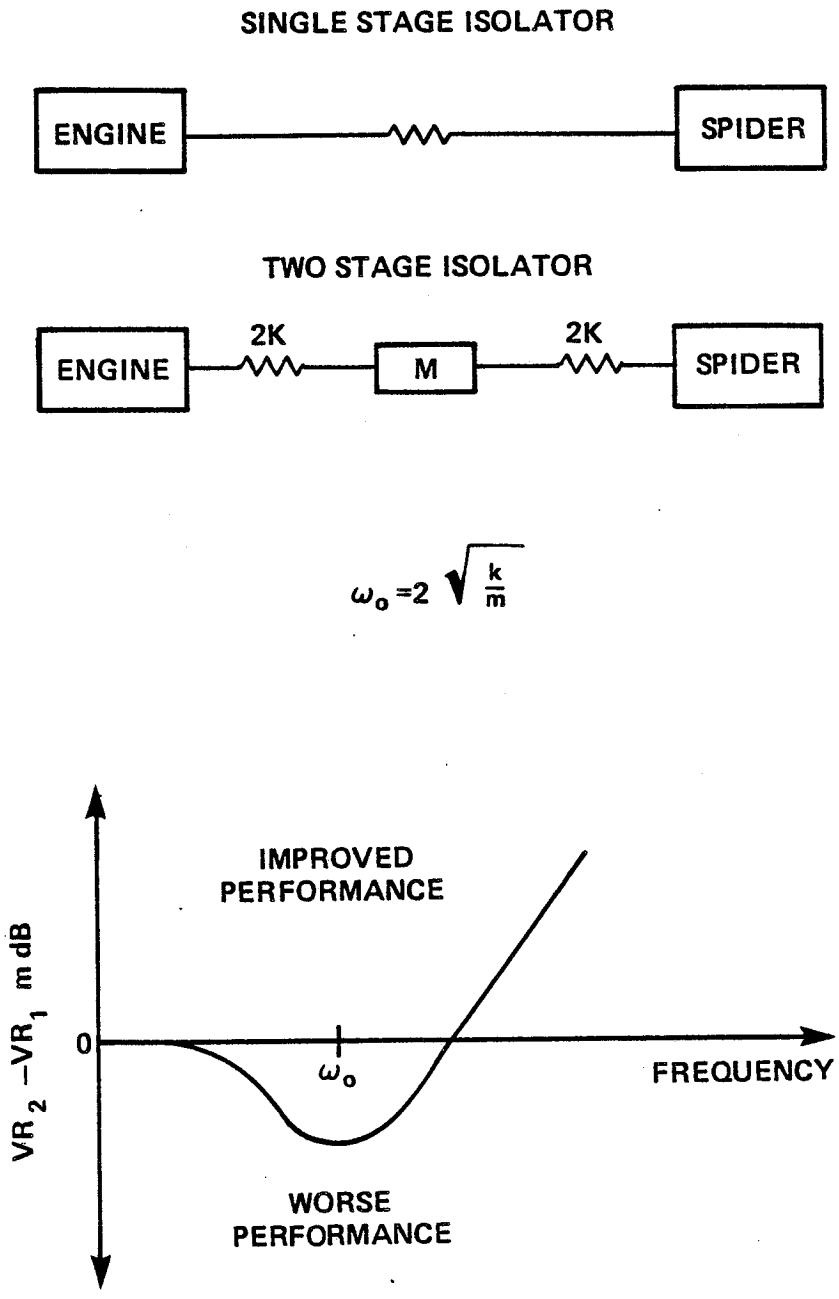

FIGURE H.25 IMPROVEMENT IN THE VIBRATION REDUCTION OF A TWO-STAGE ISOLATOR VR_2 OVER THAT OF A SINGLE-STAGE ISOLATOR VR_1.

A two-stage isolator is very useful where high static stiffness is required along with good high frequency vibration isolation. The high static stiffness ensures that the source will not move very much relative to the structure from which it is to be isolated, when steady or low frequency loads are applied. At the same time, the isolator will provide substantial vibration isolation above ω_o. The primary disavantage of a two-stage isolator is the weight and space required for a mass of sufficient size to make ω_o low enough so as to obtain good vibration isolation in the frequency range desired.

The particular engine mount used in the R182 is not easily converted into a two-stage isolator. The two-part rubber mount requires that two seismic masses be installed as illustrated in Fig. H.26. In addition, the extremely small space available around the mount in the engine compartment severely limits the amount of mass that can be installed.

Despite these disadvantages, we did not want to change the stock mounts, since they are a proven entity on the aircraft. Consequently, we modified the existing mounts by splitting them at two locations as shown in Fig. H.26. Seismic masses were then installed at those two locations as also shown in the figure. Space restrictions constrained us to masses of no more than 17 oz. each. The initial stiffness values that were obtained from the manufacturer indicated that the mounts had a nominal stiffness of 900 lb/in. using the simplified two-stage isolation model of Fig. H.21, one would estimate

$$\frac{\omega_o}{2\pi} = f_o = 91 \text{ Hz}$$

This frequency is not as low as desired, but is sufficiently low to demonstrate some benefits in the frequency range of interest. Unfortunately, after receiving the mounts from the

manufacturer and performing some preliminary measurements, it became clear that the mounts were some ten times stiffer in the axial direction than originally had been indicated. The radial stiffness at 840 lb/in. was, however, close to the value that had been originally quoted.

To test the performance of the two-stage mount, the sound pressure level was measured in the cabin while exciting the single stage isolator attached to the lower left spider mount. The measurement was then repeated with the two-stage mount installed using the same input acceleration levels. In both cases the excitation was applied to the engine side of the mounts in the lateral or radial direction. Figure H.27 presents the results of these measurements. The two-stage mount reduces the cabin noise level in the 250 to 500 Hz range, but increases it slightly at frequencies below 200 Hz.

The equation expressing the ratio of the spider vibration with a two-stage mount, V_2, to that with a single-stage mount, V_1, is given by

$$\frac{V_2}{V_1} \approx \frac{\left(1 + \frac{Z_s}{\kappa/j\omega}\right)}{\left[2 - \left(\frac{\omega}{\omega_o}\right)^2 \frac{Z_s}{2\kappa/j\omega} + 1 - \left(\frac{\omega}{\omega_o}\right)^2\right.}$$

where Zs is the spider impedance, κ is the stiffness of the single-stage isolator, $\omega_o = \sqrt{\frac{2\kappa}{M}}$, and M is the total mass added to the mount. The equation assumes that the source (the engine) impedance is high compared to the spider mount impedance.

In the lateral direction where the mount stiffness is approximately 840 lb/in it is reasonable to make the approximation $\kappa/j\omega \ll Z_s$ (see Fig. H.19). The equation then simplifies to

$$\frac{V_2}{V_1} \approx \frac{2}{2 - (\frac{\omega}{\omega_o})^2}$$

If, in addition, one allows for some damping, then

$$|\frac{V_2}{V_1}|^2 = \frac{4}{(2 - \frac{\omega}{\omega_o})^2)^2 + \eta^2 (\frac{\omega}{\omega_o})^2} \quad .$$

For $\eta = 1$, the predicted performance curve is as shown in Fig. H.27. The mount is clearly not performing as expected. The fact that the mount is very stiff in the axial direction may, through cross-coupling effects, be responsible for the apparent increase in stiffness i.e., the measured performance curve appears to be shifted to higher frequency relative to the predicted performance. Even more important is the fact that the two-stage mount does not show increasingly better performance than the single-stage mount above $f = \sqrt{2}$ fo = 123 Hz. The lack of improved performance may be due to thickness resonances in the elastomer, but the cause is presently uncertain.

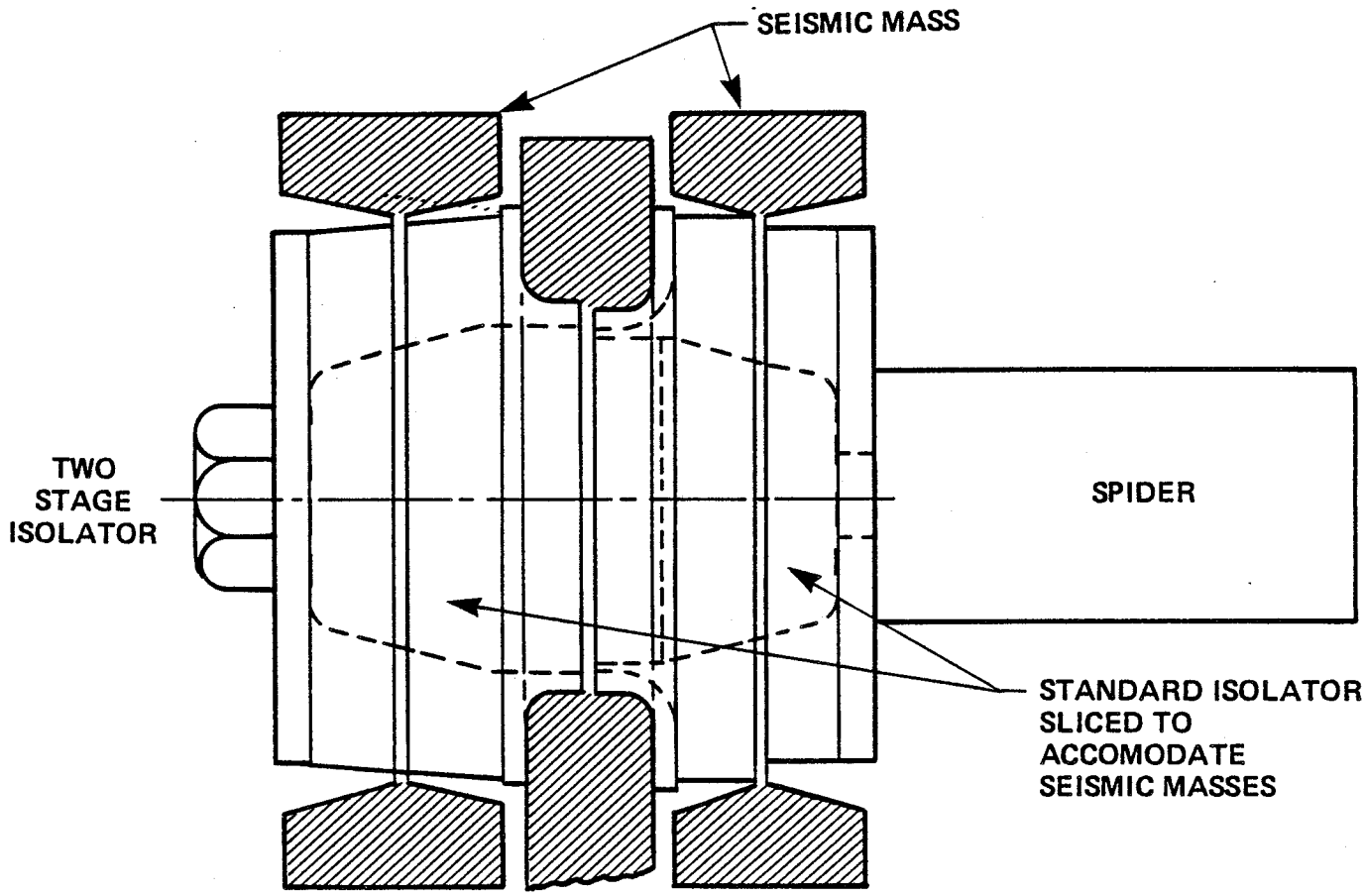

FIGURE H.26. SIMPLIFIED TWO-STAGE ISOLATOR MODEL.

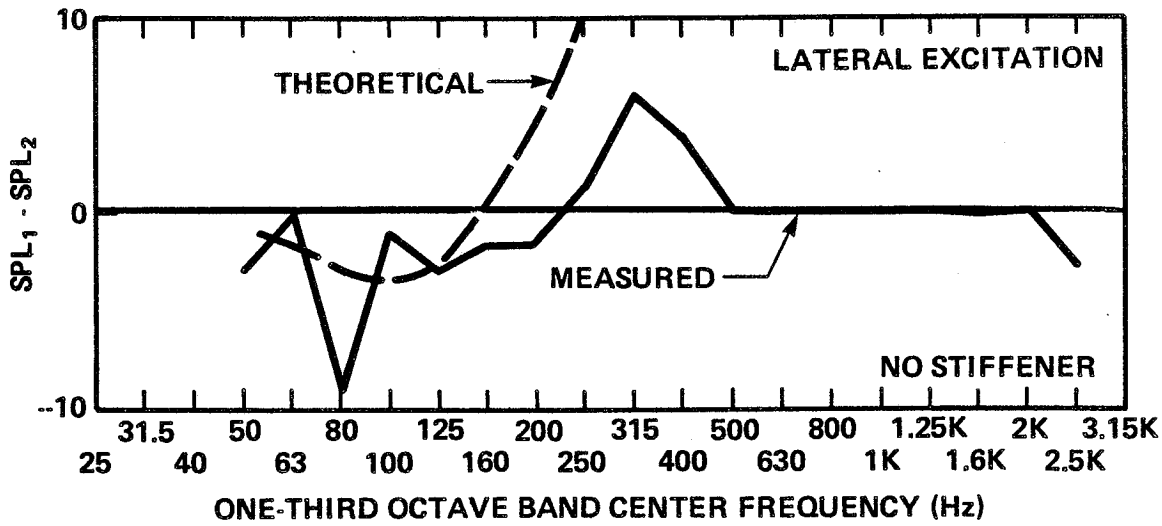

Note: (A positive change means the cabin sound pressure level is lower with the two stage mount.) Excitation was applied to the lower left mount in the lateral or radial direction at the engine side of the mount.

FIGURE H.27. CHANGE IN CABIN SOUND PRESSURE LEVEL WHEN A TWO-STAGE MOUNT IS SUBSTITUTED FOR A SINGLE-STAGE MOUNT.

H.8 Applicability of Results to Other Aircraft

Discussions with engineering managers in the general aviation industry suggest that the details of the structureborne engine noise test reported here are not universally applicable because of the following industry practices:

a) Vibration isolators are supplied by neither the engine nor the airframe manufacturer. A vendor specializing in elastomeric engine mounts designs the isolators based on engine weight, rotation rate, and maximum allowable engine movement. The engine "foundation'" i.e. airframe, is assumed to be infinitely rigid for these design calculations. The approximate 1-to-1 ratio between engine weight and empty fuselage weight suggests that the assumption of rigid mounting is rather poor.

b) The engine/isolator/airframe combination derived as in a) above invariably results in unacceptably high levels of vibration. Modifications are made to the isolators and/or the engine mount spider, often on a "cut and try" basis, until the vibration problem is minimized.

c) Measured and/or predicted values of the mechanical input impedance to the engine mount spider are, in general, unavailable.

d) Some aircraft have "bed-mounted" engines in which the engine is supported at four points in a horizontal plane rather than the radially inclined rear supports used in the R182.

The many variables implied in a) - d) would indicate that vibration and mounting point impedance measurements (or models) for the specific aircraft of interest are required. The coupling with the firewall structure and the dynamics of the mounting

spider are obviously problems. Designers should be prepared for an exhaustive series of analyses, component tests, and full aircraft tests to successfully arrive at treatment concepts for reducing structureborne noise from the engine/propeller combination.

One approach which should be investigated in order to bypass the problem of the spider dynamics is to locate the isolation system at the point where the spider joins the airframe. That point is perhaps the stiffest point on the airframe and therefore offers the potential for lower mechanical admittances and more consistent dynamic behavior, thus allowing more straightforward application of isolator design principals.

APPENDIX I

CONSIDERATIONS RELATING TO SENSOR PERFORMANCE IN THE MEASUREMENT OF SOUND IN MOVING AIRSTREAMS AND ON AIRCRAFT SURFACES

I. CONSIDERATIONS RELATING TO SENSOR PERFORMANCE IN THE MEASUREMENT OF SOUND IN MOVING AIRSTREAMS AND ON AIRCRAFT SURFACES

I.1 Introduction

Localized exterior acoustic measurements are required to perform diagnostic measurements on aircraft. In general, such measurements can be made with microphones (or dynamic pressure sensors) which are mounted on sting supports, or on the exterior surfaces of the aircraft.

Microphones placed in moving airstreams are sensitive to non-acoustic as well as acoustic pressures. If the flow is highly turbulent, such as is the case in the boundary layer of an aircraft and in the wake of propellers, wings, and protrusions, the flow-induced pressures can easily dominate the acoustic pressures. A microphone placed in a low-turbulence airstream will also be subject to non-acoustic pressures generated by its own boundary layer interacting with the acoustically "transparent" openings to the sensing area and other surface discontinuities. These non-acoustic pressures must be accounted for when attempting to interpret in-flow measurements.

Other effects of placing microphones in airstreams include the generation of acoustic energy by flow interaction with the microphone body, fairings, clamps, support stands, guy wires, tape, and even small screws. Since the source of this acoustic energy is very close to the sensing area of the microphone, it can also mask the sound which one is trying to measure. A final effect which may be encountered when carrying out measurements in flow is spurious output of a microphone caused by vibration. Such signals may be generated by the vibration-induced motion of the diaphragm or motion of internal conductors. Buffeting of microphone supports caused by turbulent in-flow or vortex shedding may lead to such effects in flight test or wind tunnel applications.

I.2 Prediction of Microphone Output Caused by Non-Acoustic Pressures

I.2.1 General considerations

The non-acoustic effects of flow on microphone output consist of "embedded" pressure fluctuations, i.e., those caused by vorticity in the flow, and "induced" pressure fluctuations caused by interactions between turbulence and the microphone. There is no way for a single microphone to be made insensitive to "embedded" pressure fluctuations which have a length scale much larger than the sensing area; indeed ported or specially-adapted microphones are often used to quantify the unsteady non-acoustic pressures in jets and engine exhausts. Induced pressures are a function of the details of unsteady inflow and the particular microphone geometry. Extensive modeling and measurement efforts have been underway for years to describe the wavenumber spectrum of turbulent boundary layers on smooth and rough walls [I.1]. Such studies are applicable to predicting the hydrodynamically-induced output of flush-mounted microphones or pressure sensors if and when the sensor is immersed in a flow field identical to that which has been modeled. In aircraft flight test situations, the flow fields seldom correspond to the idealized cases most studied. Therefore, empirical data must be consulted in such situations.

I.2.2 Cylindrical microphones with streamlined nosecones

No completely definitive study has been made to model the response of typical condenser or piezoelectric or piezoresistive microphones to self-induced as well as externally-induced pressures. However, some studies are available which can be used for guidance.

The often-used Bruel and Kjaer (B&K) condenser microphone family is also the most-studied. Unfortunately, the B&K

literature (I.1, I.2, and operation manuals for each type of microphone) quotes induced noise levels derived from a spinning rig in which the microphones operated in their own wake. Therefore, these data show excessive induced noise levels, and to date have not been supplemented or replaced with data taken from microphones immersed in more representative and better-documented flow environments.

A more definitive set of data was derived by Noiseux et al [I.3 through I.5] using both a low turbulence flow in a quiet semi-anechoic wind tunnel, and a controlled source of high turbulence, also in a quiet free jet wind tunnel environment. For the case of a low turbulence flow, Noiseaux [I.4 and I.5] produced a set of "self-noise curves (one-third octave band spectra) and corresponding turbulence spectra. These data covered a speed range of 25 - 71.2 m/s (82-235 fps); the overall rms turbulence intensity $\frac{\sqrt{u^2}}{U}$ was less than .003 for all speed ranges. A very low noise microphone support and fairing of the preamplifier body were used. Noiseux postulated a simple model that predicted the pressures induced by the turbulent inflow to be proportional to the mean dynamic pressure of the flow at the microphone and the local turbulence intensity. However, to achieve a good normalization of the data, he required an empirical correction of the amplitude by a factor of $\sqrt{U}$, where U is the local velocity. Thus, at constant Strouhal number, his normalization suggests a U^5 dependence rather than the expected U^4 dependence. It is possible that his data for low turbulence flows included some contribution of the tunnel background or microphone support acoustic pressures. His data are presented in normalized form in Figure I.1. It can be safely stated that these data represent a probable practical lower bound on self-noise of B&K microphones with conventional bullet-shaped nose cones in low turbulence flow. The data in Figure I.1 are for microphones aligned with the flow direction (0° incidence). For

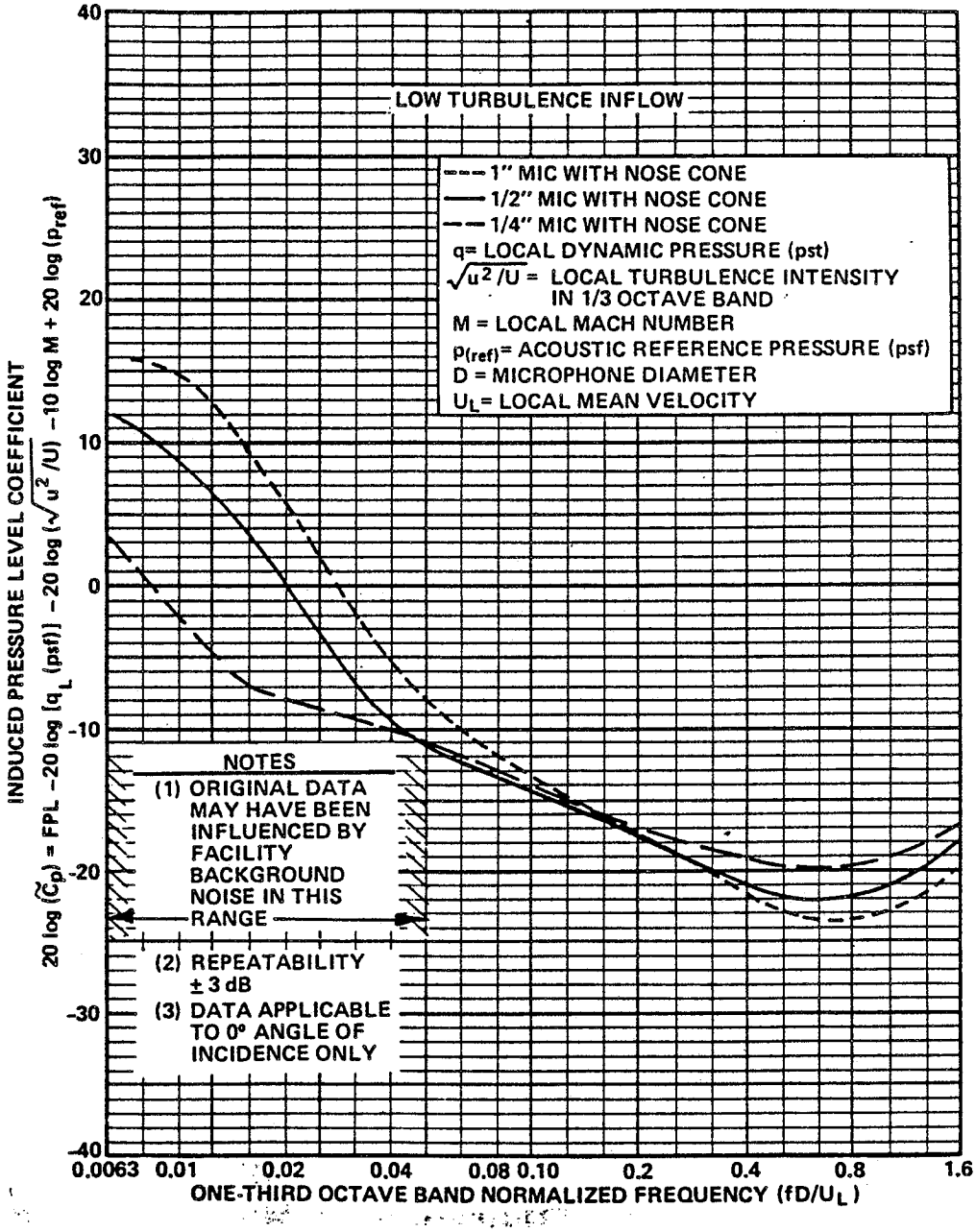

FIGURE I.1 INDUCED PRESSURE LEVEL COEFFICIENT FOR LOW TURBULENCE INFLOW.

flows not aligned with the microphone axis, the induced levels increase non-linearly as a function of incidence angle.

Turning to data from a separate study by Noiseux [I.3], one finds that for high turbulence levels, the data collapse was reasonably good using the same model, although a different normalized value is found, presumably because a different mechanism is dominant in each case. From this data, one can derive a separate curve for use in high turbulence flows (Fig. I.2). Note again that this data is for mean flow directions which are aligned with the microphone axis; for flows at other angles, the induced pressures increase with increasing "angle of attack."

It should again be noted that neither of the above curves provides a complete general description of the relationship between flow field parameters, microphone geometry, and "induced" noise. However, since the data were acquired at flow speeds comparable to those likely to be experienced in the test program, the lack of generality in their application does not significantly affect the levels predicted using these curves. It should also be noted that in other tests using the same facility in which Noiseux's data was derived, higher self-noise levels were measured when careful fairing of the microphone stands was not carried out.

I.2.3 Surface-mounted and flush-mounted sensors

When conducting flight tests aimed at quantifying the external acoustic environment on the skin of an aircraft, one seldom has the luxury of using externally-mounted streamlined condensor microphones which are both outside the aircraft's turbulent boundary layer and movable. Therefore, flush-mounted microphones are usually used. Such flush-mounted microphones used singly can usually detect discrete frequency acoustic levels

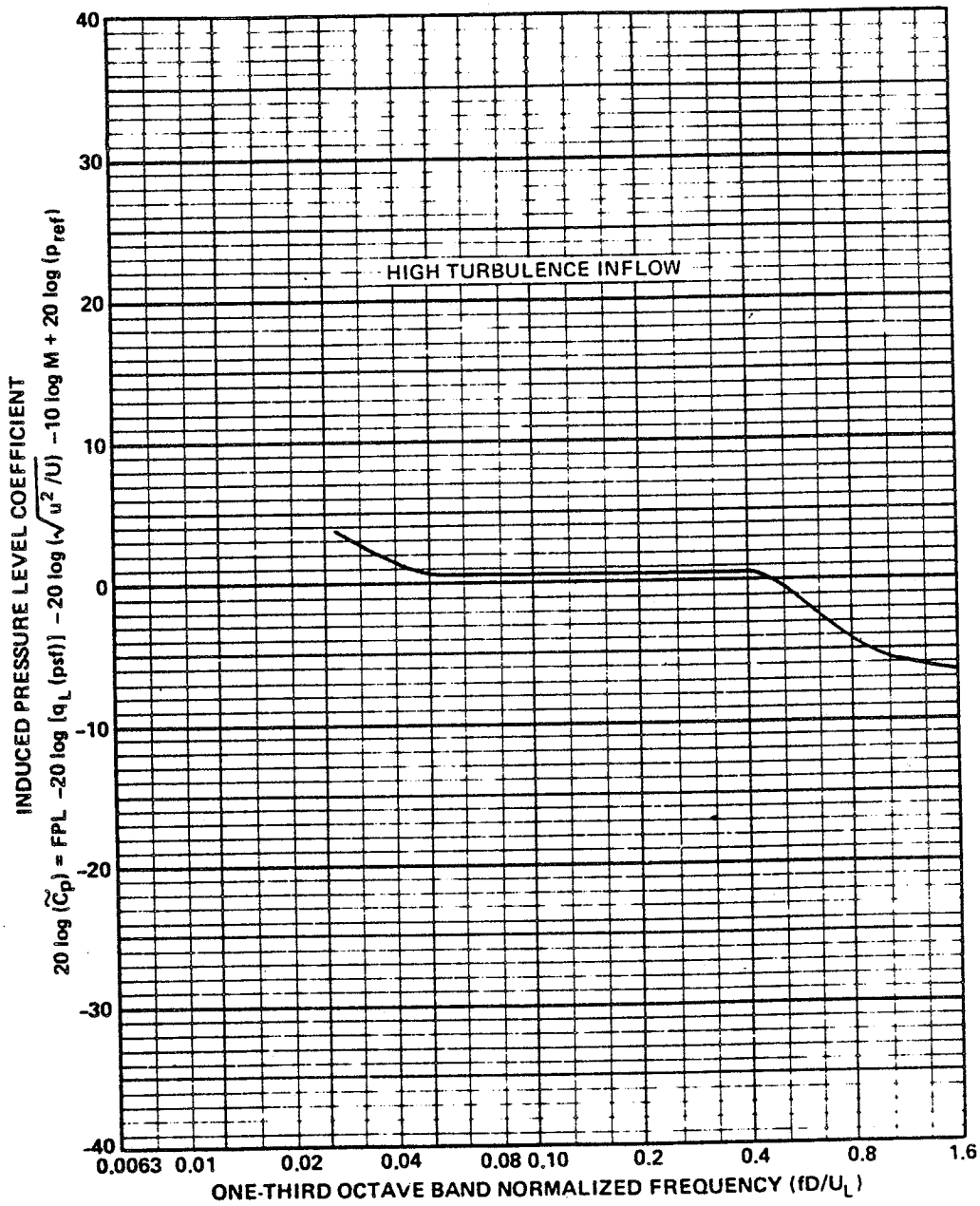

FIGURE I.2 INDUCED PRESSURE LEVEL COEFFICIENT FOR HIGH TURBULENCE INFLOW.

above the level of hydrodynamic pressures, but usually experience high levels of broadband hydrodynamic excitation which may mask all but the most intense broadband acoustic energy. (See App. G, Sec. G.2 for typical levels of hydrodynamic excitation.) The broadband performance can be improved by use of several sensors in an array, which have their outputs recorded simultaneously; the use of such arrays can also provide the detailed definition of the exterior field required to utilize recently-developed analytical models for sound transmission into aerospace vehicles. However, flush-mounted arrays required penetration of the fuselage structure, or replacing one or more windows or doors with instrumented counterparts. In this program, it was not possible to drill holes in the test aircraft (flight vehicles) nor did the opportunity to utilize an instrumented window or door blank arise.

In order to obtain some localized definition of the exterior sound field, a small rugged dynamic pressure sensor was used in conjunction with a nosecone fairing which was aimed at reducing the contamination of the output by turbulent boundary layer pressures. This device, which became known as the "stick-on mic," is described further below.

Figure I.3 provides a sketch of the "stick-on mic." This mic was actually a 0.635 (1/4 in) diameter x 2.5 cm (1 in) long dynamic piezoelectric pressure sensor (currently marketed by Vibro-Meter Corporation as Model 376 Dynamic Pressure Sensor), which has a steel body with a thin steel diaphragm welded to the sensing end and a standard microdot connector at the other end. The electronic noise floor was measured to be equivalent to 60 dB SPL (re 2×10^{-5} N/m^2) in third octave bands from 25 Hz to 4 kHz; for a sinusoidal vibration of 1 g rms, the transverse vibration sensitivity was equivalent to 103 dB SPL (re 2×10^{-5} N/m^2).

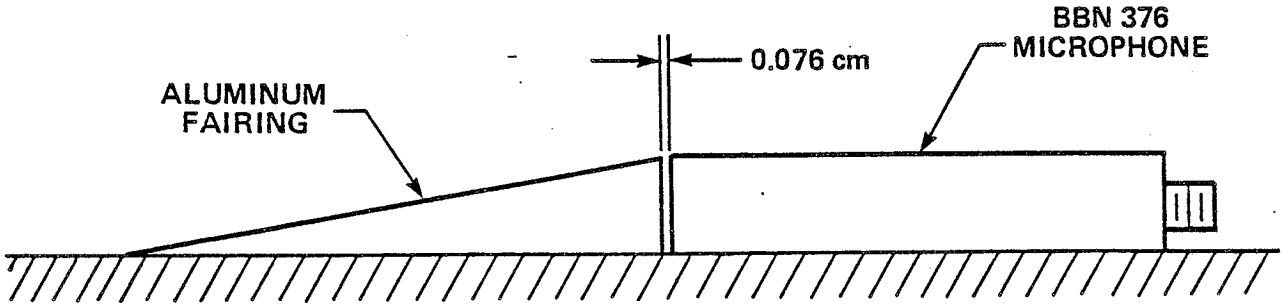

The sensor body was fitted with a non-contacting fairing which was set at .0762 cm (0.030 in) ahead of the diaphragm through use of a piece of skin stick. Both the acoustic sensitivity and hydrodynamically-induced self-noise were carefully checked against standard sensors or standard sensor configurations.

Figure I.4 compares the output of the surface-mounted sensor with that of a 1.25 cm dia. condensor microphone (pressure type) located 5.1 cm above the surface upon which the "stick-on mic" was mounted; the excitation field was grazing (propagating parallel to the surface). The data in this figure shows that the acoustic response of the sensor in its surface-mounted condition is excellent to 20 kHz (presumably the low frequency response is also excellent if the excitation levels are above the electronic noise floor).

The sensitivity to flow-induced pressures was investigated in the BBN Acoustic Wind Tunnel. The output of the surface-mounted (stick-on sensor) was compared with that of a comparable sensor carefully flush-mounted in the wall of the wind tunnel's

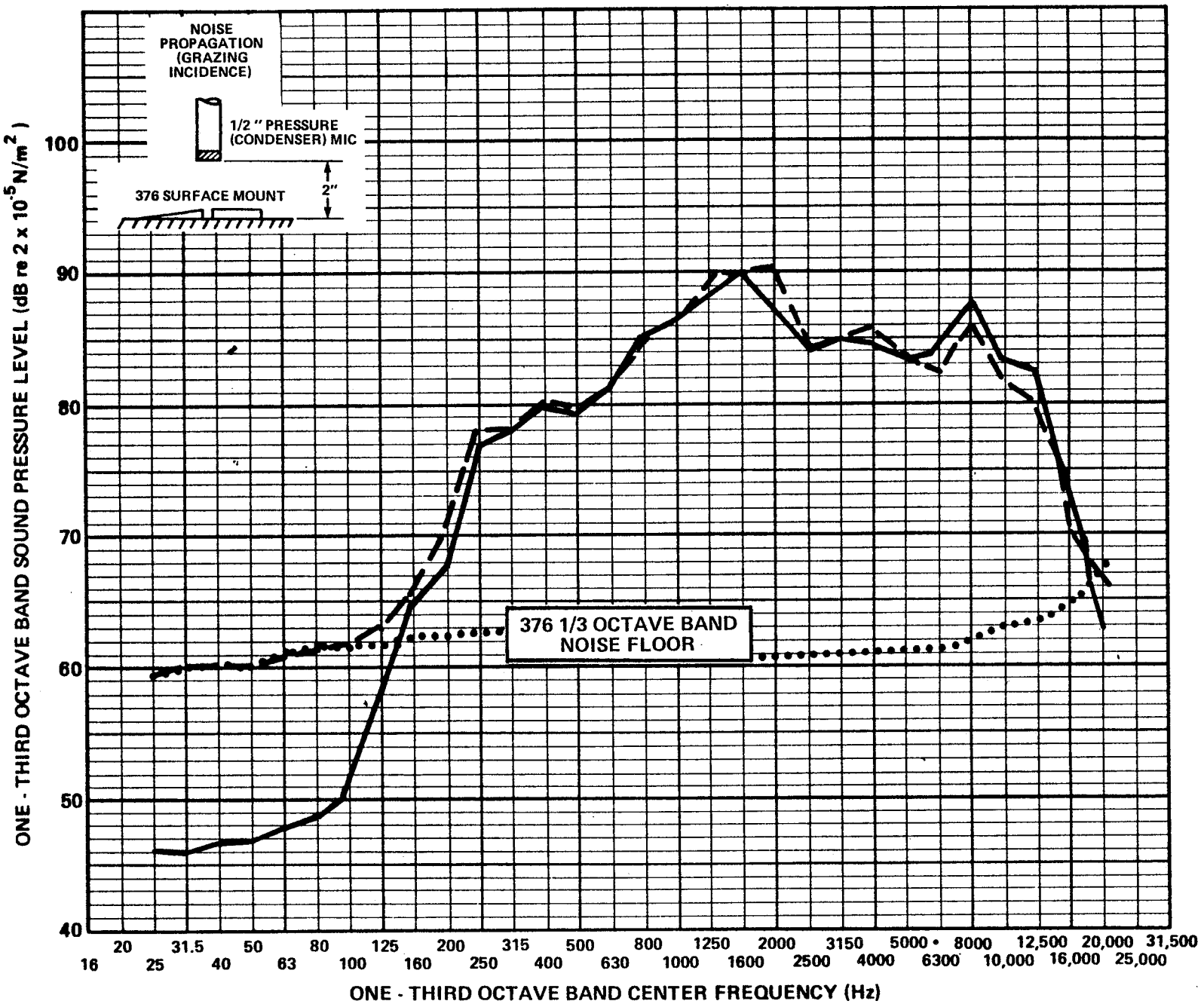

FIGURE I.4 COMPARISON OF OUTPUT OF "STICK-ON MICROPHONE" AND CONDENSOR MICROPHONE.

square (122 x 122 cm) nozzle, near the center of one of the walls. The sensors were about 2.5 cm apart in the lateral direction, and about 15 cm from the nozzle exit. Flow speeds from 31 m/s to 62 m/s were investigated for the nominal thin boundary-layer/low free-stream-turbulence condition, and for the case where a "trip" (4 mm step) was placed about 30 cm upstream to create a thick turbulent boundary layer.

Figures I.5(a) through I.5(d) show the results for the thin boundary-layer/low free-stream-turbulence case. From these figures, it can be seen that the surface-mounted sensor has higher "self noise" levels than the 0.625 cm sensor mounted flush in the wall, and that, (not surprisingly) when the side-by-side configuration was tested, the surface-mounted sensor disturbed the flow enough to cause increased low frequency output of the flush-mounted sensor. The reason for the higher output of the surface-mounted sensor configuration is undoubtedly related to its protrusion into the high velocity region of the flow, causing higher fluctuating pressures, and to local flow separation in the thin gap between the nose cone fairing and the sensing diaphragm.

Comparison of the four figures also shows that the "SPL" spectra for each configuration scale in amplitude in proportion to 40 log U_∞ (20 log q_∞), and shift in frequency in closest proportion to U_∞. Such consistent "Strouhal" scaling behavior is indicative of hydrodynamic pressures typical of turbulent boundary layers or separated flow phenomena and also allows estimates to be made of the non-acoustic output of sensors mounted in low turbulence regions on aircraft (or in wind tunnels).

When the upstream "trip" was used to create a thick turbulent boundary layer over the sensors, the spectra shifted to lower frequencies (predictably, due to the increased eddy scale) and the output of the surface-mounted and flush-mounted sensors

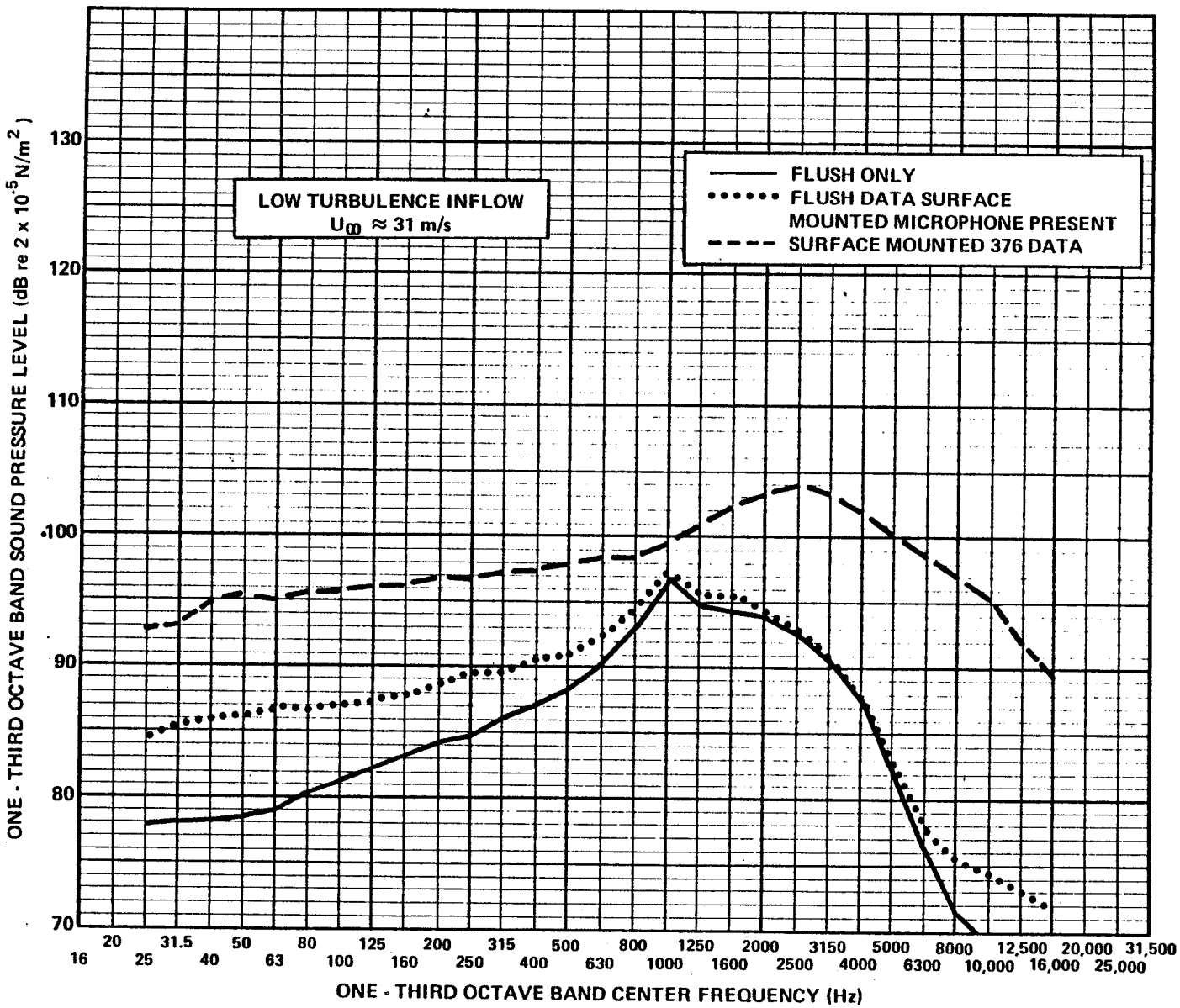

FIGURE I.5(a) COMPARISON OF OUTPUT OF SURFACE-MOUNTED ("STICK-ON") PRESSURE SENSOR WITH FLUSH-MOUNTED SENSOR; LOW TURBULENCE INFLOW.

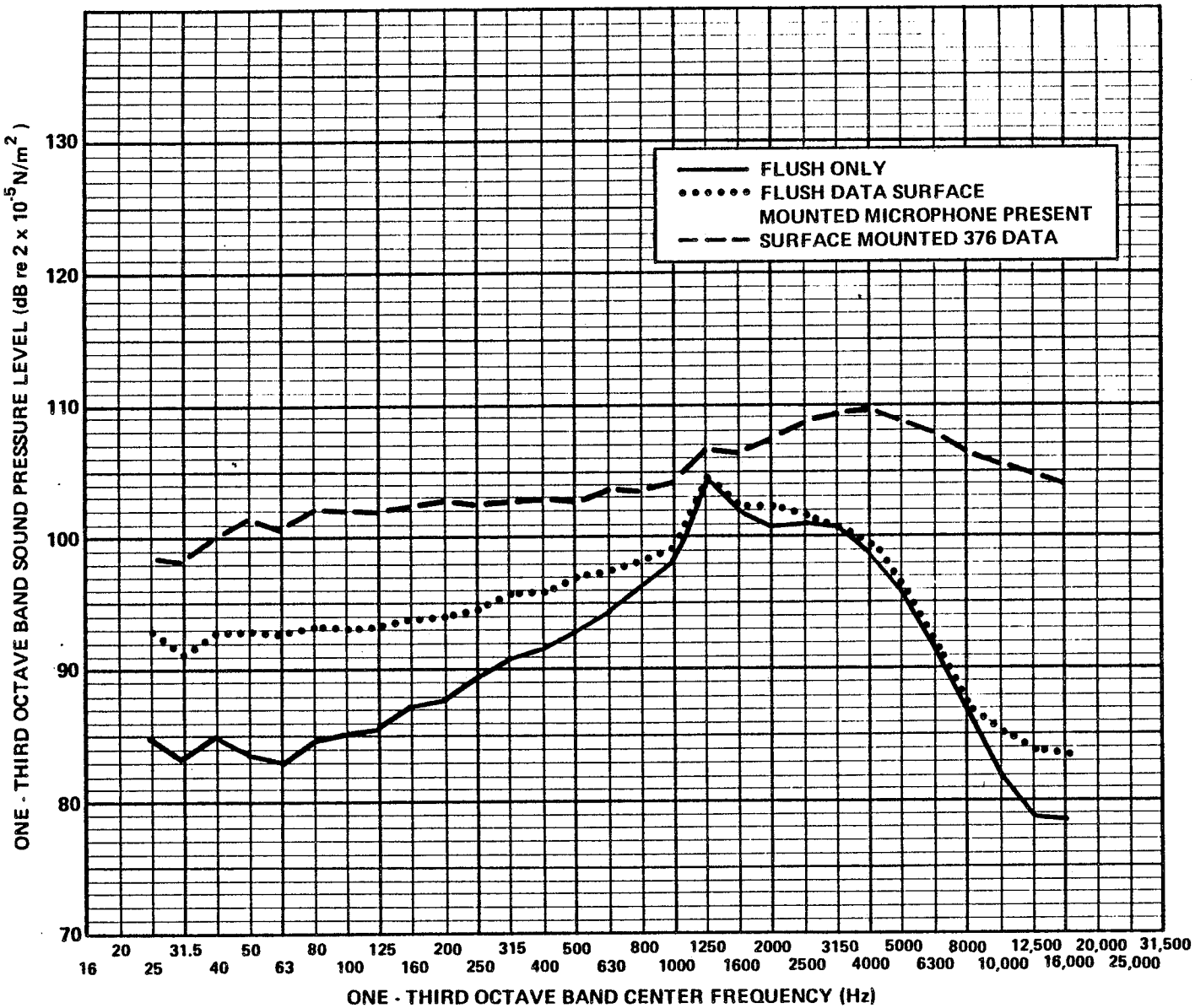

FIGURE I.5(b) COMPARISON OF OUTPUT OF SURFACE-MOUNTED ("STICK-ON") PRESSURE SENSOR WITH FLUSH-MOUNTED SENSOR; LOW TURBULENCE INFLOW; U_∞ = 44m/s

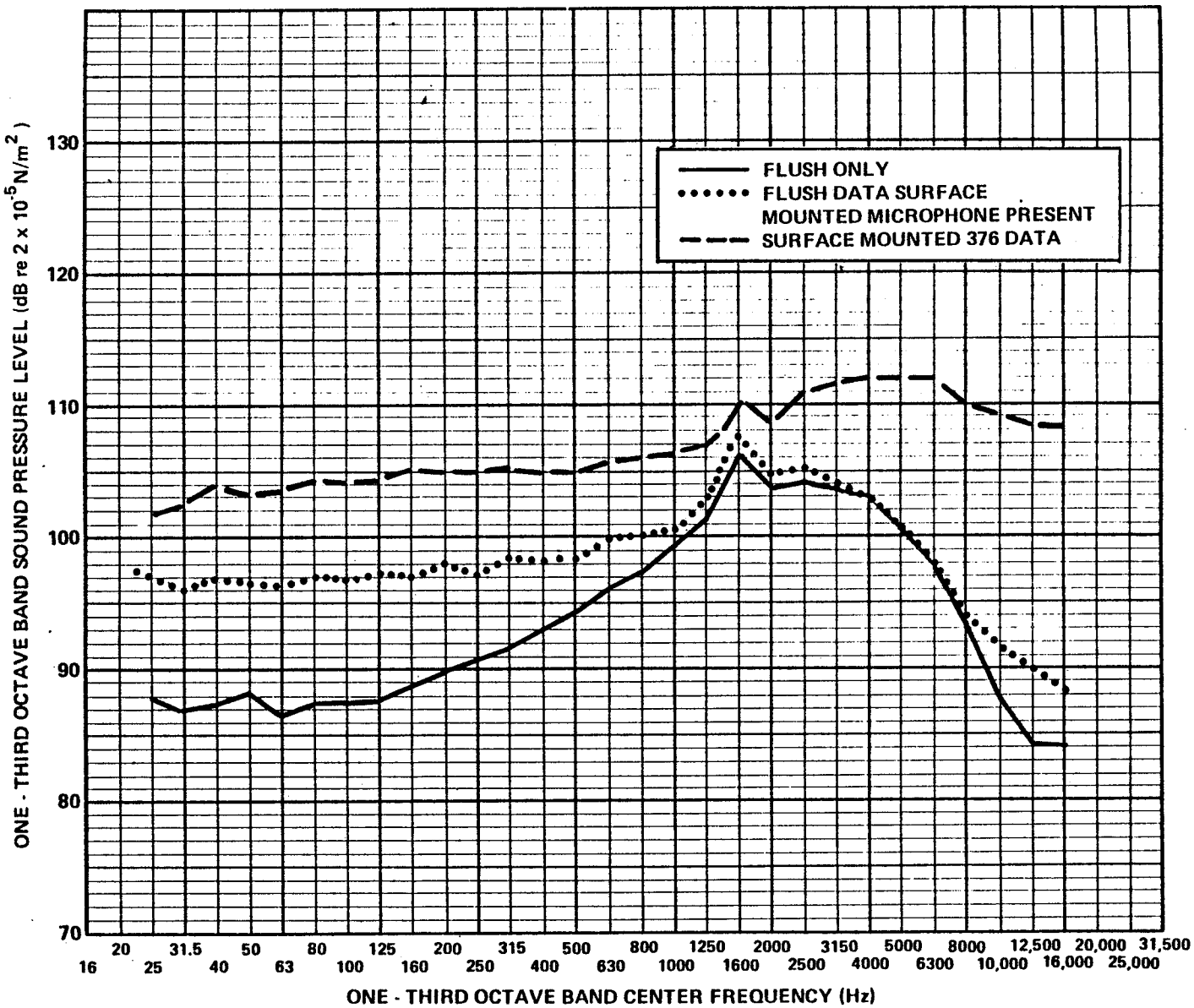

FIGURE I.5(c) COMPARISON OF OUTPUT OF SURFACE-MOUNTED ("STICK-ON") PRESSURE SENSOR WITH FLUSH-MOUNTED SENSOR; LOW TURBULENCE INFLOW; U_∞ = 53 m/s

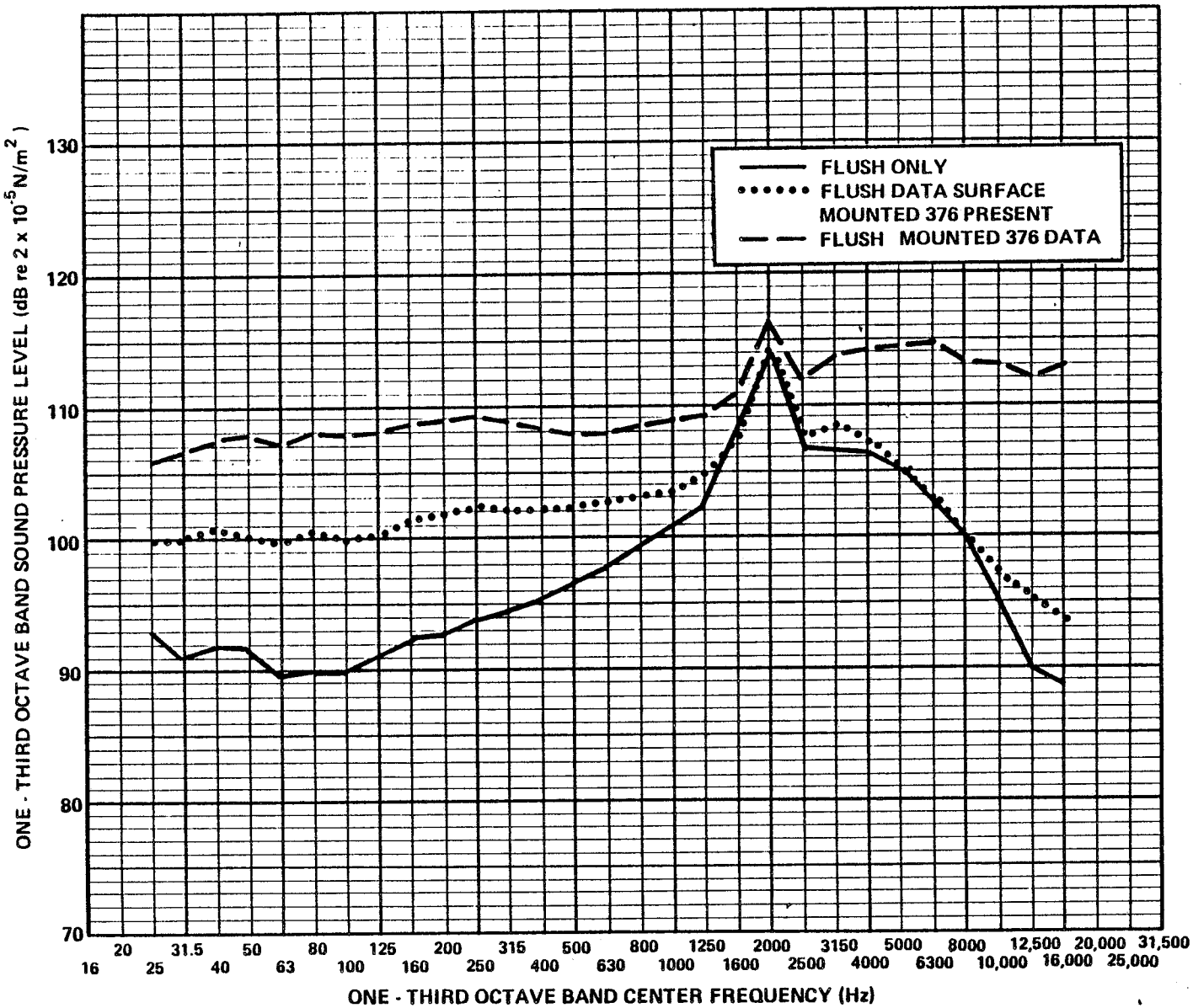

FIGURE I.5(d) COMPARISON OF OUTPUT OF SURFACE-MOUNTED ("STICK-ON") PRESSURE SENSOR WITH FLUSH-MOUNTED SENSOR; LOW TURBULENCE INFLOW; U_∞ = 62 m/s.

was essentially identical below 1 kHz; above 1 kHz, the sensor outputs differed systematically, with the "stick-on" sensor showing higher levels (levels similar to the previous case). Figures I.6(a) through I.6(d) illustrate these comparisons for free stream velocities ranging from 31 m/s to 62 m/s.

As was the case for the untripped boundary layer flow, the spectra for each configuration of the sensor(s) obey a 40 log U_∞ (20 log q) scaling relationship at constant Strouhal number (i.e., $f \propto U_\infty$). The particular spectra shown in Figure I.6(a) through I.6(d) are not particularly useful for estimating self-noise levels of such sensor configurations since the output will depend upon local details of the flow field on the aircraft. However, for lack of other data, one could use these spectra, properly scaled for differences in velocity (or q) to roughly estimate self-noise levels for "stick-on" (surface-mounted) microphones when one suspects the microphone to be immersed in a thick turbulent boundary layer. However, the procedures referenced in App. G should also be consulted to provide another estimate for hydrodynamically-induced pressures.

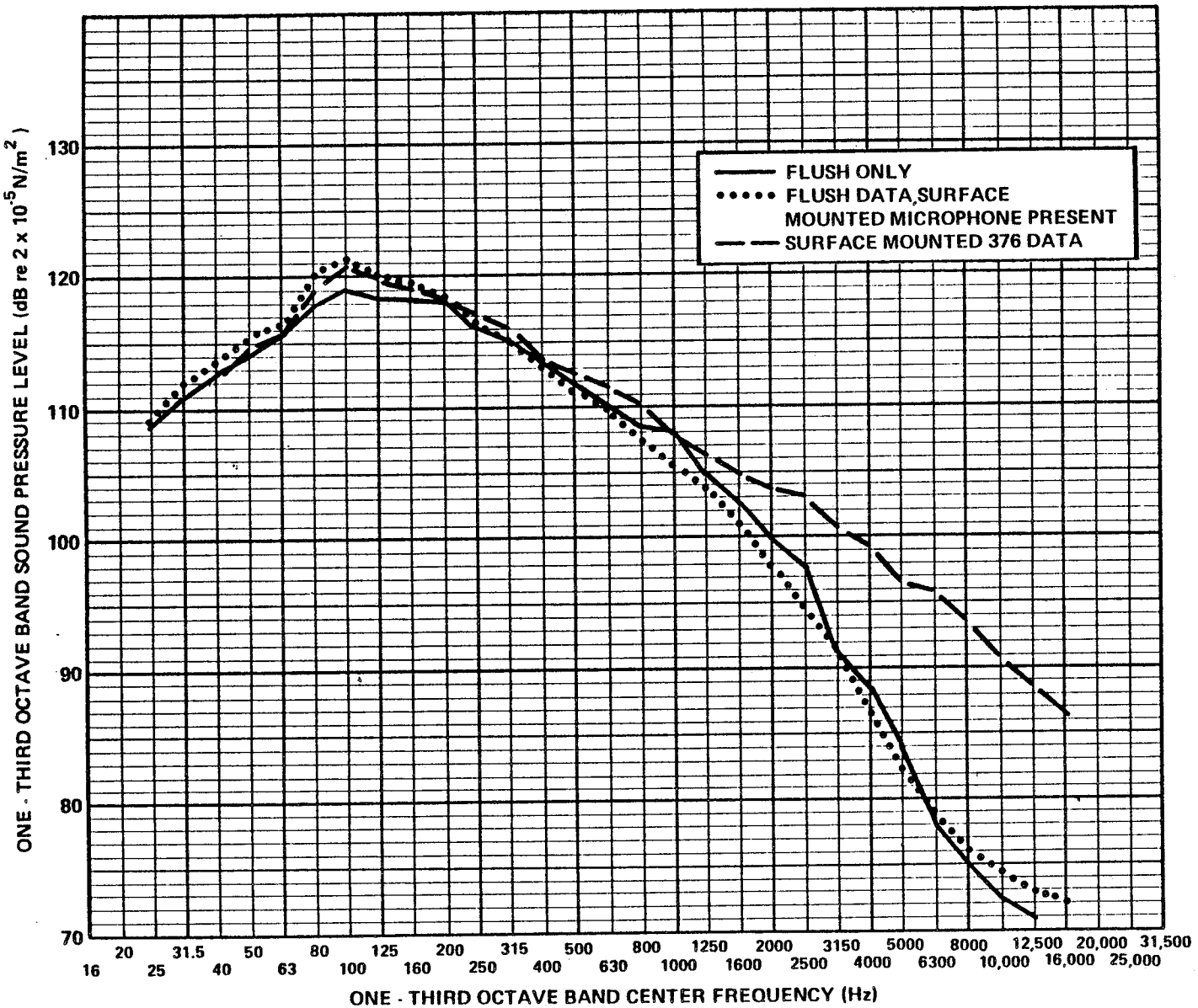

FIGURE I.6(a) COMPARISON OF OUTPUT OF SURFACE-MOUNTED ("STICK-ON") PRESSURE SENSOR WITH FLUSH-MOUNTED SENSOR; HIGHLY TURBULENT BOUNDARY LAYER; U_∞ = 31 m/s.

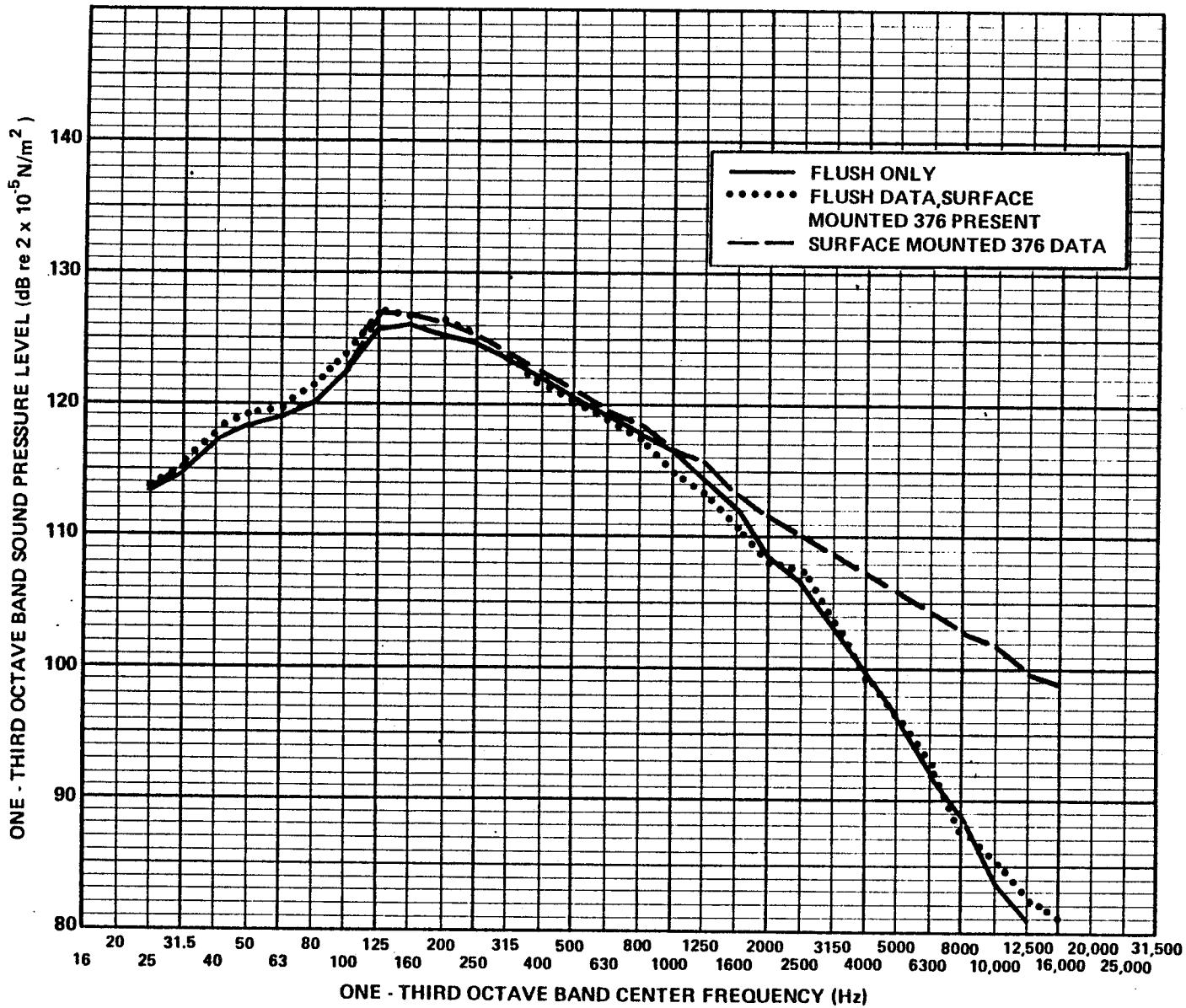

FIGURE I.6(b) COMPARISON OF OUTPUT OF SURFACE-MOUNTED ("STICK-ON") PRESSURE SENSOR WITH FLUSH-MOUNTED SENSOR; HIGHLY TURBULENT BOUNDARY LAYER; U_∞ = 44 m/s.

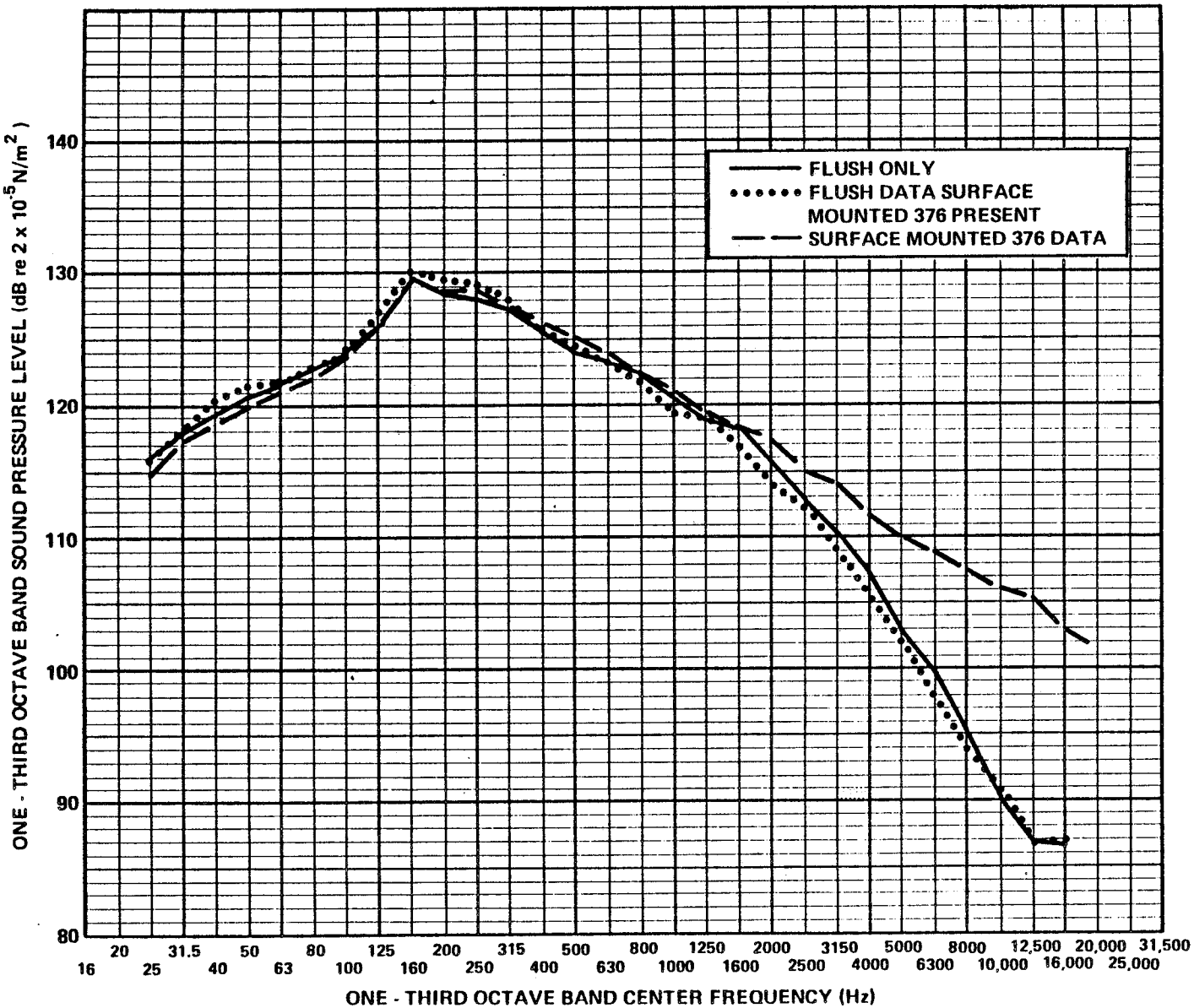

FIGURE I.6(c) COMPARISON OF OUTPUT OF SURFACE-MOUNTED ("STICK-ON") PRESSURE SENSOR WITH FLUSH-MOUNTED SENSOR; HIGHLY TURBULENT BOUNDARY LAYER; U_∞ = 53 m/s

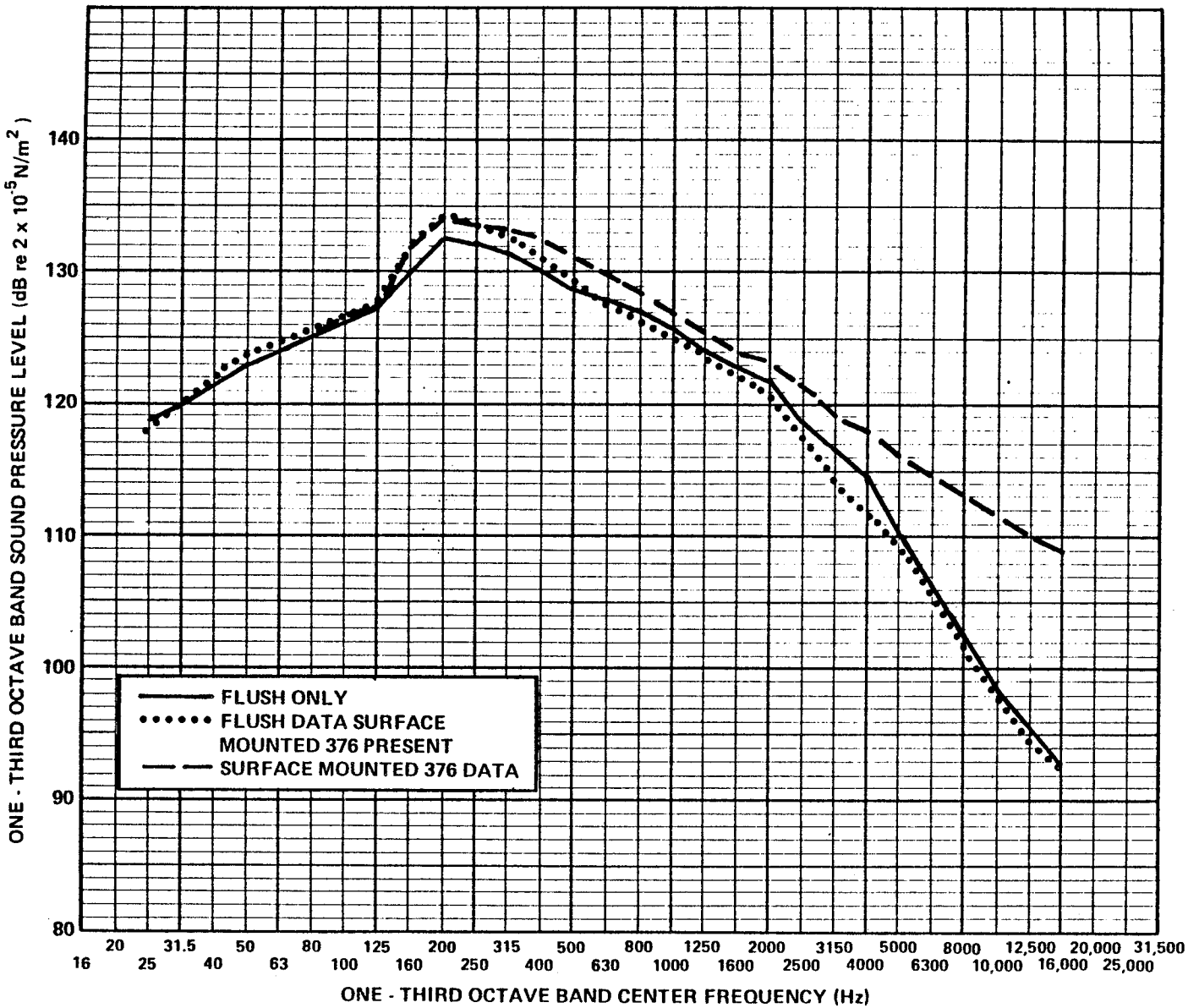

FIGURE I.6(d) COMPARISON OF OUTPUT OF SURFACE-MOUNTED ("STICK-ON") PRESSURE SENSOR WITH FLUSH-MOUNTED SENSOR; HIGHLY TURBULENT BOUNDARY LAYER; U_∞ = 62 m/s